Growth and characterization of cuprous oxide absorbers for photovoltaics

Chithira Venugopalan Kartha

UNIVERSITÉ DE STRASBOURG

ÉCOLE DOCTORALE Mathématiques, Science de l´Information et de l´Ingénieur

UMR 7357

THÈSE présentée par :

Chithira VENUGOPALAN KARTHA

soutenue le : **12 Décembre 2022**

pour obtenir le grade de : **Docteur de l'université de Strasbourg**
Discipline/ Spécialité : Physique de la Matière Condensée

Growth and Characterization of Cuprous Oxide Absorbers for Photovoltaics

RAPPORTEURS :

M.BARREAU Nicolas	Maître de conférences HDR, IMN, Université de Nantes
M.EL MARSSI Mimoun	Professeur, LPMC Université de Picardie Jules Verne, Amiens

AUTRES MEMBRES DU JURY :

Mme.VIART Nathalie	Professeur, IPCMS, CNRS- Université de Strasbourg
M.DESCHANVRES Jean-Luc	Chargé de recherche HDR, LMGP, CNRS- Université Grenoble Alpes

---

THÈSE dirigée par :

M.SLAOUI Abdelilah	Directeur de recherche, ICube, CNRS- Université de Strasbourg
M.FIX Thomas	Chargé de recherche HDR, ICube, CNRS- Université de Strasbourg

---

INVITE :

M. FERBLANTIER Gérald	Maître de conférences, ICube, CNRS- Université de Strasbourg

Titre en français :

Croissance et caractérisation d’absorbeurs à base d’oxyde cuivreux pour le photovoltaïque

To my grandmother
(Achamma)

ACKNOWLEDGEMENT

I would like to express my heartfelt gratitude to all those who have supported and guided me during the course of my PhD journey.

First and foremost, I would like to thank the members of the jury for their time, effort, and expertise in evaluating my work and attending my defense in Strasbourg. I am grateful for your invaluable insights and constructive feedbacks during the defense which have undoubtedly improved the value of my work.

I am deeply grateful to my thesis director, Dr. Abdelilah Slaoui for his guidance, support and encouragement throughout my PhD. Your insights and feedbacks have been instrumental in shaping my research and helping me to develop a deeper understanding of the subject. Your guidance and expertise in this field have helped me to grow as a researcher.

I would also like to thank my thesis co-director, Dr. Thomas Fix for his support, patience, knowledge, and motivation throughout my work. Thank you for always being available to guide me throughout my time in ICube.

I would also like to thank Dr. Gérald Ferblantier for his support and guidance throughout this journey. Thank you for passing on your wisdom in Magnetron Sputtering of thin films and for teaching me to independently work with the deposition technique.

I am grateful to Yi-Teng Huang from Cambridge University and Dr. R.Hoye from Imperial College London for their collaboration and willingness to carry out measurements in their laboratory. The results from their measurements of my samples have played a huge role in the shaping of my work and I am deeply indebted to them.

I am thankful to Prof. Jean-Luc Rehspringer, Dr.Guy Schmerber, Silviu Colis, Marc Lenertz and Cedric Leuvrey from IPCMS for their invaluable contributions in the different stages of my work in the past three years.

A special thanks to Stephane Roques and Romain Vollondat for their friendly attitude, encouragement and always being ready to help which made my life in the lab easier.

I would also like to thank my colleagues from C^3-FAB platform of ICube Laboratory especially, Dominique Muller, Yann Le Gall, Jeremy Bartringer and Nicolas Zimmermann for their help and support throughout my time in ICube.

I am deeply grateful to my family especially my parents for their unwavering love and support. Your belief in me and encouragement to pursue my dreams has been invaluable and has helped me reach this point in my academic career.

Finally, I would like to thank my husband for his love, support and understanding during this journey. Your encouragement and belief in me have been a constant source of motivation and strength.

I am grateful to all of you for your contributions to my academic journey and helping me to reach this important milestone.

Chithira Venugopalan Kartha

TABLE OF CONTENTS

INTRODUCTION

All oxide-solar cells are one of the most researched and currently growing photovoltaic technology. It involves the use of oxides in all the layers of a solar cell. Among the oxide absorbers, Cu_2O is one of the most promising material. Apart from its non-toxicity and abundant material availability, it has a high absorption coefficient and favourable direct bandgap which makes them attractive as an absorber. Even though good quality Cu_2O could be obtained via several growth techniques, their preparation method is found to be critical in their absorber efficiency. Better performing solar cells with Cu_2O absorbers, with over 5 % efficiency is only reported for thermally oxidised Cu_2O obtained by the oxidation of copper sheets at very high temperatures. Investigating the properties of Cu_2O grown via different techniques and comparing their absorber properties with the Cu_2O prepared via thermal oxidation will help to better understand the difference and will allow to engineer Cu_2O thin films using alternate techniques to improve their efficiency as an absorber.

The work of thesis focusses on the preparation and optimization of Cu_2O absorber via three techniques of Pulsed Laser Deposition (PLD), Magnetron Sputtering and Thermal Oxidation. Their properties are investigated in detail and later the optimized absorbers are compared to get a clear picture on the influence of the preparation method on their absorber properties.

This thesis is divided into five chapters. Chapter 01 gives an introduction into the basic material properties of photovoltaic absorber followed by a focus on the oxide absorbers and their different types. It also gives insights into all-oxide photovoltaics and state of the art all-oxide solar cells with different absorbers. The basic properties of Cu_2O, including its crystallographic structure, optical and electrical properties and a review on the different preparation methods is also outlined.

Chapter 2 gives a detailed description on the PLD deposited Cu_xO, optimization of the deposition parameters and their properties. Na ion implantation on the PLD Cu_2O and an analysis on its impact on the properties is also illustrated in Chapter 2.

Optimization of the films via magnetron sputtering by varying the deposition parameters is outlined in detail in Chapter 3 including the characterizations of the sputtered films structurally, optically, and electrically.

Thermal oxidation of Cu foils at elevated temperature is another technique followed to obtain Cu_2O films which is described in detail in Chapter 4. Optimization of the oxidation conditions and etching properties to obtain good quality thermally oxidized Cu_2O is also illustrated.

Chapter 5 outlines the state-of-the-art Cu_2O heterojunctions, and the photovoltaic devices realized using the films grown via PLD, magnetron sputtering and thermal oxidation in this work. The difference in the performance of the Cu_2O absorbers grown via different techniques are explained using advanced characterization techniques which helps to better understand the change in their properties and their quality via different techniques.

This work could pave the way for a better understanding of the growth techniques to obtain phase pure Cu_2O films via PLD, magnetron sputtering, and thermal oxidation and a detailed comparative study of the films grown via different techniques. By also implementing the prepared films as absorbers in all oxide solar cells a better picture of its application as an absorber is also illustrated.

1 CHAPTER : LITERATURE BACKGROUND

1.1 INTRODUCTION

Increase in the power demand unproportionally to the available non-conventional energy sources makes it critically necessary to shift to renewable energy sources. Owing to the potential of sun as an abundantly available source of energy it is viable to explore this energy source as an alternative. On an average the Earth surface receives approximately 343 W/m^2 of solar energy[1]. Even by considering the percentage of energy reflected or scattered back and the uneven distribution of radiation intensity in the different parts of usable land surface, the potential from sun is ten thousand times higher than the energy demand. In recent years, even though there has been notable growth in renewable generation, especially from solar (increase of 148 TWh) , the development is much slower contradicting its potential[2]. The main reason being the high fabrication and installation cost of the current commercially dominating first generation solar cells using Si absorbers. Owing to their higher fabrication costs, they have a higher energy payback time[3]. Additionally the current lab record efficiency of mono-crystalline Si solar cells (26.7%)[4],[5] is close to their maximum attainable theoretical efficiency of 29 % from the Shockley-Queisser limit[6]. Hence, there has been a momentum in the research of alternative materials which can potentially bring down the cost of production of solar cells since the past many decades. After the Si based solar cells the next most widely popular technology is the thin film technology dominated by CIGS and CdTe solar cells. Thin film solar cell (second -generation technology) utilizes strong light absorber layers of only few micrometers thickness and compared to the first generation, thin film solar cells require only less semiconductor material, their modules are lightweight and are less expensive. Thin film technologies had a market share of approximately 6 % in 2021[4] and is a continuously growing technology with great potential.

1.2 PHOTOVOLTAIC ABSORBER

The light absorbing layer is the most significant part of a solar cell. The main classification of solar cells is based on the absorber material used. They are responsible for the absorption of photons and in turn generation of charge carriers. There are several criterions to be fulfilled for a material to be eligible to be used as an absorber in a solar cell. First and foremost, the material should be able to excite electrons from thermal equilibrium upon absorption of photons. However, there isn´t a perfect ´´selection metric`` which helps to easily determine the potential of a material as an absorber. One of the foremost parameters to be considered is the bandgap. If the valence band maximum and conduction band minimum of a material are aligned with respect to momentum, such a material have direct bandgap, thus their transitions are vertical and mostly radiative (Figure 1.1(a)). For an indirect bandgap material on the other hand, the conduction band minimum and valance band maximum are not aligned with respect to momentum and thus due to the relative difference in the momentum, for the conservation, a phonon is involved. During the de-excitation, apart from the energy emitted via photons, some energy is emitted in form of phonons. Hence, they have phonon assisted transition unlike photon assisted transitions in a direct bandgap semiconductor (Figure 1.1(b)). Si is an indirect bandgap semiconductor, whereas GaAs is a direct bandgap semiconductor.

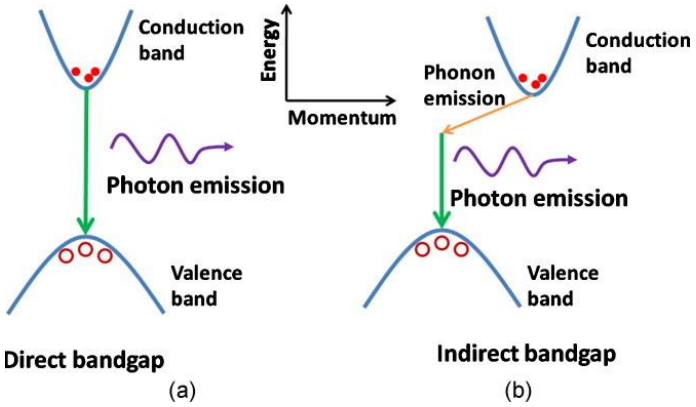

Figure 1.1 Schematic illustration of photon emission in (a) direct bandgap semiconductor (b) indirect bandgap semiconductor[7]

Even though, both direct and indirect bandgap semiconductor are suitable as an absorber, the use of direct band gap semiconductors is more favoured as small amount of material (thin film) can fulfil the necessity of strong absorption. The bandgap of the material determines the part of

the solar spectrum that the material absorbs. Low bandgap materials are more suitable to absorb low energy photons and high bandgap materials for high energy photons. Hence, using a combination of different materials is favoured sometimes for the better absorption of photons of a range of energies. However, if the bandgap is too low, the photons will have more energy available after excitation, which will be converted into heat, which is not preferred in a solar cell. The Shockley-Queisser Limit[6] is a prediction of maximum solar cell efficiency with respect to the bandgap of the absorbing material used. Figure 1.2 shows the variation of solar cell efficiency with band gap and the most suitable range of bandgap to obtain maximum theoretical efficiency above 25 % is ~ 0.9 -1.7 eV.

Absorption coefficient of a material is a measure of how far the photons penetrate through the material before it gets absorbed. The absorption coefficient is a wavelength and material dependent parameter. Higher absorption coefficient (~ 10^5 cm^{-1}) is always an important factor determining the potential of a material as a good absorber[8]. Minority carrier diffusion length is also an important factor determining the better efficiency of an absorber as higher minority carrier diffusion lengths allows for their better diffusion to the junction. The inverse of the absorption coefficient should be shorter than the minority carrier diffusion length to avoid recombination before reaching the electrodes. Therefore, higher mobility, diffusion coefficient, diffusion length and lifetime are important parameters determining the transport of charge carriers. Moreover, it is important to have an appropriate thickness of absorber such that absorption is not increased compromising the minority carrier diffusion length. Ideally, the film thickness should be greater than two times the inverse of absorption coefficient.

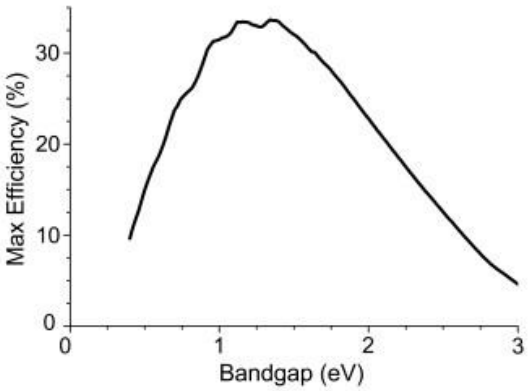

Figure 1.2 Variation of the maximum efficiency of single p-n junction solar cell with bandgap according to Shockely-Queisser limit[6]

An ideal absorber material should also have high concentration of donor or acceptor atoms depending on the doping type. However, increase in carrier concentration above a threshold will also increase recombination's (Auger recombination) and thus lowering the efficiency of solar cells.

1.2.1 Oxide Absorbers

Oxides are earth abundant and stable compounds. They contain at least one oxygen atom apart from other elements. Depending on the number of elements other than oxygen, there are binary oxides or complex oxides. Oxides can be metallic, semiconductor or insulator and can be used for multiple applications in a solar cell. They can be the light absorbers, transparent electrodes, transport layers or can be used to fulfil other unique functionalities. Metal oxides are widely used oxides for their application in photovoltaics as they are chemically stable, less toxic, and easier to fabricate. The chemical bond between oxygen and metal are rather strong and insoluble in solvents including water hence it is more feasible to use them in solar cells compared to organometallic perovskites. Most of the absorber oxides are p-type and their low mobility which leads to high charge recombination during charge transport and collection is a drawback. However, the high extinction coefficient of oxides is another advantage of oxide absorbers so that thin layer of absorber can fulfil full absorption of solar radiation[9] and to an extent overcome the recombination problem.

Within the oxide family, transition metal oxides (TMOs) are the widely used materials for photovoltaic conversion ability as they have semiconductor properties. In these compounds the oxygen is bonded to an element in 3 to 12 groups (metal with partially filled d subshell) in the periodic table. Metal oxides have higher bandgap which makes them potentially suitable light harvesters.

Among oxide absorbers, the most popular are the Cu-O based oxides. There are three stable compounds of copper oxides namely cuprous oxide (Cu_2O), cupric oxide (CuO) and paramelaconite (Cu_4O_3)[10]. The band gap of the copper oxides can be tuned by varying the phase of Cu-O compounds thus covering a range of bandgaps from 1.4-2.2 eV[11]. There has been wide research in solar cells with Cu-O absorbers since many decades among them, apart from Cu_2O, CuO solar cells are also widely investigated[12]–[16]. But the maximum achieved efficiency of solar cells using CuO is still below 1 % even though they have higher absorption coefficient compared to Cu_2O films. Bhaumik et.al have claimed to have achieved 2.88 %

efficiency with an incorporation of an optically active CuO nanopowders with ZnO/CuO based thin film solar cells[16]. Kaphle et.al have achieved 2.11 % efficiency with CuO absorbers by modifying the n type layer and adding a buffer layer[15]. Most recently, Ahmed et.al have designed a novel heterostructure with CuO thin film which have obtained an efficiency of 1.91 % but they have shown theoretically using simulation a potential for 12.09% efficiency for the design[14].

Apart from the Cu-O based absorbers, Co_3O_4, Fe_2O_3, Pb_xO_y,Bi_2O_3 [17] are other potential metal oxide absorbers[18]. Among cobalt oxides, Co_3O_4 is the most stable oxide, which is a p-type semiconductor with a direct bandgap of 1.5 eV. Even though its bandgap is so close to the ideal bandgap according to the Shockley-Queisser calculation of efficiency, the efficiencies achieved so far with Co-O absorbers are lower than the Cu-O based solar cells[18], [19]. Fe_2O_3 films also showed photovoltaic activity with rather low performance as reported by Rühle et.al with Fe_2O_3 / ZnO heterojunction[18]. Bi_2O_3 have a bandgap in the range of 1.7-3.96 eV. The ability to obtain p type and n-type conductivity with these material by tuning their fabrication methods and parameters makes it an interesting material. Even with same fabrication method, a shift from p-type to n-type Bi_2O_3 films were reported by Morasch et.al by varying the oxygen content during sputtering. They have also reported a solar cell with ITO/ Bi_2O_3 /Au with V_{oc} from 0.53-0.68 V, J_{sc} from 0.1-0.31 mA/cm^2 and efficiency varying from 0.02-0.05 % by varying the deposition parameters. There are a lot of stable lead-oxide compounds with potential absorber properties. PbO and PbO_2 are n-type semiconductors with bandgap in the range 1.9- 2.8 eV (tuning of bandgap with modifications) and 1.5-1.9 eV respectively. Schottky junction solar cells were reported with PbO absorbers but with low efficiency of 0.18 %[20]. However, none of these materials have achieved comparable PV performance to that of Cu-O based solar cells especially Cu_2O.

Another group of materials which has been popular recently are ferroelectric oxides. They are perovskites with structure ABO_3 or even double perovskites. In ferroelectric solar cells, the generated photovoltage is not limited by their bandgaps unlike the general p-n junction cells. The photo-generated carriers are transported by polarization induced internal electric field and are not localized at an interface, rather extends throughout the material which is called bulk photovoltaic effect. It has been shown experimentally by Spanier et.al that it is possible to overcome the Shockley-Queisser limit with ferroelectric absorbers which pave the way for high efficiency photovoltaic devices with single junction[21]. The most investigated ferroelectric

oxides are $BiFeO_3$(BFO), $BaTiO_3$(BTO), $LiNbO_3$(LNO), $BiMnO_3$(BMO), Pb $(Zr,Ti)O_3$ (PZT), Bi_2FeCrO_6 (BFCO). Recent advances in ferroelectric oxides with the bandgap tuning of BFO with Cr doping by Nechache et.al[22] have reported a solar cell with an efficiency of 8.1%, which is a very encouraging result for the great potential of perovskite oxides in photovoltaics.

1.3 ALL-OXIDE PHOTOVOLTAICS

Metal oxides can be used for multiple applications in a photovoltaic cell apart as an absorber namely, as transparent conducting oxides (TCO), transport layers, passivation layers etc. Owing to the chemical stability, abundancy, and non-toxicity of most of the oxides, they are becoming more popular and are very well suited for low-cost manufacturing techniques. Hence solar cells with all the layers based on metal oxide semiconductors called all-oxide solar cells are becoming a new emerging field in photovoltaics. As discussed in 1.2.1, there are numerous metal oxide semiconductors with great potential to be used as an absorber layer in a solar cell. Similarly due to the availability of wide band gap metal oxides they can be used also as transparent conducting oxide layers (TCOs) and materials such as indium tin oxide (ITO), fluorine doped tin oxide (FTO), aluminium doped zinc oxide (AZO) are already popular materials used in consumer electronics such as smart phones, flat panel displays besides in commercially available solar cells based on CdTe, CIGS, amorphous and monocrystalline Si. There are numerous binary and ternary oxides which can be used as an electron-transport layer (TiO_2,ZnO,$FeTiO_x$,$SrTiO_3$,Zn_2SnO_4), hole transport layer (NiO_x,CuO_x,MoO_3,V_2O_5,GeO_2) or as an insulating layer (Al_2O_3,ZrO_2,SiO_2) on top of the oxide electrodes to passivate any defects[23]. Additionally, for better band alignment to increase the open circuit voltage, as well as to reduce the shunt resistance in a solar cell, they can be used as window layers. One of advantages of all-oxide solar cell is that the TCO is easily compatible with the active layer.

Figure 1.3 gives a general schematics of energy band diagram of an all-oxide solar cell under short circuit condition wherein M corresponds to Metal and O to Oxygen and x and m corresponds to the stoichiometric ratios. M_xO is a window layer between the TCO and the oxide absorber $M(n_m)O_x$, which is a combinatorial light absorber material with n metals. M is the back contact metal.

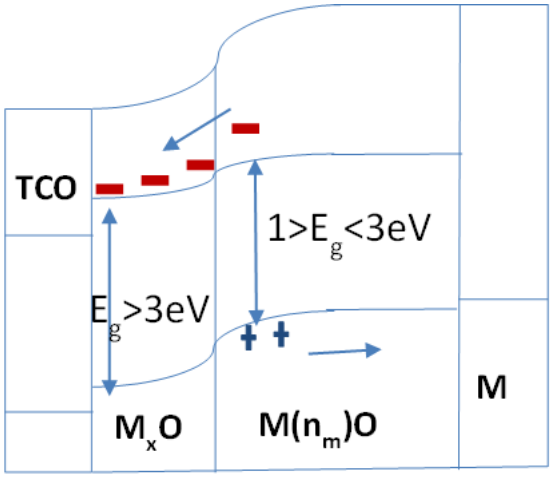

Figure 1.3. Band diagram of an all-oxide solar cell under short circuit conditions

Among all-oxide solar cells the most popular are Cu_2O based solar cells. Apart from optimizing the oxide absorbers, a focus on the improvement of transparent conducting oxide by experimenting different heterojunctions is a major part in the improvement of all-oxide solar cells. In combination with binary or ternary oxide compounds it is possible to tune the photovoltaic properties of the solar cells. Even though the most typical n- type oxide used in combination with Cu_2O is ZnO, more combinatorial TCOs with desired properties are investigated to achieve better properties. Highest reported efficiency photovoltaic cell with Cu_2O so far is with the architecture MgF_2/Al-doped $ZnO/Zn_{0.38}Ge_{0.62}O/Cu_2O$:Na which achieved a record efficiency of 8.1 %[24]. It is possible to tune the conduction or valence band positions thus tuning the conduction band offset by using ternary oxide materials. Table 1 summarizes the photovoltaic parameters of some of the Cu_2O, CuO and Co_3O_4 all-oxide solar cells with promising results.

Table 1 I-V properties of some all-oxide solar cells with Cu_2O, CuO and Co_3O_4 absorbers with promising results

System	V_{oc} (V)	J_{sc} (mA/cm^2)	PCE (%)	References
MgF_2/AZO/$Zn_{0.38}Ge_{0.62}O$/Cu_2O: Na/Au	1.1	11.00	8.1	Minami et.al ,2016[24]
MgF_2/AZO/$Al_{0.025}Ga_{0.975}O$/Cu_2O: Na/Au	0.840	10.95	6.1	Minami et.al ,2015[25]
AZO/Ga_2O_3/Cu_2O/Au	0.800	9.99	5.38	Minami et.al,2013[26]
AZO/ZnO/Cu_2O/Au or Cu_2S	0.690	10.09	3.83	Minami et.al, 2011[27]
Al-grid/AZO/a-ZTO/Cu_2O/Au /Ti/Glass	0.622	7.25	2.85	Lee et.al, 2014[28]
Al-grid/AZO/ Ga_2O_3/Cu_2O/Au /Ti/Glass	1.204	7.37	3.97	Lee et.al,2014[29]
Cu/h-BN/ Cu_2O/CuO/Au/Cr	0.650	6.90	2.2	Ergen et.al ,2015[30]
ITO/n- Cu_2O/p- Cu_2O/ITO/Glass	0.61	4.07	1.06	McShane and Choi,2012[31]
Ag/nMgO/CuO/ITO/Glass	0.326	2.13	0.25	Bhardwaj et.al,2016[12]
Au/Co_3O_4/TiO_2/FTO	0.430	0.2	0.022	Kupfer et.al,2015[19]

Another branch of all-oxide solar cells is with ferroelectric oxides. Among which only BFCO solar cells with Niobium doped $SrTiO_3$ (Nb:STO) junction have reported promising results so far which uses ITO as the top electrode[22], [32] . Table 2 summarizes the I-V parameters of BFCO all-oxide solar cells with encouraging results.

Table 2 BFCO all-oxide solar cells

System	V_{oc} (V)	J_{sc} (mA/cm^2)	PCE (%)	References
ITO/BFCO/Nb:STO	0.74	0.99	6.5	Nechache et.al,2011[32]
ITO/BFCO/SRO	0.79	11.7	3.3	Nechache et.al,2015[22]
ITO/BFCO/Nb:STO	0.84	20.6	8.1	Nechache et.al,2015[22]

1.4 CUPROUS OXIDE (Cu_2O)

Among the oxide absorbers, the most promising and investigated material is cuprous oxide. It is a semiconductor material which has been introduced as early as mid-1920s and the photoelectric effect in them was identified also much before silicon in 1930s by Lange et.al [33]. However, until the energy crisis in the 1970s which led to increase demand for low-cost solar cells, the Cu_2O absorber interest remained low. Primarily, Cu_2O is made of two very abundant and non-toxic materials, copper, and oxygen. Availability of approximately 880 million tons of copper reserves worldwide makes it a potential candidate for low-cost photovoltaics[34]. Additionally, the fact that they can be prepared via very easy techniques such as thermal oxidation of copper is a major advantage. In the study published by Wadia et.al[35], Cu_2O is identified as one of the most attractive material for photovoltaics in terms of its long-term potential among inorganic photoactive materials.

1.4.1 Crystallographic Structure

Cu_2O crystallizes in a simple cubic structure with lattice parameter 4.2696 Å. It belongs to the space group $pn3m\text{-}O_h^4$. As depicted in the crystalline structure in Figure 1.4, in a unit cell with six atoms, the two oxygen atoms (red spheres) are in body-centered cubic lattice (bcc) and four Cu atoms are in face-centered cubic sub lattice (fcc). The oxygen atoms are tetragonally coordinated with four copper atoms and copper atoms are linearly coordinated to two oxygen atoms. The concentration of copper atoms is twice that of oxygen concentration under stoichiometric conditions. The bond length between O-O is 3.68 Å, Cu-Cu is 3.01 Å, and Cu-O is 1.85 Å. The density is 6.10 g/cm^3 [32]–[34], molar mass is 143.09 g/mol and molar volume is 23.46 cm^3/mol. The melting point being 1235 °C.[36]–[38]

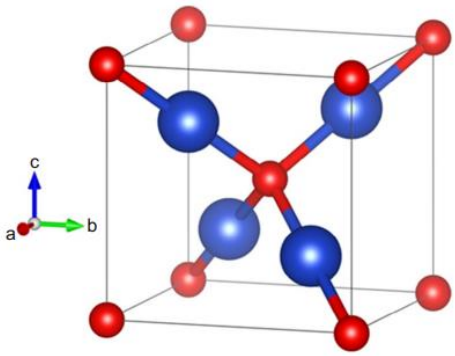

Figure 1.4 Crystalline structure of Cu_2O[17]

1.4.2 Electrical and Optical Properties

Cu_2O is a p-type defect semiconductor. It is essential to understand about the defects in Cu_2O lattice to better explain its intrinsic p-type conductivity. Frenkel defects corresponds to interstitial ions, and they do not affect the crystal stoichiometry. However, Schottky defects, which correspond to anion or cation vacancies leads to non-stoichiometry in the crystal. Basically, Cu_2O is a defect semiconductor, it is a non-stoichiometric material. The intrinsic defects in Cu_2O are from copper vacancies (one Cu missing leading to two 3-fold coordinated oxygens), copper split vacancies (nearby Cu atom occupies Cu vacancy site and coordinates four oxygens), oxygen interstitials (in octahedral , O_i^{oct} and tetrahedral coordination, O_i^{tet}). The formation energies of defects in Cu_2O for the conditions of Cu rich and poor and O rich and poor given by Scanlon et.al[39] is shown in Figure 1.5. At room temperature and atmospheric pressure, the dominant defects in Cu_2O are copper vacancies (V_{cu}) and copper split vacancy (V_{cu}^{split}) as the formation enthalpy is the lowest for these defects. The oxygen interstitial defects have much higher formation energy and are not favourable. Among the Cu vacancies, which one is more thermodynamically stable is still a matter of debate. Their formation energies reported by different theoretical studies are different. Scanlon et.al[39] reported V_{cu} at around 0.41 eV and V_{cu}^{split} at 1.24 eV wherein Soon et.al[40] reports 0.47 eV for V_{cu} and 0.78 eV for V_{cu}^{split} and Nolan et.al[41] presents 0.4 eV for both vacancies. Isseroff and Carter[42] have performed several DFT -based calculations and reported that the V_{cu} is more stable than V_{cu}^{split} by 0.21±0.03 eV. Paul et.al[43] have done deep-level transient spectroscopy studies of Cu_2O/ZnO heterostructure and found two-hole traps with activation energy 0.25 eV (trap A) and 0.45 eV (trap B). They have assigned trap A as Cu-di-vacancy and trap B as Cu-monovacancy.

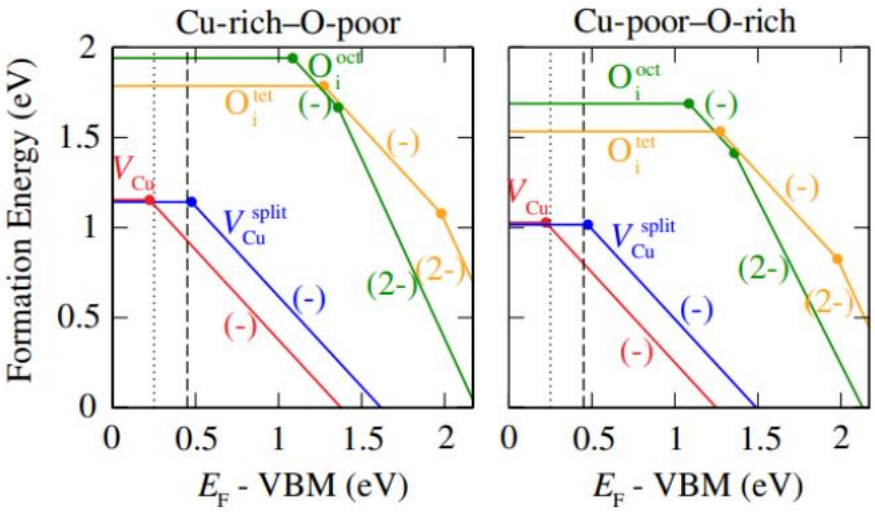

(a) (b)

Figure 1.5. Formation energies of intrinsic p-type defects in Cu_2O at (a) Cu rich and O poor (b) Cu poor and O rich conditions[39]

The concentration of V_{cu} can reach up to ~ 10^{20} cm^{-3}, however, the concentration of holes at room temperature will be only up to ~ 10^{18} cm^{-3} as all the copper vacancies will not be ionized. Brattain et.al[44] have conducted capacitance-voltage measurements on Schottky junction Cu/ Cu_2O to analyze their conductivity between 100-400 K and found that Cu_2O is a compensated semiconductor, ie. both acceptor and donors are present. The net concentration of charged defects is N_A-N_D. The acceptor level is at ~ 0.3-0.6 eV above the valence band and donor level is deep with a concentration lower than that of acceptors. They also observed that the defects might not be stable as soon after saturation begins, the conductivity increases rapidly.

The mobility (μ) of the films highly depends on the synthesis method, and can go up to 50-110 cm^2/Vs for good quality films deposited at high temperatures[25], [45]. Simple, cost-effective methods like electrodeposition produce Cu_2O films with smaller grain sizes and very low mobility. As the charge carrier collection length (L) when used in a photovoltaic device is proportional to the carrier mobility ($L = \sqrt{\frac{kT}{e}}\mu\tau$), with low mobility films the charge collection length will be below 1 μm[46], [47].

There have been few work[48]–[52] which have reported n-type conductivity of undoped Cu_2O which claims oxygen vacancies and copper interstitial defects as the source. But it is still a matter of debate[53] as thermodynamically, their formation energies are not favourable.

Cuprous oxide has a direct forbidden bandgap of ~ 2.1 eV. In the energy band diagram of Cu_2O, in Figure 1.6(a) the direct transition from the highest valence band to the lowest conduction band which occurs at the Γ-point of the Brillouin zone is schematically represented with and without spin-orbit coupling (λ). The valence band is formed by Cu $3d^{10}$ states, and the conduction band formed by empty Cu 4s states. As both the bands have same parity, it has a direct bandgap at the Brillouin zone. The $\Gamma_{25'}$ valence band is split by spin-orbit interaction into Γ_7^+ and Γ_8^+ and conduction band Γ_1 to lowest conduction band state, Γ_6^+. The absorption transitions which are parity forbidden are Γ_7^+ to Γ_6^+ (yellow), Γ_8^+ to Γ_6^+(green). The allowed optical transitions are Γ_7^+ to Γ_8^-(blue), Γ_8^+ to Γ_8^-(indigo).[36] Other inter band transitions at low temperature (4.2 K) are Γ_8^+ and Γ_6^+ , Γ_7^+ and Γ_8^- and Γ_8^+ and Γ_8^-.

Meyer et.al[36] have calculated the absorption spectrum (Figure 1.6(b)) of as-grown Cu_2O and the film annealed and have obtained well defined excitonic peaks after annealing. The absorption coefficient reaches ~ 10^5 cm^{-1} at 2.6 eV. In the absorption coefficient spectrum, the contributions of four exciton series (yellow, green, blue, and violet) are evident (in red curve of Figure 1.6(b)).

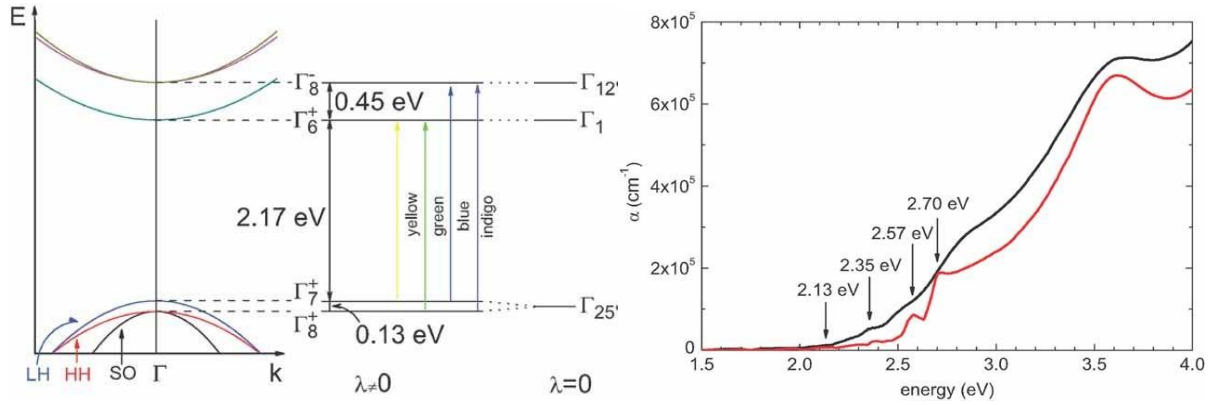

(a) (b)

Figure 1.6 (a) Energy band structure of Cu_2O at gamma point (b) Absorption coefficient spectrum of Cu_2O : as-grown (black),annealed (red)[36]

1.4.3 Cu-O Phase Diagram

In Figure 1.7 the phase diagram of Cu-O with respect to temperature and oxygen partial pressure constructed by Rakhshani et.al[9] is depicted. Pure Cu_2O in air is obtained at higher

temperature between 1000-1030 ℃ even though it is close to Cu_2O-CuO boundary. Below 1000 ℃, the stable phase is CuO at atmospheric pressure. Even though Cu_2O is unstable at room temperature, since the formation kinetics of CuO is slow, Cu_2O is considered stable. The oxidation mechanism is still not clearly understood as the oxidation kinetics is influenced by several factors such as oxygen partial pressure, temperature, sample type, its crystal orientation, grain size, impurities, lattice defects etc. From the Ellingham diagram of copper, which shows the temperature dependence of compound stability, the CuO phase can be formed only by further oxidation of Cu_2O because, Cu is in equilibrium with Cu_2O at atmospheric pressure and cannot co-exist with CuO phase[54].

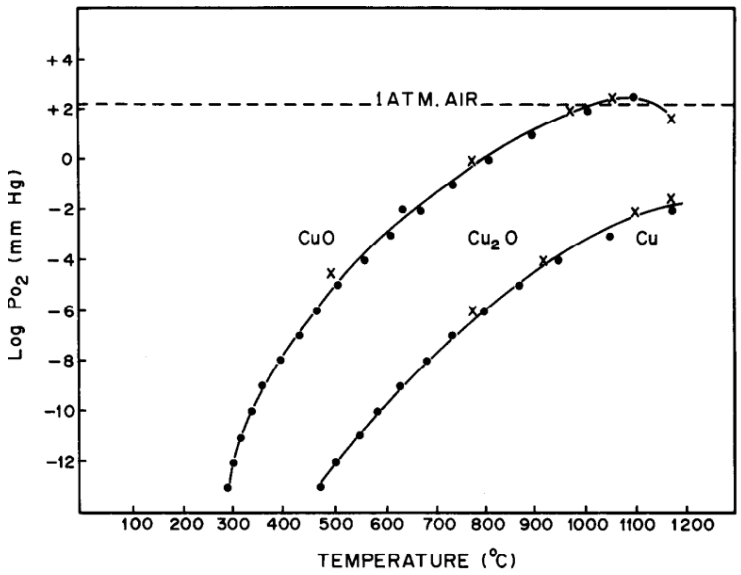

Figure 1.7 Phase diagram of Cu-O by Rakhshani et.al[9]

1.4.4 Cu_2O Growth: Overview

As the fundamental properties of cuprous oxide films highly depend on the growth technique and deposition conditions, they are important factors in obtaining films with specific properties for various applications. Especially for the application as absorbers in a solar cell, the optical and electrical properties are key criteria for best performing cells. There are several methods for the growth of Cu_2O, both vacuum and non-vacuum techniques, chemical and physical processes. The most popular among them are electrodeposition[46], [49]–[51], [55], [56], magnetron sputtering[57]–[60] and thermal oxidation[26], [27], [45], [61]. Electrodeposition is one of the cheap and simplest methods to obtain thin and uniform films. Cu_2O can be deposited on any conductive substrate which is the cathode and as the anode, copper is used with a

potential difference of less than 0.5 V between them. Cathodic reduction of alkaline solution of a cupric complex salt yields Cu_2O[9]. The smaller grain size of Cu_2O and electron collection distance of 53-88 nm increases recombination losses in electrodeposited Cu_2O[46], [62]. Even though, photovoltaic devices with Cu_2O grown via variety of techniques have been reported, the best performing Cu_2O solar cells are with thermally oxidized absorbers[24]–[26]. As can be seen Figure 1.8, which shows the efficiency of solar cells with the different preparation methods of Cu_2O absorber, all the better performing solar cells are with thermally oxidized Cu_2O. Other popular methods for preparation are pulsed laser deposition, atomic layer deposition, chemical vapour deposition, however such solar cells have not yet reported conversion efficiency above 5 %[23]. As explained in 1.4.3, obtaining the Cu_2O phase is very challenging as several factors influence the phase and CuO is more stable at room temperature. To obtain Cu_2O without any parasitic CuO, detail deposition parameter optimizations is necessary. In this work three main synthesis routes were followed to obtain phase pure Cu_2O namely, pulsed laser deposition (PLD), magnetron sputtering and thermal oxidation.

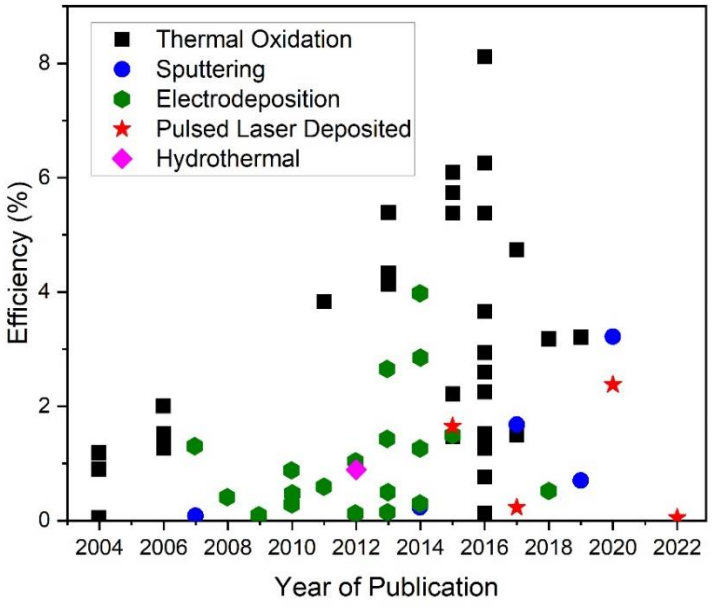

Figure 1.8 Efficiency chart of Cu_2O solar cells with their year of publication and type of preparation of Cu_2O[23], [58], [63]–[69]

a) Pulsed Laser Deposition (PLD)

Pulsed Laser Deposition (PLD) is a common physical technique to obtain high quality films. However, there are only very few reports on PLD Cu_2O[48], [52], [69]–[76] as the deposition is under non-equilibrium condition in pulsed laser deposition and it is tricky to obtain phase pure Cu_2O. Nevertheless, the properties of the PLD deposited films highly depend on the deposition parameters such as laser fluence, background gas, substrate temperature, the distance between target and substrate which allow for better control of the film properties which can be manipulated for various applications. Thermodynamic conditions play a strong influence on the Cu-O phase formed via PLD[77]. Chen et.al[70] and Liu et.al[78] have shown that an increase in chamber pressure changes plasma dynamics from the ballistic to diffuse regimes, which results in different Cu-O phases. Chen et al also show the influence of temperature, wherein they mention that at $4x10^{-4}$ mbar pressure, a variation in temperature between 400-700 °C changes the orientation of the films. Moreover, they showed that mixed films of CuO and Cu_2O are obtained at higher pressures above $1x10^{-3}$ mbar and CuO films are formed above $4x10^{-2}$ mbar. However, Jawad et al[79] claim that films deposited at a fixed oxygen partial pressure of 10^{-3} mbar and different temperatures allow the control of the film's phase between CuO and Cu_2O. Subramaniyan et.al[80] have managed to obtain phase pure Cu_2O at $3x10^{-4}$ mbar oxygen partial pressure and temperature in the range of 308-325 °C where CuO is the equilibrium phase, by varying the total chamber pressure which they explain to have a non-monotonic effect on Cu-O formation. Later, Farhad et.al[81] claim to have obtained p-type films at room temperature at an oxygen partial pressure of 2 - $3x10^{-3}$ mbar. Carrier transport properties in Cu_2O strongly affects stoichiometric deviations. Post-deposition treatments are found to improve the quality of films. Matsuzaki et.al[82] have obtained Cu_2O epitaxial films with high hole mobilities upto 90 cm^2/Vs after annealing at 750 °C.

b) Magnetron sputtering

Another very popular technique for thin film deposition of Cu_2O is sputtering[57]–[60], [68], [83]–[89]. Like any other thin film techniques, the properties of the film highly depend on the deposition conditions. Additionally, both DC (direct-current) and RF sputtering can be used for the Cu_2O film deposition and Cu target is used magnetron sputtering helps to get highly uniform films at relatively high growth rate and good control of the stoichiometry of the films with varying the deposition parameters such as substrate temperature, gas flow rates, pressure, and

target power density. One of the main parameters to be considered is the ratio of argon and oxygen flow rate. The phase of the film can be controlled with gas flow and oxygen partial pressure[57], [60], [85]. Mixed phase films of Cu and Cu_2O was observed at oxygen partial pressures from 1.7- 4.9 $x10^{-2}$ Pa due to insufficient oxygen to react with copper and high sputtering yield of copper. Further increase in oxygen partial pressure leads to single phase Cu_4O_3. Balance of optimum oxygen partial pressure and gas flow is required for pure Cu_2O. Apart from obtaining phase pure Cu_2O, improvement of the optical and electrical properties is the primary goal for all the deposition optimizations. As reported by Reddy et.al[59] increase in sputtering pressure causes stresses in the film affecting the lattice parameter. By increasing the pressure, the films changed from polycrystalline to amorphous nature. Variation of sputter pressure had influenced the orientation of the films wherein at low pressure both (1 1 1) and (2 0 0) were observed while only (1 1 1) oriented films at low pressures. Also, high surface roughness was observed for high pressure (> 4 Pa) prepared films. Resistivity also increased with pressure and hole mobility decreased. Better electrical properties were exhibited by films deposited at pressure of 1.5 Pa. Zhang et.al[60] have shown that with RF sputtering, the resistivity can be decreased by increasing the oxygen concentration in the gas flow as excess oxygen will generate acceptor levels located below Fermi level. They have also reported decrease in the bandgap of the film along with the resistivity change. Paul et.al[43] reported increase in the concentration of Cu-di-vacancy with oxygen flow rate during deposition and the dominant trap changes from Cu-mono-vacancy to Cu-di-vacancy. They have also observed improvement in the crystal quality of Cu_2O with the increase in the substrate temperature during deposition. Influence of substrate temperature on the hole mobility was observed in many work[43],[83],[90]. Unlike PLD, via sputtering, pure Cu_2O films are reported at low temperatures in the range of 200-400 °C[57], [84], [91] and also at room temperature[68], [86], [88]. Increase in the carrier concentration with deposition temperature is also reported which shows that the defect density decreased with temperature. Similarly, Ishizuka et.al[90] have increased the electrical properties especially the hole mobility to 60 cm^2/Vs by sputtering Cu_2O at high temperature of 500 °C. Lee et.al have found that apart from increase in hall mobility the morphology of films vary with substrate temperature[83].

Post annealing of the Cu_2O films is another way to improve the carrier mobility and lower the resistivity and is shown by Nordseth et.al[89] wherein by post annealing the films at 900 °C increased its mobility from 10 cm^2/Vs to 50 cm^2/Vs. Even though the annealing has increased

the grain size, it also led to the increase of roughness from 8.0 to 20.6 nm and bandgap from 2.06 eV to 2.19 eV. They have explained that it is due to the partial elimination of defect states and more phase pure films. The absorptance of the films also decreased after annealing due to the decrease in the grain-boundary scattering. Wang et.al[86] have done post annealing in air at different temperatures and found that annealing at temperature below 300 ℃ avoids further oxidation of films to CuO annealing in air also removes oxygen vacancies and reducing defect scattering. Another interesting work wherein the Cu_2O films preparation by vacuum annealing of magnetron sputtered CuO is reported by Murali et.al[92] the have obtained higher grain size and carrier mobility of 51 cm^2/Vs via this method of preparation.

Doping of pure sputtered Cu_2O films is another popular technique to improve its properties and have been reported by many in the literature with elements such as N, Ag, Si, Ge[88],[90], [93],[94]. Nitrogen is the most common dopant used and have improved the electrical properties by improving the hole concentration[87]. In the thesis of M.Nyborg[95], nitrogen is implanted to Cu_2O and observed increased carrier concentration because nitrogen substitute oxygen and act as an acceptor in the films. A shallow acceptor level was observed at about 170 meV above the valance band. Further, Na doping of sputtered Cu_2O by Ke et al[58] is found to increase the hole concentration and lower the resistivity and also enhance the crystalline properties of Cu_2O. They observed that Na impurities substitutes Cu sites in the lattice forming Na-O thus increasing the Cu vacancies and improving the electrical properties of the film. Na is a dopant of great potential to improve the photovoltaic properties as the highest efficiency Cu_2O solar cell reported so far is with Na doped Cu_2O[24],[61]. In the study of Minami et.al[61] the resistivity values of Na doped thermally oxidized Cu_2O decreased to 3.95 $x10^{-2}$ Ω.cm, mobility increased to 100 $cm^2/V.s$ and hole concentration increased to 10^{19} cm^{-3}. Improvement in the conduction of Cu_2O by passivation of defects with hydrogen or cyanide is another method[94], [96],[97]. Hydrogen implantation on sputtered Cu_2O is done by Raj Kumar et.al[94] to passivate both the acceptor defects and compensate donor defects. They have shown that increase in H^+ doses limit the acceptor level formation as they occupy Cu vacancy site, thereby decreasing the carrier density with increased doses. A reduction in the compensation ratio was observed when the implantation dose increased, which is due to decrease in compensating defects due to passivation and is also similar to what was observed by Ishizuka et.al[97].

c) Thermal Oxidation

All the metals tend to oxidize and the simplest of it is at room temperature when exposed to ambient air or oxygen wherein a thin oxide layer is formed. At high temperatures, by controlling the diffusion of oxygen atoms and chemical reactivity of metal, the thermal oxidation process can be controlled[98]. Thermal oxidation is the most widely used method for the preparation of highly efficient Cu_2O for photovoltaic application. Thermally oxidized Cu_2O have shown better performance as an absorber compared to Cu_2O prepared via other techniques as can be clearly seen in Figure 1.8. Thermal oxidation is a complex chemical process wherein the oxides are grown at elevated temperatures (above 1000 ℃) in an oxidant gradient. The starting material is copper foil. The properties of the films depend on the purity of Cu foil, temperature, film thickness, duration of oxidation, oxidant partial pressure and crystallographic orientations. Depending on the thickness of the copper foil used for oxidation the time for oxidation can be adjusted to completely oxidize the foil[98].The oxidation of Cu foil happens in mainly two steps, namely nucleation and growth. Initial step is the oxygen chemisorption, followed by nucleation thus forming Cu_2O nano islands which happens in areas where nucleation energy is lower like at grain boundaries or near dislocations. Finally, the growth of continuous oxide layer and coalescence of the islands. These steps are schematically depicted in Figure 1.9(a). Absorbed oxygen atoms occupy the hollow site on Cu(100) forming nano-sized c(2x2)-O ordered domains separated by oxygen deficit zigzag shaped anti-phase boundaries. Such nano sized domains disperse the stress associated with the oxygen absorption. Large domains of c(2x2)-O forms with coalescence of nano domains which are unstable after 0.3 ML coverage of oxygen. This stress leads to slow transition to a missing-row type surface reconstruction into the stable $(2\sqrt{2} \times \sqrt{2})R45°$-O structure[99]. Lahtonen et.al[100] studied in detail the oxidation process of Cu by carrying out time lapsed constant current topographic STM images during the entire oxidation process of pure Cu (1 0 0). They have measured the oxygen coverage by XPS during the process. This work has led to better understanding of the oxidation process. As shown in the CCT STM images in Figure 1.9(b), there is no visible change until the oxygen exposure is 551 L (oxygen coverage of 0.4 ML) and the formation of $(2\sqrt{2} \times \sqrt{2})R45°$-O can be seen as depressions in Figure 1.9 (b)(d). During this reconstruction, ejection of every fourth Cu (001) atom occurs from the surface. When the oxygen exposure further increases and reaches 1738 L a well-ordered island appears at the junction of two c(2x2)-O. The $(2\sqrt{2} \times \sqrt{2})R45°$-O phase continues to grow with oxygen exposure and c(2x2)-O reduces to one-dimensional

stripes appearing as depressions. As the oxygen exposure is increased these ordered islands grows further.[100]

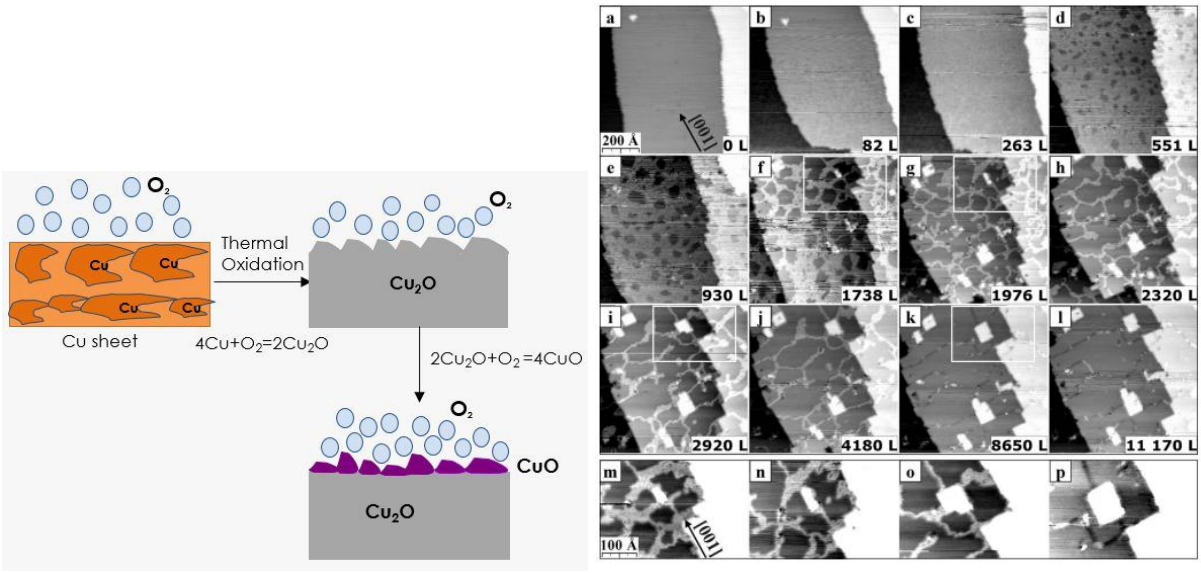

(a) (b)

Figure 1.9 (a) Schematics of cuprous oxide formation (b) copper oxidation stages from time lapsed sequential CCT STM during oxidation of clean Cu (100) surface extracted from Lahtonen et.al [100]

Most of the work in the literature related to thermally oxidized Cu_2O carry out the oxidation at higher temperatures of 1000-1050 ℃ with thin Cu sheets of 100-200 µm thickness[26],[45], [67],[101]–[104]. Musa et.al[104] studied the influence of oxidation temperature in the physical and electrical properties of Cu_2O by heating in a range of temperature from 200-1050 ℃. They observed mixed phase of CuO and Cu_2O at temperatures below 1040 ℃. Between 1040-1050 ℃ only Cu_2O phase was observed which further oxidises to CuO with long oxidation time. The CuO formed on top of Cu_2O can be selectively removed via etching in nitric acid (HNO_3) solution. They have also reported that after etching the gaps between the crystal grains disappeared. Choudhary et.al[98] tried oxidation at low temperature from room temperature to 450 ℃. As the starting material they have used Cu deposited on glass and silicon via vacuum assisted thermal evaporation technique. During the oxidation in ambient air at low temperature range (250 °C – 320 °C) they reported Cu_2O phase and beginning of CuO formation with increase in temperature. The oxidation was carried out in air or dry air by Minami et.al[102]. However in the work by Ievskaya et.al[101], they introduced oxygen with 10,000 ppm flow

rate during the oxidation process. The influence of oxygen partial pressure was studied by Lahtonen et.al [100] by carrying out the thermal oxidation at pressure of 8.0 $x10^{-7}$ and 3.7$x10^{-2}$ mbar. The have reported that at low pressure regime the $(2\sqrt{2} \times \sqrt{2})R45°$-O surface reconstruction is relatively inert which is critical for the further migration of oxygen atoms deeper into Cu and formation of Cu_2O.

Post treatment of oxidized Cu_2O done by Musa et.al[104] involves quenching which helps to stop the further oxidation and cooling down in air results in folding of the samples due to compressive stress. Additionally, as can be observed in the phase diagram (Figure 1.7), further oxidation of Cu_2O for longer time leads to CuO formation hence quenching the film helps to prevent oxidizing to CuO to an extent. To heal any defects occurred during oxidation at high temperature, annealing the thermally oxidized foils have led to lowering the resistivity and converting from polycrystalline films to nearly single crystals[104]. Zang et.al[103] have also reported that after annealing the absorbance of the film improved.

Doping oxidized Cu_2O films with Na is reported to improve the electrical properties of the film thereby giving better conversion efficiency when used as an absorber[61]. The doping is achieved by covering with Na compound powder and annealing at 400-800 °C for 1.30 h in Ar/N_2 gas. An increase in hole concentration of the films upto 10^{19} cm^{-3} is observed as Na atom at intersitial site in the lattice leads to increased Cu vacancies due to charge compensation[61]. With the Na doped Cu_2O sheets as the absorber layer, efficiency higher than 5 % (upto 8.1 %) is achieved which is not yet reported for Cu_2O solar cells with absorbers prepared via other techniques[24]. This is an attractive result with high potential for further improvement of Cu_2O photovoltaic application.

1.5 REFERENCES OF CHAPTER 01

[1] N. Belyakov, 'Chapter Seventeen - Solar energy', in *Sustainable Power Generation*, N. Belyakov, Ed. Academic Press, 2019, pp. 417–438. doi: https://doi.org/10.1016/B978-0-12-817012-0.00031-1.

[2] British Petroleum Company, *BP Statistical Review of World Energy 2021*, 70th ed. British Petroleum Co, 2021.

[3] N. Espinosa, M. Hösel, D. Angmo, and F. C. Krebs, 'Solar cells with one-day energy payback for the factories of the future', *Energy Environ. Sci.*, vol. 5, no. 1, pp. 5117–5132, 2012, doi: 10.1039/C1EE02728J.

[4] F. Ise and P. P. GmbH, 'Photovoltaics Report', p. 52.

[5] M. A. Green, E. D. Dunlop, J. Hohl-Ebinger, M. Yoshita, N. Kopidakis, and X. Hao, 'Solar cell efficiency tables (Version 58)', *Progress in Photovoltaics: Research and Applications*, vol. 29, no. 7, pp. 657–667, 2021, doi: https://doi.org/10.1002/pip.3444.

[6] W. Shockley and H. J. Queisser, 'Detailed Balance Limit of Efficiency of p-n Junction Solar Cells', *Journal of Applied Physics*, vol. 32, no. 3, pp. 510–519, 1961, doi: 10.1063/1.1736034.

[7] G. Sun, 'Intersubband approach to silicon based lasers—circumventing the indirect bandgap limitation', *Adv. Opt. Photon.*, vol. 3, no. 1, pp. 53–87, Mar. 2011, doi: 10.1364/AOP.3.000053.

[8] K. L. Chopra, P. D. Paulson, and V. Dutta, 'Thin-film solar cells: an overview', *Progress in Photovoltaics: Research and Applications*, vol. 12, no. 2–3, pp. 69–92, 2004, doi: https://doi.org/10.1002/pip.541.

[9] A. E. Rakhshani, 'Preparation, characteristics and photovoltaic properties of cuprous oxide—a review', *Solid-State Electronics*, vol. 29, no. 1, pp. 7–17, 1986, doi: https://doi.org/10.1016/0038-1101(86)90191-7.

[10] A. Pérez-Tomás, A. Mingorance, D. Tanenbaum, and M. Lira-Cantú, 'Metal Oxides in Photovoltaics: All-Oxide, Ferroic, and Perovskite Solar Cells', in *The Future of Semiconductor Oxides in Next-Generation Solar Cells*, Elsevier, 2018, pp. 267–356. doi: 10.1016/B978-0-12-811165-9.00008-9.

[11] A. Y. Anderson *et al.*, 'Quantum Efficiency and Bandgap Analysis for Combinatorial Photovoltaics: Sorting Activity of Cu–O Compounds in All-Oxide Device Libraries', *ACS Comb. Sci.*, vol. 16, no. 2, pp. 53–65, Feb. 2014, doi: 10.1021/co3001583.

[12] R. Bhardwaj, R. Barman, and D. Kaur, 'Improved photovoltaic effect in CuO/Zn1−xMgxO heterojunction solar cell by pulsed laser deposition', *Materials Letters*, vol. 185, pp. 230–234, 2016, doi: https://doi.org/10.1016/j.matlet.2016.08.092.

[13] J. Morasch, H. F. Wardenga, W. Jaegermann, and A. Klein, 'Influence of grain boundaries and interfaces on the electronic structure of polycrystalline CuO thin films', *physica status solidi (a)*, vol. 213, no. 6, pp. 1615–1624, 2016, doi: https://doi.org/10.1002/pssa.201533018.

[14] S. Ahmmed, A. Aktar, S. Tabassum, M. H. Rahman, M. F. Rahman, and A. B. M. Ismail, 'CuO based solar cell with V2O5 BSF layer: Theoretical validation of experimental data', *Superlattices and Microstructures*, vol. 151, p. 106830, 2021, doi: https://doi.org/10.1016/j.spmi.2021.106830.

[15] A. Kaphle, E. Echeverria, D. N. Mcllroy, and P. Hari, 'Enhancement in the performance of nanostructured CuO–ZnO solar cells by band alignment', *RSC Adv.*, vol. 10, no. 13, pp. 7839–7854, 2020, doi: 10.1039/C9RA10771A.

[16] A. Bhaumik, A. Haque, P. Karnati, M. F. N. Taufique, R. Patel, and K. Ghosh, 'Copper oxide based nanostructures for improved solar cell efficiency', *Thin Solid Films*, vol. 572, pp. 126–133, 2014, doi: https://doi.org/10.1016/j.tsf.2014.09.056.
[17] T. Dimopoulos, 'All-Oxide Solar Cells', in *The Future of Semiconductor Oxides in Next-Generation Solar Cells*, Elsevier, 2018, pp. 439–480. doi: 10.1016/B978-0-12-811165-9.00011-9.
[18] S. Rühle *et al.*, 'All-Oxide Photovoltaics', *J. Phys. Chem. Lett.*, vol. 3, no. 24, pp. 3755–3764, Dec. 2012, doi: 10.1021/jz3017039.
[19] B. Kupfer *et al.*, 'Thin Film Co3O4/TiO2 Heterojunction Solar Cells', *Advanced Energy Materials*, vol. 5, no. 1, p. 1401007, 2015, doi: https://doi.org/10.1002/aenm.201401007.
[20] L. M. Droessler, H. E. Assender, and A. A. R. Watt, 'Thermally deposited lead oxides for thin film photovoltaics', *Materials Letters*, vol. 71, pp. 51–53, 2012, doi: https://doi.org/10.1016/j.matlet.2011.12.027.
[21] J. E. Spanier *et al.*, 'Power conversion efficiency exceeding the Shockley–Queisser limit in a ferroelectric insulator', *Nature Photonics*, vol. 10, no. 9, pp. 611–616, Sep. 2016, doi: 10.1038/nphoton.2016.143.
[22] R. Nechache *et al.*, 'Bandgap tuning of multiferroic oxide solar cells', *Nature Photonics*, vol. 9, no. 1, pp. 61–67, Jan. 2015, doi: 10.1038/nphoton.2014.255.
[23] M. Coll *et al.*, 'Towards Oxide Electronics: a Roadmap', *Applied Surface Science*, vol. 482, pp. 1–93, Jul. 2019, doi: 10.1016/j.apsusc.2019.03.312.
[24] T. Minami, Y. Nishi, and T. Miyata, 'Efficiency enhancement using a $Zn_{1-x}Ge_x$-O thin film as an n-type window layer in Cu_2O-based heterojunction solar cells', *Appl. Phys. Express*, vol. 9, no. 5, p. 052301, May 2016, doi: 10.7567/APEX.9.052301.
[25] T. Minami, Y. Nishi, and T. Miyata, 'Heterojunction solar cell with 6% efficiency based on an n-type aluminum–gallium–oxide thin film and p-type sodium-doped Cu2O sheet', *Applied Physics Express*, vol. 8, no. 2, p. 022301, Jan. 2015, doi: 10.7567/apex.8.022301.
[26] T. Minami, Y. Nishi, and T. Miyata, 'High-Efficiency Cu_2O-Based Heterojunction Solar Cells Fabricated Using a Ga_2O_3 Thin Film as N-Type Layer', *Appl. Phys. Express*, vol. 6, no. 4, p. 044101, Apr. 2013, doi: 10.7567/APEX.6.044101.
[27] T. Minami, Y. Nishi, T. Miyata, and J. Nomoto, 'High-Efficiency Oxide Solar Cells with ZnO/Cu_2O Heterojunction Fabricated on Thermally Oxidized Cu_2O Sheets', *Appl. Phys. Express*, vol. 4, no. 6, p. 062301, May 2011, doi: 10.1143/APEX.4.062301.
[28] S. W. Lee *et al.*, 'Improved Cu2O-Based Solar Cells Using Atomic Layer Deposition to Control the Cu Oxidation State at the p-n Junction', *Advanced Energy Materials*, vol. 4, no. 11, p. 1301916, 2014, doi: https://doi.org/10.1002/aenm.201301916.
[29] Y. S. Lee *et al.*, 'Atomic Layer Deposited Gallium Oxide Buffer Layer Enables 1.2 V Open-Circuit Voltage in Cuprous Oxide Solar Cells', *Advanced Materials*, vol. 26, no. 27, pp. 4704–4710, 2014, doi: https://doi.org/10.1002/adma.201401054.
[30] O. Ergen, A. Gibb, O. Vazquez-Mena, W. R. Regan, and A. Zettl, 'Metal insulator semiconductor solar cell devices based on a Cu2O substrate utilizing h-BN as an insulating and passivating layer', *Applied Physics Letters*, vol. 106, no. 10, p. 103904, 2015, doi: 10.1063/1.4914181.
[31] C. M. McShane and K.-S. Choi, 'Junction studies on electrochemically fabricated p–n Cu2O homojunction solar cells for efficiency enhancement', *Phys. Chem. Chem. Phys.*, vol. 14, no. 17, pp. 6112–6118, 2012, doi: 10.1039/C2CP40502D.
[32] R. Nechache *et al.*, 'Photovoltaic properties of Bi2FeCrO6 epitaxial thin films', *Applied Physics Letters*, vol. 98, no. 20, p. 202902, 2011, doi: 10.1063/1.3590270.
[33] B. Lange, A. St John, and others, 'Photoelements and their Application', 1938.

[34] US Geological Survey, ‘Mineral Commodity Summaries 2022’, Reston,VA, 2022.
[35] C. Wadia, A. P. Alivisatos, and D. M. Kammen, ‘Materials Availability Expands the Opportunity for Large-Scale Photovoltaics Deployment’, *Environ. Sci. Technol.*, vol. 43, no. 6, pp. 2072–2077, Mar. 2009, doi: 10.1021/es8019534.
[36] B. K. Meyer *et al.*, ‘Binary copper oxide semiconductors: From materials towards devices’, *physica status solidi (b)*, vol. 249, no. 8, pp. 1487–1509, 2012, doi: https://doi.org/10.1002/pssb.201248128.
[37] C. Gattinoni and A. Michaelides, ‘Atomistic details of oxide surfaces and surface oxidation: the example of copper and its oxides’, *Surface Science Reports*, vol. 70, no. 3, pp. 424–447, 2015, doi: https://doi.org/10.1016/j.surfrep.2015.07.001.
[38] R. Wick and S. D. Tilley, ‘Photovoltaic and Photoelectrochemical Solar Energy Conversion with Cu2O’, *J. Phys. Chem. C*, vol. 119, no. 47, pp. 26243–26257, Nov. 2015, doi: 10.1021/acs.jpcc.5b08397.
[39] D. O. Scanlon, B. J. Morgan, G. W. Watson, and A. Walsh, ‘Acceptor Levels in p-Type $\mathrmCu_2\mathbfO$: Rationalizing Theory and Experiment’, *Phys. Rev. Lett.*, vol. 103, no. 9, p. 096405, Aug. 2009, doi: 10.1103/PhysRevLett.103.096405.
[40] A. Soon, X.-Y. Cui, B. Delley, S.-H. Wei, and C. Stampfl, ‘Native defect-induced multifarious magnetism in nonstoichiometric cuprous oxide: First-principles study of bulk and surface properties of $\textCu_2\ensuremath-\ensuremath\delta\textO$’, *Phys. Rev. B*, vol. 79, no. 3, p. 035205, Jan. 2009, doi: 10.1103/PhysRevB.79.035205.
[41] M. Nolan and S. D. Elliott, ‘The p-type conduction mechanism in Cu2O: a first principles study’, *Phys. Chem. Chem. Phys.*, vol. 8, no. 45, pp. 5350–5358, 2006, doi: 10.1039/B611969G.
[42] L. Y. Isseroff and E. A. Carter, ‘Electronic Structure of Pure and Doped Cuprous Oxide with Copper Vacancies: Suppression of Trap States’, *Chem. Mater.*, vol. 25, no. 3, pp. 253–265, Feb. 2013, doi: 10.1021/cm3040278.
[43] G. K. Paul, Y. Nawa, H. Sato, T. Sakurai, and K. Akimoto, ‘Defects in Cu2O studied by deep level transient spectroscopy’, *Appl. Phys. Lett.*, vol. 88, no. 14, p. 141901, Apr. 2006, doi: 10.1063/1.2175492.
[44] W. H. Brattain, ‘The Copper Oxide Rectifier’, *Rev. Mod. Phys.*, vol. 23, no. 3, pp. 203–212, Jul. 1951, doi: 10.1103/RevModPhys.23.203.
[45] Y. Nishi, T. Miyata, and T. Minami, ‘The impact of heterojunction formation temperature on obtainable conversion efficiency in n-ZnO/p-Cu2O solar cells’, *Thin Solid Films*, vol. 528, pp. 72–76, 2013, doi: https://doi.org/10.1016/j.tsf.2012.09.090.
[46] A. Paracchino, J. C. Brauer, J.-E. Moser, E. Thimsen, and M. Graetzel, ‘Synthesis and Characterization of High-Photoactivity Electrodeposited Cu2O Solar Absorber by Photoelectrochemistry and Ultrafast Spectroscopy’, *J. Phys. Chem. C*, vol. 116, no. 13, pp. 7341–7350, Apr. 2012, doi: 10.1021/jp301176y.
[47] K. P. Musselman, A. Marin, L. Schmidt-Mende, and J. L. MacManus-Driscoll, ‘Incompatible Length Scales in Nanostructured Cu2O Solar Cells’, *Advanced Functional Materials*, vol. 22, no. 10, pp. 2202–2208, 2012, doi: https://doi.org/10.1002/adfm.201102263.
[48] M. F. Jawad, R. A. Ismail, and K. Z. Yahea, ‘Preparation of nanocrystalline Cu2O thin film by pulsed laser deposition’, *J Mater Sci: Mater Electron*, vol. 22, no. 9, pp. 1244–1247, Sep. 2011, doi: 10.1007/s10854-011-0294-0.
[49] K. Han and M. Tao, ‘Electrochemically deposited p–n homojunction cuprous oxide solar cells’, *Solar Energy Materials and Solar Cells*, vol. 93, no. 1, pp. 153–157, 2009, doi: https://doi.org/10.1016/j.solmat.2008.09.023.

[50] Z. Xi *et al.*, 'Study on the effect of annealing on the electrical properties of n-type cuprous oxide', *Thin Solid Films*, vol. 520, no. 7, pp. 2708–2710, 2012, doi: https://doi.org/10.1016/j.tsf.2011.11.044.
[51] C. Zhu and M. J. Panzer, 'Synthesis of Zn:Cu2O Thin Films Using a Single Step Electrodeposition for Photovoltaic Applications', *ACS Appl. Mater. Interfaces*, vol. 7, no. 10, pp. 5624–5628, Mar. 2015, doi: 10.1021/acsami.5b00643.
[52] M. Xu, X. Liu, W. Xu, H. Xu, X. Hao, and X. Feng, 'Low resistivity phase-pure n-type Cu2O films realized via post-deposition nitrogen plasma treatment', *Journal of Alloys and Compounds*, vol. 769, pp. 484–489, Nov. 2018, doi: 10.1016/j.jallcom.2018.08.048.
[53] D. O. Scanlon and G. W. Watson, 'Undoped n-Type Cu2O: Fact or Fiction?', *J. Phys. Chem. Lett.*, vol. 1, no. 17, pp. 2582–2585, Sep. 2010, doi: 10.1021/jz100962n.
[54] A. Dubois-Salomon, *Chimie de l'etat solide*, Paris:Ed.Masson. Paris, 1978.
[55] P. De Jongh, D. Vanmaekelbergh, and J. Kelly, 'Cu2O: electrodeposition and characterization', *Chemistry of materials*, vol. 11, no. 12, pp. 3512–3517, 1999.
[56] J. Han *et al.*, 'Mechanistic investigation on tuning the conductivity type of cuprous oxide (Cu2O) thin films via deposition potential', *International Journal of Hydrogen Energy*, vol. 43, no. 30, pp. 13764–13777, Jul. 2018, doi: 10.1016/j.ijhydene.2018.02.121.
[57] S. Dolai, S. Das, S. Hussain, R. Bhar, and A. K. Pal, 'Cuprous oxide (Cu2O) thin films prepared by reactive d.c. sputtering technique', *Vacuum*, vol. 141, pp. 296–306, Jul. 2017, doi: 10.1016/j.vacuum.2017.04.033.
[58] N. H. Ke, P. T. K. Loan, D. A. Tuan, H. T. Dat, C. V. Tran, and L. V. T. Hung, 'The characteristics of IGZO/ZnO/Cu2O:Na thin film solar cells fabricated by DC magnetron sputtering method', *Journal of Photochemistry and Photobiology A: Chemistry*, vol. 349, pp. 100–107, Dec. 2017, doi: 10.1016/j.jphotochem.2017.09.016.
[59] A. S. Reddy, S. Uthanna, and P. S. Reddy, 'Properties of dc magnetron sputtered Cu2O films prepared at different sputtering pressures', *Applied Surface Science*, vol. 253, no. 12, pp. 5287–5292, Apr. 2007, doi: 10.1016/j.apsusc.2006.11.051.
[60] L. Zhang, L. McMillon, and J. McNatt, 'Gas-dependent bandgap and electrical conductivity of Cu2O thin films', *Solar Energy Materials and Solar Cells*, vol. 108, pp. 230–234, Jan. 2013, doi: 10.1016/j.solmat.2012.05.010.
[61] T. Minami, Y. Nishi, and T. Miyata, 'Impact of incorporating sodium into polycrystalline p-type Cu2O for heterojunction solar cell applications', *Applied Physics Letters*, vol. 105, no. 21, p. 212104, 2014, doi: 10.1063/1.4902879.
[62] C. G. Morales-Guio, S. D. Tilley, H. Vrubel, M. Grätzel, and X. Hu, 'Hydrogen evolution from a copper(I) oxide photocathode coated with an amorphous molybdenum sulphide catalyst', *Nature Communications*, vol. 5, no. 1, p. 3059, Jan. 2014, doi: 10.1038/ncomms4059.
[63] Z. Zang, 'Efficiency enhancement of ZnO/Cu2O solar cells with well oriented and micrometer grain sized Cu2O films', *Applied Physics Letters*, vol. 112, no. 4, p. 042106, 2018, doi: 10.1063/1.5017002.
[64] G. Wisz, P. Sawicka-Chudy, R. Yavorskyi, P. Potera, M. Bester, and Ł. Głowa, 'TiO2/Cu2O heterojunctions for photovoltaic cells application produced by reactive magnetron sputtering', *Materials Today: Proceedings*, vol. 35, pp. 552–557, 2021, doi: https://doi.org/10.1016/j.matpr.2019.10.054.
[65] M. H. Tran, J. Y. Cho, S. Sinha, M. G. Gang, and J. Heo, 'Cu2O/ZnO heterojunction thin-film solar cells: the effect of electrodeposition condition and thickness of Cu2O', *Thin Solid Films*, vol. 661, pp. 132–136, 2018, doi: https://doi.org/10.1016/j.tsf.2018.07.023.

[66] Y. Tolstova, S. T. Omelchenko, R. E. Blackwell, A. M. Shing, and H. A. Atwater, 'Polycrystalline Cu2O photovoltaic devices incorporating Zn(O,S) window layers', *Solar Energy Materials and Solar Cells*, vol. 160, pp. 340–345, 2017, doi: https://doi.org/10.1016/j.solmat.2016.10.049.
[67] T. Miyata, H. Tokunaga, K. Watanabe, N. Ikenaga, and T. Minami, 'Photovoltaic properties of low-damage magnetron-sputtered n-type ZnO thin film/p-type Cu2O sheet heterojunction solar cells', *Thin Solid Films*, vol. 697, p. 137825, Mar. 2020, doi: 10.1016/j.tsf.2020.137825.
[68] A. Kumar Rana, D.-K. Ban, M. Patel, J.-H. Yun, and J. Kim, 'A transparent photovoltaic device based on Cu2O/ZnO/AZO for see-through applications', *Materials Letters*, vol. 255, p. 126517, Nov. 2019, doi: 10.1016/j.matlet.2019.126517.
[69] K. Wang *et al.*, 'Heteroepitaxial growth of Cu2O films on Nb-SrTiO3 substrates and their photovoltaic properties', *Ceramics International*, vol. 43, no. 18, pp. 16232–16237, Dec. 2017, doi: 10.1016/j.ceramint.2017.08.205.
[70] Chen Aiping, Hua Long, Xiangcheng Li, Yuhua Li, Guang Yang*, Peixiang Lu, 'Controlled growth and characteristics of single-phase Cu2O and CuO films by pulsed laser deposition', *Vaccum*, vol. 83, pp. 927–930, 2009, doi: 10.1016/j.vacuum.2008.10.003.
[71] M. A. Ahmed, 'Study of Structural and Optical Properties of Cu2OThin Film Prepared by Rapid Thermal Annealing Using Nd-YAG Laser', *nq*, vol. 18, no. 2, pp. 15–22, Feb. 2020, doi: 10.14704/nq.2020.18.2.NQ20119.
[72] S. F. U. Farhad, D. Cherns, J. A. Smith, N. A. Fox, and D. J. Fermín, 'Pulsed laser deposition of single phase n- and p-type Cu2O thin films with low resistivity', *Materials & Design*, vol. 193, p. 108848, Aug. 2020, doi: 10.1016/j.matdes.2020.108848.
[73] S. H. Wee, P.-S. Huang, J.-K. Lee, and A. Goyal, 'Heteroepitaxial Cu2O thin film solar cell on metallic substrates', *Sci Rep*, vol. 5, no. 1, p. 16272, Dec. 2015, doi: 10.1038/srep16272.
[74] M. Pustan, C. Birleanu, V. Merie, L. Zarbo, S. Garabagiu, and D. Marconi, 'Effect of deposition oxygen pressure on the properties of cuprous oxide thin films', *IOP Conf. Ser.: Mater. Sci. Eng.*, vol. 724, no. 1, p. 012052, Jan. 2020, doi: 10.1088/1757-899X/724/1/012052.
[75] X. Liu, M. Xu, X. Zhang, W. Wang, X. Feng, and A. Song, 'Pulsed-laser-deposited, single-crystalline Cu2O films with low resistivity achieved through manipulating the oxygen pressure', *Applied Surface Science*, vol. 435, pp. 305–311, Mar. 2018, doi: 10.1016/j.apsusc.2017.11.119.
[76] G. Kaur, A. Mitra, and K. L. Yadav, 'Influence of oxygen pressure on the growth and physical properties of pulsed laser deposited Cu2O thin films', *J Mater Sci: Mater Electron*, vol. 26, no. 12, pp. 9689–9699, Dec. 2015, doi: 10.1007/s10854-015-3636-5.
[77] S. B. Ogale, P. G. Bilurkar, N. Mate, S. M. Kanetkar, N. Parikh, and B. Patnaik, 'Deposition of copper oxide thin films on different substrates by pulsed excimer laser ablation', *Journal of Applied Physics*, vol. 72, no. 8, pp. 3765–3769, Oct. 1992, doi: 10.1063/1.352271.
[78] X. Liu, M. Xu, X. Zhang, W. Wang, X. Feng, and A. Song, 'Pulsed-laser-deposited, single-crystalline Cu2O films with low resistivity achieved through manipulating the oxygen pressure', *Applied Surface Science*, vol. 435, pp. 305–311, Mar. 2018, doi: 10.1016/j.apsusc.2017.11.119.

[79] M. F. Jawad, R. A. Ismail, and K. Z. Yahea, ‘Preparation of nanocrystalline Cu2O thin film by pulsed laser deposition’, *J Mater Sci: Mater Electron*, vol. 22, no. 9, pp. 1244–1247, Sep. 2011, doi: 10.1007/s10854-011-0294-0.

[80] A. Subramaniyan *et al.*, ‘Non-equilibrium deposition of phase pure Cu2O thin films at reduced growth temperature’, *APL Materials*, vol. 2, no. 2, p. 022105, 2014, doi: 10.1063/1.4865457.

[81] S. F. U. Farhad, R. F. Webster, and D. Cherns, ‘Electron microscopy and diffraction studies of pulsed laser deposited cuprous oxide thin films grown at low substrate temperatures’, *Materialia*, vol. 3, pp. 230–238, Nov. 2018, doi: 10.1016/j.mtla.2018.08.032.

[82] K. Matsuzaki, K. Nomura, H. Yanagi, T. Kamiya, M. Hirano, and H. Hosono, ‘Effects of post-annealing on (110) Cu $_2$ O epitaxial films and origin of low mobility in Cu $_2$ O thin-film transistor: Effects of post-annealing on (110) Cu $_2$ O epitaxial films’, *phys. stat. sol. (a)*, vol. 206, no. 9, pp. 2192–2197, Sep. 2009, doi: 10.1002/pssa.200881795.

[83] Y. S. Lee, M. T. Winkler, S. C. Siah, R. Brandt, and T. Buonassisi, ‘Hall mobility of cuprous oxide thin films deposited by reactive direct-current magnetron sputtering’, *Appl. Phys. Lett.*, vol. 98, no. 19, p. 192115, May 2011, doi: 10.1063/1.3589810.

[84] I. J. T. Jensen *et al.*, ‘Interface phenomena in magnetron sputtered Cu $_2$ O/ZnO heterostructures’, *J. Phys.: Condens. Matter*, vol. 29, no. 43, p. 435002, Nov. 2017, doi: 10.1088/1361-648X/aa8799.

[85] H. Zhu, J. Zhang, C. Li, F. Pan, T. Wang, and B. Huang, ‘Cu2O thin films deposited by reactive direct current magnetron sputtering’, *Thin Solid Films*, vol. 517, no. 19, pp. 5700–5704, Aug. 2009, doi: 10.1016/j.tsf.2009.02.127.

[86] Y. Wang, P. Miska, D. Pilloud, D. Horwat, F. Mücklich, and J. F. Pierson, ‘Transmittance enhancement and optical band gap widening of Cu $_2$ O thin films after air annealing’, *Journal of Applied Physics*, vol. 115, no. 7, p. 073505, Feb. 2014, doi: 10.1063/1.4865957.

[87] A. H. Shukor, H. A. Alhattab, and I. Takano, ‘Electrical and optical properties of copper oxide thin films prepared by DC magnetron sputtering’, *Journal of Vacuum Science & Technology B*, vol. 38, no. 1, p. 012803, Jan. 2020, doi: 10.1116/1.5131518.

[88] Y. Takiguchi, Y. Takei, K. Nakada, and S. Miyajima, ‘Fabrication and characterization of sputtered Cu $_2$ O:N/c-Si heterojunction diode’, *Appl. Phys. Lett.*, vol. 111, no. 9, p. 093501, Aug. 2017, doi: 10.1063/1.4986084.

[89] Ø. Nordseth *et al.*, ‘Characterization of Cuprous Oxide Thin Films for Application in Solar Cells’, *DF*, vol. 22, pp. 65–73, May 2019, doi: 10.4028/www.scientific.net/DF.22.65.

[90] S. Ishizuka and K. Akimoto, ‘Control of the growth orientation and electrical properties of polycrystalline Cu2O thin films by group-IV elements doping’, *Appl. Phys. Lett.*, vol. 85, no. 21, pp. 4920–4922, Nov. 2004, doi: 10.1063/1.1827352.

[91] P. Sawicka-Chudy *et al.*, ‘Optical and structural properties of Cu 2 O thin film as active layer in solar cells prepared by DC reactive magnetron sputtering’, *Archives of Metallurgy and Materials*, vol. 64, pp. 243–250, Jan. 2019, doi: 10.24425/amm.2019.126244.

[92] D. S. Murali, S. Kumar, R. J. Choudhary, A. D. Wadikar, M. K. Jain, and A. Subrahmanyam, ‘Synthesis of Cu $_2$ O from CuO thin films: Optical and electrical properties’, *AIP Advances*, vol. 5, no. 4, p. 047143, Apr. 2015, doi: 10.1063/1.4919323.

[93] C. C. Tseng, J. H. Hsieh, S. J. Liu, and W. Wu, 'Effects of Ag contents and deposition temperatures on the electrical and optical behaviors of Ag-doped Cu2O thin films', *Thin Solid Films*, vol. 518, no. 5, pp. 1407–1410, Dec. 2009, doi: 10.1016/j.tsf.2009.09.116.
[94] R. Kumar, K. Bergum, H. N. Riise, E. Monakhov, A. Galeckas, and B. G. Svensson, 'Impact of post annealing and hydrogen implantation on functional properties of Cu2O thin films for photovoltaic applications', *Journal of Alloys and Compounds*, vol. 825, p. 153982, Jun. 2020, doi: 10.1016/j.jallcom.2020.153982.
[95] M. Nyborg, 'Nitrogen Doping of Sputtered Cuprous Oxide Thin Films by Ion Implantation', Master Thesis, University of Oslo, 2017.
[96] N. Tabuchi and H. Matsumura, 'Control of Carrier Concentration in Thin Cuprous Oxide Cu2O Films by Atomic Hydrogen', *Japanese Journal of Applied Physics*, vol. 41, no. Part 1, No. 8, pp. 5060–5063, Aug. 2002, doi: 10.1143/jjap.41.5060.
[97] S. Ishizuka *et al.*, 'Passivation of defects in polycrystalline Cu2O thin films by hydrogen or cyanide treatment', *Applied Surface Science*, vol. 216, no. 1, pp. 94–97, 2003, doi: https://doi.org/10.1016/S0169-4332(03)00485-9.
[98] S. Choudhary *et al.*, 'Oxidation mechanism of thin Cu films: A gateway towards the formation of single oxide phase', *AIP Advances*, vol. 8, no. 5, p. 055114, May 2018, doi: 10.1063/1.5028407.
[99] P. A. Korzhavyi and B. Johansson, 'Literature review on the properties of cuprous oxide Cu2O and the process of copper oxidation', p. 41.
[100] K. Lahtonen, M. Hirsimäki, M. Lampimäki, and M. Valden, 'Oxygen adsorption-induced nanostructures and island formation on Cu{100}: Bridging the gap between the formation of surface confined oxygen chemisorption layer and oxide formation', *J. Chem. Phys.*, vol. 129, no. 12, p. 124703, Sep. 2008, doi: 10.1063/1.2980347.
[101] Y. Ievskaya, R. L. Z. Hoye, A. Sadhanala, K. P. Musselman, and J. L. MacManus-Driscoll, 'Improved Heterojunction Quality in Cu_2O-based Solar Cells Through the Optimization of Atmospheric Pressure Spatial Atomic Layer Deposited $Zn_{1-x}Mg_xO$', *JoVE*, no. 113, p. 53501, Jul. 2016, doi: 10.3791/53501.
[102] T. Minami, H. Tanaka, T. Shimakawa, T. Miyata, and H. Sato, 'High-Efficiency Oxide Heterojunction Solar Cells Using Cu $_2$ O Sheets', *Jpn. J. Appl. Phys.*, vol. 43, no. No. 7A, pp. L917–L919, Jun. 2004, doi: 10.1143/JJAP.43.L917.
[103] Z. Zang, 'Efficiency enhancement of ZnO/Cu $_2$ O solar cells with well oriented and micrometer grain sized Cu $_2$ O films', *Appl. Phys. Lett.*, vol. 112, no. 4, p. 042106, Jan. 2018, doi: 10.1063/1.5017002.
[104] A. O. Musa, T. Akomolafe, and M. J. Carter, 'Production of cuprous oxide, a solar cell material, by thermal oxidation and a study of its physical and electrical properties', *Solar Energy Materials and Solar Cells*, p. 12, 1998.

2. CHAPTER : PULSED LASER DEPOSITION OF Cu_2O THIN FILMS

2.1 INTRODUCTION

This chapter aims to describe the growth of pure Cu_2O films via Pulsed Laser Deposition (PLD). Pulsed Laser Deposition is a popular and promising technique for the deposition of high-quality thin films. It is a vacuum-based physical technique. It mainly involves two steps namely plasma plume generation and expansion. The entire process happens inside a vacuum chamber. By controlling the oxygen gas flow, deposition at different oxygen partial pressures can be achieved. Several factors such as background gas partial pressure, temperature of deposition, laser fluence, deposition time and target-substrate distance, influence the structural, electrical, and stoichiometric properties of the PLD deposited thin films. A detailed description on the fundamental principles and process of PLD is outlined in Appendix. Using this method for the deposition of oxide films requires good control of the oxygen content as the background gas can highly influence the stoichiometry of the deposited oxide film. Due to the deposition at non-equilibrium conditions, PLD is not a much popular growth technique for Cu_2O films as obtaining phase pure films is difficult. By just varying the deposition temperature and oxygen partial pressure, and keeping all other parameters constant, the phase of the Cu_xO film is controlled in this work. A detailed analysis of the films via several characterization techniques is described in this chapter.

In the first section hereafter, the deposition parameters for PLD of the films is described. A CuO target is used as the starting material and the films are deposited at varying substrate temperatures at both high and low oxygen partial pressures. As apart from the oxygen partial pressure, the substrate temperature can also influence the background gas density around the substrate, it is also an important factor influencing the phase of the deposited films. The influence of the substrate temperature and partial pressure on the stoichiometry of the films thoroughly discussed in the second section. This section aims to better understand if a control of the film stoichiometry can be achieved by varying these two parameters. Additionally, the influence on the quality and crystallinity of the films on the deposition parameters is outlined here. To better understand the variation in the film properties, four samples representing different configuration of the PLD Cu_xO films are used.

As morphology and roughness of the film surface is an important criterion for employing the films for photovoltaic applications, it is necessary to understand the microstructural variation in the optimized Cu_2O films deposited at different conditions. This was achieved with the help of advanced microscopic techniques and the results are discussed towards the end of the structural analysis section. Additionally, for designing a good absorber material, their optical and electrical properties are of at most significance. The optical properties of the films are described in the third section of this chapter. The influence on the optical parameters such as Transmittance, Absorption coefficient, Bandgap, Photoluminescence, which are critical parameters for a photovoltaic absorber are discussed for the PLD deposited Cu_xO films of different configurations in this section. Electrical properties of the films are discussed in the fourth section and thereby choosing the most optimized deposition parameters for PLD of Cu_2O absorbers. Towards the end of this chapter, early studies on sodium (Na) ion implantation carried out on optimized PLD Cu_2O films is also discussed. This section aims to understand the change in the electrical properties of the films with the introduction of Na ions. Finally, a conclusion section is also included to summarize the findings from the optimization and characterization of PLD Cu_2O films.

The content of this chapter has been partly published as a scientific paper titled “Insights into Cu_2O Thin Film Absorber via Pulsed Laser Deposition” in the journal Ceramics International[1].

2.2 EXPERIMENTAL DETAILS OF Cu_XO DEPOSITION

The Cu_xO films were deposited in a PLD chamber at ICube using a CuO target. 5 mg of CuO powder (99.995%, Alfa Aesar) was carefully weighed and cold pressed into a pellet and later sintered at 900 °C for 1 hour with argon flow to prepare the target. The sintered target was then pasted onto a holder and dried overnight before loading into the PLD chamber. The substrate for the deposition was attached to the substrate holder using silver paste. The substrate holder is also a heater used for depositions under elevated temperatures. Most of the films in the work which were used to study the characteristics of the films were deposited on quartz substrates of (10 mm x10 mm) size, as quartz substrates are more stable at high temperatures.

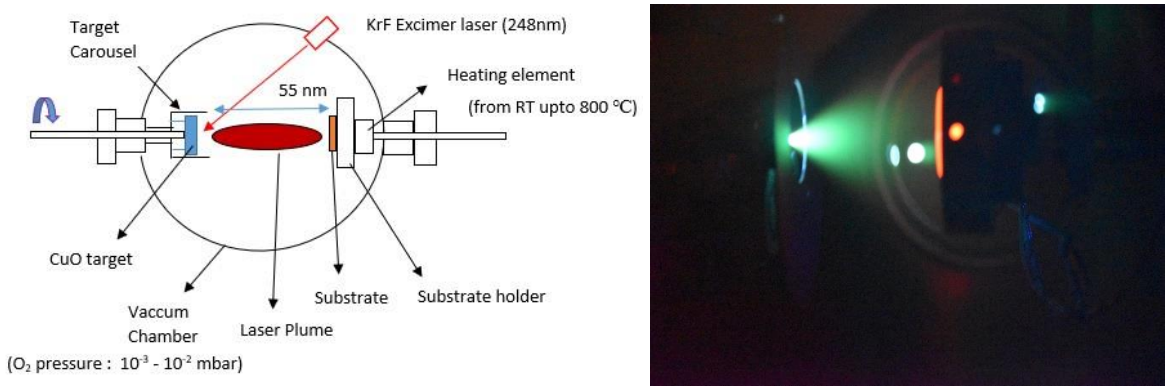

(a) (b)

Figure 2.1 (a) Schematics of the PLD setup with parameters (b) A photo of plasma plume during the PLD deposition of Cu_2O film on a heated substrate

Figure 2.1(a) outlines the schematics of the PLD setup with the parameters. The deposition was carried out using a KrF excimer laser (248 nm) at a repetition rate of 10 Hz with 1-2 J/cm^2 laser fluence on the target. The target-substrate distance was fixed at 55 mm. The plasma plume is a collection of luminous ions/molecules/atoms formed by the vaporization of the CuO target as can be seen as green colour in the photo in Figure 2.1(b). Films were prepared at a range of temperatures from room temperature up to 800 °C and oxygen partial pressures (P_{O2}) of 10^{-2} and 10^{-3} mbar for a detailed study of the film composition and properties. After the deposition, the samples were cooled down naturally under the same oxygen partial pressure used for the deposition. The films were then structurally analysed to understand their stoichiometry which is detailed in the next section.

2.3 STRUCTURAL ANALYSIS OF THE PLD Cu_xO FILMS

2.3.1 Stoichiometry and Phase Analysis

The stoichiometry of the deposited films and the thickness were analysed using Rutherford Backscattering Spectroscopy (RBS) using-1.5 MeV He^+ particles from the Van de Graaff accelerator (HVEE KN4000) facility at ICube. The samples were tilted at an angle of 45 degrees for all the measurements and a Si detector with resolution of 12 keV was used. It is a technique which can be used for the elemental analysis and thickness determination of the films. Ion beams of high energies in the range of MeV is made to incident on the film (Figure 2.2(a)), and the energy distribution and the number of the backscattered ions from the atoms is measured near the surface region, which thus allows for the determination of the atomic masses and a distribution of the target elements as a function of depth below the surface[2]. Since the spot size for RBS technique is 1 mm^2, a better understanding of the atomic composition of the films can be achieved better than any other local characterization techniques. The ions elastically scattered from the atoms with an energy characteristic to the mass of the struck atom. By detecting the energy of the backscattered ions using the detector gives a back scattering spectrum (counts per channel vs channel number) as depicted in Figure 2.2(b). The channel number is linearly proportional to the backscattered ion energy. Each peak in the spectrum corresponds to an element in the film and the width of the peak corresponds to the energy loss of the ions within the material.[2] Even though the error of this measurement depends primarily on the quality of the film, an error of 10-15% can be expected.

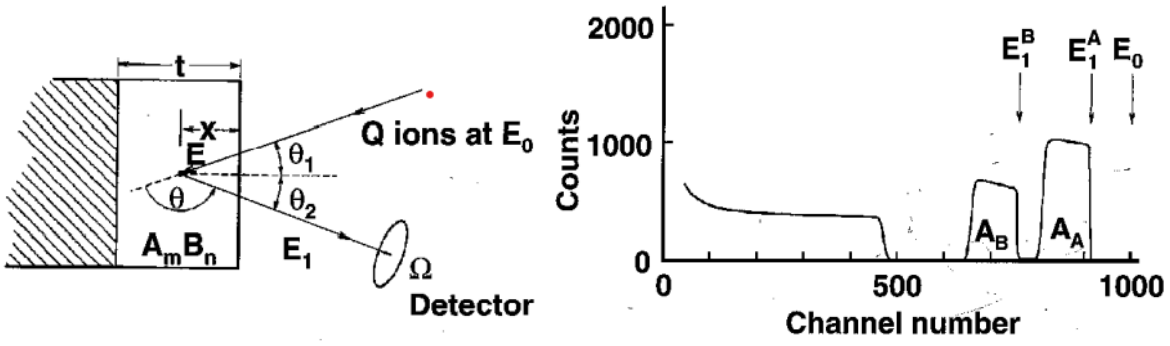

(a) (b)

Figure 2.2 (a) Basic illustration of the back scattering spectroscopy (b) RBS spectrum for a compound A_mB_n on a low mass substrate[2]

Using RBS to determine the stoichiometry of Cu_2O films is not straightforward as determination of the oxygen concentration is tricky. Figure 2.3(a) shows an RBS spectrum of a PLD deposited Cu_2O film, the experimental spectra is fitted using simulation by adjusting the simulation parameters. The height of the peak plateau gives the copper concentration, and the width gives the appropriate thickness of the film and as can be seen the oxygen peak is wide. However, since oxygen concentration is proportional to that of copper in Cu_2O, the oxygen concentration can be calculated with respect to copper. This is achieved using the simulation tool SAM[3]. Figure 2.3(b) shows the simulation parameters, wherein approximate thickness of the film in angstroms and the concentration are adjusted to obtain a fitting simulation curve. Here, two isotopes of Cu are used, hence the total concentration of copper is 0.7+0.3 and oxygen concentration is 0.5 with respect to Cu which corresponds to the stoichiometry of Cu_2O phase.

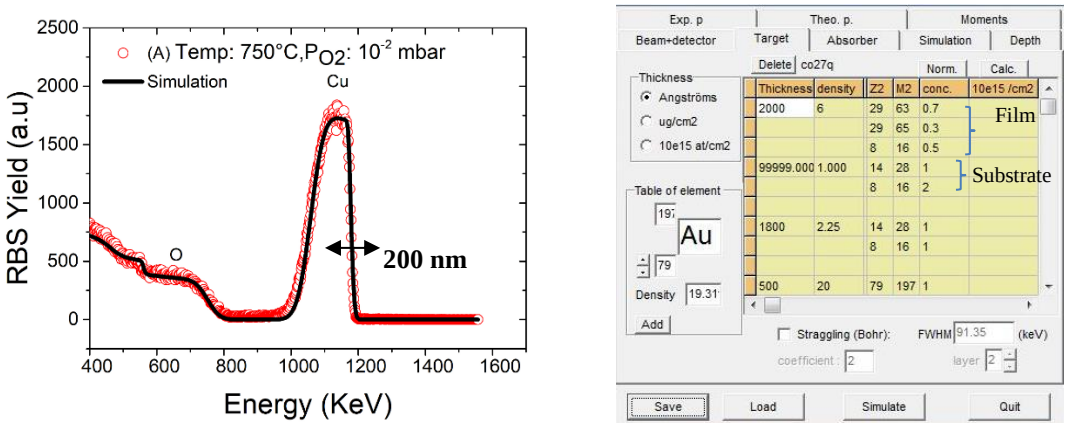

(a) (b)

Figure 2.3 (a) RBS yield vs Energy of Cu_2O film deposited at 750 °C, 10^{-2} mbar $O_{2p\text{-}p}$ on quartz (b) A screenshot from the SAM tool with the simulation parameters

Figure 2.4 shows the variation of the oxygen concentration with respect to copper in Cu_xO films deposited at two different partial pressures of oxygen by varying the deposition temperature. The variation in the stoichiometry of the film is very sensitive to the deposition parameters and only in a limited deposition window phase pure Cu_2O films were obtained without any trace of CuO similar to the findings of Wee et.al[4]. As can be seen in Figure 2.4, varying the oxygen partial pressure keeping the temperature constant, resulted in a stoichiometry variation. The Cu_2O stoichiometry was achieved at two conditions. At a higher oxygen partial pressure of 10^{-2} mbar and a higher temperature of 750 °C (sample A in Figure 2.4) the oxygen to copper ratio was 0.5 which corresponds to Cu_2O phase. Similar deposition condition was repeated thrice to

check the reproducibility and two of them coincided. The deviation of the third sample to ratio of 0.75 could be due to the difference in the sample preparation time which can lead to change in the pumping system and laser alignment. Additionally, a sample deposited at vacuum and later annealed in the PLD chamber at 750 °C and 10^{-2} mbar were found to be stoichiometrically identical. However, at 750 °C temperature with lower P_{O2}, the oxygen to copper ratio corresponds to CuO phase. The reason for this change could be due to the reduction of background gas resistance at elevated substrate temperatures which changes the background gas density within the chamber thus influencing the precursors in the gas phase apart from the thermal effect on the surface kinetics as explained by Sambri et.al[5]. The RBS spectrum of both the films can be seen in Figure 2.5(a). The film at lower P_{O2} is thinner than the one at higher P_{O2} and the oxygen concentration is higher.

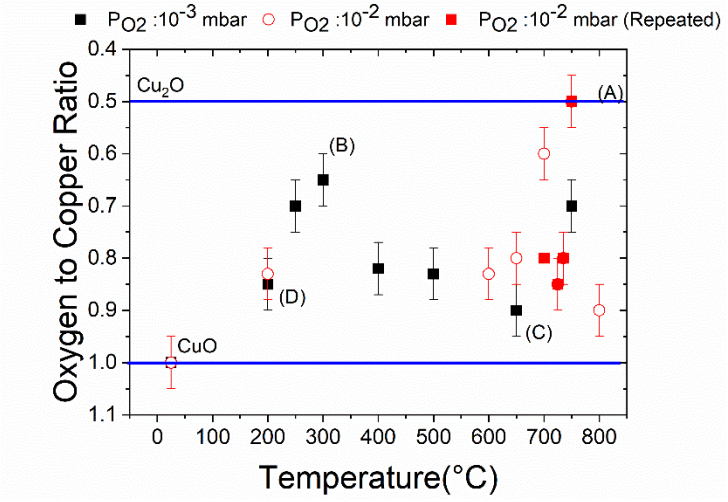

Figure 2.4 Oxygen to copper ratio in Cu_xO v.s temperature at 10^{-2} mbar and 10^{-3} mbar oxygen partial pressures (estimated from RBS measurements)

Oxygen concentration close to Cu_2O (0.65) was also observed for the sample prepared at oxygen partial pressure of 10^{-3} mbar and temperature of 300 °C (sample B in Figure 2.4). For a low temperature range of deposition (200-300 °C), lower oxygen partial pressure is favored as can be seen if the sample B and C are compared in Figure 2.4. Higher amount of oxygen results in the formation of CuO at lower temperatures. In the RBS spectrum of sample B shown in Figure 2.5 (b), the copper has diffused into the quartz substrate during deposition. Similar diffusion was observed in all the films deposited at lower temperatures, as can be seen in Figure 2.5 (c) and (d), which could be because the surface diffusion ability of the vapour atoms depends on the substrate temperature. High temperature favors quick and defect free crystalline film

growth while low temperature results in disordered or amorphous structures. As can be seen in the Figure 2.5 (c) and inset of Figure 2.5(d) the width of the Cu peak in the RBS spectrum varies for the films deposited under similar conditions apart from the temperature at both the oxygen partial pressures. This could also be because of the variation in the quality of the films such as roughness, crystallinity etc.

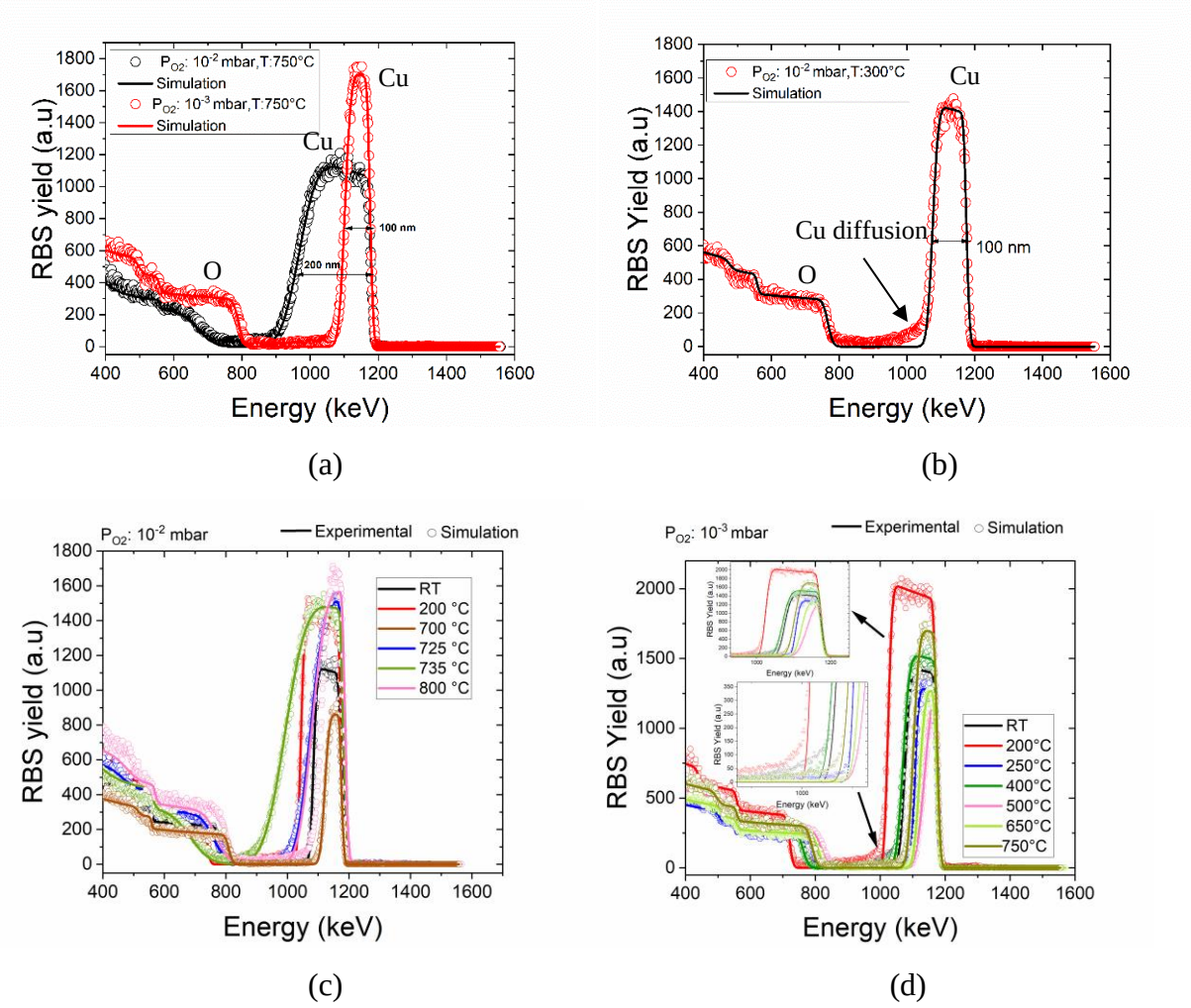

Figure 2.5 (a)RBS spectrum of Cu_xO film prepared at same temperature but different oxygen partial pressure (b) RBS spectrum of Cu_2O film deposited at 300 °C, 10^{-3} mbar P_{O2}. RBS spectrum of PLD films deposited at different temperatures and (c) P_{O2}: 10^{-2} mbar (d) P_{O2}: 10^{-3} mbar

The thickness of the films found from the RBS spectra of the films, which were deposited for similar time duration was not found to be same. The influence of temperature and oxygen partial pressure on the thickness of the films deposited is not found to follow a common trend. The thickness of the film deposited via PLD depends on several physical parameters, including

physical parameters such as fluence on the target, sticking coefficient, re-evaporation rate and surface diffusion coefficient of adatoms.[6] After a threshold temperature, the sticking coefficient decreases while re-evaporation rate increases with increase in temperature[6] Surface diffusion coefficient also increases with temperature, so it is possible that the film thickness decreases with temperature which was observed in the case of some of the films in this work. But as there is an interplay of several factors on the film formation, it is difficult to conclude about a trend in the thickness with the substrate temperature variation.

Additionally, at higher oxygen partial pressures, the film was found to be very sensitive to even 25 °C change in temperature (between 700-750 °C in Figure 2.4). This behavior was consistent when the samples were repeated, which might be due to the influence of the substrate temperature on the background gas density[5].

The Cu_xO films were also deposited at room temperature at both the oxygen partial pressures of 10^{-2} mbar and 10^{-3} mbar. Unlike reported by Farhad et.al[7], our room temperature deposited films had CuO stoichiometry as expected from the phase diagram.

In order to confirm the phase of the films determined via RBS and to study about the structural quality of the films, Raman spectroscopy studies were carried out and are discussed in the next section.

2.3.2 Raman Features of the PLD Films

Raman spectroscopy is another powerful technique to determine the phase of the film as it gives the structural fingerprint of a molecule. This spectroscopic tool helps to identify the vibrational modes in a material. When a sample is illuminated with a monochromatic light source, apart from absorption and transmission, scattering of the incident light occurs. The scattering can be Rayleigh (elastic) scattering and Raman (inelastic) scattering. Around 1% of the total scattered photons undergo inelastic scattering with lower or higher energy (frequency) than the incident photons. This energy difference corresponds to the chemical bonds within the material and the shift from the original light source is represented in wavenumber (cm^{-1}). There are two Raman scattering process depending on the frequency of the scattered photons namely Stokes ($v_s < v_i$) and Anti-Stokes ($v_s > v_i$).

As the Cu_2O unit cell contains 6 atoms, 15 optical phonon modes and 3 acoustic lattice vibrations are possible. Their symmetry at k=0 are:

$$A_{2u} \oplus E_u \oplus T_{2g} \oplus 3T_{1u} \oplus T_{2u}$$

Phonons with A, E, and T symmetry are one, two-and three-fold degenerate, respectively. The acoustic phonons have T_{1u} symmetry. The intrinsic p-type conductivity of Cu_2O which originates from V_{cu} (copper vacancies) and V_{cu}^{split} (copper split vacancies) are defects which has a characteristic site symmetry depending on their location in the unit cell of Cu_2O. Due to the non-stoichiometry of Cu_2O caused by point defects such as vacancies and interstitials, the local symmetry is reduced, and the Raman selection rules are no longer followed in the case of Cu_2O. Hence, the experimental Raman spectra of Cu_2O will have signals from infrared active, silent or defect modes irrespective of the method of synthesis[8]. However, the intensity and the number of lattice modes observed varies.

A Horiba LabRAM ARAMIS Raman spectrometer with 532 nm laser excitation was used to study the Raman footprints of the deposited films in this work. Raman spectroscopic analysis of the PLD films revealed a similar phase as from the stoichiometry analysis from RBS. RRUFF is a digitalization project which provides free access to approximately 3,500 mineral spectra[9]. The Raman spectra in this work are compared with the spectra in the RRUFF reference database using 532 nm laser excitation. Hence the peak positions are based on similar conditions in the reference and experimental spectra.

The vibrational modes of Cu_2O were observed in the film deposited at 750 °C and 10^{-2} mbar (sample A in Figure 2.4) and 300 °C and 10^{-3} mbar (sample B in Figure 2.4) as can be seen in Figure 2.6. Apart from the T_{2g} mode at around ~ 480-500 cm^{-1}, E_u mode, T_{1u} mode, second-order E_u ($2E_u$) mode, A_{2u} mode and multi phonon process (MPP) mode were observed at 109 cm^{-1}, 145 cm^{-1}, 216 cm^{-1}, and 310 cm^{-1}, 412 cm^{-1} respectively in both the films and it matches with the Cu_2O reference (RRUFF reference: R140763). The T_{1u} mode corresponds to phonons activated by defects namely copper vacancies and copper split vacancy which is the origin of p-type conductivity in Cu_2O[8] , which is observed in both the films. Additionally, the intensity ratio of peaks at 145 cm^{-1} (T_{1u}) and 216 cm^{-1}($2E_u$) is sensitive to surface damages[10]. Comparing both the Cu_2O films (A and B), film B might have more surface damages as the ratio is 0.80 while for film A is 0.43. The raman peaks found in the CuO film are corresponding to A_g mode at ~ 270-300 cm^{-1} and B_g mode at ~346-350 and ~ 630 cm^{-1} according to the RRUFF reference (R120076). Similar to the stoichiometry observed using RBS, via Raman spectroscopy it was also confirmed that some films were pure CuO (the room temperature deposited at 10^{-3} mbar in Figure 2.6 (a) and (b)) while some others were a mixture of both the phases. It was also observed that vibrational modes of CuO were absent in some of

the films which had an oxygen-copper ratio close to that of a CuO or a mixture of both the phases. This shows that RBS is a more reliable technique in the stoichiometry identification as for Raman spectroscopy the spot size is smaller. Room temperature deposited film at 10^{-2} mbar (Figure 2.6 (a)) had an additional peak at ~ 527 cm^{-1} corresponding to the vibrational mode of Cu_4O_3[11] apart from the CuO peaks. Cu_4O_3 (Paramelaconite) is another common oxide of copper intermediate between CuO and Cu_2O.

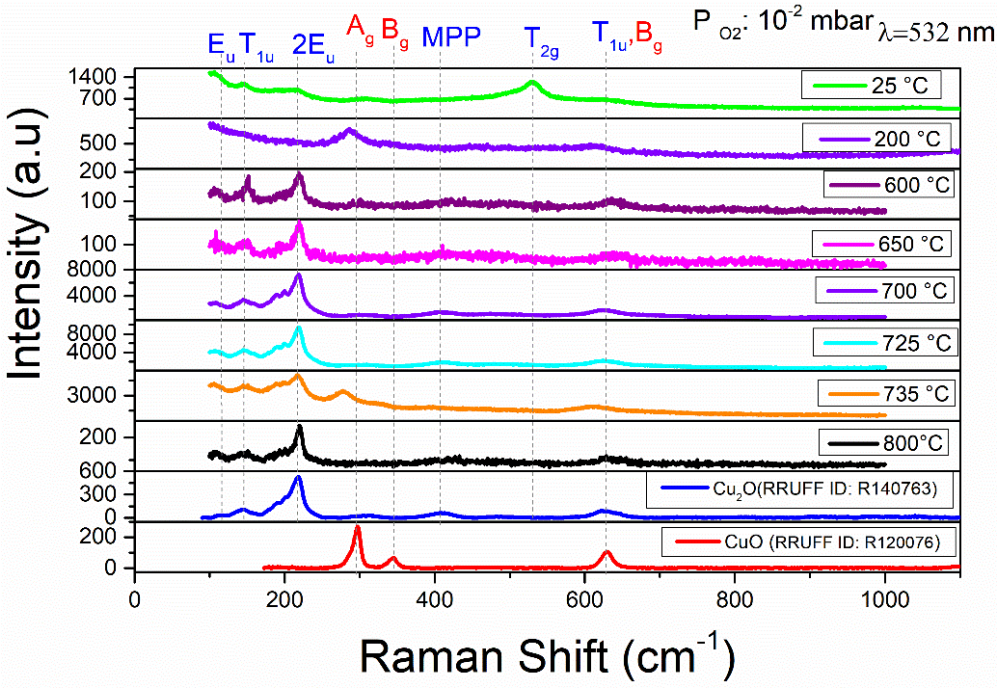

(a)

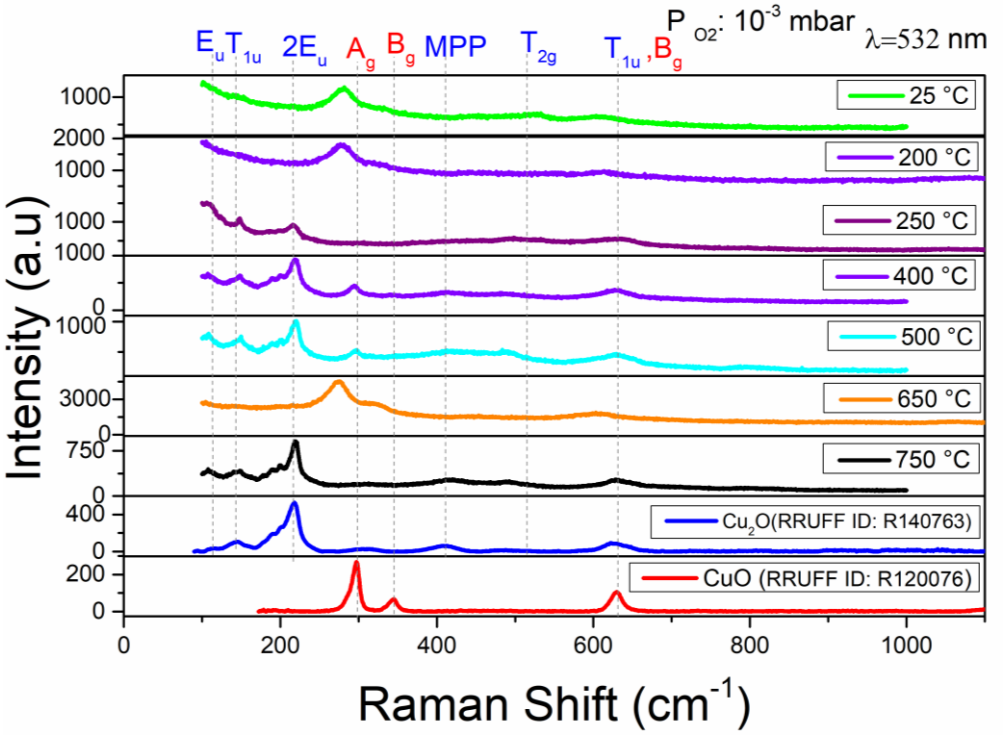

(b)

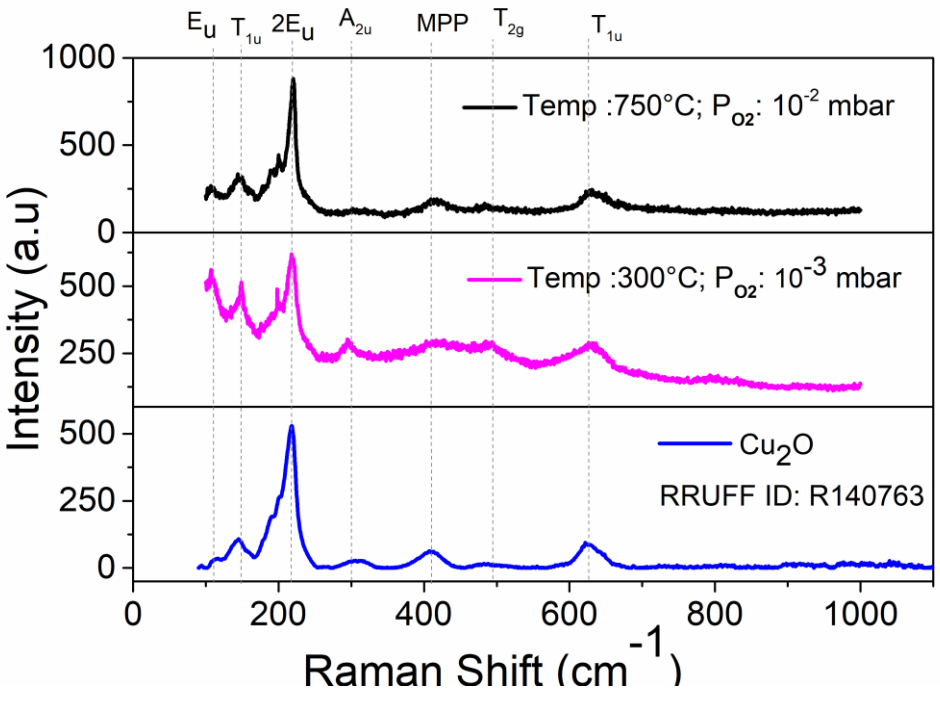

(c)

Figure 2.6 Raman spectra of the PLD deposited Cu_xO films at different temperatures and (a) P_{O2}: 10^{-2} mbar (b) P_{O2}: 10^{-3} mbar (c) Raman spectra of the PLD deposited Cu_2O films on quartz along with references from RRUFF database translated for viewing purpose

For the better performance of the thin films, crystallinity is an important criterion. The structural analysis on a larger scale was performed using X-ray diffraction technique. The shape, position and intensity of the diffraction peaks provide information about the structure of the film, defects (vacancies, dislocations), crystallite sizes, crystalline structure of phases etc.

2.3.3 Crystallinity and Lattice Parameters of the films

Crystallographic structure of the PLD deposited Cu_2O films were analysed using X-ray diffraction (XRD) studies. XRD can be used to measure the crystallinity, orientation, and spaces between the plane of atoms. Due to the comparable wavelength of X-rays and the distance between atoms in a crystal, when a crystalline sample is probed with an X-ray, diffraction patterns are produced due to interference with atomic planes. The scattered X-ray is measured and is used to analyze the crystal structure. Bragg´s law which determine the diffraction when an incoming X-ray of wavelength λ falls on a crystal at an angle θ is given by

$$n\lambda = 2.d.\sin\theta \qquad \textbf{2.1}$$

where d is the interplanar spacing and n is the order of diffraction.

Since XRD technique is very sensitive to nanometer thicknesses it is a useful characterization technique for thin films. Additionally, it can be used to analyse the dislocations, stresses, and composition in thin films.

Table 3 Experimental Details of Samples

Sample	Temperature	Oxygen Partial Pressure
A	750 °C	10^{-2} mbar
B	300 °C	10^{-3} mbar
C	650 °C	10^{-3} mbar
D	200 °C	10^{-2} mbar

X-ray diffraction studies in this work were carried out using a Rigaku Smartlab diffractometer equipped with a monochromatic source delivering a Cu $K\alpha_1$ incident beam (45 kV, 200 mA, 0.154056 nm) and Bruker-AXS D8 Advance X-ray diffractometer with $CuK\alpha_1$ radiation (λ =

0.154056 nm). The diffraction peaks of the PLD films were clearly visible only when measured at a grazing angle of 3°. For a better understanding on the influence of temperature and oxygen partial pressure for the controlled growth of Cu_2O and CuO films, the results of four samples, as they represent the various configurations of the PLD deposited Cu_xO films, are discussed in more detail. The growth conditions of the four samples are summarized in Table 3. All the films were crystallized and were polycrystalline as the grains had different orientation directions. From the XRD pattern in Figure 2.7(a) the Cu_2O film at higher temperature (film A) is better crystalline than the one at lower temperature (film B). At a higher substrate temperature the adatoms can settle down in densely packed form on the surface thus leading to better crystallinity[6]. The preferred orientation of the Cu_2O film (film A) is (2 0 0) direction while that of film B is (1 1 1) like the reference. The X-ray diffractogram of sample A and B at a grazing angle of 3° exhibit significant Cu_2O peaks for (2 0 0), (3 1 1), (2 2 0), and (1 1 1) with no secondary CuO phase, which is in good agreement with the RBS and Raman results. Film C and D however had no Cu_2O peaks as can be seen in Figure 2.7(b). The shift of (-1 1 1) peak in film C to 2θ ~ 36° could be because of strain in the film.

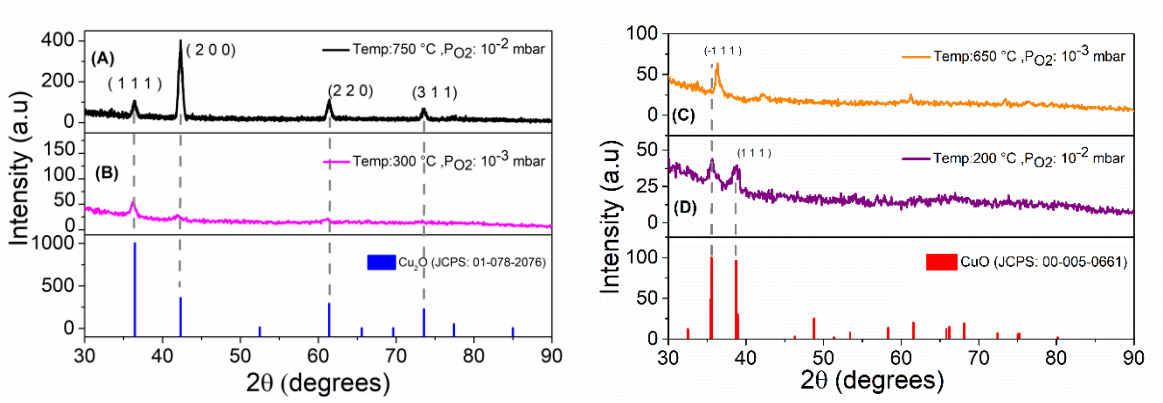

(a) (b)

Figure 2.7 Grazing angle X-ray diffraction pattern of (a) A and B (b) C and D on quartz and reference of Cu_2O and CuO from the ICCD database

Lattice parameters of the Cu_2O films were calculated from the XRD pattern and listed in Table 4. The broadening of the diffraction peaks gives the structural information of the material. The mean grain size (L) of the crystallites is given by the Scherrer equation[12]:

$$L=k\lambda / \beta \cos \theta \qquad \textbf{2.2}$$

where k is the Scherrer constant, λ is the X-ray wavelength, β is the full width half maximum (FWHM) of the intensity peak and θ is the Bragg angle. Sample A is found to have larger crystallite size (15.1±0.6 nm) than all the four samples. The grain size shows a decreasing trend with temperature comparing Sample A and Sample D (10.4 ± 0.9 nm).

Lattice constant of the films were calculated from the equation:

$$a = d_{hkl} * \sqrt{(h^2+k^2+l^2)} \quad \textbf{2.3}$$

The lattice constant of pure Cu_2O film is 4.27 Å according to JCPS:01-078-2076. Film A has a lattice constant similar to that of pure Cu_2O from the reference which is an indication of good film quality. However, film B has a deviation of approximately 0.5 % from the pure Cu_2O film could be an indication of lattice strain in the films. Additionally, the higher full width half maximum of the peaks in film B over film A could be an indication of lattice strain, point defects and/or dislocations in the material apart from the instrumental effects. The stress in the films was calculated from the measured lattice constant using the equation[14], [15]:

$$\sigma = (-E\ (a-a_0))/2\upsilon a_0 \quad \textbf{2.4}$$

Where E is the Youngs Modulous of Cu_2O (30 GPa), a is the lattice parameter of the bulk, a_0 is the measured lattice parameter of the film and υ is the poissons ratio of Cu_2O (0.45)[14], [16]. Comparing all the four films, film A has very low tensile stress of 0.01 GPa whereas film B had tensile stress of 0.22 GPa. Film C has a tensile stress of 0.07 GPa while film D have a compressive stress of 0.57 GPa. The d-spacing of the high temperature deposited Cu_2O film (film A) are expected values for the dominant peaks of pure Cu_2O film and a slight deviation was observed for the low temperature deposited film (sample B) as expected. Detailed study on all the crystalline parameters points to film A deposited at 750 °C, 10^{-2} mbar to be of better-quality.

As from all the elemental and phase analysis point to two conditions for Cu_2O films, before confirming the best deposition optimized conditions, it is necessary to study the morphology and roughness of the films, especially for its application as a photovoltaic absorber. A uniform coverage with more flat film is desirable to avoid any short circuits when employed in a photovoltaic cell.

Table 4 Lattice Parameters, Crystallites Sizes and Micro strain of Samples A and B calculated from the X-ray diffraction peaks

Sample	2θ (°)	FWHM (°)	d spacing (Å)	Grain Size (nm)	Lattice Constant (Å)
(A)	36.39	0.57	2.46	14.69	4.27
	42.31	0.59	2.13	14.48	4.27
	61.38	0.59	1.51	15.48	4.27
	73.56	0.63	1.29	15.79	4.27
(B)	36.23	0.63	2.47	13.25	4.29
	41.93	1.41	2.15	6.02	4.30
	61.01	0.91	1.52	10.18	4.29

2.3.4 Morphology and Roughness of the Cu_2O Films

To better understand the morphology of the Cu_2O films, they were analyzed using a scanning electron microscope (SEM). It allows to obtain high quality images with high resolution and magnification thus revealing the topography of the films. An electron beam is incident on the film, and the electron from the beam interacts with atoms at various depth within the material resulting in different types of electrons (primary back scattered electrons (BSE), secondary electrons (SE), Auger electrons) and photons (X-rays) emission. The secondary scattered electrons emitted from the film can be detected using a secondary electron detector to create a scanned image with varied brightness (intensity) depending on the roughness differences on the surface of the film. While the SE electrons are emitted from the top surface of the material, BSE have much high energy and they are emitted from much deeper locations within the film. Hence, BSE images have lower resolution than the SE images (order of nm´s). BSE electrons gives information on the distribution of different elements in a film (lighter elements in dark) while the elemental distribution can be mapped by detecting the energy or wavelength of the X-rays by Energy Dispersive X-ray spectroscopy (EDS) or Wavelength Dispersive X-ray spectroscopy (WDS). This is achieved by detecting the X-ray photon emitted due to the relaxation of exited

charge from the inner shell of atoms. This energy will be unique to different elements in a sample and can be hence used for their detection[17] However, since it is difficult to detect oxygen, such an analysis is not feasible in the case of Cu_2O films. The morphology of the two PLD Cu_2O films were analyzed by scanning electron microscopy performed using a Gemini 500-Zeiss apparatus.

Figure 2.8 (a) and (c) confirms that the Cu_2O film deposited at 750 °C,10^{-2} mbar on quartz is polycrystalline.Rectangular shaped grains randomly arranges with rather fewer holes is visible in the image which is preferable for photovoltaic applications. Higher grain size than the calculated values from the diffraction peaks is visible in the SEM image which could be an indication that the broadening of the diffraction peak is not just due to the influence of grain size but rather be also due to defects or stress in the material. However, for the film B deposited at 300 °C,10^{-2} mbar, the grain size is much smaller and it has a flat morphology as can be seen in Figure 2.8 (c). Similar change in the morphology of the films deposited at lower temperatures was also reported by Subramaniyan et.al[18]. In a more wider magnification, presence of holes (marked in red in Figure 2.8 (d)) and lots of splashing can be observed.Surface damages in this film B was already revealed in the Raman spectroscopy analysis in 2.3.2. Splashing arise from the accumulation of ions which can create short-circuits which is not favourable for its application in a photovoltaic cell. Apart from the influence of substrate temperature the lower oxygen partical pressure during deposition of film B is also a factor for the holes /cracks in the film. Similar observations were reported in the literature for PLD films[6]. A decrease in the stress and strain of the films deposited at higher substrate temperature calculated from the diffraction peaks in 2.3.3 is due to higher crystallite size and compactness achieved with temperature confirmed from the SEM images.

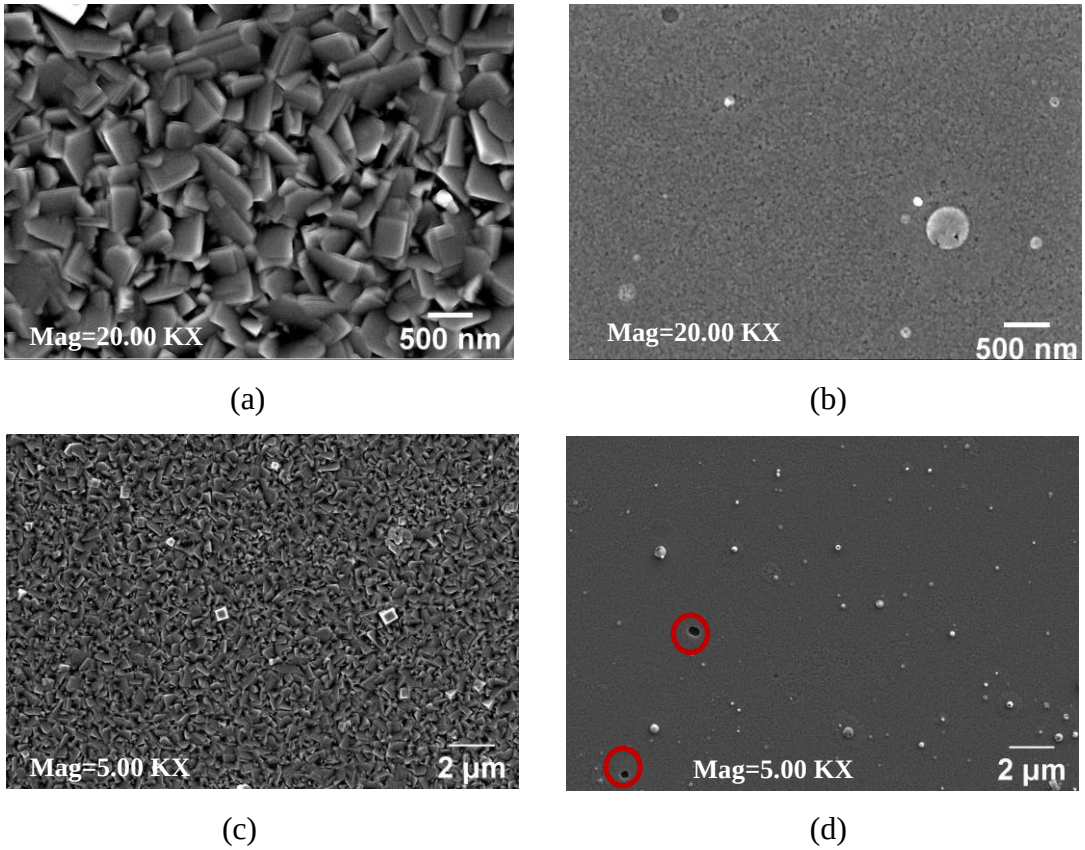

Figure 2.8 Secondary Electron images of Cu_2O films at different magnifications (a) and (c) Film A deposited at 750 °C,10^{-2} mbar on quartz (b) and (d) Film B deposited at 300 °C,10^{-3} mbar on quartz (holes in films is marked in red)

Another microscopy technique followed to determine the topography and roughness of the films was Atomic Force Microscopy (AFM). In AFM technique, a small tip attached to a cantilever which scans over the surface of the film and interacts with the atoms. It measures the force with which the tip gets deflected by the peaks and valleys due to attraction or repulsion. The deflection is measured and converted into an electric signal which helps to create a topographic graph of the surface[19]. It is a very high-resolution technique with orders of magnitude in nanometers. The roughness of the Cu_2O films (approximately 100 nm thick) was found out using a NT-MDT SMENA Atomic Force Microscope (AFM). The Cu_2O film deposited at 750 °C,10^{-2} mbar (film A) was rough with RMS roughness of 47 nm while the film B deposited at 300 °C,10^{-3} mbar was smooth with RMS roughness of 7 nm. As can be seen in the 3D AFM view of film A in Figure 2.9(a), it has larger grains with a height of 0.27 µm. Even though film B has a smooth surface, large splashing causes uneven surface as can be seen in the three dimensional view of the AFM scan in Figure 2.9 (b).

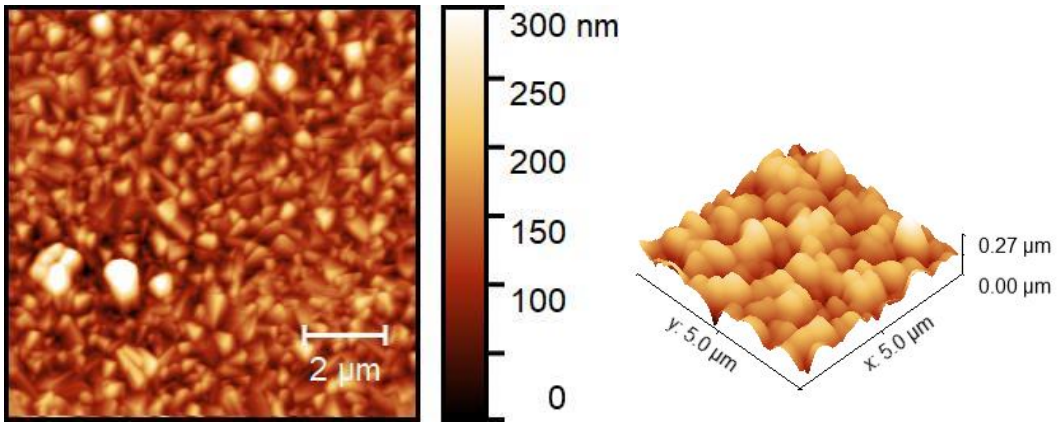

(a)

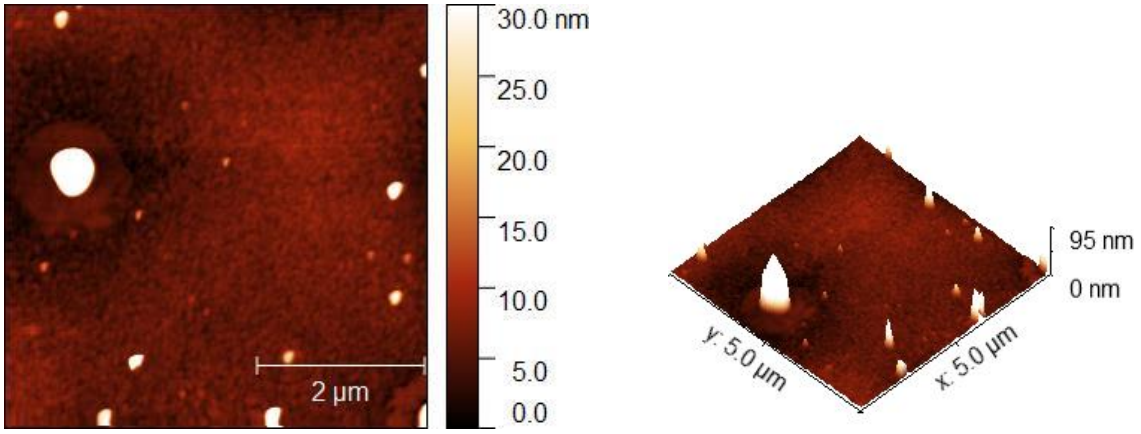

(b)

Figure 2.9 AFM image (5 µm x 5 µm) in two-dimensional and three-dimensional view of Cu_2O film (~ 100 nm thick) deposited at (a) 750 °C,10^{-2} mbar (b) 300 °C,10^{-3} mbar on quartz

2.4 OPTICAL PROPERTIES

The detailed structural analysis using different techniques revealed the elemental composition and structural quality difference of the PLD deposited films at different deposition conditions. In the following section, the optical properties of the different films such as transmittance, bandgap, absorption coefficient and photoluminescence were analysed to investigate its potential as an absorber.

2.4.1 UV-VIS Spectroscopy

The transmittance of the films was measured via UV-VIS spectroscopy using Perkin-Elmer Lambda 19 UV/Vis/NIR spectrophotometer**.** The absorbance of the films was calculated from the transmission spectra using the equation:

$$absorbance = 2 - \log(\%T) \qquad \textbf{2.5}$$

Reflectance was not taken into account for the absorbance calculations. Both the Cu_2O films had good absorbance in the visible region of the electromagnetic spectrum as can be seen in Figure 2.10 (a) and (b). Film A deposited at 750 °C and 10^{-2} mbar which was found to have better quality in the structural analysis is found to have higher absorbance (zero transmittance) between the wavelengths of 200-450 nm range and an absorption threshold between 450-630 nm. However, the Cu_2O film deposited at 300 °C and 10^{-3} mbar (Figure 2.10(b)) have a high absorbance (low transmittance) for a narrow wavelength (~200-300 nm) and then the absorbance decays exponentially, the exciton binding energy might be lower in film B compared to film A. For the films C and D similar fast decay in absorbance with wavelength in the visible region can be observed in Figure 2.10 (c) and (d).

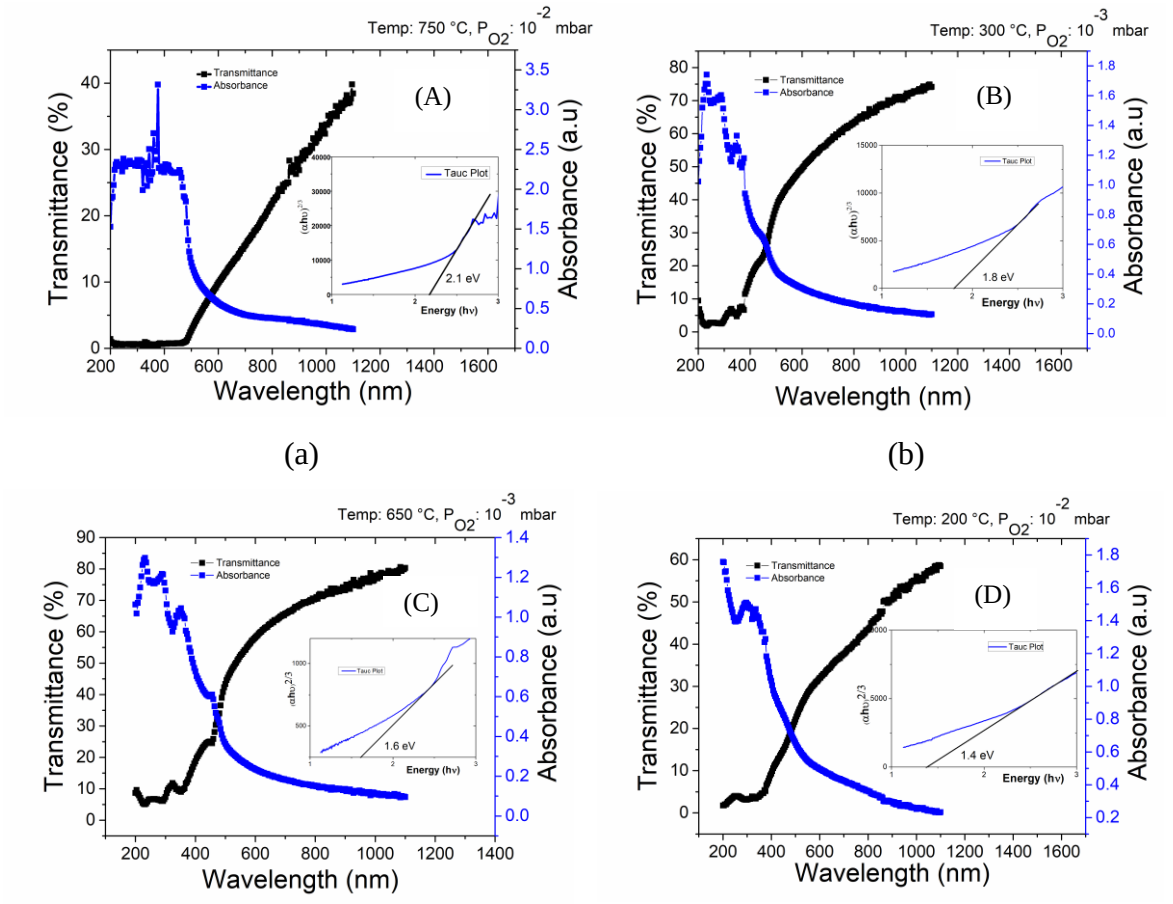

Figure 2.10 Transmittance and Absorbance spectra of the PLD deposited films at (a) 750 °C and 10^{-2} mbar (b) 300 °C and 10^{-3} mbar (c) 650 °C and 10^{-3} mbar (d) 200 °C and 10^{-2} mbar on quartz with their corresponding tauc plots in the inset

The bandgap of the films was calculated from the transmission spectrum with the help of Tauc plot ($h\upsilon$ vs $(\alpha h\upsilon)^{1/r}$) (inset of Figure 2.10). Since Cu_2O have direct forbidden transitions, the exponent r=3/2[20], [21] was used for the calculations and for the CuO films, r=2 considering they have indirect bandgap. Film A have a bandgap of 2.05±0.05 eV which corresponds to Cu_2O from literature and film B have a bandgap of 1.80±0.10 eV. The lower optical bandgap of film B compared to film A might be due to defect states in the bandgap thus reducing the effective bandgap. For CuO films, the bandgap varies from 1.2-2.6 eV depending on the preparation conditions[22]. Films C and D have a bandgap in the range of 1.4-1.5 eV which corresponds to that of oxygen rich CuO phase.

While designing an absorber, one of the important optical properties is the absorption coefficient. Absorption coefficient is a measure of the ability of a material to absorb the incident

photon of a particular wavelength. It is important to understand how far the absorbed photons travel in a film before it is absorbed so that appropriate thickness of the film can be chosen. Films with high absorption coefficient allows to have thinner absorber layers in a solar cell.

2.4.2 Absorption Coefficient from Ellipsometry

Ellipsometry analysis on the PLD films were carried out to determine the absorption coefficient of the films. It is a non-destructive technique which can be used to determine the complex refractive index of an unknown material or the thickness of a thin film. This technique is very useful if interpreted with a suitable model. A linearly polarized beam is made to incident on a sample surface at an angle Φ which gets reflected (elliptically polarized). The change in the polarization of the beam after interaction with the sample is measured.

In the plane of incidence, the incident light decomposes into two components namely s (perpendicular) and p (parallel) polarized light. The complex reflection coefficient is the ratio of these two components with amplitude Ψ and phase difference Δ. Using numerical models, a suitable fit of the theoretical and measured Ψ, Δ is obtained. The model uses Fresnel´s equations to predict the response with the chosen fit parameter of optical constants (n, k) or the layer thickness.

A Horiba Uvisel Lt M200 FGMS (210-880 nm) spectroscopic ellipsometer was used for the measurements in this work. The dispersion models used for Cu_2O and CuO are the Triple Tauc Lorentz and simple Tauc Lorentz formulas respectively[23]. The figure of merit related to χ-squared values was below 0.6 for the Cu_2O samples. As can be seen in Figure 2.11 (a), both the Cu_2O films (A and B) have a high absorption coefficient in the range of 10^6 cm^{-1} in the visible region which is a preferrable for the application as an absorber.

The peak at 560 nm corresponds to yellow exciton transition (E_{OA} edge) and 2D exciton transitions at 349 nm (E_{1A}) and at 290 nm (E_{1B}) is visible for the film A, deposited at 750 °C, 10^{-2} mbar, which is similar to that of Cu_2O in the literature[24]. The visibility of 2D exciton peaks at room temperature for the Cu_2O films is due to its high binding energy (~ 150 meV) and is a validation of the good quality of films. However, for film B (300 °C,10^{-3} mbar) apart from the 2D exciton transitions, the indigo exciton peak (E_{OD} edge) at 440 nm is visible. The indigo exciton peaks are usually not observed in good quality films as it is sensitive to surface damages. This further confirms the poor surface quality of the film B revealed in the structural characterizations. As the symmetry of the CuO crystal is low compared to Cu_2O, the spectra of

CuO does not have sharp structures as in Cu_2O. Similar behavior was observed in the films C and D (Figure 2.11(b)). The absorption coefficient peak is from E_4 transition at 315 nm which is similar to that of CuO[25].

For the application of the Cu_2O films deposited via PLD as an absorber, it is necessary to understand the absorption/emission process within the electronic energy levels when it interacts with light. Photoluminescence spectroscopy studies were conducted on the films, as it helps to identify impurity levels, defects and recombination mechanisms and also gives information on the electronic bandgap.

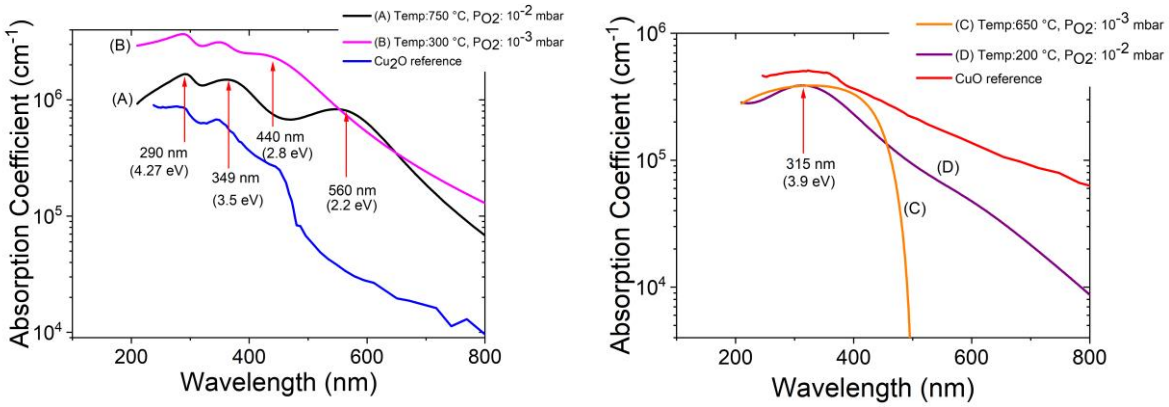

(a) (b)

Figure 2.11 Variation of absorption coefficient v.s wavelength of (a) film A and B (b) C and D deposited at different temperatures and pressures on quartz.

2.4.3 Photoluminescence

Photoluminescence (PL) spectroscopy is a contactless, non-destructive optical characterization technique widely used to study the electronic structure and defects in a material. When a material is optically excited by a light source of appropriate wavelength, the excited carriers relax to the ground state by emission of light (photon) which can be measured using a spectrometer to give information on the material quality, impurities, bandgap, recombination mechanisms and discrete energy states of a material. In this work, the Photoluminescence measurements were done in the same setup of Raman spectroscopy, a Horiba LabRAM ARAMIS Raman spectrometer using a 532 nm HeNe laser of 100 mW output at room temperature.

Photoluminescence studies were carried out on all the samples prepared at different temperatures in the two oxygen partial pressures. However, a PL signal was not observed in all of them. Additionally, among the films that gave a signal, a narrow PL peak was only observed in the Cu_2O film deposited at 750 °C, 10^{-2} mbar (film A) as shown in Figure 2.12 (a). The peak was at 1.97 eV which corresponds to the near-band edge emission. However, for film B, a wider peak at 1.97 eV and an additional PL peak at 2.13 eV was observed (Figure 2.12 (a)). It could be a defect band which needs further studies for confirmation. The other two peaks in the spectra are from the quartz substrates. PL spectra of a bare quartz substrate was measured to confirm this. A wider PL peak was observed for the films C and D as can be seen in Figure 2.12 (b). The wider PL spectrum points to poor film quality with defect states. The quartz peaks are also visible in these spectra at 682 nm and 730 nm.

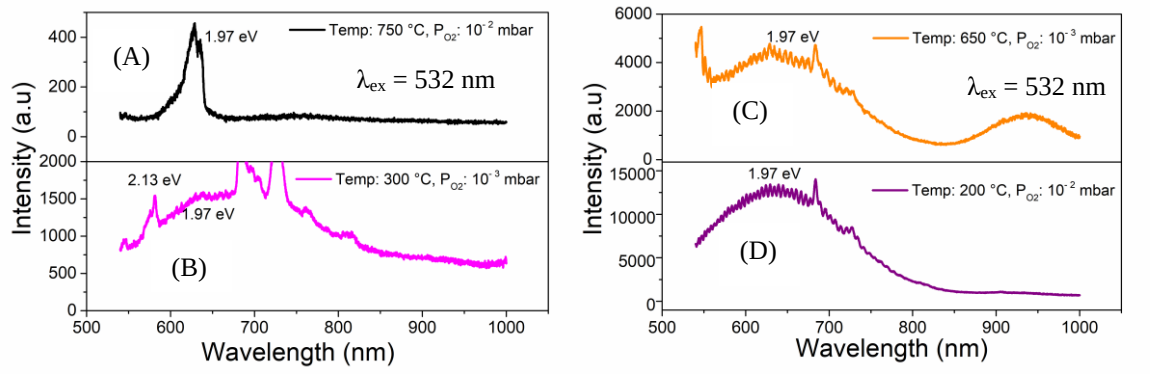

(a) (b)

Figure 2.12 Photoluminescence spectra for films (a) A (750 °C, 10^{-2} mbar) and B (300 °C, 10^{-3} mbar) (b) C (650 °C, 10^{-3} mbar) and D (200 °C, 10^{-2} mbar) at an excitation wavelength of 532 nm on quartz substrates

Another basic physical property of a material is the work function. It is important to have information on the work function of a material when designing interfaces. The work function of the Cu_2O film varies with synthesis and its determination is significant to form appropriate heterojunctions.

2.4.3.1 Work function Measurements

Kelvin Probe (KP) measurements were carried out to determine the work function of the PLD deposited Cu_2O films. Determination of work-function via Kelvin probe is not a straight-forward technique as it measures the contact potential difference between the probe and the

material. Hence, the work function of the probe needs to be calculated with a reference material (with known work function) before using it on the sample to be measured.

When the sample and the reference electrodes are electrically connected, electrons flow from metal of lower work function to larger work function and thus creating an electric potential (Figure 2.13(a)). This electric potential will be the difference in their work functions. To measure this, a counter potential is applied and the point where the equilibrium is achieved is monitored (Figure 2.13(b)). The value of counter potential where the electric transfer stops is the contact potential difference (CPD) between the reference and the sample. This is measured by vibrating the probe at a frequency ω and monitoring the AC (ω) using a lock in amplifier.

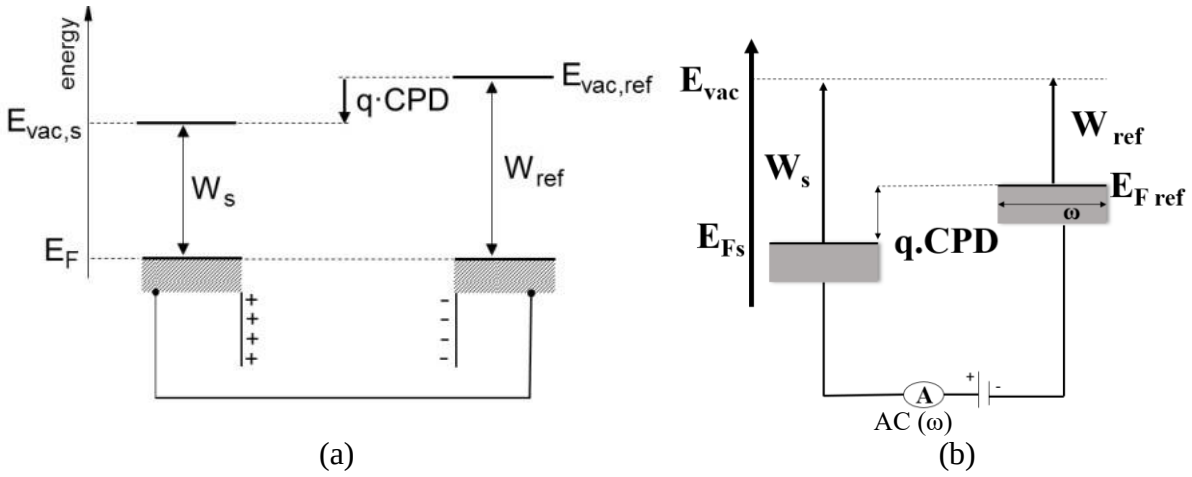

Figure 2.13 Schematics of Kelvin Probe measurement process wherein (a)reference electrode and sample are electrically connected [26] (b) Application of counter potential to measure CPD

The work function of all the samples were determined using a single point Kelvin Probe from KP Technology (KP020) with a 2 mm diameter gold tip with resolution of 1-3 meV. The work function of the films depends on several factors and synthesis routes just being one of them, hence a general trend was not observed in the values of the films. Most of the films showed work function in the range of 4.9-5.3 eV. Further, the work function of film A from Kelvin probe measurements is 4.98 eV which is similar to the literature for Cu_2O film[27], [28]. Similar value was also observed for the film deposited at 700 °C, 10^{-2} mbar. CuO film can have a work function in the wide range of 4.7-5.5 eV[29] so with the work function value it is hard to distinguish the phases.

2.5 ELECTRICAL PROPERTIES OF THE PLD DEPOSITED FILMS

Electrical properties are another crucial criterion for choosing an absorber. A high carrier concentration without compromising the mobility is very critical. This section discusses the change in the carrier properties of the PLD deposited films of different configurations studied using Hall Effect Measurement technique.

2.5.1 Hall Effect Measurement

Hall Effect measurement is a useful and widely used electrical characterization technique for thin films. It uses a 4-point probe measurement. There are two configurations possible for this type and Van der Pauw configuration is used in this work for the Hall Effect Measurements. The film is contacted using four probes on the perimeter and a current is passed through and the voltage is measured from which the sheet resistance is calculated. The resistivity of the film can be measured from the sheet resistance for a known thickness. In the hall effect measurement while the electrical current (I) is applied longitudinal direction to the sample, a perpendicular magnetic field B is applied. This causes accumulation of charge carriers on one side of the film due to the deflection due to the Lorentz force thus building a Hall voltage (V_H) which is given by:

$$V_H = \frac{I.B}{n.t.q} \qquad \textbf{2.6}$$

where t is the thickness, n is the charge carrier concentration and q is the elementary charge. Depending on the polarity of the Hall voltage, the n and p type conductors can be distinguished. The PLD deposited films were analyzed using a four-point probe measurement in Van der Pauw configuration by an Ecopia Hall effect measurement system (HMS-5000) at room temperature. Even though Hall effect measurements were carried out in all the films deposited via PLD, only few of them showed a conducting behaviour. All the conducting films showed p-type conductivity irrespective of the stoichiometry and hall concentration in the range of 10^{15} cm^{-3} (Figure 2.14 (c)), which is consistent with the Cu_2O films prepared via other techniques[30]–[32]. Among all the films, approximately 100 nm thick film A deposited at 750 °C and 10^{-2} was the least resistive and had the highest hall mobility as can be seen in Figure 2.14 (a) and (b). It showed a resistivity as low as 16 Ω·cm and high mobility of 30 $cm^2/(V{\cdot}s)$ at room temperature. Table 5 outlines a comparison of the electrical properties of the best performing PLD deposited

Cu_2O film (film A) with the Cu_2O films deposited via other popular techniques. The bulk concentration and resistivity values are comparable to the PLD deposited films in the literature.

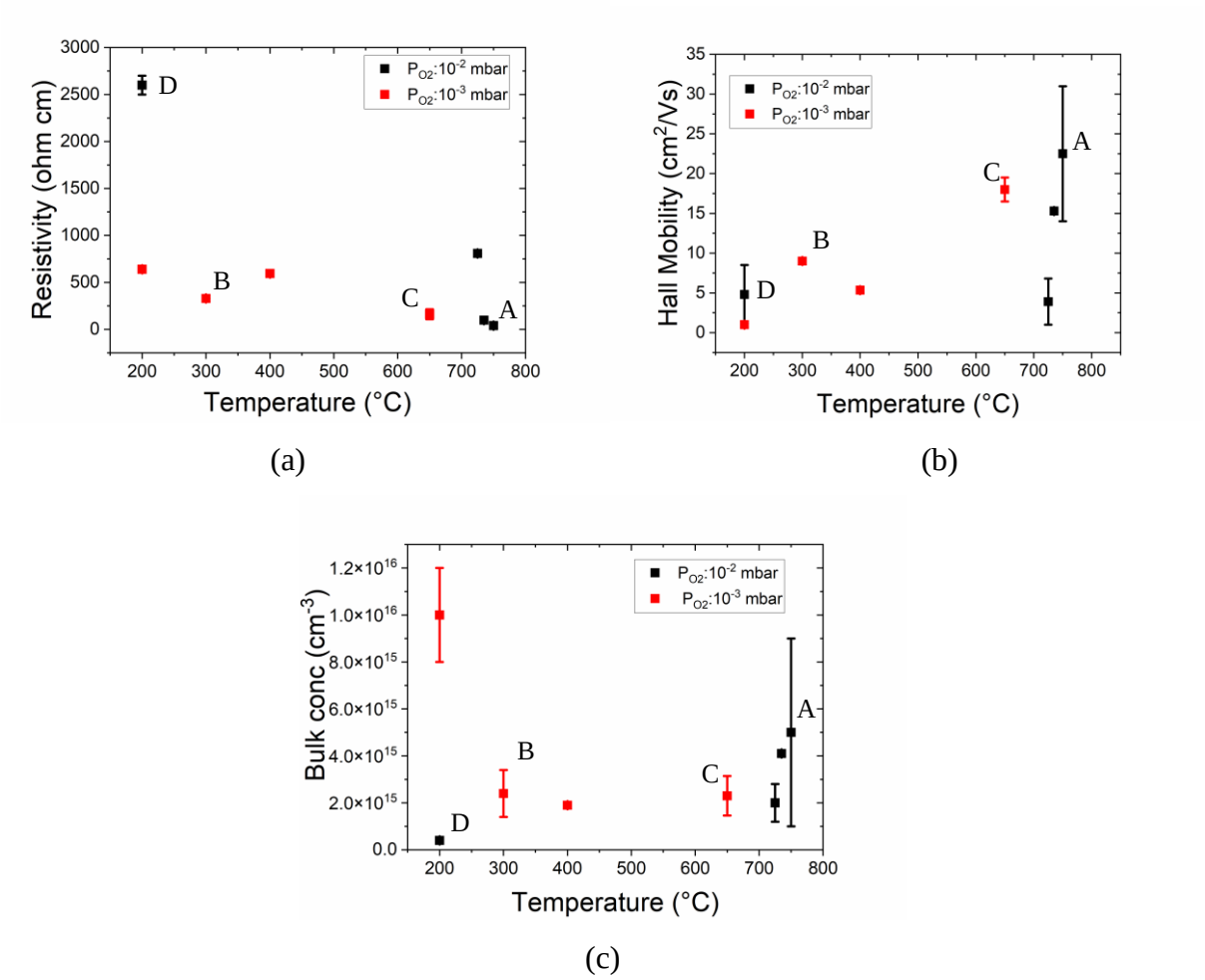

Figure 2.14 Electrical properties of the PLD deposited Cu_xO films (~100 nm thick) at two oxygen partial pressures of 10^{-2} and 10^{-3} mbar (a)Resistivity (b)Hall Mobility (c)bulk concentration as a function of substrate temperature

The film A was remeasured after 2 years (film left in ambient air) to check its stability and was found to have a resistivity of 23 Ω·cm and mobility of 27 cm^2/(V·s). This stability in the conductivity exhibited by the film A which also was the best quality film according to the structural and optical characterizations is a promising factor for its application in devices[33]. It also showed higher mobility without deteriorating the carrier concentration than most of the films via PLD reported in the literature[7], [34]. To the best of our knowledge, all the previous work which have reported high mobility without compromising the carrier concentration was on single-crystal substrates.

Film B deposited at 300 °C and10^{-3} mbar which also had shown a stoichiometry close to Cu_2O however had a rather higher resistivity and low mobility. The poor surface quality of the films revealed in the structural characterizations could be a reason for this. Film C deposited at 650 °C and 10^{-3} mbar had a comparable resistivity and mobility to that of film A. This film had a stoichiometry close to CuO in the RBS analysis.

Table 5 Electrical properties of the Cu_2O film via different techniques

Type of Preparation	Resistivity (Ω·cm)	Mobility ($cm^2/(V·s)$)	Bulk concentration (cm^{-3})	Reference
PLD	16-64	14.0-31.0	$1.0x10^{15}$– $9x10^{15}$	This work
PLD	60	26	$1x10^{13}$ – $1x10^{16}$	Wee et.al, Ogale et.al,Ran et.al[33], [35], [36]
Sputtering (RF)	$2x10^{-1}$- $4x10^{-2}$	0.08-2.23	$5.8x10^{18}$ – $2.1x10^{21}$	Zhang et.al[37]
Thermal Oxidation	$1x10^{3}$	100.00	$1.0x10^{13}$ – $1.0x10^{14}$	Minami et.al[38]
Electrodeposition	$2.7x10^{4}$-$3.3x10^{6}$	0.4-1.8	10^{12}-10^{14}	Mizuno et.al[39]
ALD	64-160	42-92	$2x10^{15}$-$7x10^{15}$	Sekkat et.al[40]

Improvement in the Cu_2O film properties by doping with different materials have been discussed in Chapter 01. Among them the most popular dopant which have shown to improve the efficiency of Cu_2O solar cells from 2-5 %[41], [42]to upto 8.1 %[43] is sodium (Na). Sodium doping on thermally oxidised Cu_2O were achieved by the group of Minami et.al by post annealing the sheets with NaCl powder. This method however does not allow for a better control on the amount of Na dopant. We have tried to use ion implantation to implant Na into optimized PLD deposited Cu_2O films. The following section outlines the results of this studies.

2.6 SODIUM IMPLANTATION ON PLD Cu_2O FILM

Even though, the most efficient solar cells with Cu_2O absorbers are Na doped[41], [43] from literature, analysis of the change in Cu_2O properties after Na doping is not yet studied in detail. In order to deeply understand the change in the Cu_2O thin film properties which in turn improves the solar cell efficiency, Na ions were introduced into best performing PLD Cu_2O thin film (deposited at 750 °C and 10^{-2} mbar) via ion implantation. Ion implantation allows introduction of a given element into a material by controlling the depth and quantity of the species introduced. Thus, ion implantation provides the advantage of controlling the dose of Na introduced into the lattice thus helping to carefully study the effect of Na. A 200 kV implanter (EATON 200 MC) was used for the implantation. It can accelerate ions up to mass 115 (In) at voltages between 1 and 180 kV. It is equipped with a scanning magnet for mass selection after a 20 kV pre-acceleration. NaCl powder was used as the ion source, which was vaporized in the furnace and separated to Na^+ and Cl^- by electromagnets. Subsequently Na+ is used as the ion beam. Six doses (number of atoms/cm^2) of Na ions were introduced into the Cu_2O films at 40 keV energy to study its impact on the properties of the films. The depth profile or the ion distribution as a function of depth for the implantation was determined using SRIM software at the various doses of Na ions and is shown in Figure 2.15. A gaussian distribution of ions is achieved at an energy of 40 keV for 100 nm film.

Several doses of Na from 1e12 to 1e16 atoms/cm^2 were implanted in 100 nm thick Cu_2O film deposited at 750 °C and 10^{-2} mbar. Rapid Thermal Annealing (RTA) of the implanted samples was found to be necessary to crystallize the sample after implantation. RTA was carried out in two temperatures namely at 600 °C and 750 °C, each for 30 seconds in argon atmosphere. As for this study, a different CuO target was used, slight variation in the electrical properties of the reference can be observed compared to the values stated before.

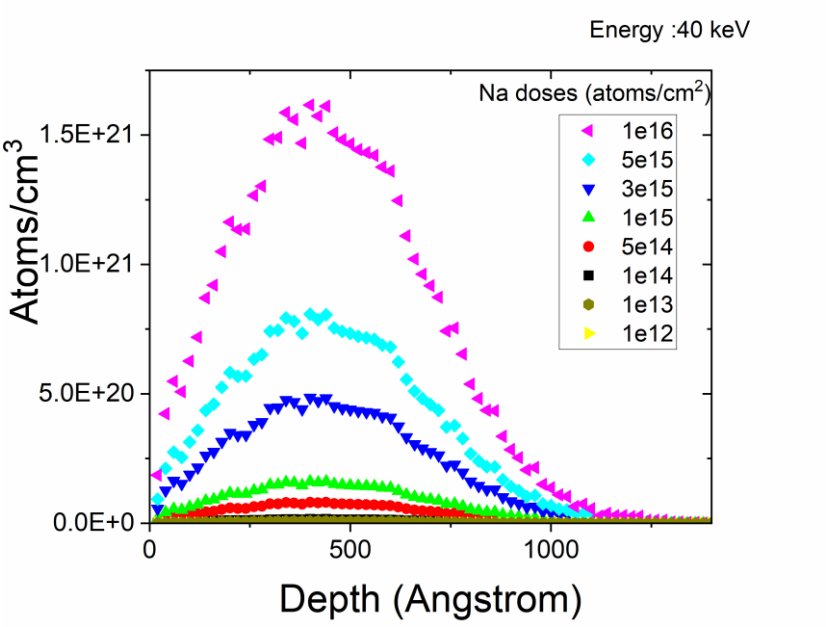

Figure 2.15 Stimulated ion distribution as a function of depth for the different doses of Na ions at 40 keV energy

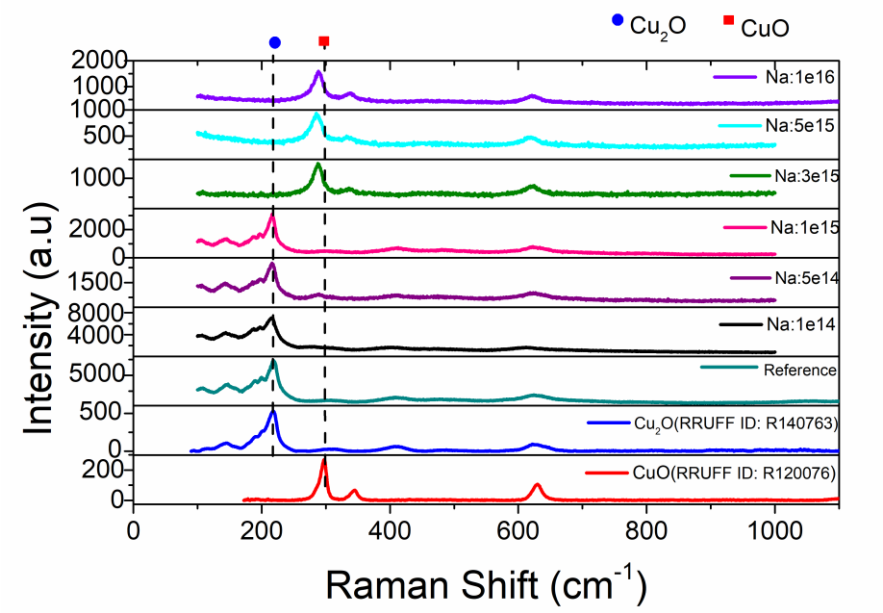

Figure 2.16 Raman spectra of the Na implanted sample after RTA at 600 °C

Raman analysis of the films after implantation revealed that implantation at higher doses of Na namely 5 e15 and 1e16 atoms/cm^2 have changed the phase of the film to CuO. Improvement in the films electrical properties was observed for lower dose of implantation (10^{14} cm^{-3}) after RTA at 600 °C. The bulk concentration of the films increased by a factor of 100 after

implantation and RTA, even though there was not much improvement in mobility (Table 6 , rows 3-5). This could be because, Na bonds with oxygen, as a substitute to Cu thus forming Na_2O, which in turn increases the Cu vacancies in the Cu_2O films. Minami et.al[45] have also observed increase in the hole concentration with Na content without much change in the mobility and have suggested that it can be attributed to the increase in copper vacancy due to incorporation of Na atom in the interstitial site. An oxygen vacancy (V_O) is self-compensated by two copper vacancies in an undoped Cu_2O. When a V_o^+ donor is associated with Na donor, a copper vacancy is released thus increasing the hole concentration.

The impact of this increase in bulk concentration for Cu_2O absorber was analyzed via simulation studies using AFORS-HET simulation software[44] and was found to improve the overall performance of the solar cell (Table 7) which in turn led to efficiency improvement from 0.96 % to 9.66 % when the acceptor concentration (N_A) increased from $1e^{+14}$ to $1e^{+19}$ cm^{-3}. Figure 2.17(a) shows the increase in current density with the acceptor concentration. Improvement in the absorption coefficient of the films was observed with Na implantation as can be seen in Figure 2.17(b). Na ions might have passivated the dangling bonds in Cu_2O which acts as point defects.

Table 6 Hall Effect Measurement of Na implanted Cu_2O thin films

Sl.No	Na dose ($atoms/cm^2$)	RTA	Bulk concentration (cm^{-3})	Mobility (cm^2/Vs)	Resistivity (Ωcm)
1	0	no	+6e+14	10.66	907
2	0	yes	+2e+15	3.70	882
3	10^{14}	yes	+5e+17	16.00	0.76
4	10^{15}	yes	+5e+17	16.00	0.76
5	10^{16}	no	+4e+19	0.16	1.65
6	10^{12}	yes	+1e+16	17.0	23.8
7	10^{13}	yes	+1e+16	16.1	39.6
8	10^{14}	yes	+1e+16	12.3	54.0
9	$5x10^{14}$	yes	+6.3e+15	8.0	170.0
10	$1x10^{15}$	yes	+6.5e+15	8.3	117.0

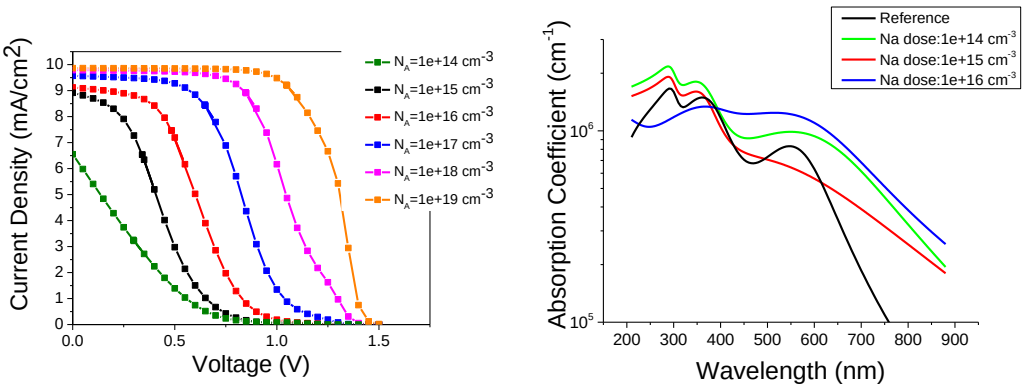

(a) (b)

Figure 2.17 (a) Variation of current density with acceptor concentration from simulation of ITO//Cu_2O/ZnO/AZO solar cell (AFORS-HET) (b)Experimental absorption coefficient of implanted Cu_2O films

Table 7. Simulated solar cell parameters of ITO//Cu_2O/ZnO/AZO at different acceptor concentrations and constant hole mobility of 23 $cm^2/V.s$

Acceptor conc. (cm^{-3})	Open circuit Voltage (V)	Short Circuit Current Density (mA/cm^2)	Fill Factor (%)	Efficiency (%)
1e+14	0.6	6.55	25	0.96
1e+15	0.7	8.91	35	2.18
1e+16	0.85	9.12	47	3.62
1e+17	1.05	9.57	54	5.47
1e+18	1.3	9.79	59	7.56
1e+19	1.4	9.87	69	9.66

Even though, promising results on the conductivity increase of the Cu_2O film by controlling the Na doses were achieved, upon repeating the same doses the result could not be reproduced. Additionally, new doses were also trialed but improvement in the bulk concentration was not observed. The results from other doses are outlined in Table 6 (rows 6-10). The films were not conducting after implantation of the doses 3e15 and 5e15 atoms/cm^2. Further to check if the initial improvement in the bulk concentration was an effect of the implantation process, oxygen

implantation at a lower dose of 1e14 atoms/cm^2 was carried out. But no improvement in the electrical properties were observed.

2.7 CONCLUSION

In this chapter, a detailed description on the optimization of Cu_2O film deposition via PLD was described. All the films deposited at varied temperatures at two oxygen partial pressures were analysed via RBS and Raman spectroscopy to find that phase pure Cu_2O films can be obtained only in a narrow window of temperature and oxygen partial pressure. Under the conditions wherein this work was carried out Cu_2O without any trace of CuO were obtained at both high temperature and low temperature by varying the oxygen partial pressures. The Cu_2O stoichiometry was obtained at 750 °C and 10^{-2} mbar as well as at 300 °C and 10^{-3} mbar. The structural properties of the films were analysed using XRD to find that the film deposited at higher temperature was of better quality. SEM and AFM further confirmed the surface quality of the film. The absorbance as well as the absorption coefficient obtained from the ellipsometry measurements were the highest for these films. Moreover, a narrow emission peak at 1.97 eV was seen in the PL measurement which matches with the Cu_2O band gap. Also, the best Cu_2O film exhibited the lowest resistivity and highest mobility without compromising on the carrier concentration. Altogether by performing several structural, optical and electrical characterization techniques, it was confirmed that the optimised PLD Cu_2O film with suitable properties of an absorber can be obtained at 750 °C and 10^{-2} mbar.

As the best performing Cu_2O based solar cells are Na doped, to study the impact of Na on the properties of Cu_2O, Na ions were implanted at varied doses on the optimized Cu_2O film to analyse the change in the film properties. Even though the first trial showed promising results with an increase in the bulk concentration of the films. The results could not be reproduced.

2.8 REFERENCES OF CHAPTER 02

[1] C. V. Kartha *et al.*, 'Insights into Cu2O thin film absorber via pulsed laser deposition', *Ceramics International*, vol. 48, no. 11, pp. 15274–15281, 2022, doi: https://doi.org/10.1016/j.ceramint.2022.02.061.

[2] J. Leavitt, L. McIntyre, M. Weller, J. Tesmer, and M. Nastasi, 'Handbook of Modern Ion Beam Materials Analysis', *Materials Research Society, Pittsburgh*, p. 37, 1995.

[3] J. P. Stoquert, F. Pêcheux, Y. Hervé, H. Marchal, R. Stuck, and P. Siffert, 'VRBS: A virtual RBS simulation tool for ion beam analysis', *Nuclear Instruments and Methods in Physics Research Section B: Beam Interactions with Materials and Atoms*, vol. 136–138, pp. 1152–1156, 1998, doi: https://doi.org/10.1016/S0168-583X(97)00807-0.

[4] S. H. Wee, P.-S. Huang, J.-K. Lee, and A. Goyal, 'Heteroepitaxial Cu2O thin film solar cell on metallic substrates', *Sci Rep*, vol. 5, no. 1, p. 16272, Dec. 2015, doi: 10.1038/srep16272.

[5] A. Sambri, M. Radovic', X. Wang, S. Amoruso, F. M. Granozio, and R. Bruzzese, 'Substrate heating effects on the propagation dynamics of laser produced plume during pulsed laser deposition of oxides', *Applied Surface Science*, vol. 254, no. 4, pp. 790–793, 2007, doi: https://doi.org/10.1016/j.apsusc.2007.07.183.

[6] S. Behera and A. Khare, 'Influence of substrate temperature and oxygen pressure on the structural and optical properties of polycrystalline BaTiO3 thin films grown by PLD', *Materials Science in Semiconductor Processing*, vol. 140, p. 106379, 2022, doi: https://doi.org/10.1016/j.mssp.2021.106379.

[7] S. F. U. Farhad, D. Cherns, J. A. Smith, N. A. Fox, and D. J. Fermín, 'Pulsed laser deposition of single phase n- and p-type Cu2O thin films with low resistivity', *Materials & Design*, vol. 193, p. 108848, Aug. 2020, doi: 10.1016/j.matdes.2020.108848.

[8] T. Sander *et al.*, 'Correlation of intrinsic point defects and the Raman modes of cuprous oxide', *Phys. Rev. B*, vol. 90, no. 4, p. 045203, Jul. 2014, doi: 10.1103/PhysRevB.90.045203.

[9] B. Lafuente, R. T. Downs, H. Yang, and N. Stone, '1. The power of databases: The RRUFF project', in *Highlights in Mineralogical Crystallography*, T. Armbruster and R. M. Danisi, Eds. Berlin, München, Boston: De Gruyter (O), 2015, pp. 1–30. doi: doi:10.1515/9783110417104-003.

[10] A. Compaan, 'Surface damage effects on allowed and forbidden phonon raman scattering in cuprous oxide', *Solid State Communications*, vol. 16, no. 3, pp. 293–296, Feb. 1975, doi: 10.1016/0038-1098(75)90171-4.

[11] L. Debbichi, M. C. Marco de Lucas, J. F. Pierson, and P. Krüger, 'Vibrational Properties of CuO and Cu4O3 from First-Principles Calculations, and Raman and Infrared Spectroscopy', *J. Phys. Chem. C*, vol. 116, no. 18, pp. 10232–10237, May 2012, doi: 10.1021/jp303096m.

[12] A. L. Patterson, 'The Scherrer Formula for X-Ray Particle Size Determination', *Phys. Rev.*, vol. 56, no. 10, pp. 978–982, Nov. 1939, doi: 10.1103/PhysRev.56.978.

[13] A. R. Stokes and A. J. C. Wilson, 'The diffraction of X rays by distorted crystal aggregates - I', *Proceedings of the Physical Society*, vol. 56, no. 3, pp. 174–181, May 1944, doi: 10.1088/0959-5309/56/3/303.

[14] A. S. Reddy, S. Uthanna, and P. S. Reddy, 'Properties of dc magnetron sputtered Cu2O films prepared at different sputtering pressures', *Applied Surface Science*, vol. 253, no. 12, pp. 5287–5292, Apr. 2007, doi: 10.1016/j.apsusc.2006.11.051.

[15] M. Ohring, ‘The Materials Science of Thin Solid films’. Academic Press,New York, 1992.
[16] J. Hallberg and R. C. Hanson, ‘The elastic constants of cuprous oxide’, *physica status solidi (b)*, vol. 42, no. 1, pp. 305–310, 1970, doi: https://doi.org/10.1002/pssb.19700420131.
[17] A. Buckley, ‘J. I. Goldstein, D. E. Newbury, P. Echlin, D. C. Joy, A. D. RomigJr, C. E. Lyman, C. Fiori & E. Lifshin 1992. Scanning Electron Microscopy and X-Ray Microanalysis. A Text for Biologists, Materials Scientists, and Geologists, 2nd ed. xviii 820 pp. New York, London: Plenum Press. Price US $49.50 (hard covers). ISBN 0 306 44175 6.’, *Geological Magazine*, vol. 130, no. 3, pp. 402–403, 1993, doi: 10.1017/S0016756800020276.
[18] A. Subramaniyan *et al.*, ‘Non-equilibrium deposition of phase pure Cu2O thin films at reduced growth temperature’, *APL Materials*, vol. 2, no. 2, p. 022105, Feb. 2014, doi: 10.1063/1.4865457.
[19] G. Binnig, C. F. Quate, and Ch. Gerber, ‘Atomic Force Microscope’, *Phys. Rev. Lett.*, vol. 56, no. 9, pp. 930–933, Mar. 1986, doi: 10.1103/PhysRevLett.56.930.
[20] V. T. Agekyan, ‘Spectroscopic properties of semiconductor crystals with direct forbidden energy gap’, *physica status solidi (a)*, vol. 43, no. 1, pp. 11–42, 1977, doi: https://doi.org/10.1002/pssa.2210430102.
[21] Y. Wang *et al.*, ‘Electronic structures of Cu2O,Cu4O3, and CuO: A joint experimental and theoretical study’, *Phys. Rev. B*, vol. 94, no. 24, p. 245418, Dec. 2016, doi: 10.1103/PhysRevB.94.245418.
[22] L. Xu, G. Zheng, S. Pei, and J. Wang, ‘Investigation of optical bandgap variation and photoluminescence behavior in nanocrystalline CuO thin films’, *Optik*, vol. 158, pp. 382–390, 2018, doi: https://doi.org/10.1016/j.ijleo.2017.12.138.
[23] G. E. Jellison and F. A. Modine, ‘Parameterization of the optical functions of amorphous materials in the interband region’, *Applied Physics Letters*, vol. 69, no. 3, pp. 371–373, 1996, doi: 10.1063/1.118064.
[24] T. Ito, T. Kawashima, H. Yamaguchi, T. Masumi, and S. Adachi, ‘Optical Properties of Cu 2O Studied by Spectroscopic Ellipsometry’, *Journal of the Physical Society of Japan*, vol. 67, no. 6, pp. 2125–2131, 1998, doi: 10.1143/JPSJ.67.2125.
[25] T. Ito, H. Yamaguchi, T. Masumi, and S. Adachi, ‘Optical Properties of CuO Studied by Spectroscopic Ellipsometry’, *Journal of the Physical Society of Japan*, vol. 67, no. 9, pp. 3304–3309, 1998, doi: 10.1143/JPSJ.67.3304.
[26] T. Dittrich and S. Fengler, *Surface Photovoltage Analysis of Photoactive Materials*. WORLD SCIENTIFIC (EUROPE), 2020. doi: 10.1142/q0227.
[27] W.-Y. Yang and S.-W. Rhee, ‘Effect of electrode material on the resistance switching of Cu2O film’, *Applied Physics Letters*, vol. 91, no. 23, p. 232907, 2007, doi: 10.1063/1.2822403.
[28] J. Deuermeier *et al.*, ‘Visualization of nanocrystalline CuO in the grain boundaries of Cu2O thin films and effect on band bending and film resistivity’, *APL Materials*, vol. 6, no. 9, p. 096103, 2018, doi: 10.1063/1.5042046.
[29] J. Morasch, H. F. Wardenga, W. Jaegermann, and A. Klein, ‘Influence of grain boundaries and interfaces on the electronic structure of polycrystalline CuO thin films’, *physica status solidi (a)*, vol. 213, no. 6, pp. 1615–1624, 2016, doi: https://doi.org/10.1002/pssa.201533018.

[30] Ø. Nordseth *et al.*, 'Characterization of Cuprous Oxide Thin Films for Application in Solar Cells', *DF*, vol. 22, pp. 65–73, May 2019, doi: 10.4028/www.scientific.net/DF.22.65.
[31] H. Rahal, R. Kihal, A. M. Affoune, and S. Rahal, 'Electrodeposition and characterization of Cu2O thin films using sodium thiosulfate as an additive for photovoltaic solar cells', *Chinese Journal of Chemical Engineering*, vol. 26, no. 2, pp. 421–427, 2018, doi: https://doi.org/10.1016/j.cjche.2017.06.023.
[32] H. Matsumura, A. Fujii, and T. Kitatani, 'Properties of High-MobilityCu2OFilms Prepared by Thermal Oxidation of Cu at Low Temperatures', *Japanese Journal of Applied Physics*, vol. 35, no. Part 1, No. 11, pp. 5631–5636, Nov. 1996, doi: 10.1143/jjap.35.5631.
[33] S. H. Wee, P.-S. Huang, J.-K. Lee, and A. Goyal, 'Heteroepitaxial Cu2O thin film solar cell on metallic substrates', *Sci Rep*, vol. 5, no. 1, p. 16272, Dec. 2015, doi: 10.1038/srep16272.
[34] X. Liu, M. Xu, X. Zhang, W. Wang, X. Feng, and A. Song, 'Pulsed-laser-deposited, single-crystalline Cu2O films with low resistivity achieved through manipulating the oxygen pressure', *Applied Surface Science*, vol. 435, pp. 305–311, Mar. 2018, doi: 10.1016/j.apsusc.2017.11.119.
[35] S. B. Ogale, P. G. Bilurkar, N. Mate, S. M. Kanetkar, N. Parikh, and B. Patnaik, 'Deposition of copper oxide thin films on different substrates by pulsed excimer laser ablation', *Journal of Applied Physics*, vol. 72, no. 8, pp. 3765–3769, Oct. 1992, doi: 10.1063/1.352271.
[36] F.-Y. Ran, H. Hiramatsu, H. Hosono, T. Kamiya, and M. Taniguti, 'Detection of dead layers and defects in polycrystalline Cu_2O thin-film transistors by x-ray reflectivity and photoresponse spectroscopy analyses', *Journal of Vacuum Science & Technology B, Nanotechnology and Microelectronics: Materials, Processing, Measurement, and Phenomena*, vol. 33, no. 5, p. 051211, Sep. 2015, doi: 10.1116/1.4929445.
[37] L. Zhang, L. McMillon, and J. McNatt, 'Gas-dependent bandgap and electrical conductivity of Cu2O thin films', *Solar Energy Materials and Solar Cells*, vol. 108, pp. 230–234, Jan. 2013, doi: 10.1016/j.solmat.2012.05.010.
[38] T. Minami, Y. Nishi, and T. Miyata, 'Impact of incorporating sodium into polycrystalline p-type Cu_2O for heterojunction solar cell applications', *Appl. Phys. Lett.*, vol. 105, no. 21, p. 212104, Nov. 2014, doi: 10.1063/1.4902879.
[39] K. Mizuno *et al.*, 'Structural and Electrical Characterizations of Electrodeposited p-Type Semiconductor Cu2O Films', *Journal of The Electrochemical Society*, vol. 152, pp. C179–C182, Mar. 2005, doi: 10.1149/1.1862478.
[40] A. Sekkat *et al.*, 'Open-air printing of Cu2O thin films with high hole mobility for semitransparent solar harvesters', *Commun Mater*, vol. 2, no. 1, p. 78, Dec. 2021, doi: 10.1038/s43246-021-00181-8.
[41] T. Minami, T. Miyata, and Y. Nishi, 'Efficiency improvement of Cu2O-based heterojunction solar cells fabricated using thermally oxidized copper sheets', *Thin Solid Films*, vol. 559, pp. 105–111, May 2014, doi: 10.1016/j.tsf.2013.11.026.
[42] T. Minami, Y. Nishi, T. Miyata, and J. Nomoto, 'High-Efficiency Oxide Solar Cells with ZnO/Cu_2O Heterojunction Fabricated on Thermally Oxidized Cu_2O Sheets', *Appl. Phys. Express*, vol. 4, no. 6, p. 062301, May 2011, doi: 10.1143/APEX.4.062301.
[43] T. Minami, Y. Nishi, and T. Miyata, 'Efficiency enhancement using a $Zn_{1-x}Ge_x$-O thin film as an n-type window layer in Cu_2O-based heterojunction solar cells', *Appl. Phys. Express*, vol. 9, no. 5, p. 052301, May 2016, doi: 10.7567/APEX.9.052301.

[44] R. Varache, C. Leendertz, M. E. Gueunier-Farret, J. Haschke, D. Muñoz, and L. Korte, ‘Investigation of selective junctions using a newly developed tunnel current model for solar cell applications’, *Solar Energy Materials and Solar Cells*, vol. 141, pp. 14–23, 2015, doi: https://doi.org/10.1016/j.solmat.2015.05.014.
[45] T. Minami, T. Miyata, and Y. Nishi, ‘Relationship between the electrical properties of the n-oxide and p-Cu 2 O layers and the photovoltaic properties of Cu 2 O-based heterojunction solar cells’, *Solar Energy Materials and Solar Cells*, vol. 147, pp. 85–93, Apr. 2016, doi: 10.1016/j.solmat.2015.11.033.

3. CHAPTER : MAGNETRON SPUTTERING OF Cu_2O THIN FILMS

3.1 INTRODUCTION

As described in chapter 1, one of the main aim of this thesis is to study the properties of Cu_2O thin films prepared via different techniques and to analyse their potential as a photovoltaic absorber. In the previous chapter Cu_2O thin film optimization via PLD has been discussed and their basic structural, optical and electrical properties were presented. Magnetron sputtering is another popular thin film deposition technique which provides a good control on the stoichiometry of the films by varying the deposition parameters. It provides high uniformity at a relatively high growth rate. Similar to other thin film deposition techniques, the film properties and stoichiometry can be controlled by varying the substrate temperature, gas flow rates, target power density, sputtering gas pressure. A detailed description of the sputtering deposition technique is given in the Appendix.

Even though magnetron sputtering is one of the popular Cu_2O growth techniques, majority of the work in literature are using DC magnetron sputtering[1]–[6]. Here, we have optimized the Cu_2O thin film deposition via RF sputtering, and the influence of the different deposition parameters on the properties of the films are analysed to find the optimized Cu_2O film with absorbing properties.

Similar to PLD, depositing phase pure Cu_2O film is challenging. In the first section of this chapter the influence of different deposition parameters on the film stoichiometry is discussed using the techniques of RBS, XRD and Raman spectroscopy. Even though, deposition temperature and sputtering pressure was varied along with sputtering power and reactive gas flow rate, since more variation between Cu_2O and CuO was observed with the variation of sputtering power and reactive gas flow rate, the results of these two parameters will be discussed in detail.

Further in the following section, the structural properties like vibrational modes, crystallographic structure, lattice parameters, morphology, and surface roughness of the Cu_2O film sputtered at optimized conditions is analysed. The potential of employing the film as a photovoltaic absorber is discussed by the detailed analysis of the optical and electrical properties of the film in the section three and four respectively. Influence of post annealing on the properties of the film is also discussed towards the end of this chapter which is followed by a conclusion on the findings from the analysis elucidated in this chapter.

3.2 CUPROUS OXIDE PHASE OPTIMIZATION

The stoichiometry of the sputtered films was determined with the help of Rutherford Backscattering Spectroscopy (RBS) and further, the best deposition parameters for Cu_2O film was confirmed by identifying the Raman peak´s signatures and the X-ray Diffraction spectra. Similar to the characterization of PLD films discussed in Chapter 2, RBS measurements were done using -1.5 MeV He^+ beam from the Van de Graaff accelerator (HVEE KN4000). The films were tilted at an angle of 45 degrees for all the measurements. The oxygen to copper ratio was calculated from the RBS spectra with the help of simulation tool SAM[7]. For optimizing the deposition parameters for Cu_2O phase, one parameter each was varied keeping the rest of the parameters constant.

For the deposition of Cu_2O films via magnetron sputtering, commercially brought high purity (99.99+ %) Cu target of diameter 50 mm from Goodfellow was used. The deposition parameters were optimized by varying the deposition temperature, sputtering power, sputtering pressure and gas flow rate. After depositing at different temperatures, the best substrate temperature was chosen which had a closest phase to that of Cu_2O. Table 8 lists the deposition parameters. All the films used for the analysis of their properties were sputtered for a duration of 20 min. The thickness was measured using a Dektak 150 model Profilometer by creating a step on a Si substrate during the deposition.

Table 8 Parameters during Sputtering Deposition of the Cu_xO thin films

Sputtering Target	Pure Copper Target
Substrate	Quartz (15 mm x15 mm)
Target-Substrate Distance	25 cm
Sputtering Pressure	3.4 mTorr
Substrate Temperature	300 ℃

A Horiba LabRAM ARAMIS Raman spectrometer with 532 nm laser excitation was used for Raman spectroscopy and a Rigaku Smartlab diffractometer equipped with a monochromatic source delivering a Cu $K\alpha_1$ incident beam (45 kV, 200 mA, 0.154056 nm) was used for the XRD measurements.

3.2.1 Variation of Sputter Power

Depositions at different sputtering powers from 30 W to 70W were carried out keeping the following parameters constant, temperature: 300 ℃, sputtering pressure: 3.4 mTorr, Ar/O_2: 8/1 sccm. Since RBS measurements can have an error upto 5-10 % depending on the quality of the films, an error of 5 % was considered for all the films. As can be seen in Figure 3.1 (a) (marked in red), the films deposited between sputtering powers of 50-55 W and the film at 65 W had an oxygen-copper ratio close to Cu_2O. At lower sputtering powers, the amount of Cu ions removed from the target will be less resulting in higher oxygen concentration in the films with respect to copper.

Raman spectroscopy analysis were performed on the films which had an O_2/Cu close to Cu_2O stoichiometry, to confirm their phase (Figure 3.1 (b)) and the film deposited at 65 W had a characteristic CuO Raman peak, additionally the film had poor adhesion to the substrate. Among the films deposited between 51-55 W, film at 51 W with oxygen to copper ratio of 0.5 from RBS was found to be a mixture of both the phases. However, the film deposited at 53 W showed vibrational modes of Cu_2O, which also showed an oxygen to copper ratio of 0.54. The simulation parameters fitted well with the experimental RBS spectrum of this film (Figure 3.1(d)(A)) and there was no visible diffusion into substrate, which is the evidence of their good quality. To analyse the crystallinity of the films, the X-ray diffraction analysis were carried out on the films deposited at 51-55 W. As can be seen in the grazing angle (3°) XRD pattern in Figure 3.1(c), even though all the films showed good crystallization, the film deposited at 53 W was better crystallized (lower FWHM) with an orientation in (2 0 0) direction. It also exhibited significant Cu_2O peaks for (1 1 1), (2 2 0) and (3 1 1). Confirming the Raman, the film deposited at 51 W was a mixture of both the phases. Hence, as the power increases the phase of the film changes from a mixture of Cu_2O and CuO (due to insufficient Cu atoms) to Cu_2O phase only. Cu_2O phase without any parasitic phase was obtained only for a narrow sputtering power range between 52 W - 55 W. Further increase in the power leads to pure CuO phase. Similar control on the stoichiometry of the films by controlling the sputtering power was also reported by Shukor et.al using DC sputtering[5]. Ooi et.al[8] have observed this behaviour in RF magnetron sputtered films, wherein they obtained a mixed phase film due to the copper and oxygen concentration variation inside the chamber at lower sputtering pressures. Ogwu et.al[9], [10] have shown that further increase in the sputtering power above a threshold, will increase the energy and flux ratio of the species in the particle flux, changing the film stoichiometry from

Cu_2O to CuO. As the formation kinetics of CuO is slower than Cu_2O, and the dissociation of oxygen to oxygen ions and atoms depend on the RF power. So, at lower powers, metallic copper can be observed and with the increase in power (to upto 800 W), oxygen rich films will be formed[9].

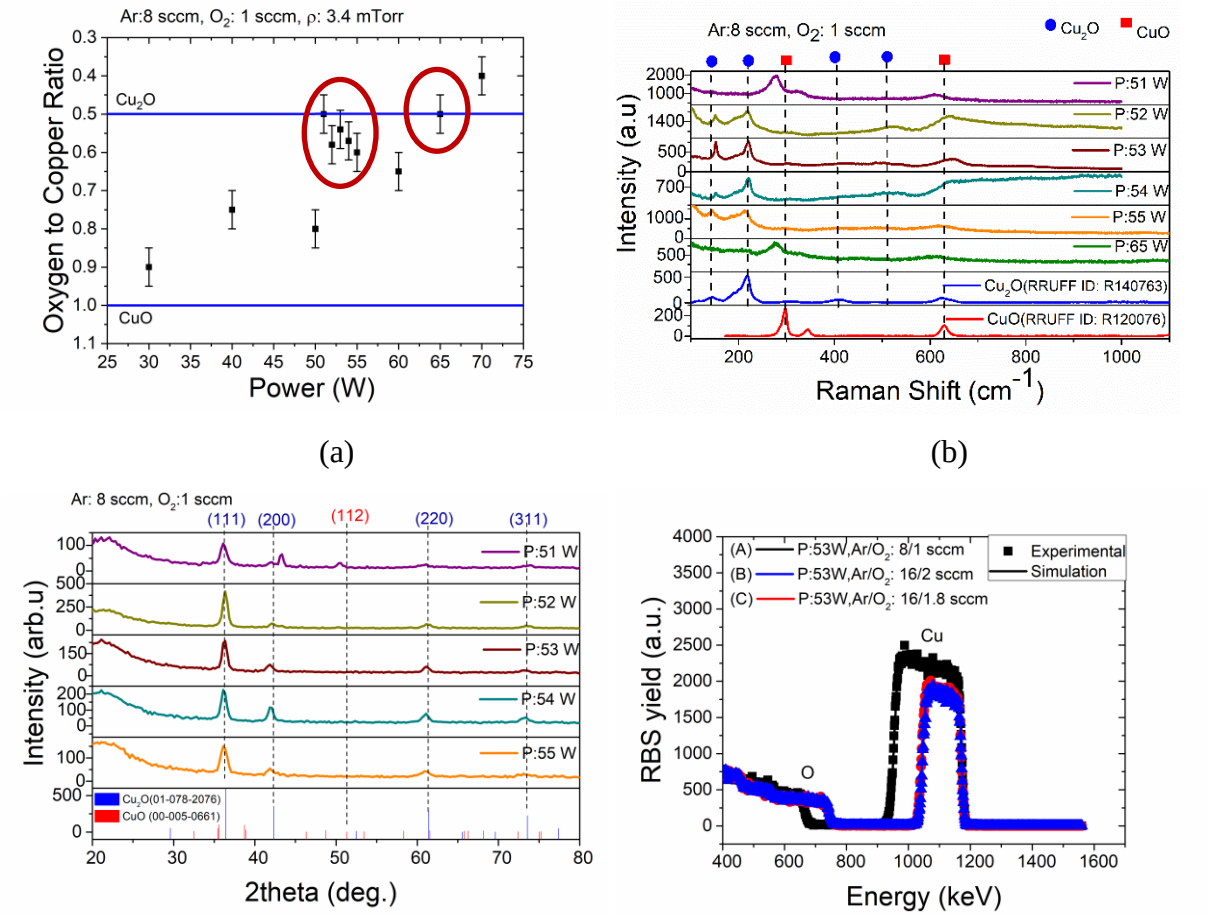

Figure 3.1 (a) Oxygen to copper ratio of sputtered thin films deposited at Ar/O_2: 8/1 sccm and varied sputtering pressures (estimated from RBS measurements)(b) Raman spectra of films deposited at Ar/O_2: 8/1 sccm and sputtering powers of 50-55 W and 65 W at 532 nm excitation wavelength (c) Grazing angle (3°) XRD pattern of the sputtered films deposited at Ar/O_2: 8/1 sccm and varied sputtering pressures (d)RBS yield vs Energy of sputtered thin films

To further optimize the films, keeping the power constant at 53 W, the oxygen flow rate was varied. According to previous works[3], [4], [11], for the deposition of films of Cu_2O stoichiometry, the ratio of the sputtering gas and the reactive gas is a critical criterion. A phase

control of the films by changing the reactive gas flow were observed by Dolai et al[3] and Zhu et.al[6] for DC magnetron sputtered Cu_2O films and Zhang et.al[12] and Ogwu et .al[9] in RF sputtered films. Hence to get a more range to control the O_2 flow rate, keeping the ratio of Ar:O constant at 8:1, the flow rate was doubled for both the gases. Further, the O_2 flow rate was changed keeping the Argon at constant flow. The influence of this recative gas variation on the phase of the films is discussed in the following section.

3.2.2 Variation of Oxygen Flow Rate

Keeping the sputtering power at 53 W and argon flow constant at 16 sccm, oxygen flow rate was varied from 1.5 sccm to 2.5 sccm to study the change in the stoichiometry of the films. Unlike expected, by doubling both the argon and oxygen flow rate, keeping their ratio constant,a change in the phase of the films was observed as can be seen from the O/Cu ratio estimated from RBS in Figure 3.2(a). The oxygen to copper ratio was 0.54 for a flow rate of Ar/O: 8/1 sccm while it increased to 0.71 when the flow rate doubled to Ar/O: 16/2 sccm. When at higher reactive gas flow, increase in the oxygen availability had led to formation of CuO films. Hence above 2 sccm all the films showed CuO stoichiometry as can be seen from the RBS, Raman and XRD results in Figure 3.2. At lower flow rate of 1.5 sscm, the O/Cu estimated from RBS results were contradicting with the Raman spectra. The films were a mixture of both Cu_2O and CuO phase. For a lower oxygen flow rate, below 1.7 sccm films had the presence of both the phases. Between oxygen flow rate of 1.7-1.9 sccm the film had Raman vibrational modes of Cu_2O (RRUFF ID:R140763).

All the films were crystalline with an orientation in the direction of (1 1 1) in the XRD pattern (Figure 3.2(c)). The intensity of diffraction peak at (1 1 1) increased with the increase of gas flow rate upto 1.8 sccm.Similar increase with gas flow rate was also reported by Zhu et.al[85]. At 1.8 sccm flow rate, strong diffraction peaks at (1 1 1) and additional peaks of the planes (2 0 0), (2 2 0) and (3 1 1) of Cu_2O were observed. For the films deposited at lower flow rates of 1.5-1.7 sccm , diffraction peak of non oxidised Cu (1 1 1) (JCPDS : 85-1326) was observed as can be seen in Figure 3.2(c). This mixture is due to the lack of oxygen at lower flow rates. The RBS spectra of the film at 1.8 sccm is shown in Figure 3.1(d)(C) and is fitting to the simulation results.

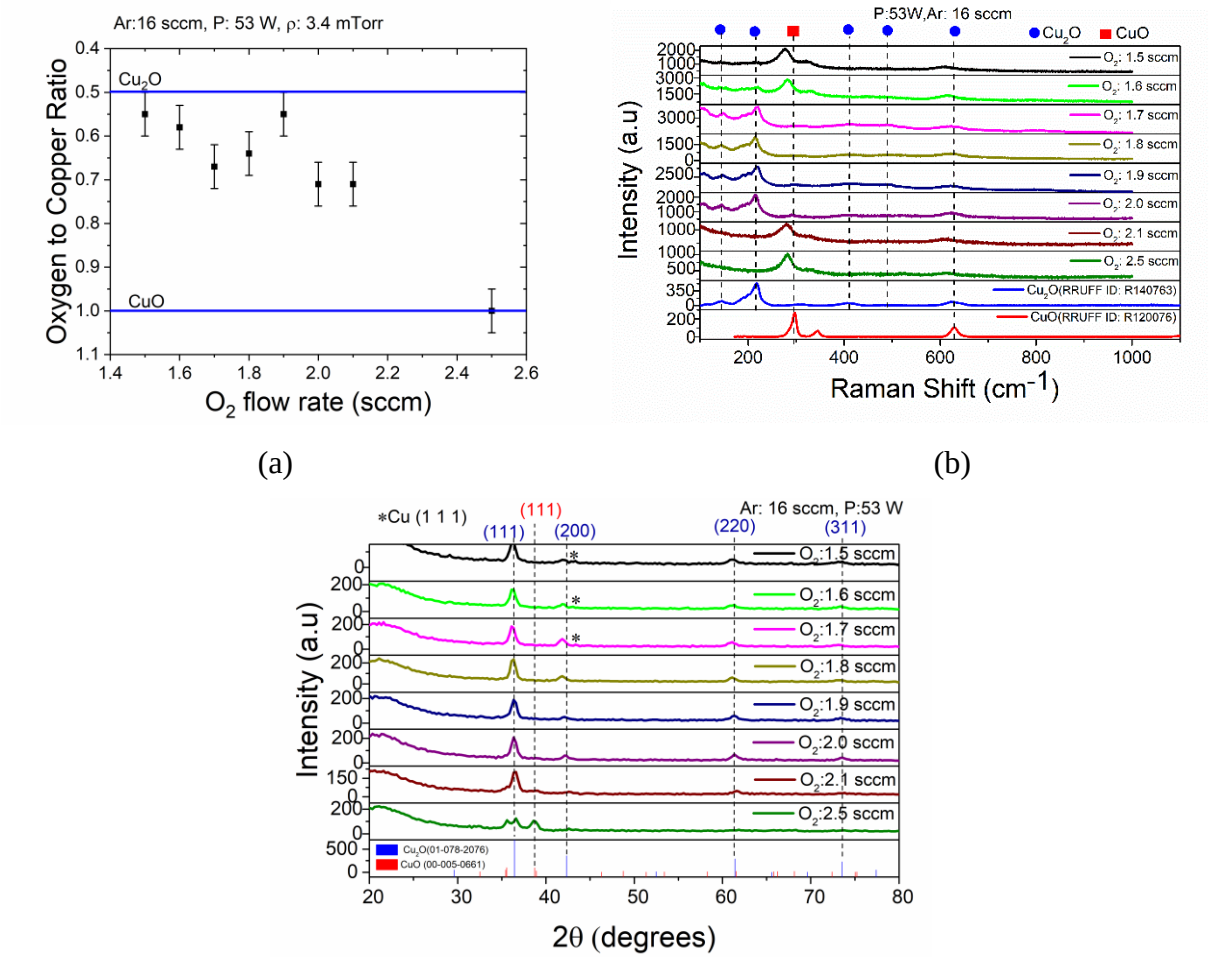

Figure 3.2 (a) Oxygen to copper ratio of sputtered thin films deposited at 53 W, Ar:16 sccm and varied oxygen flow rate(estimated from RBS measurements) (b)Raman of sputtered thin films deposited at 53 W, Ar:16 sccm and varied oxygen flow rate at 532 nm excitation wavelength (c) Grazing angle (3°) XRD pattern of films deposited at 53 W at varied O_2 flow rate

To analyse also the influence of the sputtering pressure, keeping all the rest of the parameters constant (53 W, Ar/O2 : 16 /1.8 sccm, 300 °C) the phase of the films were analysed using Raman spectroscopy by varying the sputtering pressure between 2.8-3.6 mTorr in steps of 0.2 mTorr. It was found that within a pressure window of 2.8-3.6 mTorr , all the films had Cu_2O phase and there was no influence of sputtering pressure on the film stoichiometry in this range. Hence comparing the results of elemental analysis using RBS, structural characterization using Raman and XRD, the best optimized deposition parametrs to obtain single phase Cu_2O film were P: 53 W, Ar/O2 : 16 /1.8 sccm, T:300 °C. The quality of this film (called reference

sputtered film) and its optical and electrical properties were further analysed for its potential as an absorber using several techniques and is discussed in the following sections.

3.3 STRUCTURAL CHARACTERIZATION OF SPUTTERED Cu_2O

The structural properties of the phase optimised sputtered Cu_2O films were studied using Raman spectroscopy and X-ray Diffraction studies. As discussed in the previous section, characteristic peaks of Cu_2O films were observed in the film with the presence of E_u mode, T_{1u} mode, second-order E_u ($2E_u$) mode, A_{2u} mode, multi phonon process (MPP) mode and T_{2g} mode at 106 cm^{-1}, 145 cm^{-1}, 216 cm^{-1}, 310 cm^{-1} 412 cm^{-1} and ~ 500 cm^{-1}, as can be seen Figure 3.3 (a). Compared to the Raman peak of PLD Cu_2O film in Figure 2.6 (c), the reference sputtered film has a higher T_{1u} signal which is due to the presence of higher copper vacancies and interstitials in the film[13]. Hence a higher carrier concentration over the film deposited via PLD route can be expected for the sputtered Cu_2O. The intensity ratio of T_{1u} and $2E_u$ mode for the sputtered film was 0.66 which is higher than the PLD film (0.43), this is an indication of surface damages in the film which needs to be investigated[14]. However, the ratio is smaller compared to the PLD film deposited at an identical temperature. Thin films deposited at elevated temperatures will have higher quality due to better crystallization. However, the sputtered films were deposited at lower temperature of 300 ℃ and this particular film has a better surface quality than the PLD film deposited at 300 ℃, which is promising.

The crystalline structure of the reference sputtered film was studied with the help of X-ray diffraction studies (Figure 3.3(b)) and its lattice parameters are listed in Table 9. The mean grain size of the film was calculated from the Scherrer´s equation[15] and was found to be 10.1 nm. The smaller grain size has led to an increase lattice constant of 4.3±0.02 Å for the film. More than 1 % deviation from the pure Cu_2O film could be because of lattice strain, defects or dislocations in the material. The stress in the film was calculated from the lattice constant and was found to be 0.21. The stress is several times higher than that was observed in the best PLD film. However, it is similar to the PLD film at 300 ℃. Hence the difference could be related to the change in the crystallite size associated with the deposition temperature. The sputtered film had a microstrain (Ɛ) of 5.46±4.5 calculated using the Stokes-Wilson relation[16]. The surface quality of the film was further analysed using advanced microscopic techniques for a better understanding and the results are discussed in the next section.

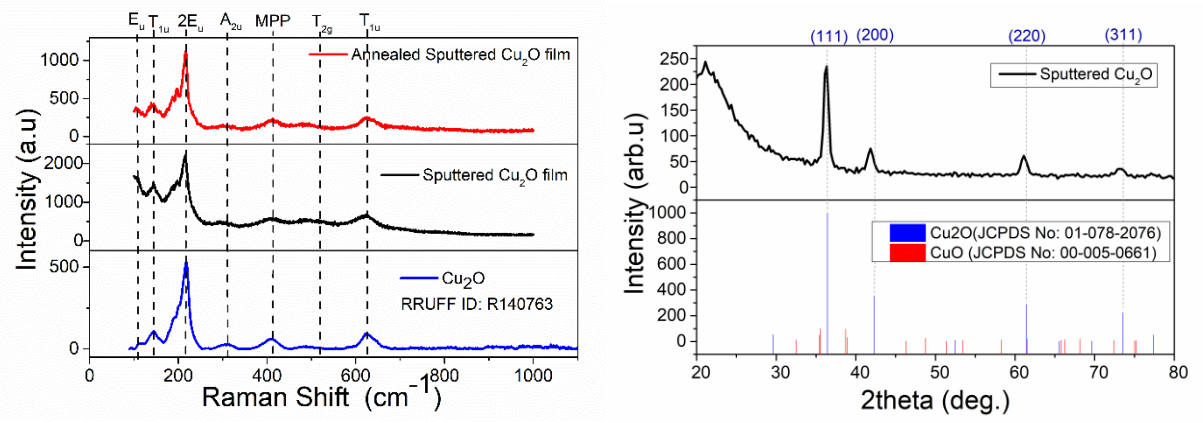

(a) (b)

Figure 3.3 (a) Raman spectra of magnetron sputtered Cu_2O film at 532 nm excitation wavelength(b) Grazing angle XRD pattern of the sputtered Cu_2O film

Table 9 Lattice Parameters, Crystallites Sizes and Micro strain of sputtered Cu_2O film calculated from the X-ray diffraction peaks

2θ (°)	FWHM (°)	d spacing (Å)	Grain Size (nm)	Lattice Constant (Å)
36.27	0.74	2.48	11.2	4.29
41.97	0.083	2.16	11.02	4.32
61.12	0.93	1.51	9.87	4.29
73.20	1.19	1.29	8.31	4.28

3.3.1 Morphology and Roughness of the Cu_2O Films

Scanning electron microscopy analysis of the sputtered Cu_2O film revealed flat morphology with smaller grains confirming the calculated values from the diffraction peaks. A Gemini 500-Zeiss apparatus was used for the SEM measurements. The films were uniformly covered with no visible holes in the films, as can be seen in the wider magnification image in Figure 3.4(b). Unlike the PLD film deposited at 300 °C there were only fewer splashings present in the film which points to their better surface quality than the PLD Cu_2O film at lower temperature. Higher

stress in the sputtered film compared to the best PLD film (at 750 °C,10^{-2} mbar) calculated from the XRD peaks is due to the smaller crystalline size confirmed via XRD and SEM . The PLD film had larger grains with well defined boundaries.The morphology of the films were also studied using an NT-MDT SMENA Atomic Force Microscope (AFM). The smooth surface of the film was also visible in the three dimensional view of the AFM image as can be seen in Figure 3.4(d) .The grains were very small with a height of less than 33 nm. The sputtered film had a flat morphology with an RMS roughness of only 2.7 nm which is much smaller than both the PLD deposited films at high and low temperatures.

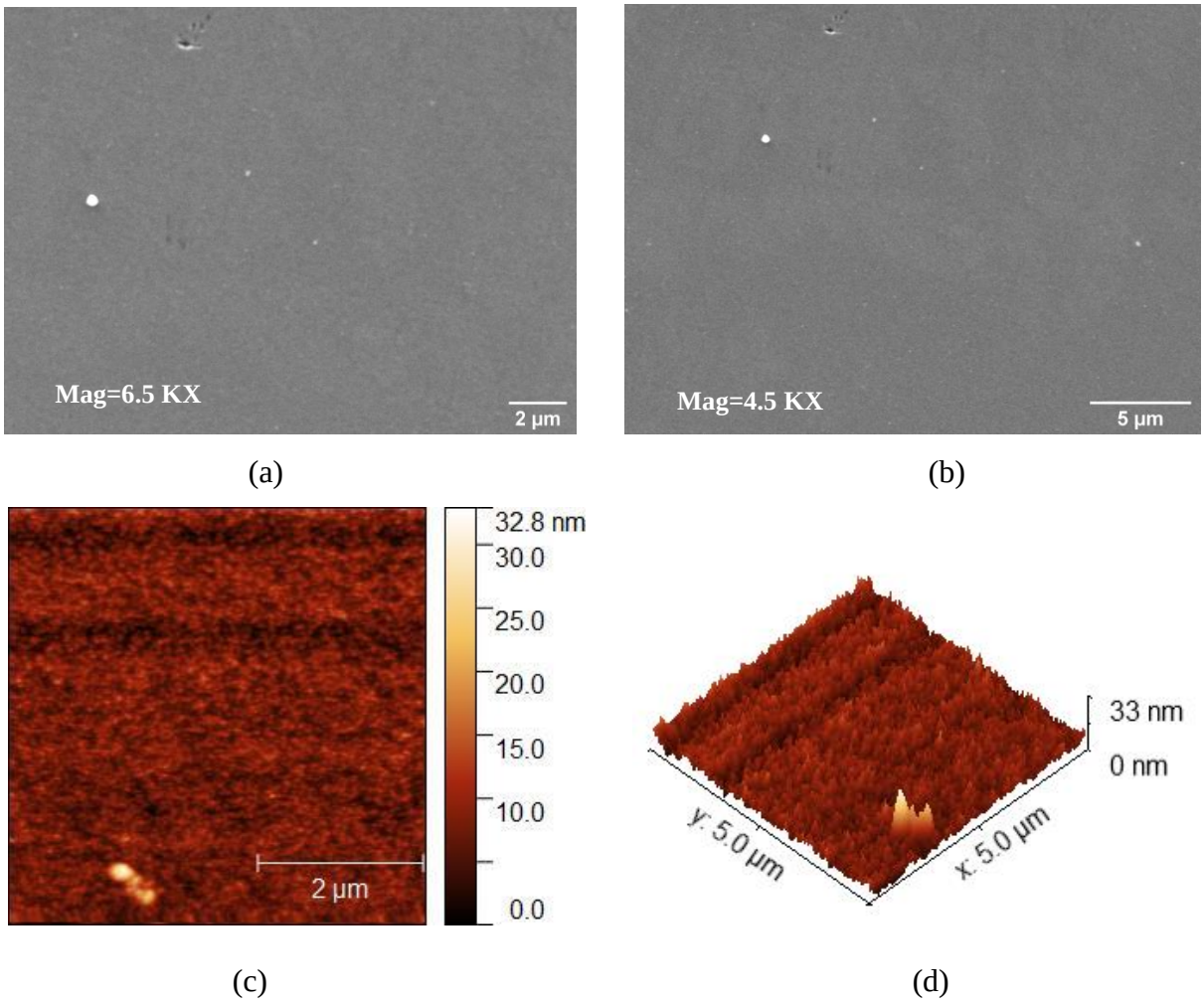

Figure 3.4 (a) and (b) Secondary electron images of Cu_2O film deposited by RF magnetron sputtering at different magnifications. AFM image (5 µm x 5 µm) of sputtered Cu_2O film (c) in two-dimension (d) in three-dimension

Thus from the detailed structural analysis of the optimized Cu_2O film via magnetron sputtering, then reference sputtered film has exhibited good surface quality which makes it suitable for

opto-electronic applications. It is promising that the film sputtered at 300 ℃ have comparable surface quality to that of the best PLD film (deposited at 750 ℃) apart from the grain size, as it allows for the use of flexible substrates. Also in some cases, high temperature growth of absorber is not favourable during the growth of a solar cell when the underlying layer is not compatible with high temperatures.However, further anlaysis of optical and electrical properties of the film is necessary to confirm its potential for the application in a solar cell and is discussed in the upcoming sections.

3.4 OPTICAL PROPERTIES

Apart from the good structural quality, an absorber layer should have good optical properties which helps to increase the overall photovoltaic conversion efficiency. The bandgap, absorption coefficient and photoluminescence of the films will be discussed in this section.

3.4.1 Absorption Properties

The transmittance of the reference sputtered film was measured using UV-VIS spectroscopy using a Perkin-Elmer Lambda 19 UV/Vis/NIR spectrophotometer. From the transmission spectra, absorbance was calculated. Reflectance was not taken into account for the absorbance calculations. As can be seen in Figure 3.5(a) the sputtered film exhibited a high absorbance in the ultra-violet and the blue region of the visible spectrum (200-500 nm) which is similar to that of PLD film. The optical bandgap of the films were calculated from the transmission spectra using Tauc plot ($h\upsilon$ vs $(\alpha h\upsilon)^{1/r}$). Since Cu_2O have direct forbidden bandgap, an exponent of 3/2 was used for the calculations. As can be seen in the Tauc plot in the inset of Figure 3.5(a), the sputtered film had an optical bandgap of 2.3 eV which is higher than PLD film. As in Cu_2O, transition between the valence band maximum and conduction band minimum is forbidden, the calculated optical bandgap is between the valence band maximum and the second energy level of conduction band [17]. Hence the real bandgap of the film will be smaller than 2.3 eV. A variation in the bandgap of the film due to different synthesis route was already reported in the literature[3], [18]–[20] . A similar bandgap was reported for RF magnetron sputtered film by Hari prasad et.al[21].

The optical absorption coefficient of the film was determined from a Horiba Uvisel Lt M200 FGMS (210-880 nm) spectroscopic ellipsometer. Dispersion model based on Triple Tauc Lorentz formula was used for the film[22].The appearance of steps in the absorption coefficient

of Cu_2O as can be seen in Figure 3.5(b) is due to simultaneous creation and destruction of phonons along with excitons which makes the spectra similar to that of semiconductors with indirect edges[23], [24]. Even though, on comparison to the PLD films, the absorption coefficient of the sputtered film is lower as can be seen in Figure 3.5(b), a high absorption coefficient in the range of 10^6-10^5 cm^{-1} in the visible region was observed in the film which make them suitable for an absorber.

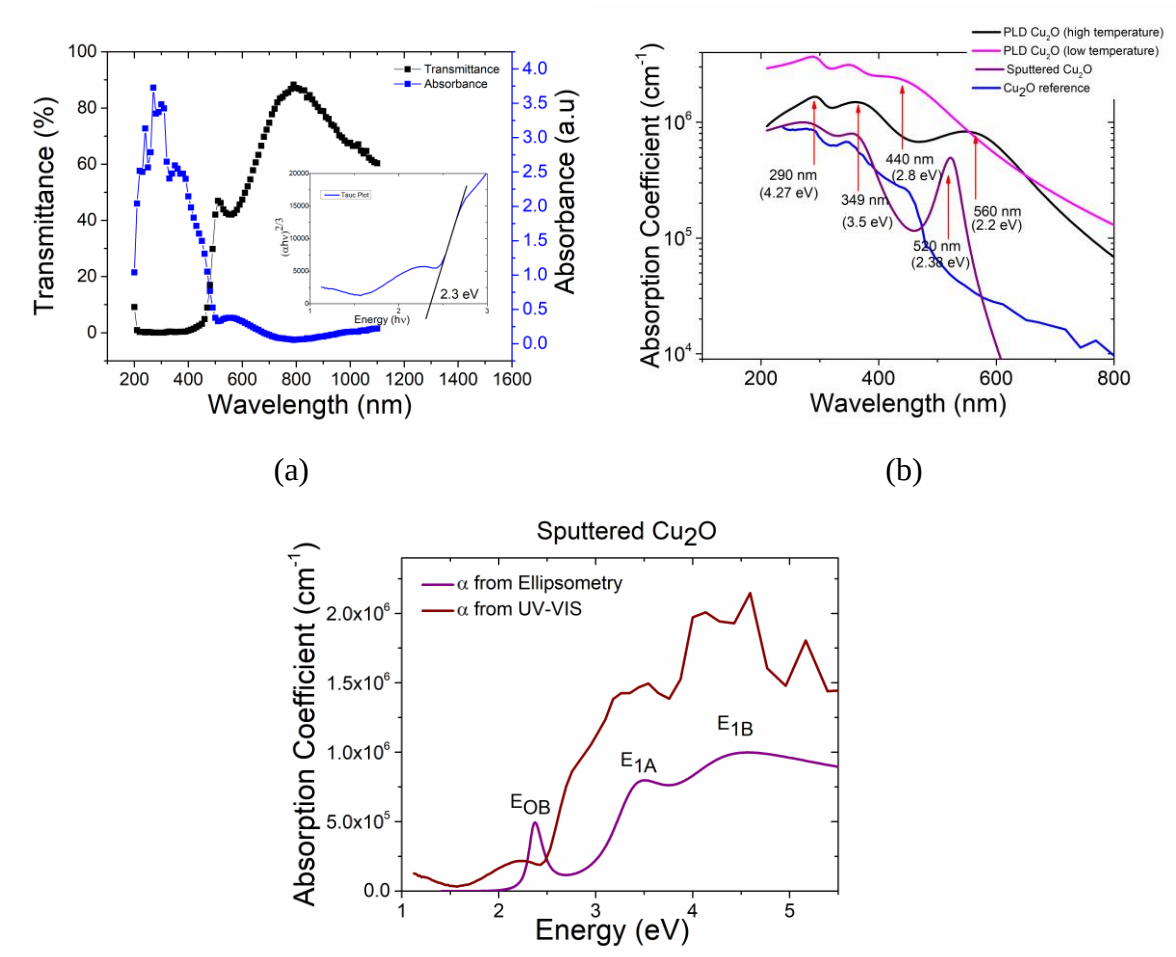

Figure 3.5 (a) Wavelength depended Transmittance and Absorbance of the Cu_2O film sputtered at 53 W, Ar/O: 16/1.8 sccm and tauc plot in the inset (b) Absorption coefficient spectra of the Cu_2O film from ellipsometry measurements via different techniques and reference[25] (c) Absorption coefficient with respect to energy of the sputtered Cu_2O film on quartz from Ellipsometry and UV-VIS spectroscopy

In the energy vs absorption coefficient plot calculated from the ellipsometry and transmittance measurements in Figure 3.5(c), the absorption coefficient is zero below the bandgap (from ellipsometry), unlike reported by Malerba et.al[26] and Wang et.al[17], which is an evidence that there are no sub-gap absorption due to defects in the film. However, in the spectra calculated from UV-VIS measurements, a non-zero absorption coefficient below bandgap is visible. The excitonic peaks corresponding to the E_{OB} edge (green exciton) and 2D exciton transitions of E_{1A} (3.5 eV) and E_{1B} (4.3 eV) was visible in the absorption spectra[25]. The yellow and green excitonic transitions in Cu_2O are dipole forbidden due to same parity. However, yellow excitonic transition was observed in the best PLD film and green excitonic transitions in the sputtered Cu_2O film. The green excitonic transition was not visible in the absorption coefficient spectra from UV-VIS spectroscopy measurements It has been reported that these forbidden transitions may be observed as weak quadrupolar transition due to stress or symmetry effects in the crystal[24]. For the PLD film, the yellow exciton peak is weak as can be seen Figure 3.5(b) but a strong green exciton peak in the sputtered film might be due to stress in the film which was also observed in the calculations from the diffraction peaks. The influence of this on the photoluminescence of the film is discussed in the next section.

3.4.2 Photoluminescence of Sputtered Films

For a better understanding on the emission characteristics of the film upon illumination, to study about the recombination mechanisms, discrete energy states and defects in the sputtered Cu_2O film, Photoluminescence (PL) spectroscopy analysis was carried out at room temperature. An Andor iStar DH740 CCI-010 system connected to a grating spectrometer (Andor SR303i) at the Cambridge University was used for the PL measurements. An excitation wavelength of 400 nm was used to measure the photoluminescence spectrum of the sample. This measurement was performed by Yi-Teng Huang from the Optoelectronics Group of Cavendish Laboratory at Cambridge University as part of a collaboration with Dr. Robert Hoye.

As can be seen in Figure 3.6, four PL peaks were observed in the film. A distinct peak corresponding to the near band edge emission can be seen at ~ 630 nm (1.97 eV). Similar PL peak was also observed in the PLD film. A strong intensity peak at ~735 nm (1.68 eV) and a narrow peak at ~798 nm (1.55 eV) is also visible. According to the deep level transient absorption spectroscopy studies carried out by Paul et.al[27] to understand the defects in Cu_2O films, two trap levels corresponding to Cu vacancy (V_{cu}) and Cu-di vacancy(V_{cu}^{split}) are present

at 0.45 eV and 0.25 eV above the valance band edge. Hence the peak at 1.55 eV can be assigned to V_{cu} and the peak at 1.68 eV could be the V_{cu}^{split}. Paul et.al[27] also observed that the peak of V_{cu}^{split} diminishes with improved crystallinity. This may be the reason this peak was not observed in the PLD film. A wider peak was observed at ~ 460 nm (2.69 eV) which could be due to the interband transition ($\Gamma_7^+ \rightarrow \Gamma_8^-$). Similar wide peak above 2 eV in the PL was also reported by Wang et.al[17].

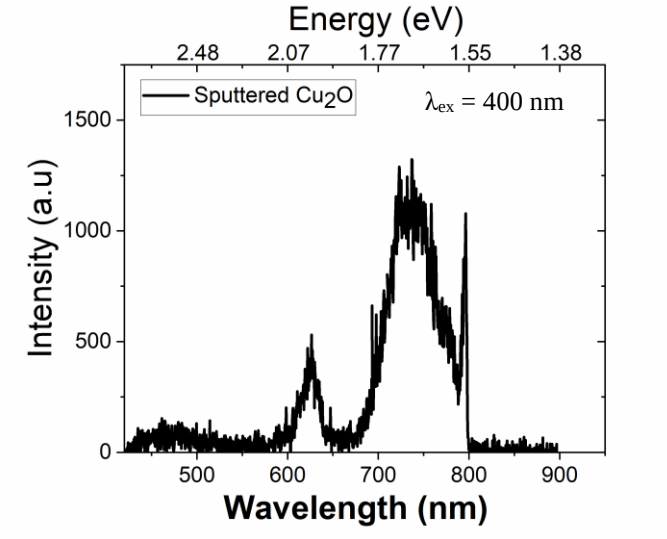

Figure 3.6 Photoluminescence spectra of the sputtered Cu_2O film at an excitation wavelength of 400 nm on quartz substrate

Hence from the optical property analysis, despite lacking the quality compared to the optimized PLD Cu_2O film, the sputtered film has the potential properties for a good photovoltaic absorber. A detailed analysis also on the electrical properties of the film is necessary to understand about the carrier properties of the film for its application in a photovoltaic cell.

3.5 CARRIER PROPERTIES OF THE SPUTTERED FILMS

In order to choose a good absorber, it is important for it to have good electrical properties as the charge generation, transport and separation are crucial factors in the conversion efficiency of a solar cell. An Ecopia Hall effect measurement system (HMS-5000) in Van der Pauw configuration was used for the measurement of the carrier properties of the sputtered films at room temperature.

Not all the films deposited at different sputtering conditions were conducting. However, all the conducting films were p-type with a higher carrier concentration in the range of 10^{17} cm^{-3}. It is higher than most of the reported values for RF magnetron sputtered films in the literature[17], [28], [29]. The hole concentration was the highest for the optimized Cu_2O film deposited at 1.8 sccm oxygen flow as can be seen in Figure 3.7.Eventhough there is no major difference in the hole concentration of the three films deposited at different oxygen flow rates, the resistivity of the films deposited at 1.9 sccm is more than 5 orders of magnitude higher than the film at 1.8 sccm oxygen flow rate. This variation could be due to the difference in the crystallinity of the films as discussed during the X-ray diffraction characterization in 3.2.2. The resistivity of the optimized sputtered Cu_2O film deposited at 1.8 sccm was as low as 16.2±0.01 **Ω**cm. The reference sputtered film also had an increased mobility due to the crystallinity, as improved crystallinity increases the grain size thus reducing the scattering from the interface states along the grain boundaries which are negatively charged. This in turn improves the mobility of the films.

Compared to the PLD films, the mobility of the sputtered films are lower but is comparable to the mobility of sputtered films in the literature[28]–[30]. This is because compared to the PLD films, the carrier concentration of the sputtered films is higher which leads to higher ionized centers (native defects). Scattering from these ionized centers reduces the mobility of the films[31].

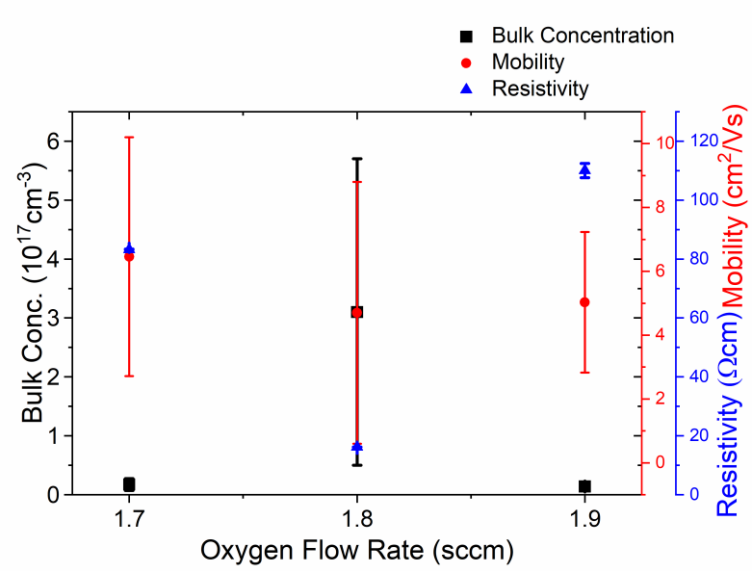

Figure 3.7 Carrier properties of the sputtered Cu_xO films estimated from the hall measurements, deposited at a power of 53 W, argon flow rate of 16 sccm and different oxygen flow rates

Hence, comparing the electrical properties of the sputtered films, lower hole mobility is a major concern in its application as an absorber. In the literature, post annealing has been reported to improve the hall mobility of the films. To study potential of improvement in the electrical properties, the optimized sputtered films were post annealed and the results will be discussed in the next section.

3.6 POST-ANNEALING OF THE SPUTTERED Cu_2O FILMS

There have been many reports in literature on the improvement in the properties of the sputtered Cu_2O films after post-annealing[17], [30], [32], [33]. The sputtered Cu_2O films deposited at optimized deposition conditions were post annealed using a rapid annealing furnace. In Rapid Thermal Annealing (RTA) the films are heated by infrared radiation using tungsten halogen lamps. The temperature is increased rapidly in a controlled atmosphere of argon, nitrogen or oxygen. In our case, a JIPELEC oven type RTP FAV4 model Rapid Annealing furnace was used for the process. RTA was carried out at 900 ℃ for 3 minutes in argon atmosphere. The colour of the film changed from yellow to a lighter shade of yellow after the process which could indicate a change in the bandgap of the film and increased transmittance. This was also observed by Wang et.al[17] after post annealing due to partial removal of defect band tail. In order to confirm the phase of the film after RTA, Raman spectroscopy analysis of the film was performed. As can be seen in Figure 3.8(a) the films showed vibrational modes of Cu_2O even after undergoing RTA.

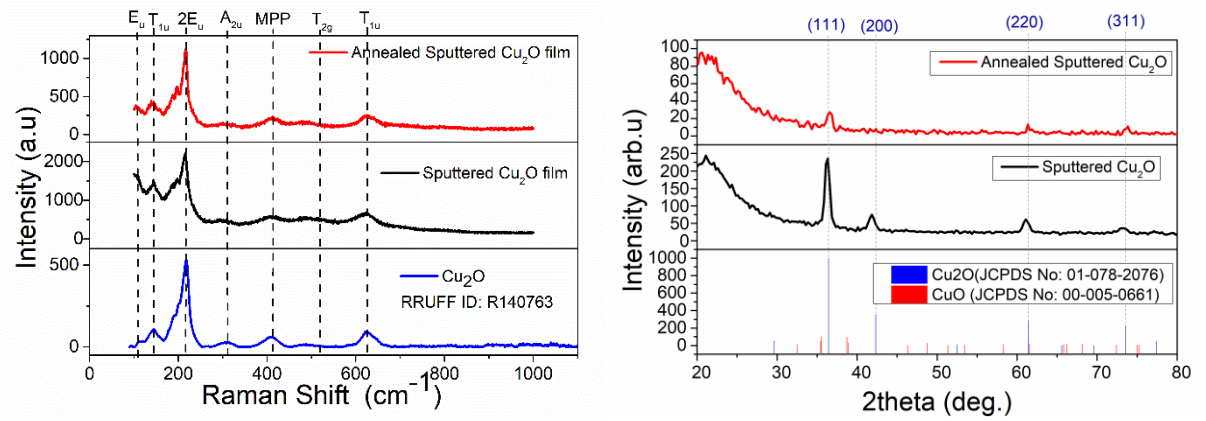

(a) (b)

Figure 3.8 (a) Raman spectra of the as grown sputtered Cu_2O film and the film annealed via RTA process (b) Diffraction peaks of the as grown sputtered Cu_2O film and the film annealed via RTA process

Further the electrical properties of the film were measured via Hall measurement. As listed in Table 10, the mobility of the films increased more than 8 times after RTA. However, the resistivity and carrier concentration decreased. To analyse the crystallinity of the film, the XRD pattern of the film was studied as can be seen in Figure 3.8 (b). It is clear that the crystallinity of the annealed film decreased after RTA from the decrease in the diffraction peak intensity.

The peak at (2 0 0) have completely diminished and the (1 1 1) peak had broadened and shifted to the right. However, as listed in Table 10, the lattice constant of the film has decreased, and the film has a compressive stress of 0.15 GPa compared to the tensile stress of 0.21 GPa before RTA. The broadening of the diffraction peak observed might be stress induced. The increased mobility observed in the films after RTA might be due to decreased carrier concentration (ionized centres or native defects). Wang et.al[17] have reported an increase in the crystallite size after annealing which led to increase in the mobility. However, in our film, even though the decrease in lattice parameter can be connected to an increase in the crystallite size, the diminished intensity of diffraction peaks contradicts this assumption. Hence it can only be assumed that upon RTA some defects in the films have decreased/removed which led to the increase in the mobility similar to the PLD Cu_2O film. As a conclusion, due to the poor structural quality, application of the RTA sputtered film as absorber is not recommended.

Table 10 Electrical properties and lattice parameters of the sputtered Cu_2O film before and after annealing

Sputtered Cu_2O Film	Bulk concentration (cm^{-3})	Resistivity (Ω.cm)	Mobility ($cm^2/V.s$)	Lattice Parameter (Å)	Stress (GPa)
Before RTA	$3.1x10^{17}±2.6x10^{17}$	16.2±0.01	4.7±4.10	4.3±0.02	0.21
After RTA	$1.3x10^{15}±1.1x10^{14}$	131.0±3.00	35.2±2.83	4.24±0.02	-0.15

3.7 CONCLUSION

This chapter was focused on the tentative to prepare phase pure Cu_2O films via RF magnetron sputtering.

The optimization of deposition parameters to obtain Cu_2O film stoichiometry was discussed. It was shown that by varying the sputtering power and the reactive gas flow rate, the phase and the structural properties of the thin film can be a varied. Phase pure Cu_2O films were obtained at a narrow range of power and oxygen flow rate. The sputtered Cu_2O film with best structural quality was obtained at a temperature of 300 ℃, power of 53 W, argon flow rate of 16 sccm and oxygen flow rate of 1.8 sccm. The structural properties of the films deposited at optimized conditions were analysed using XRD and Raman spectroscopy. Eventhough on comparison, the optimized PLD film has a superior structural quality, the sputtered film is also promising because deposition is carried out at a lower temperature than the PLD film which makes it suitable for specific applications. A flat morphology with very low surface roughness was observed in reference sputtered film via SEM and AFM analysis. The optimized film also showed high absorption coefficient and a bandgap in the range of Cu_2O in the literature. Apart from the band edge emission, PL peaks corresponding to copper vacancies which is responsible for the p-type conductivity was observed in the photoluminescence measurements of the film. Hall effect measurements revealed high carrier concentrations in the range of 10^{17} cm^{-3} with lower resistivity (16 Ωcm) for the films. The mobility (8 $cm^2/V.s$) was in comparison to the RF sputtered Cu_2O films in the literature. However, compared to the PLD film the mobility was much lower. To improve the electrical properties the sputtered film was annealed using Rapid Thermal Annealing (RTA). Even though this increased the mobility of the film to ~ 36 $cm^2/V.s$, the crystallinity of the film was affected by the process. Through the different analysis techniques described in this chapter, the best Cu_2O film using RF magnetron sputtering was identified along with its potential as an absorber was elucidated. Further in the next chapter, the growth of Cu_2O film via another very popular technique namely thermal oxidation is discussed along with its properties. Finally in the last chapter all the Cu_2O films via different routes are compared using advanced characterization techniques to better understand the influence of synthesis route of Cu_2O on its performance in a solar cell.

3.8 REFERENCES OF CHAPTER 03

[1] P. Sawicka-Chudy *et al.*, 'Optical and structural properties of Cu 2 O thin film as active layer in solar cells prepared by DC reactive magnetron sputtering', *Archives of Metallurgy and Materials*, vol. 64, pp. 243–250, Jan. 2019, doi: 10.24425/amm.2019.126244.

[2] A. S. Reddy, S. Uthanna, and P. S. Reddy, 'Properties of dc magnetron sputtered Cu2O films prepared at different sputtering pressures', *Applied Surface Science*, vol. 253, no. 12, pp. 5287–5292, Apr. 2007, doi: 10.1016/j.apsusc.2006.11.051.

[3] S. Dolai, S. Das, S. Hussain, R. Bhar, and A. K. Pal, 'Cuprous oxide (Cu2O) thin films prepared by reactive d.c. sputtering technique', *Vacuum*, vol. 141, pp. 296–306, Jul. 2017, doi: 10.1016/j.vacuum.2017.04.033.

[4] N. H. Ke, P. T. K. Loan, D. A. Tuan, H. T. Dat, C. V. Tran, and L. V. T. Hung, 'The characteristics of IGZO/ZnO/Cu2O:Na thin film solar cells fabricated by DC magnetron sputtering method', *Journal of Photochemistry and Photobiology A: Chemistry*, vol. 349, pp. 100–107, Dec. 2017, doi: 10.1016/j.jphotochem.2017.09.016.

[5] A. H. Shukor, H. A. Alhattab, and I. Takano, 'Electrical and optical properties of copper oxide thin films prepared by DC magnetron sputtering', *Journal of Vacuum Science & Technology B*, vol. 38, no. 1, p. 012803, Jan. 2020, doi: 10.1116/1.5131518.

[6] H. Zhu, J. Zhang, C. Li, F. Pan, T. Wang, and B. Huang, 'Cu2O thin films deposited by reactive direct current magnetron sputtering', *Thin Solid Films*, vol. 517, no. 19, pp. 5700–5704, Aug. 2009, doi: 10.1016/j.tsf.2009.02.127.

[7] J. P. Stoquert, F. Pêcheux, Y. Hervé, H. Marchal, R. Stuck, and P. Siffert, 'VRBS: A virtual RBS simulation tool for ion beam analysis', *Nuclear Instruments and Methods in Physics Research Section B: Beam Interactions with Materials and Atoms*, vol. 136–138, pp. 1152–1156, 1998, doi: https://doi.org/10.1016/S0168-583X(97)00807-0.

[8] P. K. Ooi, S. S. Ng, and M. J. Abdullah, 'Effects of sputtering power on properties of copper oxides thin films deposited on glass substrates', presented at the NATIONAL PHYSICS CONFERENCE 2014 (PERFIK 2014), Kuala Lumpur, Malaysia, 2015, p. 100008. doi: 10.1063/1.4915215.

[9] A. A. Ogwu, E. Bouquerel, O. Ademosu, S. Moh, E. Crossan, and F. Placido, 'The influence of rf power and oxygen flow rate during deposition on the optical transmittance of copper oxide thin films prepared by reactive magnetron sputtering', *Journal of Physics D Applied Physics*, vol. 38, no. 2, pp. 266–271, Jan. 2005, doi: 10.1088/0022-3727/38/2/011.

[10] A. A. Ogwu, T. H. Darma, and E. Bouquerel, 'Electrical resistivity of copper oxide thin films prepared by reactive magnetron sputtering', *Journal of Achievements in Materials and Manufacturing Engineering*, vol. 24, no. 1, p. 6, 2007.

[11] Y. S. Lee, M. T. Winkler, S. C. Siah, R. Brandt, and T. Buonassisi, 'Hall mobility of cuprous oxide thin films deposited by reactive direct-current magnetron sputtering', *Appl. Phys. Lett.*, vol. 98, no. 19, p. 192115, May 2011, doi: 10.1063/1.3589810.

[12] L. Zhang, L. McMillon, and J. McNatt, 'Gas-dependent bandgap and electrical conductivity of Cu2O thin films', *Solar Energy Materials and Solar Cells*, vol. 108, pp. 230–234, Jan. 2013, doi: 10.1016/j.solmat.2012.05.010.

[13] T. Sander *et al.*, 'Correlation of intrinsic point defects and the Raman modes of cuprous oxide', *Phys. Rev. B*, vol. 90, no. 4, p. 045203, Jul. 2014, doi: 10.1103/PhysRevB.90.045203.

[14] A. Compaan, ‘Surface damage effects on allowed and forbidden phonon raman scattering in cuprous oxide’, *Solid State Communications*, vol. 16, no. 3, pp. 293–296, Feb. 1975, doi: 10.1016/0038-1098(75)90171-4.
[15] A. L. Patterson, ‘The Scherrer Formula for X-Ray Particle Size Determination’, *Phys. Rev.*, vol. 56, no. 10, pp. 978–982, Nov. 1939, doi: 10.1103/PhysRev.56.978.
[16] A. R. Stokes and A. J. C. Wilson, ‘The diffraction of X rays by distorted crystal aggregates - I’, *Proceedings of the Physical Society*, vol. 56, no. 3, pp. 174–181, May 1944, doi: 10.1088/0959-5309/56/3/303.
[17] Y. Wang, P. Miska, D. Pilloud, D. Horwat, F. Mücklich, and J. F. Pierson, ‘Transmittance enhancement and optical band gap widening of Cu_2O thin films after air annealing’, *Journal of Applied Physics*, vol. 115, no. 7, p. 073505, Feb. 2014, doi: 10.1063/1.4865957.
[18] S. F. U. Farhad, D. Cherns, J. A. Smith, N. A. Fox, and D. J. Fermín, ‘Pulsed laser deposition of single phase n- and p-type Cu2O thin films with low resistivity’, *Materials & Design*, vol. 193, p. 108848, Aug. 2020, doi: 10.1016/j.matdes.2020.108848.
[19] M. T. S. Nair, L. Guerrero, O. L. Arenas, and P. K. Nair, ‘Chemically deposited copper oxide thin films: structural, optical and electrical characteristics’, *Applied Surface Science*, vol. 150, no. 1, pp. 143–151, 1999, doi: https://doi.org/10.1016/S0169-4332(99)00239-1.
[20] A. S. Reddy, G. V. Rao, S. Uthanna, and P. S. Reddy, ‘Structural and optical studies on dc reactive magnetron sputtered Cu2O films’, *Materials Letters*, vol. 60, no. 13–14, pp. 1617–1621, Jun. 2006, doi: 10.1016/j.matlet.2005.11.101.
[21] M. Hari Prasad Reddy, A. Sreedhar, and S. Uthanna, ‘Structural, surface morphological and optical properties of nanocrystalline Cu2O films prepared by RF magnetron sputtering: substrate bias effect’, *Indian Journal of Physics*, vol. 86, no. 4, pp. 291–295, Apr. 2012, doi: 10.1007/s12648-012-0057-7.
[22] G. E. Jellison and F. A. Modine, ‘Parameterization of the optical functions of amorphous materials in the interband region’, *Applied Physics Letters*, vol. 69, no. 3, pp. 371–373, 1996, doi: 10.1063/1.118064.
[23] R. J. Elliott, ‘Intensity of Optical Absorption by Excitons’, *Phys. Rev.*, vol. 108, no. 6, pp. 1384–1389, Dec. 1957, doi: 10.1103/PhysRev.108.1384.
[24] R. A. Forman, W. S. Brower, and H. S. Parker, ‘Phonons and the green exciton series in cuprous oxide, Cu2O’, *Physics Letters A*, vol. 36, no. 5, pp. 395–396, 1971, doi: https://doi.org/10.1016/0375-9601(71)90276-3.
[25] T. Ito, T. Kawashima, H. Yamaguchi, T. Masumi, and S. Adachi, ‘Optical Properties of Cu 2O Studied by Spectroscopic Ellipsometry’, *Journal of the Physical Society of Japan*, vol. 67, no. 6, pp. 2125–2131, 1998, doi: 10.1143/JPSJ.67.2125.
[26] C. Malerba, F. Biccari, C. Leonor Azanza Ricardo, M. D’Incau, P. Scardi, and A. Mittiga, ‘Absorption coefficient of bulk and thin film Cu2O’, *Solar Energy Materials and Solar Cells*, vol. 95, no. 10, pp. 2848–2854, Oct. 2011, doi: 10.1016/j.solmat.2011.05.047.
[27] G. K. Paul, Y. Nawa, H. Sato, T. Sakurai, and K. Akimoto, ‘Defects in Cu2O studied by deep level transient spectroscopy’, *Appl. Phys. Lett.*, vol. 88, no. 14, p. 141901, Apr. 2006, doi: 10.1063/1.2175492.
[28] H. Ahn and Y. Um, ‘RF Magnetron Sputtering Grown Cu2O Film Structural, Morphological, and Electrical Property Dependencies on Substrate Type’, *j nanosci nanotechnol*, vol. 15, no. 3, pp. 2342–2345, Mar. 2015, doi: 10.1166/jnn.2015.10252.

[29] S. Ishizuka, T. Maruyama, and K. Akimoto, ‘Thin-Film Deposition of Cu2O by Reactive Radio-Frequency Magnetron Sputtering’, *Japanese Journal of Applied Physics*, vol. 39, no. Part 2, No. 8A, pp. L786–L788, Aug. 2000, doi: 10.1143/jjap.39.l786.
[30] Ø. Nordseth *et al.*, ‘Characterization of Cuprous Oxide Thin Films for Application in Solar Cells’, *DF*, vol. 22, pp. 65–73, May 2019, doi: 10.4028/www.scientific.net/DF.22.65.
[31] Y. S. Lee, M. T. Winkler, S. C. Siah, R. Brandt, and T. Buonassisi, ‘Hall mobility of cuprous oxide thin films deposited by reactive direct-current magnetron sputtering’, *Appl. Phys. Lett.*, vol. 98, no. 19, p. 192115, May 2011, doi: 10.1063/1.3589810.
[32] R. Kumar, K. Bergum, H. N. Riise, E. Monakhov, A. Galeckas, and B. G. Svensson, ‘Impact of post annealing and hydrogen implantation on functional properties of Cu2O thin films for photovoltaic applications’, *Journal of Alloys and Compounds*, vol. 825, p. 153982, Jun. 2020, doi: 10.1016/j.jallcom.2020.153982.
[33] M. Nyborg, ‘Nitrogen Doping of Sputtered Cuprous Oxide Thin Films by Ion Implantation’, Master Thesis, University of Oslo, 2017.

4. CHAPTER : THERMAL OXIDATION

4.1 INTRODUCTION

In the previous chapters, preparation of Cu_2O films via two popular thin film deposition techniques, namely Pulsed Laser Deposition and RF Magnetron Sputtering was described in detail. The structural, optical and electrical properties of the films for their potential application as an absorber in a photovoltaic cell was also discussed. Among all the different preparation techniques for Cu_2O absorbers in literature, the most efficient technique producing high performing solar cells till date is thermal oxidation[1], [2]. Hence understanding the properties of the film via this technique will help to better engineer Cu_2O films towards better performing absorbers. Compared to both the other reported techniques in this work, which are vacuum based techniques, thermal oxidation is a low-cost alternative method. Thermal oxidation is a very popular technique wherein by introducing an oxidative agent at high temperature, the sample gets oxidised. Unlike PLD, during this technique the phase of the oxidised sample depends on the phase equilibrium between temperature and pressure (Figure 1.7 in chapter 1). At atmospheric pressure, Cu_2O phase is formed at higher temperatures. Even though reports on preparation of Cu_2O via thermal oxidation dates back to 1984[3] it was only in 2011 Minami et.al[4] reported above 3% efficient solar cell with Cu_2O absorber by optimising the thermal oxidation conditions. Thus, the thermal oxidation process is not straightforward and several factors such as starting copper foil purity, thickness, duration of oxidation, temperature, temperature ramp rate and oxygen concentration inside the furnace determine the phase and grain size of the deposited films. Additionally, there are no sufficient literature describing the thermal oxidation process to obtain high quality Cu_2O as obtained by Minami et.al[5].

The first section of this chapter details the experimental setup used for thermal oxidation in this work, which is followed by the optimization of the oxidised foils by varying the parameters of oxidation in the next section. Variation of oxidation duration on the phase of the foils and the influence of cooling down procedure after oxidation on the structure, morphology and photoluminescence of the foils are discussed in this section. The optimization of the etching parameters to obtain pure Cu_2O foils are discussed later and towards the end of this chapter a small comparison on the structural quality of the Cu_2O prepared via thermal oxidation, PLD and magnetron sputtering are discussed including the crystalline parameters, stress and microstrain.

4.2 EXPERIMENTAL DETAILS OF THERMAL OXIDATION

For the preparation of Cu_2O via thermal oxidation, 0.127 mm thick laminated copper foils (99.9% purity) from Alfa Aesar were used. The foils were cut into 15 x15 mm^2 square size and were cleaned in ultrasonic bath in three steps with acetone, isopropanol and deionized water to remove any dust or unwanted residues from the surface of the copper foils. Figure 4.1 shows the schematics of the thermal oxidation setup. Copper foils were placed horizontally and vertically inside the furnace in alumina crucible. The placement direction was not found to influence the phase of the film. Argon and Oxygen gas were introduced into the furnace through a mass flow controller. As it is important to monitor the amount of oxygen which has a direct influence on the formed oxidised phase, an oxygen gas analyzer was used to measure the amount of oxygen inside the furnace. To have a control on the amount of oxygen to which the Cu foil is exposed during oxidation process, it is important to flush out any oxygen inside the furnace before starting the process, this was achieved with the help of Argon gas. During the temperature ramp up, only Argon gas was introduced into the furnace (maximum flow) and oxygen concentration was monitored with the help of oxygen gas analyzer. Once the temperature has reached the set value, and the oxygen concentration inside is less than 1000 ppm (0.1 %), oxygen gas was introduced into the furnace slowly, carefully monitoring the concentration. The time for oxidation was counted from the time the oxygen concentration inside has reached the required value. The oxygen concentration during thermal oxidation was chosen based on the work of Ievskaya et.al[6]. The temperature for thermal oxidation was chosen based on the thermodynamic considerations to obtain Cu_2O phase. Musa et.al[7] have calculated 1041 ℃ as the “limiting temperature” to eliminate CuO. But they have also reported mixed phase films of Cu_2O and CuO at 1040 ℃ and only Cu_2O phase at 1050 ℃[7]. All the parameters followed for the thermal oxidation of copper foils in this work are listed in Table 11.

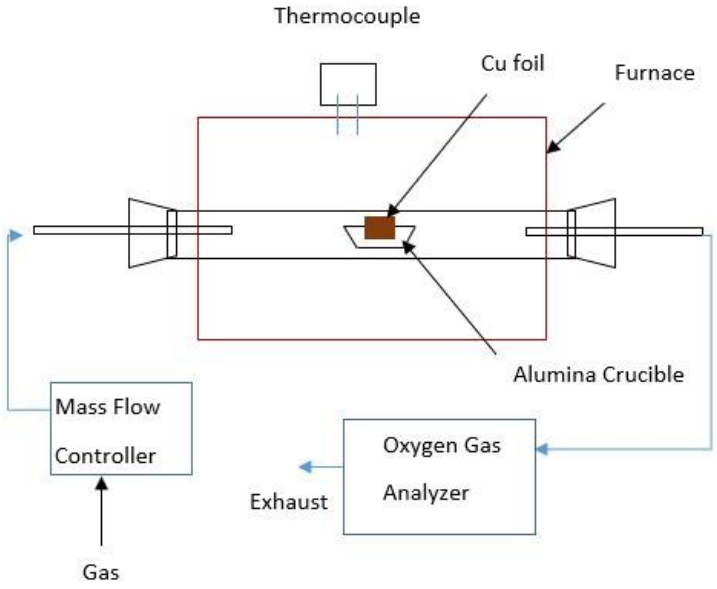

Figure 4.1 Schematics of Thermal Oxidation Setup

Table 11 Parameters during Thermal Oxidation of copper foils

Temperature	1050 ℃
Substrate	Copper Foil (15 mm x15 mm)
Temperature Ramp Rate	20 ℃/min
Oxygen concentration during oxidation	10,000 ppm
Deposition time	1 hour,1.5 hour

After thermal oxidation, the foils were cooled down inside the furnace in Argon flow. The temperature was brought down in steps of 50 °C as the sudden drop in temperature was found to heavily bend the films. In this work the influence of rapid quenching of the films at 500 ℃ and cooling down the films to room temperature inside the furnace were studied and will be discussed in the following sections.

For identifying the phase of the thermally oxidized foils, Raman spectroscopy and X-ray diffraction techniques were used. A Horiba LabRAM ARAMIS Raman spectrometer with 532 nm laser excitation was used for Raman spectroscopy and a Bruker-AXS D8 Advance X-ray diffractometer with CuKα1 radiation (λ = 0.154056 nm) was used for the XRD measurements.

To optimize the oxidised films, the influence of oxidation time and post-oxidation cooling down procedure were varied and the results will be discussed in this section.

4.3 OPTIMIZATION OF THERMALLY OXIDISED FILMS

To optimize the oxidised films, the influence of oxidation time and post-oxidation cooling down procedure were varied and the results will be discussed in this section.

4.3.1 Oxidation Duration

The duration of thermal oxidation of copper foils was varied between one hour and one and half hours to optimize the phase of the oxidised films. Figure 4.2(a) plots the Raman spectra, at an excitation wavelength of 532 nm, for the two investigated durations. Vibrational modes of only Cu_2O (T_{1u} mode, second-order E_u ($2E_u$) mode, and multi phonon process (MPP) mode) was visible in the raman spectra of the film oxidized for 1 hour duration as can be seen in Figure 4.2(a) in comparison to the reference (RRUFF ID:R140763). In contrast, for the film oxidized for 1.5 hours along with the Raman signature peaks of Cu_2O, vibrational modes of CuO are clearly visible. Thus, the thermally oxidised foil with longer duration of oxidation has changed its phase from pure Cu_2O phase to a mixture of Cu_2O and CuO.

As Raman spectroscopy is a local surface analysis technique, further X-ray diffraction studies of the film were carried out to confirm the Cu_2O phase. In the diffraction pattern given in Figure 4.2(b), both the films were crystalline with a preferred orientation of (1 1 1). Comparing the intensity of diffraction peaks, it seems that longer oxidation duration improves the crystallinity of the films. The diffraction peak (2 0 0) has completely disappeared after oxidation for 1.5 hours, which might be due to texturing in the films or due to preferential direction growth as can be seen from the increased intensity of (1 1 1) peak. Similar to the results from Raman spectroscopy, the 1.5 hour oxidized foil showed multiple planes corresponding to CuO phase apart from Cu_2O. In the foil oxidised for an hour, apart from the two very small peaks corresponding to the (0 0 2) and (2 0 0) planes of CuO, (1 1 0), (1 1 1) and (2 2 2) planes of Cu_2O were observed. This is because intrinsically, thermally oxidized Cu_2O films will have small traces of CuO, which gets formed when the oxidized foil meets air after oxidation. Chemical etching of the films is hence recommended before using the film as an absorber. Detailed discussion on the etching parameter optimization and results are discussed towards the end of this chapter.

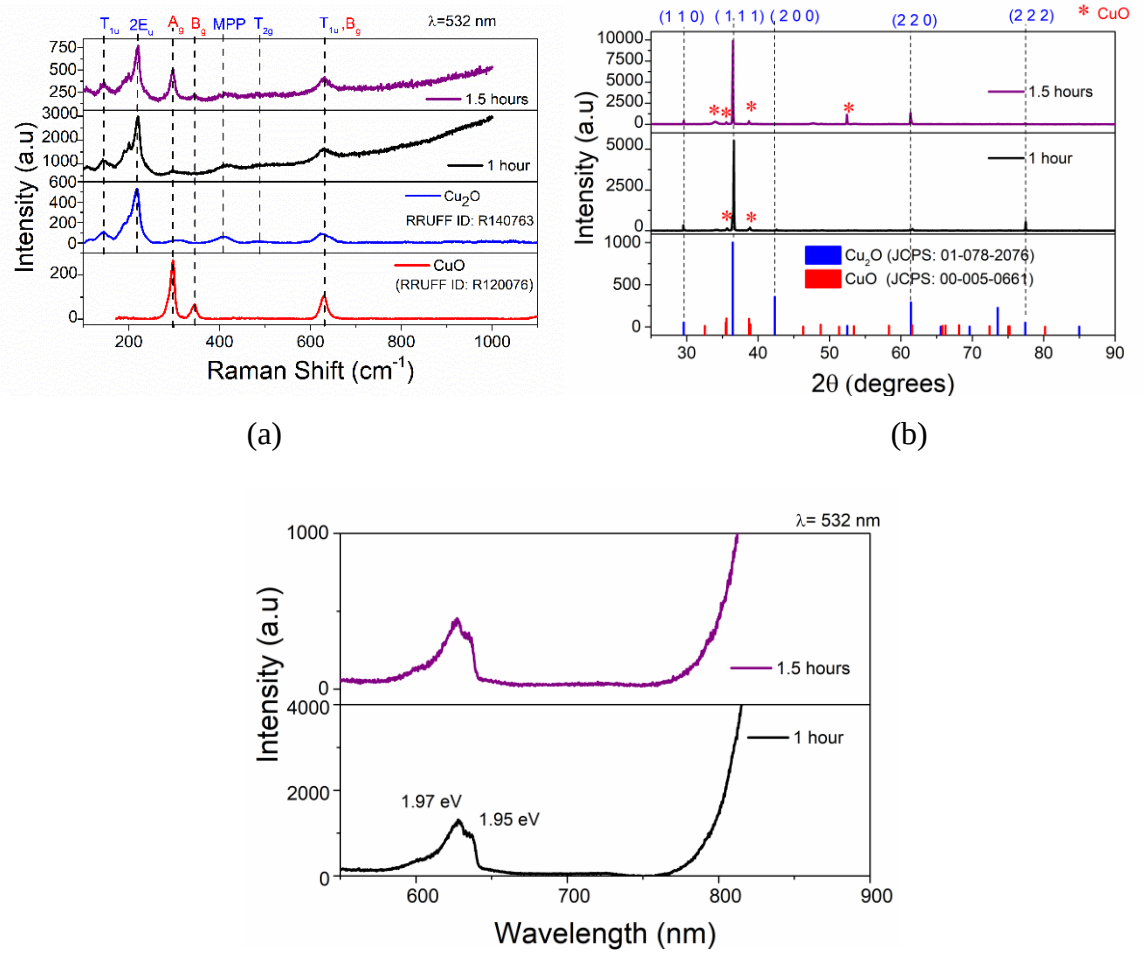

Figure 4.2 Structural Properties of thermally oxidized copper foils for a duration of 1 hour and 1.5 hours (a) Raman spectrum at an excitation wavelength of 532 nm (b) X-ray diffraction pattern (c) Photoluminescence spectra at an excitation wavelength of 532 nm

For employing the film for absorber application, influence of the oxidation duration on the emission characteristics of the oxidised foil was also monitored with the help of photoluminescence measurements. As can be seen in Figure 4.2(c), both the films had two PL peaks, precisely at 1.97 eV and 1.95 eV which could be due to the near band edge emission. The PL intensity was found to be highest for the foil oxidized for 1 hr. The foil oxidized for longer duration might have other non-radiative recombination pathways such as defects. Hence when comparing the foils oxidised for 1 and 1.5 hours, the foil at 1 hr has comparatively less amount of CuO on the surface and higher PL signal.

One of the major issues faced during the thermal oxidation of Cu_2O was the bending/folding of the foils after thermal oxidation. This is a major concern while using these films for solar cells

as it becomes difficult to deposit the back electrode and to establish a contact. Additionally, it is possible that the small CuO peaks observed in the 1 hr oxidised foils might be due to further oxidation of the foils during the cooling down process as there will be smaller amount of oxygen inside the furnace even after completely turning off the oxygen flow. In the oxidation process reported by Ievskaya et.al[6] and Musa et.al[7] rapid quenching of the foils is described and as suggested by Musa et.al it helps to prevent the compressive stress on the oxidised foils. To improve the oxidised foils, and to possibly avoid the bending, rapid quenching was also carried out in this work and a comparison on the properties of oxidised foils which was rapidly quenched versus those that were cooled down to room temperature (RT) are discussed in the next section.

4.3.2 Effect of Quenching Process

To avoid the further oxidation of the foils after thermal oxidation during the cooling down process, and to improve the quality of the foils, the foils oxidised for 1 hour were rapidly quenched at 500 °C by dipping in deionized water. The Raman spectrum of this quenched film is reported in Figure 4.3(a). Unlike expected and reported by others in the literature[7], it can be seen that the spectrum exhibits a vibrational mode of CuO in the raman analysis apart from Cu_2O. A detailed analysis on XRD (Figure 4.3(b)) showed that only one diffraction peak of Cu_2O corresponding to (1 1 0) plane was visible in the rapidly quenched foil. Additionally, this diffraction peak at 29.5° shifted to 22.5°. This shift could be due to an increase in the interplanar spacing (d) to 3.9 Å, according to the Bragg´s law (Equation 2.1 in chapter 02). The d value for the foil cooled down to room temperature in the furnace was 3.02 Å. This change in the d value might be due to change in the lattice parameters. The lattice constant for the rapidly quenched was calculated to be 5.58 Å while for the RT cooled foil was 4.27 Å. This is a clear indication of increased lattice strain, defects or dislocations in the foil. The crystallographic orientation of the foil also changed from (1 1 0) to (1 1 1) when the foil was cooled down to room temperature. Hence the rapidly quenched foils were found to be poor in surface quality compared to the room temperature cooled down foil. Further, the foils were still bended unlike reported by Musa et.al[7].

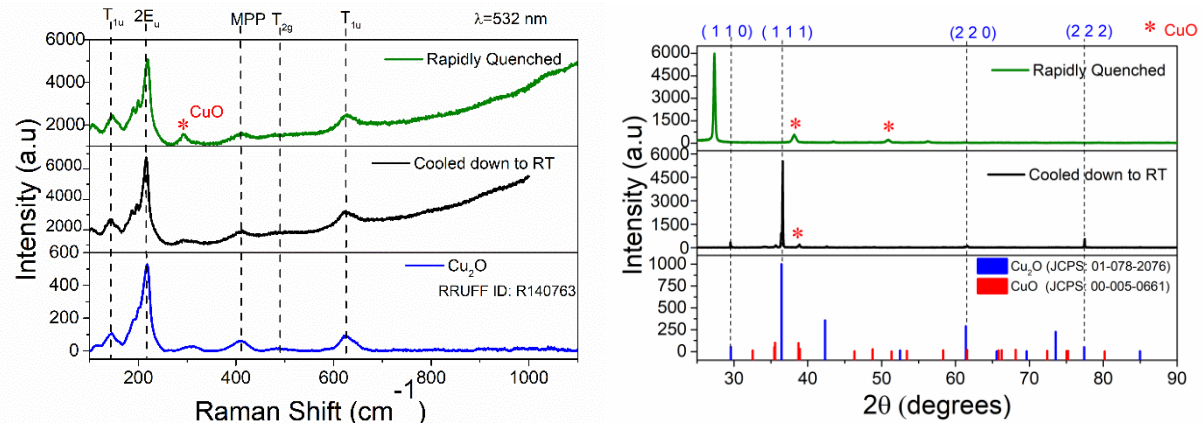

(a) (b)

Figure 4.3 Structural characterization of the thermally oxidised foils rapidly quenched and the foils which were cooled down to room temperature (RT) inside the furnace (a) Raman spectra at an excitation wavelength of 532 nm (b) X-ray diffraction patterns

The influence of the cooling process on the morphology of the oxidised foils were also investigated using microscopy techniques. The grains were clearly visible in the optical microscopy (from the Raman setup) images as can be seen in Figure 4.4(a) and (b). Rapid quenching of the foils after thermal oxidation have resulted in smaller grains. For a better understanding of the influence of cooling procedure on the surface structure of the foils, scanning electron microscopy of the thermally oxidised foils were carried out. Even though much variation in the grain size was not observed in the SEM images, comparing the magnified images in Figure 4.4(d) and (f) the morphology revealed a difference in surface morphology between the foils. The brighter areas in Figure 4.4(d) seems to be a coating of CuO on Cu_2O. Similar morphology was reported by Musa et.al[7] for an oxidised film at 900 °C. Moreover, in the rapidly quenched foils, larger cracks are visible which can cause short circuits during its application in a photovoltaic cell.

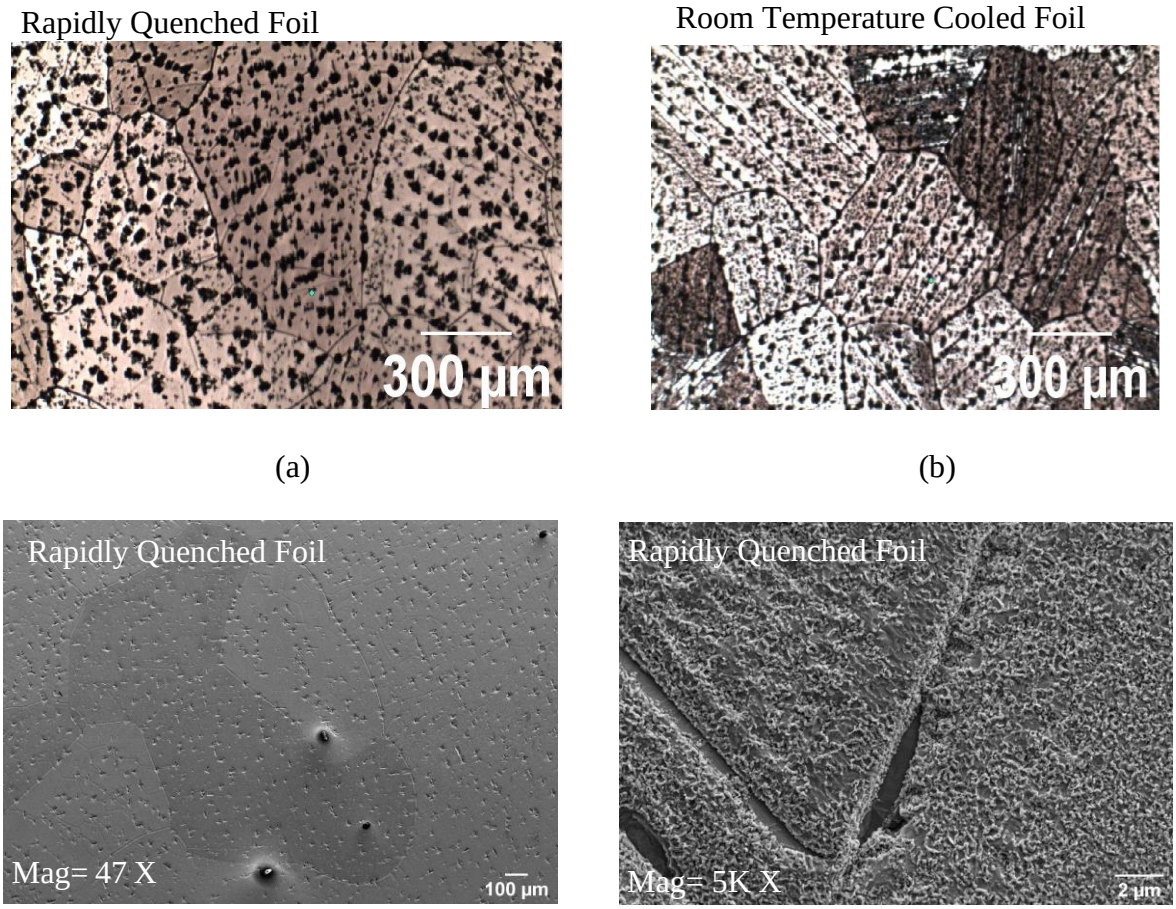

Figure 4.4 Optical microscope image at a magnification of 5X of (a) a rapidly quenched foil (b) room temperature cooled down oxidised foil. Secondary electron images of (c) and (d) rapidly quenched oxidised foil ,(e) and (f) a thermally oxidised foil cooled down to room temperature

Photoluminescence of the foils were also measured for further confirmation on the superior quality of the foil cooled down to room temperature. As can be seen in Figure 4.5 apart from the two PL peaks at 1.95 eV and 1.97 eV an additional wider PL peak at ~ 1.48 eV was observed in the rapidly quenched foil. This might be due to the presence of CuO, which can have a bandgap value smaller than Cu_2O via thermal oxidation.

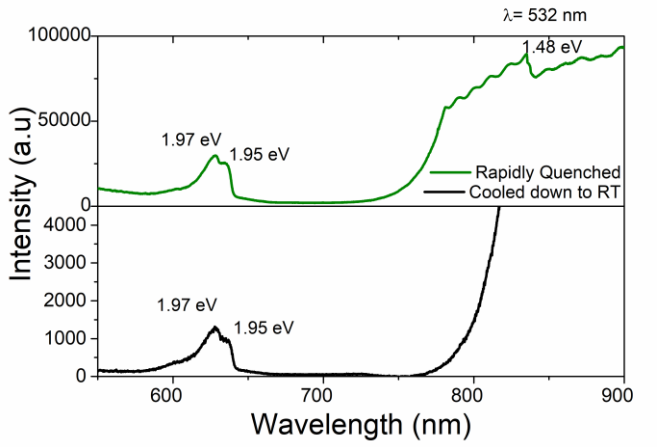

Figure 4.5 Photoluminescence spectrum of thermally oxidised foil rapidly quenched and cooled down to room temperature

Thus, the structural, morphology and photoluminescence analysis of the thermally oxidised foils cooled down via two different methods, points to the better quality and suitability of the foil cooled down to room temperature in the furnace for the application as an absorber. However, in the XRD pattern of even the optimized foils, small peaks of CuO are visible as it is very difficult to obtain only Cu_2O via thermal oxidation due to the low stability. Consequently, while making heterojunctions with thermally oxidised films, it is important to remove the parasitic CuO phase for better performance of the solar cell. This can be achieved by chemically etching the foils to carefully remove CuO. Optimization of the etching conditions are discussed in the next section.

4.4 OPTIMIZATION OF ETCHING PARAMETERS

Parasitic CuO traces on the top of the thermally oxidized Cu_2O were etched with a solution of 69 % concentrated HNO_3 (Nitric acid) and deionized water[6]. The etching parameters namely the acid concentration and etching time were varied in order to find the best conditions. As Raman Spectroscopy was an easily accessible technique to monitor the effect of etching on the phase of the film, etching optimizations were carried out on a sample with visible CuO peak in Raman which was prepared before the optimization of oxygen concentration inside the furnace using oxygen gas analyzer.

Etching trials were carried out using two concentrations of nitric acid, namely, 10% HNO_3 + 90 % H_2O (deionized) and 20% HNO_3 + 80 % H_2O (deionized). The duration of etching was varied between 10-60 seconds in steps of 10 seconds before transferring the foil from etching solution to isopropanol. The etched film was then ultrasonically cleaned using isopropanol and deionized water and dried with nitrogen. The 10% HNO_3 + 90 % H_2O was found to be a very low concentration for etching, as the unwanted CuO peaks, even after 60 s dipping in the etching solution did not diminish in the raman spectra. Further increasing the concentration of the etchant to 20% HNO_3 + 80 % H_2O, CuO peaks were diminished. After 50 s of treatment, a complete was elimination of CuO and pure Cu_2O phase was observed as can be seen in the raman spectra in Figure 4.6 (a). The vibrational mode of CuO at 298 cm^{-1} completely diminished in the foil etched for 50 seconds. Hence the CuO traces can be completely removed from the thermally oxidised foil by etching for 50 s in a solution of 20% HNO_3 + 80 % H_2O.

It was also observed that, since the amount of CuO in the back of the foil is not same as at the front side as when placed horizontally during thermal oxidation, the oxygen exposure is not same, the Cu foil become visible after dipping in the etching solution. Hence to avoid this, during the etching it is recommended to drop the etching solution on the front side of the oxidised foil rather than dipping it in the etchant.

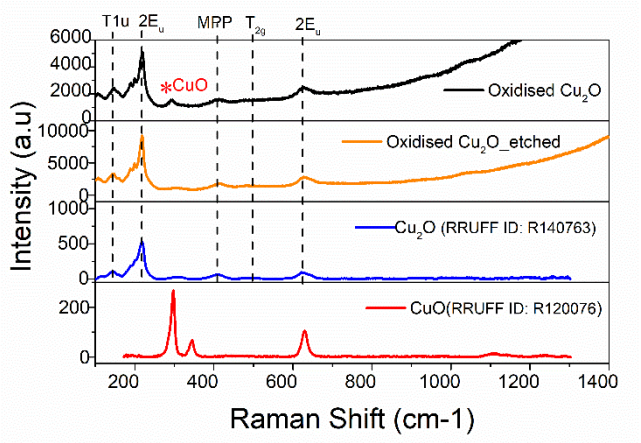

Figure 4.6 Raman spectra of the unetched and etched thermally oxidised Cu_2O

Even though the CuO phase could be successfully etched from the thermally oxidised Cu_2O, it is very important to minimize the time between etching and further deposition of an n-type doped thin film to form a heterojunction. This is because Cu_2O is unstable, and it is almost impossible to avoid CuO formation.

A comparison on the basic properties of the optimized thermally oxidised Cu_2O film with the PLD and sputtered Cu_2O will be discussed in the next section to better understand its potential as an absorber.

4.5 PROPERTIES OF THERMALLY OXIDISED Cu_2O

The structural properties of the optimized thermally oxidised Cu_2O (unetched) were analysed and compared with Cu_2O via PLD and magnetron sputtering. As discussed in the previous section, Raman signature peaks of Cu_2O were observed in the oxidised foil with the presence of E_u mode,T_{1u} mode, second-order E_u ($2E_u$) mode, A_u mode multi phonon process (MPP) mode and T_{2g} mode at 106 cm^{-1}, 145 cm^{-1}, 216 cm^{-1}, 310 cm^{-1} , 412 cm^{-1} and ~ 500 cm^{-1} as can be seen in Figure 3.3 (a). The T_{1u} signal was highest for the oxidised foils compared to Cu_2O via PLD and sputtering. The higher T_{1u} signal which is due to the presence of higher copper vacancies and interstitials in the film[8] shows that thermally oxidised foils contain a higher charge carrier concentration. The intensity ratio of T_{1u} and $2E_u$ mode is only 0.36 for the thermally oxidised which is the least compared to PLD (0.43) and sputtered (0.66) films and is an indication that thermal oxidation produce good quality Cu_2O with less surface damage[9].

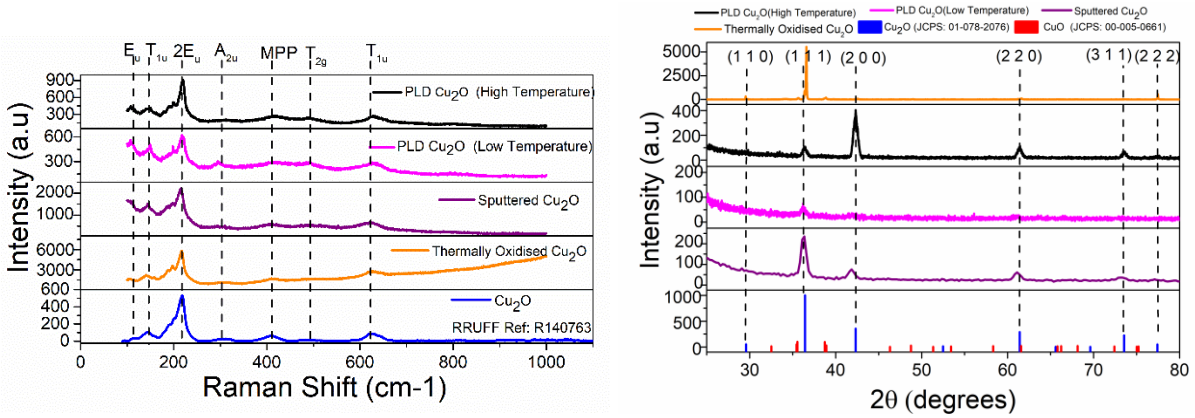

(a) (b)

Figure 4.7 (a) Raman spectra of Cu_2O via three different techniques at 532 nm excitation wavelength(b) Diffraction pattern of Cu_2O via three different techniques

Similar to sputtered Cu_2O, from the X-ray diffraction studies it was revealed that the thermally oxidised foils had a preferred orientation of (1 1 1). As expected, the oxidised foils exhibit a higher crystallinity (full width half maximum lowest) compared to the other Cu_2O films as can be seen in Figure 3.3(b). Table 12 lists the crystalline parameters calculated from the significant diffraction peaks of the thermally oxidised Cu_2O. The full width half maximum of the diffraction peaks is much smaller confirming that oxidised foils have good crystallisation.

Table 12 Lattice Parameters, Crystallites Sizes and Micro strain of thermally oxidised Cu_2O calculated from the significant X-ray diffraction peaks

2θ (°)	FWHM (°)	d spacing (Å)	Grain Size (nm)	Lattice Constant (Å)
29.53	0.07	3.02	117.35	4.27
36.59	0.09	2.45	89.06	4.25
77.47	0.08	1.23	121.40	4.26

As can be seen from Table 13, the oxidised foils show higher mean grain size of 109.3 nm from the Scherrer´s equation[10] which is seven times higher than the mean grain size of the PLD film. Increase in grain size decreases recombination and scattering at grain boundaries improving the overall electrical properties of the films. The mean lattice parameter of the oxidised foil was 4.26 Å which is close to pure Cu_2O. The oxidised foil had negligible tensile stress of 0.07 but is higher than the PLD film, which could be due to the increased grain size.

Table 13 Comparison on the Crystalline Parameters of Cu_2O prepared via different techniques

Preparation Method	d spacing (Å)	Mean Grain Size (nm)	Lattice Constant (Å)	Stress (GPa)
PLD	1.87±0.6	15.11	4.27	0.01
Magnetron Sputtering	1.88±0.6	10.1	4.3±0.02	0.21
Thermal Oxidation	2.12±0.3	109.30	4.26±0.01	0.07

Figure 4.8 compares the photoluminescence of the Cu_2O from different preparation routes. It is found that the emission peak corresponding to the near band edge emission is at the same wavelength for all the Cu_2O prepared via PLD, sputtering and thermal oxidation even though the excitation wavelength was different for the magnetron sputtered film. Furthermore, the

shape of the PL peak was identical for both the thermally oxidised and PLD Cu_2O and as expected the thermally oxidised foil showed higher intensity PL peak which is an indication that the non-radiative recombination pathways is lower for the thermally oxidised Cu_2O compared to PLD Cu_2O. Hence the density of defects might be lesser for oxidised foil than those in the PLD film. Only in the sputtered film, PL peaks at higher wavelengths are visible. The origin of this peak is not yet clear. As explained in chapter 03, this could be attributed to the presence of copper vacancies and interstitials. The reason it was not visible in the PL spectra of the other two Cu_2O could be due to the different excitation wavelength. Since the peak is broader in the near infrared (IR) region it could be due to overlapping emission from multiple defect related recombination centres which was not observed in the PLD Cu_2O and thermally oxidised foil.

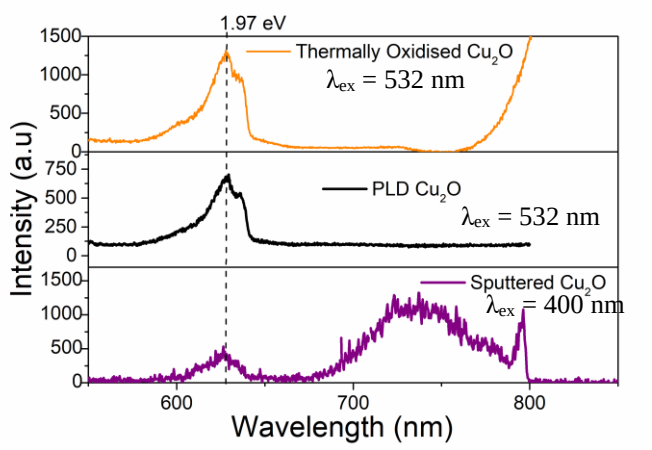

Figure 4.8 PL spectra of Cu_2O via different techniques

Apart from the better surface quality of the oxidised foils, there are a few factors limiting its application. The major problem encountered was that the oxidised foils were very fragile and breaks easily during handling or during deposition of subsequent layers on the thermally oxidised absorber. The surface roughness of the foils was analysed using Atomic Force Microscopy (Figure 4.9). Even though the roughness of the oxidized foils measured using AFM was 16.83 nm (for a 5x5 μm^2) which is smaller the PLD film, after etching the roughness was found to increase to 160 nm. But these drawbacks do not diminish its potential as an absorber and in the next chapter application of all the films in a photovoltaic cell is illustrated.

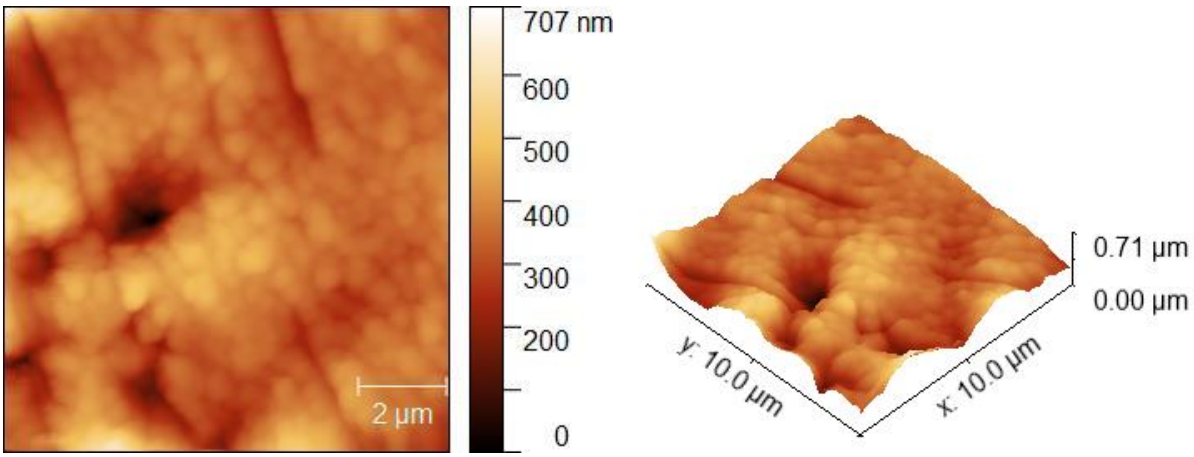

(a) (b)

Figure 4.9 AFM image of a thermally oxidised Cu_2O (unetched) (a) 2D image (10x 10 μm^2) (b) 3D image

4.6 CONCLUSION

In this chapter, optimization of Cu_2O obtained by direct thermal oxidation of copper foils was discussed. Thermal oxidation at 1050 ℃ for one hour duration and further cooling of the foils to room temperature inside the furnace was found to produce good quality Cu_2O foils with small traces of CuO. The parasitic CuO phase was removed by etching in nitric acid. The etching duration and concentration of the etchant was optimized to obtain pure Cu_2O phase. The structural properties of the thermally oxidised Cu_2O revealed better quality than the PLD and sputtered Cu_2O films. Larger grains with flat morphology were observed thanks to the scanning electron microscopy and atomic force microscopy analysis. Additionally, thermally oxidised foils showed higher photoluminescence than the PLD and sputtered Cu_2O. Even though the basic characterization of the thermally oxidised Cu_2O has shown better properties, for a better understanding of the superior performance of the thermally oxidised Cu_2O absorbers, the Cu_2O film via different techniques were analysed using advanced characterization techniques as displayed in the next chapter.

4.7 REFERENCES OF CHAPTER 04

[1] T. Minami, Y. Nishi, and T. Miyata, 'Efficiency enhancement using a Zn $_{1-x}$ Ge $_{x}$ -O thin film as an n-type window layer in Cu $_{2}$ O-based heterojunction solar cells', *Appl. Phys. Express*, vol. 9, no. 5, p. 052301, May 2016, doi: 10.7567/APEX.9.052301.

[2] T. Minami, Y. Nishi, and T. Miyata, 'Heterojunction solar cell with 6% efficiency based on an n-type aluminum–gallium–oxide thin film and p-type sodium-doped Cu2O sheet', *Applied Physics Express*, vol. 8, no. 2, p. 022301, Jan. 2015, doi: 10.7567/apex.8.022301.

[3] W. M. Sears and E. Fortin, 'Preparation and properties of Cu2O/Cu photovoltaic cells', *Solar Energy Materials*, vol. 10, pp. 93–103, May 1984.

[4] T. Minami, Y. Nishi, T. Miyata, and J. Nomoto, 'High-Efficiency Oxide Solar Cells with ZnO/Cu $_{2}$ O Heterojunction Fabricated on Thermally Oxidized Cu $_{2}$ O Sheets', *Appl. Phys. Express*, vol. 4, no. 6, p. 062301, May 2011, doi: 10.1143/APEX.4.062301.

[5] T. Minami, Y. Nishi, and T. Miyata, 'High-Efficiency Cu $_{2}$ O-Based Heterojunction Solar Cells Fabricated Using a Ga $_{2}$ O $_{3}$ Thin Film as N-Type Layer', *Appl. Phys. Express*, vol. 6, no. 4, p. 044101, Apr. 2013, doi: 10.7567/APEX.6.044101.

[6] Y. Ievskaya, R. L. Z. Hoye, A. Sadhanala, K. P. Musselman, and J. L. MacManus-Driscoll, 'Improved Heterojunction Quality in Cu_2O-based Solar Cells Through the Optimization of Atmospheric Pressure Spatial Atomic Layer Deposited $Zn_{1-x}Mg_xO$', *JoVE*, no. 113, p. 53501, Jul. 2016, doi: 10.3791/53501.

[7] A. O. Musa, T. Akomolafe, and M. J. Carter, 'Production of cuprous oxide, a solar cell material, by thermal oxidation and a study of its physical and electrical properties', *Solar Energy Materials and Solar Cells*, p. 12, 1998.

[8] T. Sander *et al.*, 'Correlation of intrinsic point defects and the Raman modes of cuprous oxide', *Phys. Rev. B*, vol. 90, no. 4, p. 045203, Jul. 2014, doi: 10.1103/PhysRevB.90.045203.

[9] A. Compaan, 'Surface damage effects on allowed and forbidden phonon raman scattering in cuprous oxide', *Solid State Communications*, vol. 16, no. 3, pp. 293–296, Feb. 1975, doi: 10.1016/0038-1098(75)90171-4.

[10] A. L. Patterson, 'The Scherrer Formula for X-Ray Particle Size Determination', *Phys. Rev.*, vol. 56, no. 10, pp. 978–982, Nov. 1939, doi: 10.1103/PhysRev.56.978.

[11] A. R. Stokes and A. J. C. Wilson, 'The diffraction of X rays by distorted crystal aggregates - I', *Proceedings of the Physical Society*, vol. 56, no. 3, pp. 174–181, May 1944, doi: 10.1088/0959-5309/56/3/303.

5. CHAPTER : ADVANCED CHARACTERIZATIONS OF Cu_2O ABSORBERS

5.1 INTRODUCTION

Preparation of Cu_2O via three different routes was described in the previous chapters. In this chapter we focus on the application of the prepared Cu_2O as absorbers in a solar cell and further advanced characterization of the films to better understand the difference in the Cu_2O absorbers prepared via PLD, RF Magnetron Sputtering and Thermal Oxidation.

The first section of this chapter describes the state-of-the-art Cu_2O heterojunctions followed by a description and properties of the different TCOs used in this work. Subsequently we discuss the performance of our Cu_2O solar cells prepared with thin film absorbers via PLD, magnetron sputtering and Cu_2O sheet via thermal oxidation. Further we compare the charge carrier dynamics, surface photovoltage, PL kinetics etc of the different Cu_2O absorbers to find an answer to why the thermally oxidised Cu_2O sheets have better photovoltaic performance.

5.2 STATE OF THE ART Cu_2O HETEROJUNCTIONS

Despite many advantages like high absorption coefficient in the visible region, suitable bandgap and good minority carrier diffusion lengths (10 μm[1]), which are likely to give high energy conversion efficiency to Cu_2O solar cells, the practically achieved efficiency till date is still lower than 10 %. One of the main challenges for the low performance of Cu_2O solar cells is that due to the intrinsic p-type conductivity of the films, to form a heterojunction with Cu_2O, an appropriate n-type layer with suitable energy band alignment is required. Since Cu_2O have a low electron affinity of 3.2 eV, the potential n-type candidates to make the junction are limited. Since Cu_2O is a self-compensated semiconductor with intrinsic defects, n-type doping to form Cu_2O homojunction is also very challenging. Additionally, since the Cu_2O surface is very reactive, it is highly susceptible to oxidation or reduction (low enthalpy of formation of Cu_2O), interfacial Cu or CuO formation further deteriorate the efficiency[1], [2]. At Cu_2O /metal Schottky junctions, Cu rich region forms regardless of the metal thus reducing the Schottky barrier height and limiting the open circuit voltage (V_{oc})[2], [3]. Hence it is important to fabricate devices with high barrier heights and stoichiometric Cu_2O at the interface. As discussed in Chapter 01, deposition of n-type TCO on polycrystalline thermally oxidised Cu_2O

have shown better performance compared to thin film heterojunctions in literature (Figure 1.8). In this chapter through different characterization techniques, we explain this change in performance of Cu_2O solar cells with the preparation method of the absorber.

The most used heterojunction partner for Cu_2O is ZnO[4]–[8]. However, due to band-edge misalignment (type -II band alignment) the built-in voltage between Cu_2O/ZnO is only 0.75-0.87 eV, limiting V_{oc} values to less than 600 mV[9]. The conduction band discontinuity between ZnO and Cu_2O is ~1.1 eV[10]. Olsen et.al[2] have mentioned that to achieve a 10 % efficient solar cell with Cu_2O, a built-in voltage of 1.4 eV is required. For a semiconductor of bandgap 2.17 eV, the Shockley-Quiesser limit for device photovoltage is ~ 1.7 eV. It has been reported in several work that Zn reduces Cu_2O at the interface forming Cu which reduces the barrier height[1],[11]. Several numerical studies have also reported that a defect layer at the interface should be introduced to match the experimentally reported properties of Cu_2O/ZnO heterojunction[12],[13]. Other Cu_2O heterojunctions investigated include AZO[14], CdO[7], Ga_2O_3[15]–[17], ITO[4]. There were also reports on the use of ternary oxides as electron selective contacts (buffer layers) at the heterojunction which increased the V_{oc} and efficiency including, Zn(O,S)[18],[19], Zn_2SnO_4[20], $(Ga_{0.975},Al_{0.025})_2O_3$[15], $ZnGa_2O_4$[21], $Zn_{0.38}Ga_{0.62}O$[22]. The intermediate buffer layer minimizes interface recombination by improving the band alignment and interface defect density. Figure 5.1 shows the photovoltaic performance of Cu_2O solar cells with different ternary compounds. By far the highest efficient solar cells based on Cu_2O with 8.1 % efficiency was reported by Minami et.al[22] with ternary buffer layer and Na doped Cu_2O. As can be seen in the table in Figure 5.1, with change in the heterojunction, the efficiency increased from 5.4 to 8.1 % which clearly shows the importance of choosing the right heterojunction partner for Cu_2O. The deposition condition as well as the method of deposition of TCO is also significant as reported by Minami et.al[23], Nishi et.al[24]. Low temperature, low damage techniques for the deposition of buffer layer will improve the performance of the solar cells with thermally oxidised Cu_2O absorbers.

Minami et.al[16],[25] have illustrated the importance of low damage deposition techniques for TCO and have demonstrated that when AZO films were deposited via PLD, the power conversion efficiency of the subsequent photovoltaic cell increased to 2.5 % compared to 1.2-1.4 % for a similar cell with AZO deposited via dc or rf magnetron sputtering. They connect this to the variation in the amount of oxygen interacting with the Cu_2O surface during the deposition of TCO.

The influence of deposition temperature and partial pressure during the deposition of the n-type on the efficiency of Cu_2O solar cell was studied by Minami et.al[26]. They have found that RT deposition of the TCO layer decreases series resistance and also observed a decrease in the shunt resistance with increase in the temperature of deposition due to the increase in the leakage current. With the increase in temperature of TCO deposition, they observed degradation of Cu_2O sheet surface and interdiffusion of metals at the interface. They have also reported that the oxygen partial pressure during deposition has no influence on the performance and the pre-deposition condition of Cu_2O surface is only significant.

Solar cell architecture	η (%)	V_{oc} (V)	J_{sc} (mA/cm^2)	FF (%)
AZO/$Zn_{0.38}Ge_{0.62}O$/Cu_2O/Au	8.10	1.1	~10	~65
AZO/$(Ga_{0.975}Al_{0.025})_2O_3$/$Cu_2O$:Na/ Au	6.25	0.84	10.8	69
AZO/$(Ga_{0.975}Al_{0.025})_2O_3$/$Cu_2O$:Na/Au	6.10	0.84	10.95	66
AZO/$(Ga_{0.975}Al_{0.025})_2O_3$/$Cu_2O$/Au	5.42	0.84	10.11	64
AZO/Al-Ga-Mg-Zn-O/Cu_2O:Na/Au	5.40	0.96	10.6	53
AZO/$ZnGa_2O_4$/Cu_2O/Au	5.36	0.81	10.22	65
AZO/$(Zn_{0.91}Mg_{0.09})_2O_3$/$Cu_2O$/Au	4.29	0.80	9.11	59
AZO/Zn_2SnO_4/Cu_2O/Au	3.64	0.63	9.93	59
AZO/$ZnSnO_3$/Cu_2O/Au	2.92	0.57	9.99	51
AZO/Zn-Sn-O/Cu_2O/Au	2.65	0.55	7.37	65
AZO/$MgIn_2O_4$/Cu_2O/Au	2.58	0.50	7.82	66
AZO/$GaInO_3$/Cu_2O/Au	2.22	0.52	8.13	52
AZO/$CuGaO_2$/Cu_2O/Au	1.49	0.33	8.09	56
AZO/Zn_2FeO_4/Cu_2O/Au	1.24	0.44	5.04	56
AZO/$CuInO_2$/Cu_2O/Au	0.75	0.29	5.35	49
AZO/$AgInO_2$/Cu_2O/Au	0.12	0.24	1.19	45
AZO/Zn_2GeO_4/Cu_2O/Au	0.03	0.35	0.21	40
AZO/Zn_2SiO_4/Cu_2O/Au	0.01	0.39	0.04	48

Figure 5.1 Performance of thermally oxidised Cu_2O absorber based solar cells with different heterojunctions with n-type ternary compounds copied from Coll et.al[27]

5.2.1 Transparent Conducting Oxides for Cu_2O

As detailed in the previous section choosing the right TCO with Cu_2O is the key in obtaining better performing photovoltaic cell. Here for the comparison of the I-V properties of the Cu_2O absorbers prepared via PLD, Magnetron sputtering and Thermal Oxidation, for forming a heterojunction, several n-type thin films were used. Their preparation and basic properties will be discussed in this section.

In this work ZnO and AZO films were prepared via PLD using commercially bought targets. Room Temperature (RT) deposition at an oxygen partial pressure of 10^{-2} mbar was chosen as the deposition parameters to avoid any damage to the Cu_2O surface. The ZnO and AZO films used in this work had good carrier concentration in the range of -10^{20} cm^{-3} and lower resistivity

in the range of 10^{-4} Ωcm. Zn_2SnO_4 (ZTO) was another TCO used in this work which was prepared via Magnetron Sputtering at 300 ℃ with carrier concentration of -10^{19} cm^{-3} and lower resistivity in the range of 10^{-3} Ωcm. Commercially bought conductive substrate of 1x1 cm^2 Nb (1 at %) doped $SrTiO_3$ (STO) (001) with a resistivity of 0.01 Ωcm which is also an n-type semiconductor was also used for epitaxial growth of Cu_2O thin film to form a heterojunction.

As from literature an n-type buffer layer of $Zn_{1-x}Ge_xO_4$ was reported to improve the efficiency of Cu_2O solar cell[24], a PLD target was prepared by mixing 5g of ZnO_2 and 3.166 g of GeO_2 followed by cold pressing and sintering at 1000 ℃. However, the films deposited at different temperatures and oxygen partial pressures were not conducting and an optimized deposition parameters could not be found.

Since the open circuit voltage from the p-type Cu_2O/n-type semiconductor is related to the diffusion potential of the heterojunction which is based on the work function of the semiconductors[28], it is important to check the work function of the TCOs before implementing the heterojunctions. The work functions of the TCOs and Cu_2O absorbers prepared via different techniques were measured using Kelvin Probe Technique and is listed in the Table 14. Work function of ZnO and AZO are similar to the value reported in literature 4.71 eV and 4.62 eV[29] respectively. The work function of ZTO is similar to the value reported for amorphous ZTO by Yeh et.al[30].

Table 14 Work function of the TCOs and the Cu_2O prepared via different techniques calculated via the Kelvin Probe Technique

Sample	Work function (eV)
ZnO	4.83
AZO	4.64
Nb:STO	4.62
ZTO	5.00
Cu_2O (PLD)	4.98
Cu_2O (Sputtering)	5.12
Cu_2O (Oxidised)	5.25

Comparing the work function difference of all the TCOs and the Cu_2O films, the ZTO film have the highest work function difference. Hence better open circuit voltage should be observed but

since the optimized deposition condition of ZTO is at 300 ℃, it might damage the surface of the Cu_2O sheet prepared via oxidation. Comparing all the Cu_2O films, the oxidised sheet have a higher work function which might be because since the measurement is done in air, CuO, which have higher work function[31] might have formed on the surface of the thermally oxidised sheet. The I-V properties of the heterojunctions with the different TCOs will be discussed in the next section.

5.3 I-V PROPERTIES OF THE Cu_2O ABSORBERS

To check the photovoltaic behaviour of the Cu_2O absorbers prepared via PLD, magnetron sputtering and thermal oxidation, solar cells were prepared and their I–V properties were measured using a AAA rated ORIEL Verasol-2 LED Solar Simulator (LSS-7120) and a Keithley 2461 Source Measure Unit. As discussed in the previous section, different TCOs were used to form a heterojunction with the p-type Cu_2O prepared via different techniques.

(a) Pulsed Laser Deposition

For the PLD Cu_2O film, even though heterojunction was formed with different TCOs, a working solar cell was obtained only for two architectures. Even though a p-n junction behaviour was indeed observed with ZnO and AZO, a current even though in micro ampere range was obtained only for the architecture with a buffer layer of $Zn_{1-x}Ge_xO_4$ between the Cu_2O and AZO. As the back contact, approximately 100 nm layer of $La_{0.67}Sr_{0.33}MnO_3$ (LSMO) was pulsed laser deposited at 750 ℃ temperature and 10^{-2} mbar oxygen partial pressure, on quartz substrate. On top of the LSMO layer, approximately 150 nm Cu_2O layer was deposited followed by 100 nm each of the buffer layer and AZO at room temperature and 10^{-2} mbar oxygen partial pressure via a steel mask of 1 mm^2 forming a solar cell with architecture Quartz//LSMO/Cu_2O/ $Zn_{1-x}Ge_xO_4$/AZO. An open-circuit voltage of 0.1 V and a small, short circuit current density of 0.02 mA/cm^2 was measured from the solar cell measured in dark and light conditions using a solar simulator at 1 sun under AM 1.5 G conditions (Figure 5.2(a)). The shape of the current density vs voltage curve can give a lot of information about resistance problems, insulation layer formation, mobility issues etc. As can be seen in Figure 5.2(a), both the dark and illuminated J-V are hanging curves (non-zero current in dark and non-saturation of current at higher voltage for light measurement) in the backward direction (0 V to negative bias). This behavior upon illumination is an indication of carrier transport problems. The hanging dark curve is due to

higher shunt resistance caused due to leakage current. Leakage current can occur in a solar cell through pinholes in the film, solar cell edges etc. A kink in the J-V curve at positive voltage values which was also observed could be an indication of carrier accumulation due to defects at interfaces, formation of energy barrier etc.

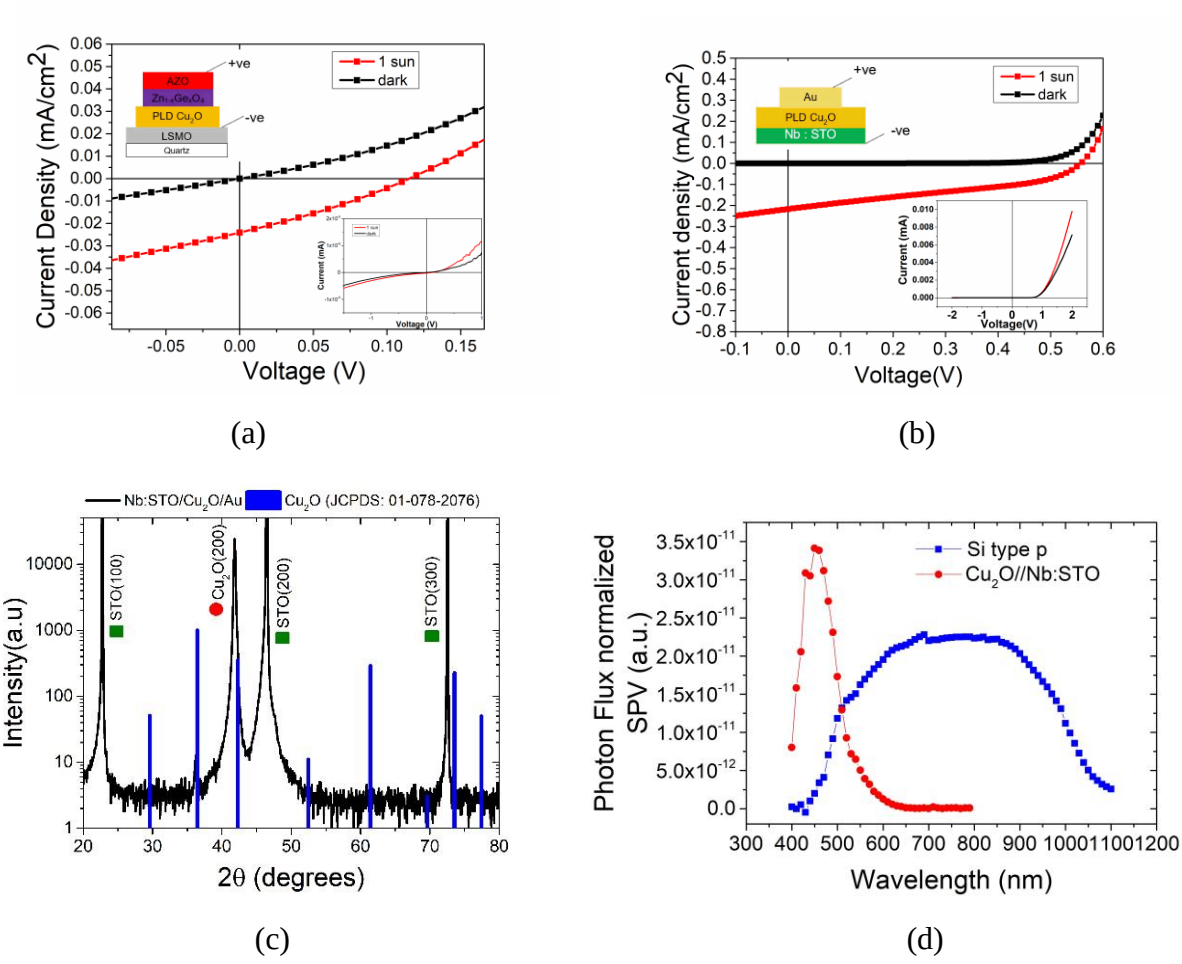

Figure 5.2 Current density vs voltage of measured in dark and 1 sun of solar cell with (a)PLD Cu_2O (b) epitaxially grown PLD Cu_2O on Nb:STO. A schematics of the corresponding solar cell architecture is given in the inset (c) θ-2θ XRD diffractogram of (0 0 1) oriented Nb:STO//Cu_2O (100 nm)/Au (7 nm) (d) Surface Photovoltage Spectroscopy of the best performing solar cell with PLD Cu_2O and p-type silicon by normalizing the SPV by the photon flux versus the wavelength of the light

To improve the performance of solar cells with PLD Cu_2O, a thin film was epitaxially grown on a crystalline and conductive substrate of Nb doped $SrTiO_3$(001). A cube-on-cube epitaxial relationship of Cu_2O and STO (Cu_2O (100)//STO (100)) in heteroepitaxial growth of the film on the substrate[32], [33], even though there is a high lattice mismatch of 8.5 % between them. The diffraction peak of this film exhibited a single peak at (200) confirming epitaxial growth

as can be seen in Figure 5.2(c). The other peaks at 2θ = 22.7°, 46.5°, and 72.5° are from STO (100), STO (200), and STO (300) respectively. Nb:STO is also an n-type semiconducting oxide forming a heterojunction with Cu_2O. A thin semitransparent layer of Au (7 nm with 58 % transmission at 550 nm) was deposited as the top electrode by evaporation through a 1 mm^2 steel mask forming a solar cell with architecture Nb:STO (001)//Cu_2O (100 nm)/Au. The solar cell exhibited a good open circuit voltage of 0.56 V but a low short circuit current density of 0.21 mA/cm^2 at AM 1.5 G conditions using a solar simulator. As can be seen from the current density vs voltage curve in Figure 5.2(b) there has been definite improvement in the photovoltaic behavior when the film was grown epitaxially. Apart from the lower thickness of Cu_2O and absorption due to Au electrode, the lower current might be due to heterojunction defects or Cu_2O defects which will be discussed in detail in the upcoming sections on advanced characterization. The solar cell exhibited an efficiency of 0.053 % and fill factor of 45 %. The efficiency is comparable to the values reported in the literature for PLD Cu_2O[32] considering a 20 % efficiency increase with optimal Cu_2O thickness (1000 nm instead of 100 nm) and influence of Au top layer which reduces the efficiency by a factor of ~ 2. The open-circuit voltage which corresponds to the built-in potential at the Nb:STO/Cu_2O heterojunction, is higher than the diffusion potential calculated from the work function difference which is 0.36 V. Hence this high V_{oc} can´t be explained solely based on the work function difference, as the diffusion potential is also influenced by the quality of the interface of Cu_2O and n-type semiconductor. As reported by Cendula et.al[28], for heterojunction solar cells, the open circuit voltage can exceed the built in voltage due to the influence of additional factors due to steps in electron affinity or density of states.

To understand more about the efficiency of charge separation in the PLD Cu_2O solar cell, as the current generated was very low from the I-V measurements, Surface Photovoltage Spectroscopy (SPS) measurements were carried out. A Kelvin Probe system (KP Technology KP020) with a 2 mm diameter gold tip and GR50–605 (Thorlabs) monochromator of 600 g/mm-1 grating was used for the spectroscopic SPV measurements. As can be seen in Figure 5.2(d) a high photon flux was visible only in the wavelength region of 400-600 nm and after 600 nm the photon flux is zero since the bandgap of the Cu_2O film (~ 2.1 eV) is higher than Si (1.1 eV). Hence compared to using a Si absorber, when using Cu_2O absorber, only higher energy photons can create charge carriers by absorption. Therefore, the current generated from

Cu_2O solar cells will be much smaller than Si based solar cells as in most of the visible region of the light, the absorption is zero for the Cu_2O absorber.

(b) Magnetron Sputtering

To analyze the I-V properties of sputtered Cu_2O, ~100 nm Cu_2O film was sputtered on ITO substrate followed by PLD of ~ 100 nm AZO layer as the top contact forming a heterojunction of Cu_2O/AZO. From the current density vs voltage characteristics measured using a solar simulator, the device showed a photovoltaic effect with an open circuit voltage of 0.26 V and short-circuit current density of 1.76 mA/cm^2(Figure 5.4(a)). The poor open-circuit voltage could be due to the high conduction band offset between Cu_2O and AZO (Figure 5.3(b)) which affects the efficient charge separation. Similar to the performance of the PLD Cu_2O solar cell with AZO, hanging curves were observed in the J-V characteristics as can be seen in Figure 5.4(a) which could be an indication of mobility issues and leakage current. Compared to the performance of PLD Cu_2O with similar heterojunction, better open circuit-voltage and short-circuit current density was observed in sputtered Cu_2O. Additionally the short circuit current density was higher than the epitaxially grown PLD Cu_2O/Nb:STO heterojunction (Table 15) which clearly shows the better quality of sputtered film over the epitaxial PLD Cu_2O. The solar cell with sputtered Cu_2O have shown a better efficiency of 0.127 % but a lower fill factor of 27.8 %. Other heterojunctions with ZnO and ZTO investigated with sputtered Cu_2O however gave lower current and open circuit voltage (less than 20 mv).

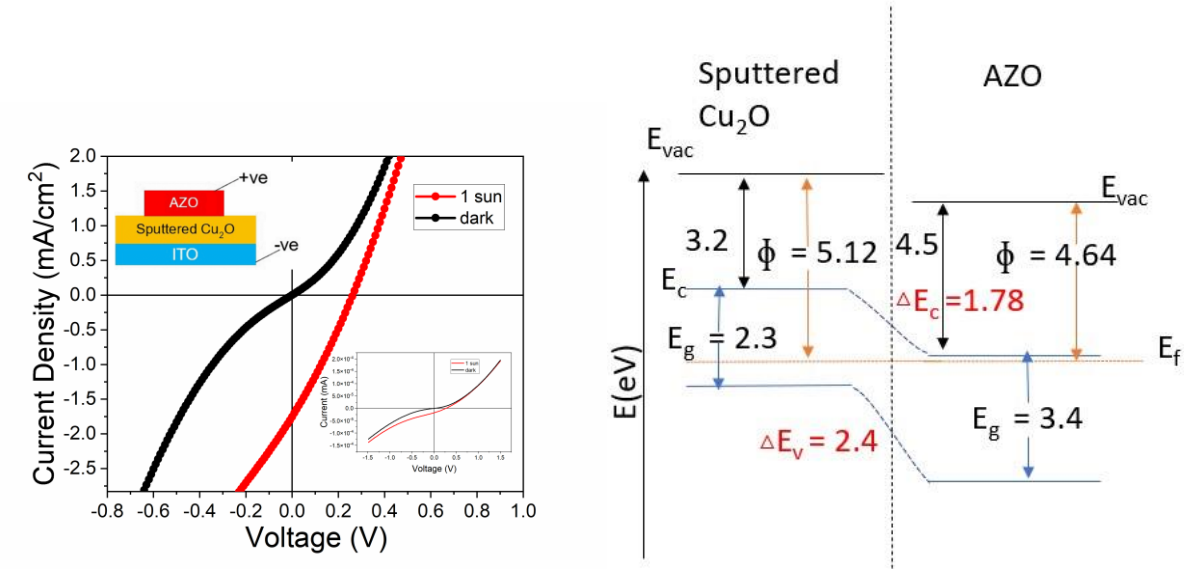

(a) (b)

Figure 5.3 (a) Current density vs voltage characteristics of ITO/Sputtered Cu_2O/AZO (b) energy band diagram of the heterojunction Cu_2O/AZO

(c) Thermal Oxidation

Compared to the sputtered Cu_2O solar cell, the thermally oxidised Cu_2O solar cell did not show much higher performance unlike expected. As can be seen in Figure 5.4(a) the shape of the J-V curve was more affected by lower shunt resistance and higher series resistance caused by leakage current and defects respectively. As can be seen from Table 15, only the short circuit current density was slightly higher than the solar cell from the sputtered Cu_2O. Unlike the sputtered Cu_2O solar cell, the heterojunction was formed with 100 nm PLD deposited ZnO (RT, 10^{-2} mbar) and further a 100 nm layer of AZO was deposited via PLD. A 100 nm Au layer was deposited via PLD at room temperature in vacuum behind the oxidised sheet as the back contact. Compared to the sputtered Cu_2O/AZO heterojunction, as can be seen in the energy band diagram in Figure 5.4(b), the band offsets had improved with thermally oxidised Cu_2O/ZnO heterojunction which should ideally reflect in the performance of the solar cell, but it was not observed. The reason for this will be further discussed based on surface photovoltage results of the heterojunction in the upcoming section on advanced characterization. For the application of thermally oxidised Cu_2O sheet in a solar cell there were many challenges including surface oxidation, large cracks/grain boundaries, bending of the films etc. Before its application into a solar cell, the Cu_2O sheet was etched to remove parasitic CuO layer at the optimized etching

conditions. The deposition of the n-type was carried out as quickly as possible but there has been exposure to air meanwhile during the transport from the etching lab to the PLD lab. Additionally, during the deposition of ZnO and AZO via PLD, the layer further gets exposed to oxygen which might have led to CuO formation at the interface which further reduces barrier height and decrease the open circuit voltage.

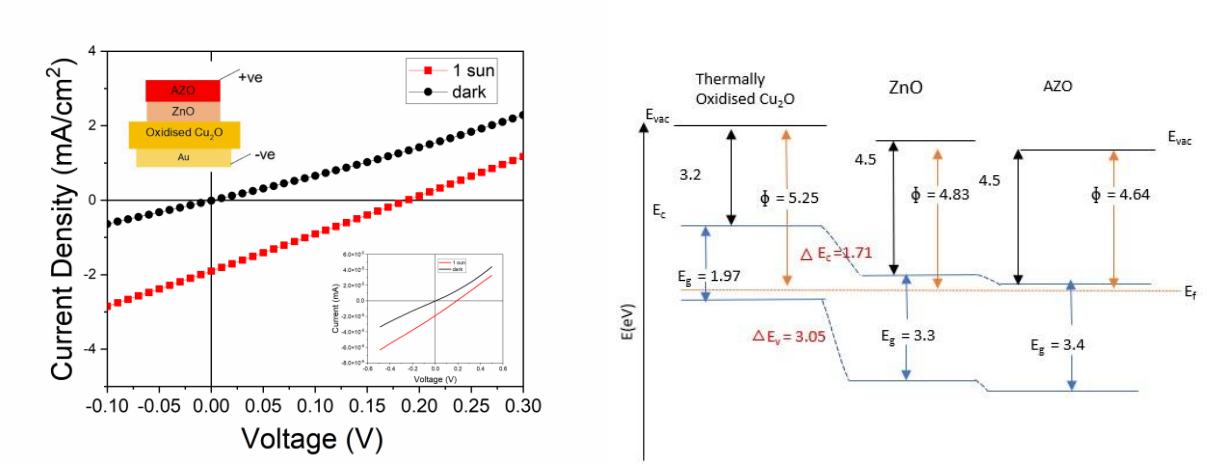

(a) (b)

Figure 5.4 (a) Current density vs voltage characteristics of Au/Oxidised Cu_2O/ZnO/AZO measured in dark and at 1 sun illumination with solar cell schematics in the inset (b) Energy band diagram of the heterojunction between Cu_2O and ZnO/AZO

Different heterojunctions of thermally oxidised Cu_2O were analysed with AZO, ZTO and $Zn_{1-x}Ge_xO_4$. But the open circuit voltage was much lower (less than 100 mV) for all the other architectures. The result discussed here are the best performing cells we obtained for all the different types of Cu_2O. We believe this variation in performance of the thermally oxidised Cu_2O is mostly because of the heterojunction defects and surface quality of thermally oxidised Cu_2O as the surface oxidation after etching cannot be controlled. Even though compared to solar cell with Si absorber the performance is much lower, the values reported here is higher than or comparable to the values reported for Cu_2O solar cells by Melo et.al [34], Jeong et al[35] and Ievskaya[36]. On comparing the photovoltaic characteristics of the different Cu_2O solar cells in this work listed in Table 15, fill factor loss is a major factor affecting the conversion efficiency.

Table 15 Characteristics of Cu_2O solar cell with the absorber layer prepared via different techniques

Solar cell architecture	Method of Preparation of Cu_2O absorber	Short circuit current density	Open circuit voltage	Efficiency	Fill Factor
Au/Cu_2O/Nb:STO	PLD	0.21 mA/cm^2	0.56 V	0.053 %	45.0 %
AZO/ Cu_2O/ITO	Magnetron Sputtering	1.76 mA/cm^2	0.26 V	0.127 %	27.8 %
AZO/ZnO/ Cu_2O/Au	Thermal Oxidation	1.90 mA/cm^2	0.19 V	0.09 %	25 %

Keeping aside the influence of the heterojunction there is a definite influence of the Cu_2O absorber prepared via different techniques on the photovoltaic performance as epitaxial growth of PLD film led to better I-V characteristics. This difference was studied in detail through several transient characterization measurements and other advanced techniques which will be discussed in detail in the next section.

5.4 ADVANCED CHARACTERIZATION OF Cu_2O ABSORBERS

To better understand the difference in the Cu_2O films prepared via PLD, magnetron sputtering and thermal oxidation, the films were characterized via several advanced characterization techniques including transient absorption, time resolved photoluminescence, surface photovoltage etc. All the measurements discussed in this section except surface photovoltage were performed by Yi-Teng Huang from the Optoelectronics Group of Cavendish Laboratory at Cambridge University as part of a collaboration with Dr. Robert Hoye from Imperial College, London.

5.4.1 Transient Absorption Spectroscopy

The excitonic states upon illumination induced by absorption are very short-lived in the order of femtoseconds or picoseconds. Longer lifetime of the excitonic states helps in efficient separation of charge carriers before recombination. Transient Absorption (TA) spectroscopy helps to better understand about these transient excited states by giving information on the kinetics of energy level transitions, spontaneous lifetimes etc. It is a pump-probe technique wherein a high intensity pump laser beam excites the sample, and another laser beam measures the absorption simultaneously. The probe laser absorption with and without pump laser helps to measure the change in absorption. At different time delays of the pump and probe, the process is repeated to measure the change in the transmitted probe pulse energy.

To understand the difference in the carrier dynamics in the PLD and sputtered Cu_2O, 100 nm of both the PLD and sputtered Cu_2O films were deposited on quartz substrates. For the long time TA, the third harmonic of 355 nm pump pulses were provided by an electronically controlled, Q-switched Nd:YVO_4 laser (Innolas Picolo 25) with a pump width ~800 ps passing through several non-linear crystals equipped. For the short-time TA, the second harmonic of 400 nm pump pulses were created from a Ti:Sapphire laser (Solstice Ace) with pump width ~100 fs passing through a beta barium borate crystal (Eksma Optics). Broadband probe pulses with wavelength ~400 – 600 nm were generated by focusing an 800 nm wavelength fundamental laser onto a CaF_2 crystal (Eksma Optics, 5mm) controlled by a digital motion controller (Mercury C-863 DC Motor Controller). The short-time measurements could be performed in transmission (TA) or reflection (TR) configuration depending on the samples and substrates. The repetition rate of the pump pulses was initially 1 kHz, but the

reflection/transmittance probe pulses from the samples with or without pump excitation ($T_{pump\ on}$, $T_{pump\ off}/R_{pump\ on}$, $R_{pump\ off}$) were collected at a rate of 500 Hz, which was controlled by a rotating chopper wheel. The reflected/transmitted pulses were collected by a monochrome line scan camera (JAI SW-4000M-PMCL; spectrograph, Andor Shamrock SR-163). These reflections/transmittances were used to calculate the TA/TR signal intensity by $\frac{\Delta R}{R} = \frac{R_{pump\ on} - R_{pump\ off}}{R_{pump\ off}}$ and $\frac{\Delta T}{T} = \frac{T_{pump\ on} - T_{pump\ off}}{T_{pump\ off}}$, respectively.

In the transient absorption peak of the PLD Cu_2O film, three spectra regions were visible. A Ground State Bleach (GSB) at ~ 2.17 eV in the spectral region of 570-575 nm, and two Photo Induced Absorption (PIA) at ~2.03 eV (562-567 nm) and ~2.19 eV (605-615 nm) as can be seen in Figure 5.5(a). The bleach signal corresponds to the depletion of valence electrons, and it matches with the optical bandgap of the film calculated in Chapter 2. The PIA could be from ortho-exciton state or absorption from copper interstitial to C2. The kinetics of the GSB peak and two PIA dips are shown in Figure 5.5(b). As can be seen in Figure 5.5(b) all the transition lifetimes were very short (~ ps) instead of µs for pure Cu_2O films from literature[37]. This could be an indication of defects in the film. The GSB and PIA dips showed an exponential decay with time constant less than 1 ps. The decay time of the GSB peak was 355 fs and PIA decayed at 883 fs and 364 fs when fitted with an exponential function as can be seen in Figure 5.5(c). This result is very similar to the values reported for Cu_2O by Shenje et.al[38] Azimi et.al[39]. Azimi et.al have reported a decay time of 0.5 ps ±0.06 and have said it to be the exciton lifetime which decays fast due to the presence of defect or trap states.

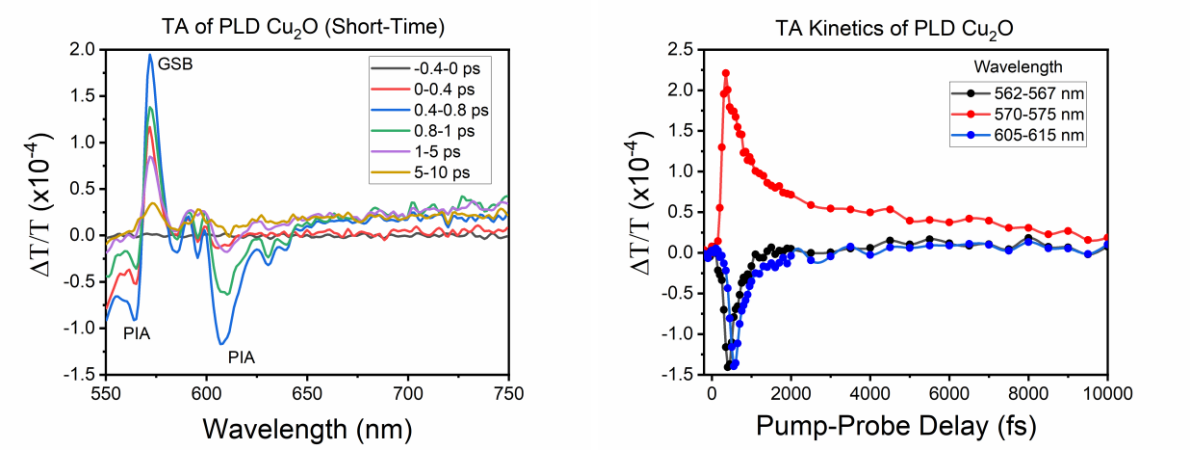

(a) (b)

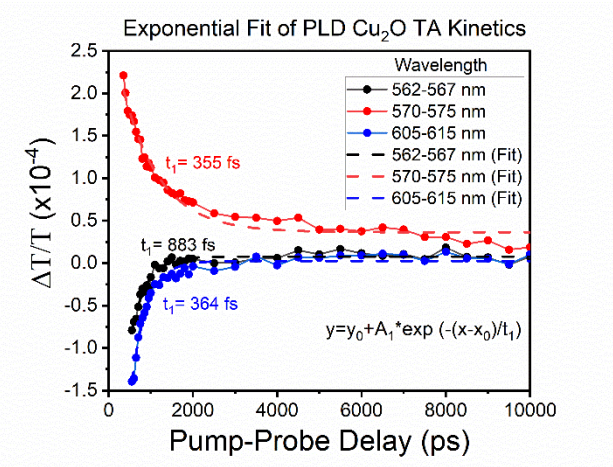

(c)

Figure 5.5 (a) Wavelength dependent Transient Absorption spectrum of the PLD Cu_2O (b) TA kinetics at different wavelengths (c) Exponential Fit of the transient absorption peaks and dips with the fitting equation

During the measurement of long-time TA of the PLD film, at 355 nm excitation wavelength and power of 400 µW, an unknown long lifetime component with a negative feature was observed at an energy state larger than the bandgap, as shown in Figure 5.6 (a). The TA kinetics of this feature at a wavelength of 540 nm (Figure 5.6(b)) was fitted by an exponential decay function with a rather longer decay time of ~ 20 ns. Azimi et.al[39] have also observed a similar long lifetime component which was stable beyond their experimental window of 8 ns which they attribute to a trap state which lowers the lifetime of the excitonic state. In our PLD Cu_2O

film, this long lifetime component was also found to persist even at different powers of laser with similar dynamics as shown in Figure 5.6(c) hence it may be power independent. This could be a trap state which is affecting excitonic transition lifetimes.

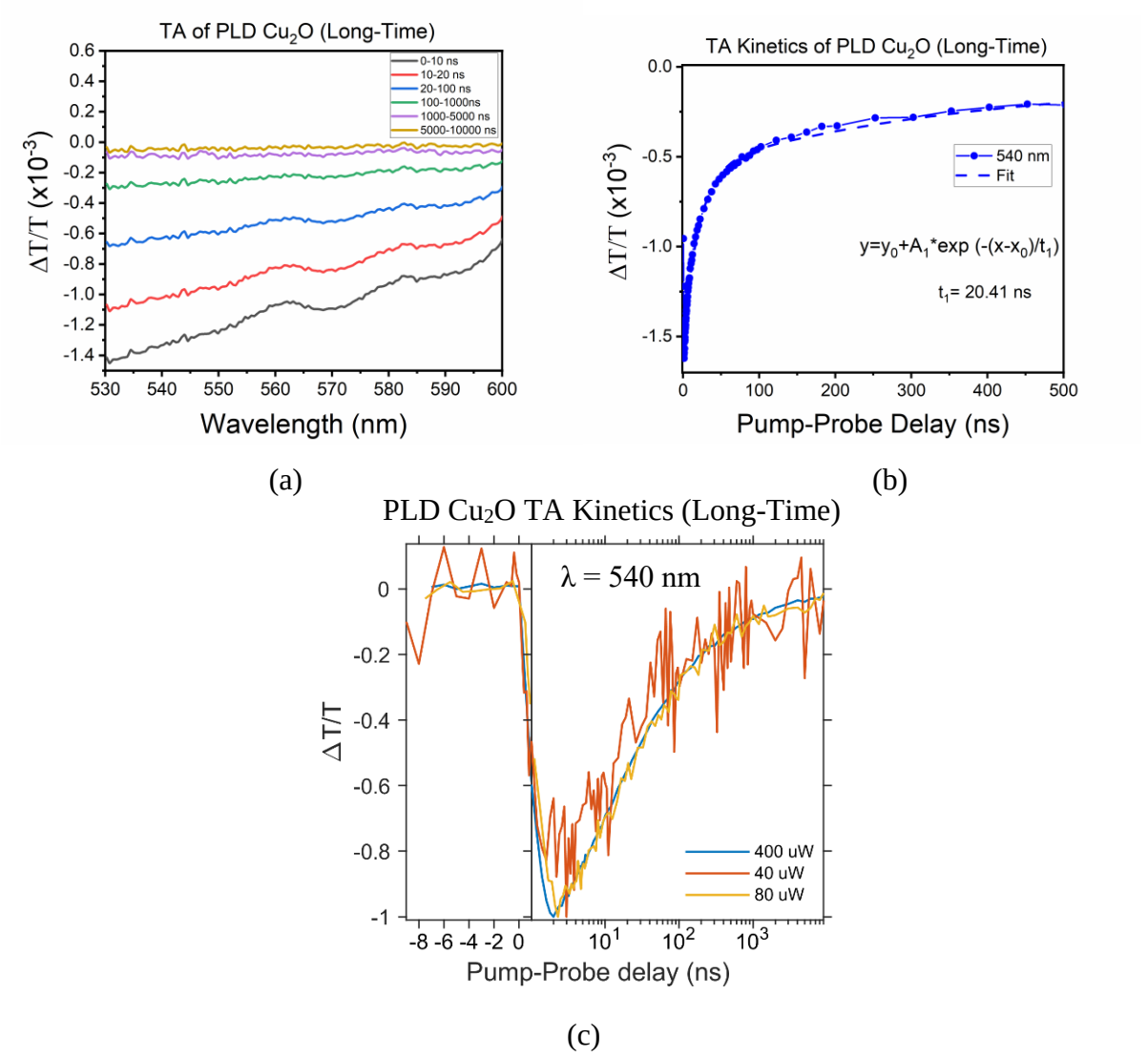

Figure 5.6 (a) Long Time TA absorption spectrum of PLD Cu_2O (b) TA kinetics of PLD Cu_2O at 540 nm fitted by an exponential decay function (c) TA kinetics at 540 nm wavelength at different excitation powers

Compared to the PLD film, the TA spectrum of the sputtered Cu_2O film had multiple peaks, two GSB signal at shorter spectral region of 420-460 nm and 600-690 nm. The GSB signal at higher wavelength is broader and was found to decay fast. Also, two PIA signals were observed with shoulder at 460-500 nm and 690-740 nm as can be seen in Figure 5.7(a). This could be due to the presence of copper vacancies or interstitials within the bandgap of the material as was also observed in the PL spectra of the film in chapter 3. The GSB signal kinetics are

different for the one at shorter wavelength and longer wavelengths as can be seen in the TA kinetics in Figure 5.7(b), so the depopulation process might be different. However, it has a similar kinetics to that of the PIA signal at 460-500 nm. The GSB signal at shorter wavelength might be associated with band-band transitions and signal is almost fluence independent as can be seen in Figure 5.7(c). The GSB peak decay can be fitted with a bi-exponential decay function with time constants 0.96 ps and 137.16 ps which is higher than that of PLD Cu_2O. Additionally, the PIA signal was also found to have a longer lifetime as the signal did not decay even at 1 ns. Further long-time TA measurement revealed that the PIA signal at 460-500 nm was found to not vanish even at 1 μs as can be seen from the long time TA spectra in Figure 5.7(d). It was also found to be fluence dependent.

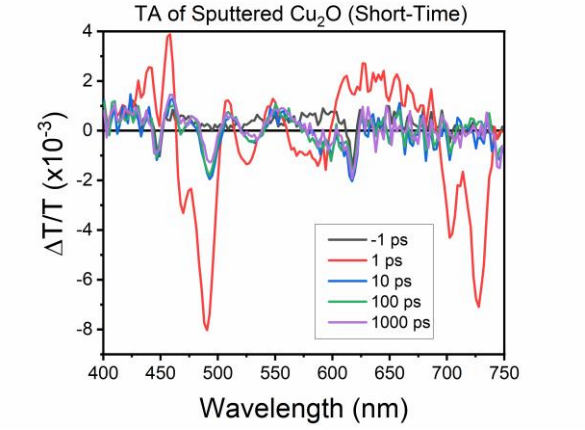

(a)

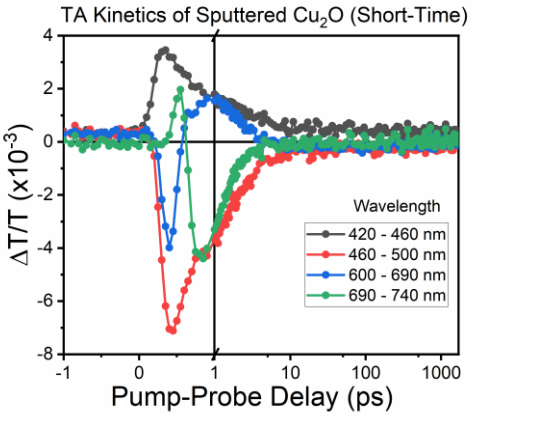

(b)

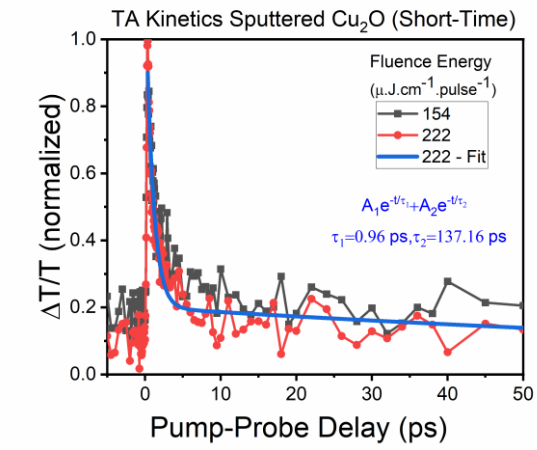

(c)

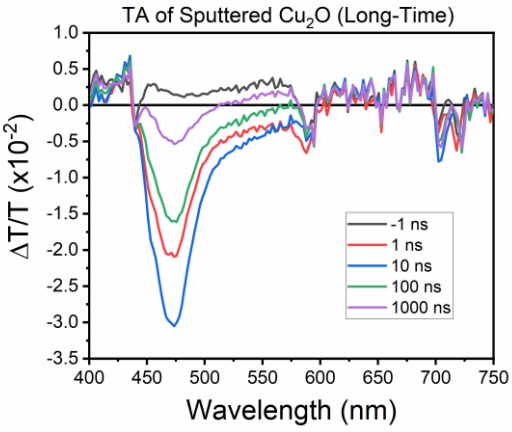

(d)

Figure 5.7 (a) Short-time wavelength dependent TA spectrum of sputtered Cu_2O (b)TA kinetics (c)Fluence dependency of TA kinetics of GSB signal at 420-460 nm (d) Long-time TA spectrum with strong PIA signal

Hence TA analysis explains the better performance of sputtered Cu_2O absorber as the excitonic lifetime is much better in the sputtered film compared to the PLD film. It is also worth noting that the long lifetime component observed in the PLD film in long time TA measurement Figure 5.6(a) which is assumed to be influencing the excitonic lifetime was not found in the sputtered Cu_2O film. To further understand about these defects influencing the carrier dynamics, investigation of any sub-bandgap absorption due to defects in the Cu_2O films were carried out with the help of Photothermal Deflection Spectroscopy (PDS) measurements.

5.4.2 Photothermal Deflection Spectroscopy (PDS)

It is often difficult to measure absorption and mostly we depend on transmission or reflectivity measurements for the same. Absorbance below the bandgap (due to sub-bandgap states) is hard to measure as the sum of transmission and reflection will be close to one and moreover, even a small error in the measurement can lead to values higher or lower than the real values. Overcoming this limitation, using PDS, the absorbance of the semiconductor can be measured in high dynamic range. It is a very sensitive technique for the measurement of absorptance. When a semiconductor absorbs lights, there will be a change in the thermal state of the sample as phonons are created by the absorbed light by non-radiative recombination and thermalization of photogenerated carriers. In PDS this change in the temperature due to photon absorption (not lost be emission) is measured indirectly using “mirage effect”. A semiconductor is illuminated with a monochromatic light and is simultaneously dipped in a liquid as shown in the schematics in Figure 5.8 (a). The change in the temperature of the sample also affects the thermodynamic property of the liquid around the sample and changes its refractive index. The refractive index of the liquid changes as a function of its distance from the semiconductor film (Figure 5.8(b)). The refractive index gradient is measured with a parallel probe beam which gets deflected at an angle β which is proportional to the absorptance of the film and power density of the pump beam. The detector detects the change in voltage which is proportional to β. Thus with the PDS measurement the absorption edge and sub-bandgap states can be studied in disordered absorbers with better resolution and precision than from UV-VIS spectroscopy measurements.[40]

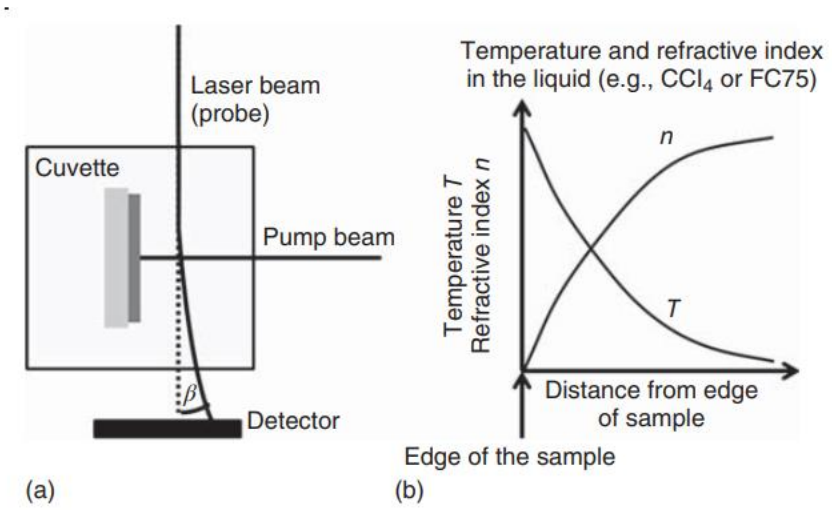

Figure 5.8 (a) Schematics of PDS Measurement (b) change in temperature /refractive index with respect to distance from film (copied from [40])

For PDS measurements, samples were prepared on Spectrosil® 2000 quartz substrates and immersed in an inert liquid FC-72 Fluorinert (3M Company), which has a high thermo-optic coefficient. Monochromatic beams were generated from a 100 W Xenon lamp (Photon Technology International) integrated with a monochromator (CVI DK240). The monochromatic beams were illuminated perpendicularly to the sample surface at a frequency of 13 Hz controlled by a mechanical chopper. Non-radiative recombination processes occurring at the sample surface will lead to a temperature gradient, and thus a refractive index gradient in the inert liquid around the sample. A 670 nm CW laser beam passing through the inert liquid in the parallel direction to the sample surface will be deflected due to the temperature gradient, and the deflected beam will be detected by a quadrant photodiode with a lock-in amplifier (Stanford Research Systems SR830).

The PDS measurement of our Cu_2O films were important to identify the defects in the films within the bandgap. The optical bandgap estimated from tauc-plot for the PLD, and sputtered film was 2.1 eV and 2.3 eV respectively. The PL peaks for both the films were centred below their optical bandgap around 1.97 eV. In the PDS measurement of the PLD and sputtered Cu_2O film, a non-zero absorbance below their bandgap was found for both the films as can be seen in Figure 5.9 (the dashed lines indicate the onset of main absorption). However, for the sputtered Cu_2O, the absorbance onset is not sharp around the bandgap and higher absorbance than the PLD film below the bandgap can be seen which could be due to higher sub-gap states in the

sputtered Cu_2O film. Presence of sub-gap states is not favoured as they lead to recombination pathways in an absorber.

For the PLD film a sharp absorbance onset around its bandgap is visible. Hence comparing both the films, the PLD film might have lower sub-gap defects than sputtered film. In the TA spectroscopy of the PLD film discussed in 5.4.1(a), the long lifetime component was observed at higher energies from the bandgap. This result from the PDS further points that the poor performance of the PLD film might not be only due to sub-gap defects or traps as it is much lower for PLD Cu_2O compared to the sputtered Cu_2O.

To better understand about the influence of these defects on the charge carrier lifetime in the Cu_2O absorbers prepared via different techniques, the PL kinetics was studied using advanced techniques such as time resolved photoluminescence and time-correlated single photon counting and is discussed in the next section.

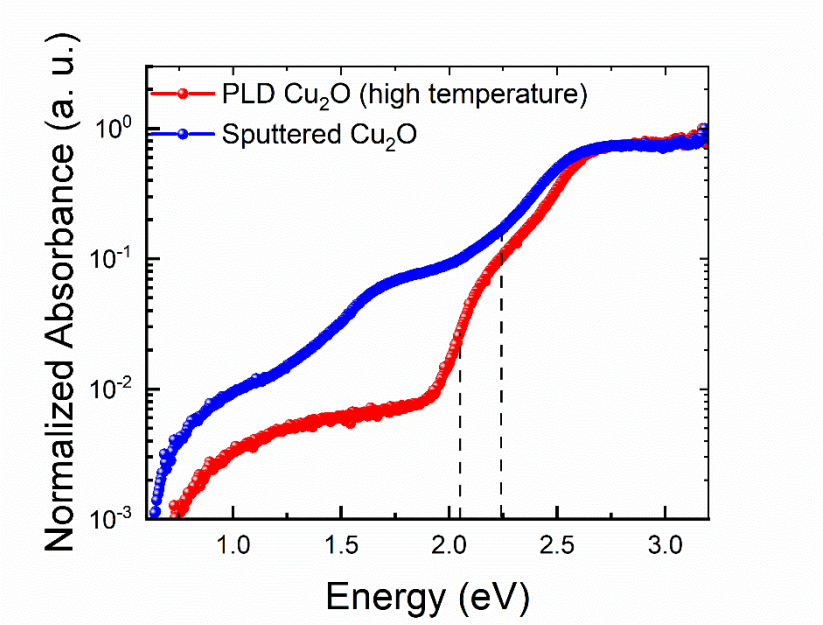

Figure 5.9 Normalized Absorbance spectra of PLD and sputtered Cu_2O measured from Photothermal Deflection Spectroscopy.

5.4.3 PL Kinetics of the Cu_2O prepared via different techniques

To compare the PL kinetics of the Cu_2O film prepared via PLD (~ 100 nm), magnetron sputtering (~100 nm) and thermal oxidation, two techniques were followed namely Time Resolved Photoluminescence (TRPL) and Time-Correlated Single Photon counting (TCSPC). TRPL is a powerful technique to investigate the decay of radiative recombination pathways of

the charge carriers. A pulsed laser excites the charge carriers in a sample and the subsequent decay of the photoluminescence is measured as a function of time. For the measurement, An Andor iStar DH740 CCI-010 system connected to a grating spectrometer (Andor SR303i) at the Cambridge University was used. An excitation wavelength of 400 nm was used to measure the photoluminescence spectrum of the sample and an intensified charge-coupled device (ICCD) camera was used to provide time and spectral resolution. The time-resolution of the ICCD camera was only 4 ns. Using TRPL, radiative recombination events only > 1 ns after excitation could be measured. So, for a better time resolution, TCSPC technique was also followed which has a time resolution of ~ 20 ps. TCSPC measurements were performed in the Edinburgh Instruments Life Spec system, FLS1000. A picosecond pulsed (~80 ps) diode laser (EPL-405, Edinburgh Instruments), with a wavelength of 405 nm was used for the excitation. The repetition rate was set at 40 kHz during the measurements. In addition, photoluminescence spectrum of the samples could also be measured in the same system by exciting the samples with a monochromatic beam from an integrated Xe light source.

(a) Pulsed Laser Deposition

For the PLD Cu_2O, three PL peaks were visible at 0 ns corresponding to band edge transition, ortho-exciton recombination and C2-V2 transition as can be seen in Figure 5.10(a). However, all the PL peaks were found to decay fast in less than 4 ns. To better understand the decay time of the exciton peak corresponding to the band edge transition, the PL kinetics of 626 nm exciton peak measured by TCSPC. To investigate the carrier lifetime the later tail of the PL kinetics was fitted using a biexponential function as shown in Figure 5.10(b). There were two decay components with a smaller lifetime of 0.05 ns and a longer lifetime of 0.58 ns. The average decay time which corresponds to the carrier lifetime was found to be ~ 315 ps. A similar fast decay of the photogenerated carriers was also reported by Li et.al[41] in TRPL measurements of Cu_2O nanocrystals prepared via chemical route. This fast decay time is not so favorable when employing these films as absorbers as the excited carriers are lost much faster via radiative recombination.

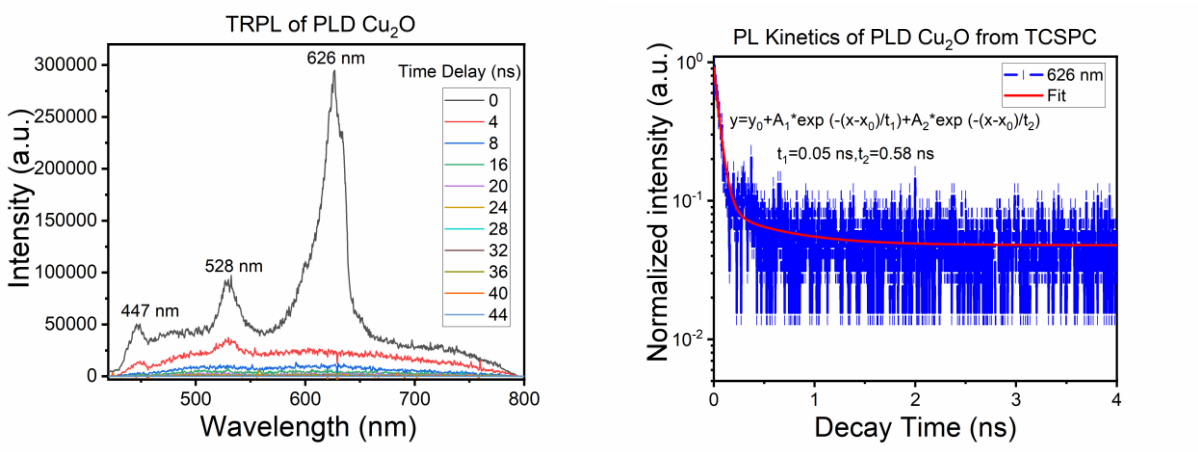

(a) (b)

Figure 5.10 (a) TRPL of PLD Cu_2O at an excitation wavelength of 400 nm (b) PL kinetics of the exciton peak at 626 nm (from TCSPC measurement at excitation wavelength of 405 nm) with its bi-exponential fit

(b) Magnetron Sputtering

In the TRPL spectrum of the sputtered Cu_2O at a similar excitation wavelength, emission peaks of trap states namely copper vacancy and copper interstitials were visible apart from the band edge transition at energies smaller than the bandgap as can be seen in Figure 5.11. This confirms the sub-bandgap absorption observed in the sputtered film from PDS. All the PL peaks were found to decay within 15 ns which is fast but was better than the PLD film (315 ps). Hence more efficient charge carrier separation is possible before recombination in the sputtered film than the PLD deposited film. This could result in better current as observed from the I-V measurement discussed in the beginning of this chapter. Strangely in the TCSPC measurement of the sputtered Cu_2O, no peaks were visible. The PL kinetics was hence hard to compare. The peak at 735 nm was found to be still visible after 15 ns. As the defect could have longer fluorescence lifetime than band edge recombination[42] this could correspond to a defect state.

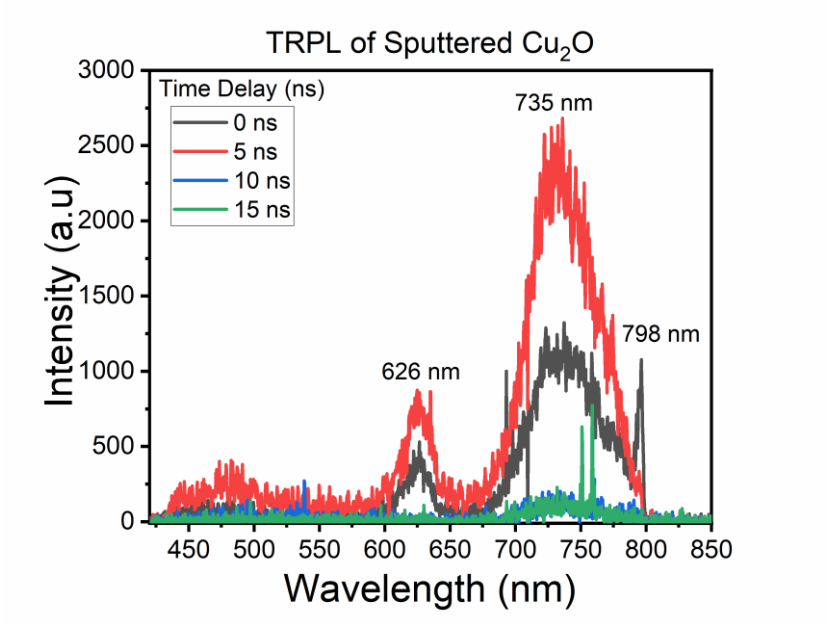

Figure 5.11 TRPL spectrum of sputtered Cu_2O film at 400 nm excitation wavelength

(c) Thermal Oxidation

To investigate the PL kinetics of the oxidised foil, TCSPC measurement was done on an unetched oxidised foil as it has a better resolution than TRPL measurement. As can be seen in Figure 5.12(a), the thermally oxidised foil had three PL peaks at an excitation of 405 nm using a monochromatic light from Xe lamp. The peak at 780 nm may not be real and it could be from the background or setup as it was not detectable in the TCSPC measurement. The band edge emission was observed at a higher wavelength of 585 nm corresponding to a bandgap of 2.1 eV. As Cu_2O have a narrow bandgap, the PL emissions might be due to contribution of defect states or from the surface other than the recombination of electron from conduction band to valence band. The decay profiles at both the wavelengths were approximately similar following a tri-exponential decay with average decay times of 3.83 ns (for 585 nm peak) and 4.14 ns (for 476 nm peak) as shown in Figure 5.12 (b) and (c). The peak at 476 nm could be a due to C2-V2 transition with a longer lifetime.

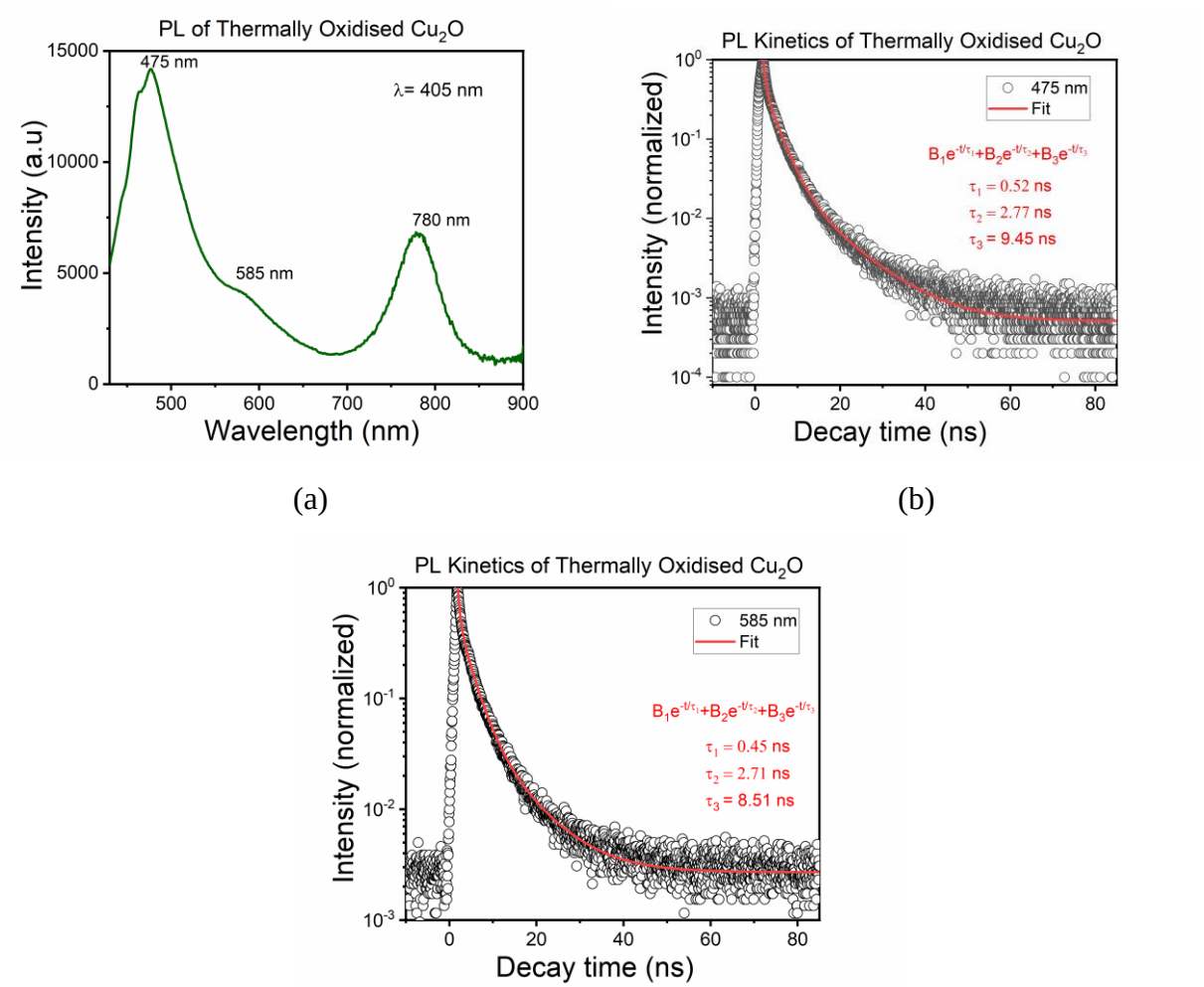

Figure 5.12 (a) PL spectrum of thermally oxidised Cu_2O at 405 nm excitation. Kinetics of the PL peaks at (b) 475 nm (c) 585 nm with a tri-exponential fit

Hence comparing the PL decay profiles of PLD Cu_2O and thermally oxidised Cu_2O sheets the decay time is more for Cu_2O from thermal oxidation which shows that the minority carrier lifetime is better, which helps in better charge separation. Even though in the sputtered Cu_2O TRPL measurement, the PL peak was not completely decayed even at 15 ns, since no PL peaks were observed in the TCSPC measurement, it is difficult to compare with the thermally oxidised Cu_2O sheet. But it can be concluded that from the PL kinetics analysis, the sputtered film and thermally oxidised sheet might have a better carrier lifetime than the PLD Cu_2O film.

As the carrier lifetime was good in thermally oxidised sheet, to understand why our thermally oxidised Cu_2O still had lower photovoltaic performance especially open-circuit voltage, surface photovoltage of the Cu_2O absorbers were measured.

5.4.4 Surface Photovoltage Measurement

Surface Photovoltage measurement is a contactless technique which helps to analyse the illumination induced variation in the surface voltage of a film. By definition, surface photovoltage (SPV) is the illumination induced change in the surface potential. When a free semiconductor with a grounded back contact is illuminated, the generation of free charge carriers by various transitions from band-band or trap-band etc results in the redistribution of charge within the surface to bulk or vice versa. This results in the variation of surface space charge region and hence the surface potential. Hence measuring SPV at different illumination intensity give information about minority carrier diffusion length and transient measurements helps to understand the dynamics of the photoinduced charge carriers. Thus, SPV is an excellent measurement technique to compare the potential application of our Cu_2O absorbers grown via different methods.

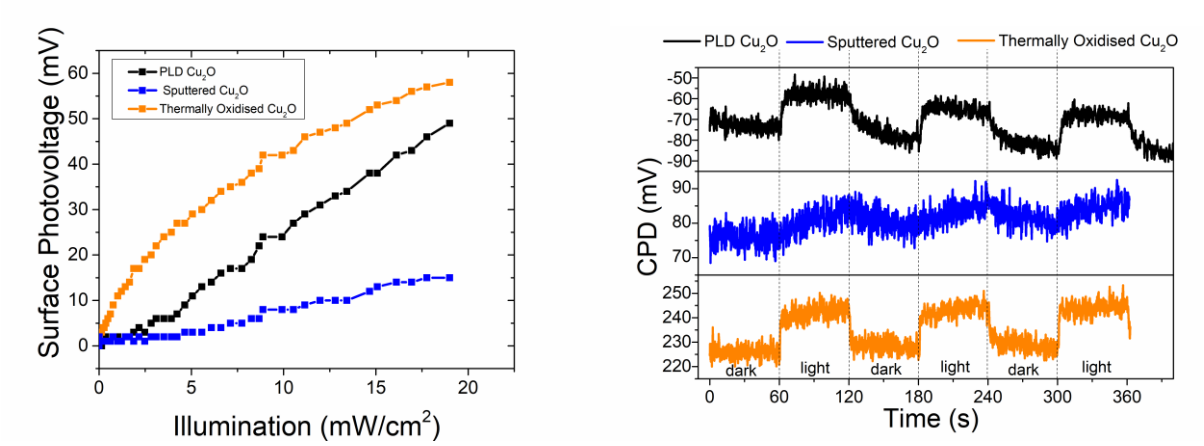

(a) (b)

Figure 5.13 (a) Surface photovoltage (SPV) of the Cu_2O samples prepared via different techniques with respect to illumination (b) Contact Potential Difference (CPD) variation at dark and light cycle conditions

SPV measurements of the Cu_2O were carried out using a single point Kelvin Probe system (KP Technology KP020) with a 2 mm diameter gold tip at ICube Laboratory. Illumination was done using a halogen source with calibrated illumination for white light SPV. The SPV signal was measured by subtracting the CPD at dark from CPD at illumination. As can be seen in Figure 5.13(a), SPV signal increases linearly for all the three samples with illumination intensity and it saturates at 56 mV for thermally oxidised sheet, at 49 mV for PLD film and was the lowest for sputtered film at 15 mV. The SPV signal of the thermally oxidised Cu_2O was the highest

followed by PLD and sputtered films. Here we also need to consider the fact that the thickness of the samples was not identical (thermally oxidised sheets have thickness in micrometre range) and the surface of the thermally oxidised foils was more textured which are some other factors which also influence the minority carrier diffusion length. Even then higher surface voltage was observed for the thermally oxidised sheets. This shows their better surface quality than the PLD and sputtered film.

The change in CPD vs time shown in Figure 5.13 (b) at light and dark cycles is also prominent for the thermally oxidised foil followed by PLD film. For the sputtered film the change was hardly detectable. This further confirms that the photo response is the highest for the thermally oxidised sheets.

To check if the poor V_{oc} observed for the solar cell, Au/thermally oxidised Cu_2O/ZnO/AZO measured in the I-V measurements (reported in 5.3(c)) is due to physical difficulty in establishing a contact on the electrodes using the probes during I-V measurements, the surface photovoltage at the heterojunction was measured at varying intensities of white light (SPV is contactless measurement). This was achieved by measuring the CPD between the heterojunction in the solar cell.

As listed in Table 16, the SPV of the heterojunction of thermally oxidised Cu_2O sheet was 500 mV at 20 mW/cm^2 illumination. However, the V_{oc} measured at 1 sun (100 mW/cm^2) was only 190 mV. For the best performed PLD solar cell, Nb:STO//PLD Cu_2O/Au with highest V_{oc} of 0.56 V, the SPV was 280 mV. At a higher illumination of 100 mW/cm^2, higher V_{oc} than the SPV at 20 mW/cm^2 could be obtained. However, this was not observed in thermally oxidised solar cells because as the films were bended and since I-V is a contact measurement there were problems in making a stable contact using the measurement probes. Hence the low voltage value measured from the I-V measurements is to an extend due to this physical issue. The high SPV voltage obtained from the SPV measurement of the thermally oxidised sheet than the PLD film shows that there is definitely higher potential for thermally oxidised Cu_2O based solar cell, and much better photovoltaic performance can be achieved.

Table 16 Comparison of SPV at heterojunction and open circuit voltage

Heterojunction	Preparation method of Cu_2O	SPV at 20 mW/cm^2	Voc from solar cell at 1 sun illumination
Epitaxial Cu_2O/Au	PLD	280 mV	560 mV
Cu_2O/ZnO/AZO	Thermal Oxidation	500 mV	190 mV

5.5 CONCLUSION

The focus of this chapter was mainly on the comparison of the different Cu_2O absorbers prepared via PLD, magnetron sputtering and thermal oxidation. On comparison of the J-V properties by forming solar cells using different heterojunctions, the PLD Cu_2O solar cell with epitaxially grown absorber layer showed the highest open circuit voltage of 0.56 V. Non-epitaxially grown PLD Cu_2O absorber was found to show very poor performance. Even though the highest short circuit current density was obtained from thermally oxidised foil (1.9 mA/cm^2), it had a poor open circuit voltage (0.19 V) and J-V characteristics compared to the sputtered and PLD films. The J-V characteristics of all the solar cells except the epitaxial Cu_2O solar cell showed mobility, series resistance and shunt problems.

Table 17 Comparison of the Cu_2O absorbers using advanced characterization techniques

Characterization Technique	Parameter	Cu_2O Absorber		
		PLD	Magnetron Sputtering	Thermal Oxidation
Transient Absorption	Exciton lifetime	0.35 ps (GSB) 0.6 ps (PIA)	69.06 ps (GSB) > 1μs (PIA)	
TRPL and TCSPC	PL Decay	315 ps	15 ns (Defect peak?)	4 ns
PDS	Sub-band gap defects	low	high	

These absorbers were then further analysed using advanced characterization techniques. Table 17 summarizes the results. From the TA measurements, it was observed that even though both the PLD and sputtered film have poor exciton lifetime due to defects, it was the lowest for the PLD film than the sputtered film. For a good Cu_2O film, without any defects, this value should be in micrometre range. A strong PIA signal was observed only in the sputtered films under long-time TA measurements. Additionally, transient absorption measurements of the PLD Cu_2O revealed a fluence independent absorption feature with a longer lifetime of 20 ns at higher energies than bandgap which could be from a trap state which is reducing the exciton lifetime to femtoseconds which was measured from short-time TA. This was not observed in the sputtered Cu_2O film which had a better lifetime.

Further, the charge carrier dynamics of the PLD, sputtered and thermally oxidised Cu_2O were analysed using TRPL and TCSPC. The PL kinetics of the PLD film showed a biexponential decay with a fast decay time of ~ 315 ps. The thermally oxidised Cu_2O sheets had a tri-exponential decay with a decay time in the range of ~ 5 ns which could be the reason for higher photocurrent observed in the I-V measurement as charge carrier separation becomes more efficient due to higher minority carrier lifetime. However, these values are much lower than Si absorbers with PL lifetime in the micrometre range[43]. Hence this lower minority carrier lifetime could also be a reason for the low performance of Cu_2O based solar cell compared to Si based solar cell. Compared to all the Cu_2O absorbers studied in this work, the thermally oxidised sheet was found to have better minority carrier lifetime. The thermally oxidised Cu_2O was also found to have higher SPV signal which is related to the minority carrier diffusion length. Moreover, the SPV measurement of the thermally oxidised Cu_2O heterojunction with ZnO/AZO revealed high photovoltage saturating at 500 mV at 20 mW/cm^2 while the experimentally measured V_{OC} of this heterojunction was only 190 mV at 100 mW/cm^2. This discrepancy points to the fact that the thermally oxidised Cu_2O have higher photovoltaic performance potential than that was measured experimentally if the physical problems encountered during contacting the electrodes by the probes during I-V measurements were solved. This aligns with the better photovoltaic performance of thermally oxidised Cu_2O reported in the literature which we have found out to be due to better surface quality, higher minority carrier lifetime and diffusion lengths through several characterization techniques.

Both the PLD and sputtered Cu_2O absorbers were found to have defects which are affecting their carrier lifetime. For the PLD film, a trap state at a higher energy state than the band gap

was found to be the prominent factor reducing the exciton lifetime while for the sputtered film several sub-bandgap defects were found to affect the charge carrier dynamics. Further improvement of Cu_2O solar cells based on thermally oxidised sheets can be achieved by engineering better heterojunctions and for the other techniques (PLD and Sputtering) improving the film quality to lower the defects in the film should be the focus.

5.6 REFERENCES OF CHAPTER 05

[1] S. S. Wilson, J. P. Bosco, Y. Tolstova, D. O. Scanlon, G. W. Watson, and H. A. Atwater, 'Interface stoichiometry control to improve device voltage and modify band alignment in ZnO/Cu2O heterojunction solar cells', *Energy Environ. Sci.*, vol. 7, no. 11, pp. 3606–3610, 2014, doi: 10.1039/C4EE01956C.

[2] L. C. Olsen, F. W. Addis, and W. Miller, 'Experimental and theoretical studies of Cu2O solar cells', *Solar Cells*, vol. 7, no. 3, pp. 247–279, 1982, doi: https://doi.org/10.1016/0379-6787(82)90050-3.

[3] L. C. Olsen, R. C. Bohara, and M. W. Urie, 'Explanation for low-efficiency Cu2O Schottky-barrier solar cells', *Applied Physics Letters*, vol. 34, no. 1, pp. 47–49, 1979, doi: 10.1063/1.90593.

[4] A. Mittiga, E. Salza, F. Sarto, M. Tucci, and R. Vasanthi, 'Heterojunction solar cell with 2% efficiency based on a Cu2O substrate', *Applied Physics Letters*, vol. 88, no. 16, p. 163502, 2006, doi: 10.1063/1.2194315.

[5] A. T. Marin, D. Muñoz-Rojas, D. C. Iza, T. Gershon, K. P. Musselman, and J. L. MacManus-Driscoll, 'Novel Atmospheric Growth Technique to Improve Both Light Absorption and Charge Collection in ZnO/Cu2O Thin Film Solar Cells', *Adv. Funct. Mater.*, vol. 23, no. 27, pp. 3413–3419, Jul. 2013, doi: 10.1002/adfm.201203243.

[6] T. Minami, Y. Nishi, T. Miyata, and J. Nomoto, 'High-Efficiency Oxide Solar Cells with ZnO/Cu $_2$ O Heterojunction Fabricated on Thermally Oxidized Cu $_2$ O Sheets', *Appl. Phys. Express*, vol. 4, no. 6, p. 062301, May 2011, doi: 10.1143/APEX.4.062301.

[7] L. Papadimitriou, N. A. Economou, and D. Trivich, 'Heterojunction solar cells on cuprous oxide', *Solar Cells*, vol. 3, no. 1, pp. 73–80, 1981, doi: https://doi.org/10.1016/0379-6787(81)90084-3.

[8] T. Miyata, H. Tokunaga, K. Watanabe, N. Ikenaga, and T. Minami, 'Photovoltaic properties of low-damage magnetron-sputtered n-type ZnO thin film/p-type Cu2O sheet heterojunction solar cells', *Thin Solid Films*, vol. 697, p. 137825, Mar. 2020, doi: 10.1016/j.tsf.2020.137825.

[9] L. M. Wong, S. Y. Chiam, J. Q. Huang, S. J. Wang, J. S. Pan, and W. K. Chim, 'Growth of Cu2O on Ga-doped ZnO and their interface energy alignment for thin film solar cells', *Journal of Applied Physics*, vol. 108, no. 3, p. 033702, 2010, doi: 10.1063/1.3465445.

[10] Z. Starowicz *et al.*, 'Investigation of the Zn and Cu oxides for heterojunction thin film solar cell application', *Microelectronic Engineering*, vol. 221, p. 111196, Jan. 2020, doi: 10.1016/j.mee.2019.111196.

[11] J. Herion, E. A. Niekisch, and G. Scharl, 'Investigation of metal oxide/cuprous oxide heterojunction solar cells', *Solar Energy Materials*, vol. 4, no. 1, pp. 101–112, 1980, doi: https://doi.org/10.1016/0165-1633(80)90022-2.

[12] Y. Takiguchi and S. Miyajima, 'Device simulation of cuprous oxide heterojunction solar cells', *Jpn. J. Appl. Phys.*, vol. 54, no. 11, p. 112303, Nov. 2015, doi: 10.7567/JJAP.54.112303.

[13] A. Sekkat, D. Bellet, G. Chichignoud, D. Muñoz-Rojas, and A. Kaminski-Cachopo, 'Unveiling Key Limitations of ZnO/Cu2O All-Oxide Solar Cells through Numerical Simulations', *ACS Appl. Energy Mater.*, vol. 5, no. 5, pp. 5423–5433, May 2022, doi: 10.1021/acsaem.1c03939.

[14] T. Minami, H. Tanaka, T. Shimakawa, T. Miyata, and H. Sato, ‘High-Efficiency Oxide Heterojunction Solar Cells Using Cu_2O Sheets’, *Jpn. J. Appl. Phys.*, vol. 43, no. No. 7A, pp. L917–L919, Jun. 2004, doi: 10.1143/JJAP.43.L917.
[15] T. Minami, Y. Nishi, and T. Miyata, ‘Heterojunction solar cell with 6% efficiency based on an n-type aluminum–gallium–oxide thin film and p-type sodium-doped Cu2O sheet’, *Applied Physics Express*, vol. 8, no. 2, p. 022301, Jan. 2015, doi: 10.7567/apex.8.022301.
[16] T. Minami, Y. Nishi, and T. Miyata, ‘High-Efficiency Cu_2O-Based Heterojunction Solar Cells Fabricated Using a Ga_2O_3 Thin Film as N-Type Layer’, *Appl. Phys. Express*, vol. 6, no. 4, p. 044101, Apr. 2013, doi: 10.7567/APEX.6.044101.
[17] Y. S. Lee *et al.*, ‘Atomic Layer Deposited Gallium Oxide Buffer Layer Enables 1.2 V Open-Circuit Voltage in Cuprous Oxide Solar Cells’, *Advanced Materials*, vol. 26, no. 27, pp. 4704–4710, 2014, doi: https://doi.org/10.1002/adma.201401054.
[18] R. E. Brandt *et al.*, ‘Band offsets of n-type electron-selective contacts on cuprous oxide (Cu2O) for photovoltaics’, *Appl. Phys. Lett.*, vol. 105, no. 26, p. 263901, Dec. 2014, doi: 10.1063/1.4905180.
[19] W. Niu, M. Zhou, Z. Ye, and L. Zhu, ‘Photoresponse enhancement of Cu2O solar cell with sulfur-doped ZnO buffer layer to mediate the interfacial band alignment’, *Solar Energy Materials and Solar Cells*, vol. 144, pp. 717–723, 2016, doi: https://doi.org/10.1016/j.solmat.2015.10.013.
[20] Y. S. Lee *et al.*, ‘Ultrathin amorphous zinc-tin-oxide buffer layer for enhancing heterojunction interface quality in metal-oxide solar cells’, *Energy Environ. Sci.*, vol. 6, no. 7, pp. 2112–2118, 2013, doi: 10.1039/C3EE24461J.
[21] T. Minami, Y. Nishi, and T. Miyata, ‘Cu2O-based solar cells using oxide semiconductors’, *Journal of Semiconductors*, vol. 37, no. 1, p. 014002, Jan. 2016, doi: 10.1088/1674-4926/37/1/014002.
[22] T. Minami, Y. Nishi, and T. Miyata, ‘Efficiency enhancement using a $Zn_{1-x}Ge_x$-O thin film as an n-type window layer in Cu_2O-based heterojunction solar cells’, *Appl. Phys. Express*, vol. 9, no. 5, p. 052301, May 2016, doi: 10.7567/APEX.9.052301.
[23] T. Minami, T. Miyata, and Y. Nishi, ‘Efficiency improvement of Cu2O-based heterojunction solar cells fabricated using thermally oxidized copper sheets’, *Thin Solid Films*, vol. 559, pp. 105–111, May 2014, doi: 10.1016/j.tsf.2013.11.026.
[24] Y. Nishi, T. Miyata, and T. Minami, ‘Effect of inserting a thin buffer layer on the efficiency in *n*-ZnO/*p*-Cu_2O heterojunction solar cells’, *Journal of Vacuum Science & Technology A: Vacuum, Surfaces, and Films*, vol. 30, no. 4, p. 04D103, Jul. 2012, doi: 10.1116/1.3698596.
[25] T. Minami, T. Miyata, K. Ihara, Y. Minamino, and S. Tsukada, ‘Effect of ZnO film deposition methods on the photovoltaic properties of ZnO–Cu2O heterojunction devices’, *Thin Solid Films*, vol. 494, no. 1, pp. 47–52, 2006, doi: https://doi.org/10.1016/j.tsf.2005.07.167.
[26] T. Minami, T. Miyata, and Y. Nishi, ‘Cu2O-based heterojunction solar cells with an Al-doped ZnO/oxide semiconductor/thermally oxidized Cu2O sheet structure’, *Solar Energy*, vol. 105, pp. 206–217, Jul. 2014, doi: 10.1016/j.solener.2014.03.036.
[27] M. Coll *et al.*, ‘Towards Oxide Electronics: a Roadmap’, *Applied Surface Science*, vol. 482, pp. 1–93, Jul. 2019, doi: 10.1016/j.apsusc.2019.03.312.
[28] P. Cendula, M. T. Mayer, J. Luo, and M. Grätzel, ‘Elucidation of photovoltage origin and charge transport in Cu2O heterojunctions for solar energy conversion’, *Sustainable Energy Fuels*, vol. 3, no. 10, pp. 2633–2641, 2019, doi: 10.1039/C9SE00385A.

[29] M. Wei, C.-F. Li, X.-R. Deng, and H. Deng, ‘Surface Work Function of Transparent Conductive ZnO Films’, *Energy Procedia*, vol. 16, pp. 76–80, 2012, doi: https://doi.org/10.1016/j.egypro.2012.01.014.

[30] T. C. Yeh, Q. Zhu, D. B. Buchholz, A. B. Martinson, R. P. H. Chang, and T. O. Mason, ‘Amorphous transparent conducting oxides in context: Work function survey, trends, and facile modification’, *Applied Surface Science*, vol. 330, pp. 405–410, 2015, doi: https://doi.org/10.1016/j.apsusc.2015.01.026.

[31] B. Singh and B. R. Mehta, ‘Relationship between nature of metal-oxide contacts and resistive switching properties of copper oxide thin film based devices’, *Thin Solid Films*, vol. 569, pp. 35–43, 2014, doi: https://doi.org/10.1016/j.tsf.2014.08.030.

[32] K. Wang *et al.*, ‘Heteroepitaxial growth of Cu2O films on Nb-SrTiO3 substrates and their photovoltaic properties’, *Ceramics International*, vol. 43, no. 18, pp. 16232–16237, Dec. 2017, doi: 10.1016/j.ceramint.2017.08.205.

[33] Z. Q. Yu *et al.*, ‘Epitaxial growth and microstructure of Cu2O nanoparticle/thin films on SrTiO3(100)’, *Nanotechnology*, vol. 18, no. 11, p. 115601, Feb. 2007, doi: 10.1088/0957-4484/18/11/115601.

[34] C. de Melo *et al.*, ‘Semi-Transparent p-Cu $_2$$ O/n-ZnO Nanoscale-Film Heterojunctions for Photodetection and Photovoltaic Applications’, *ACS Appl. Nano Mater.*, vol. 2, no. 7, pp. 4358–4366, Jul. 2019, doi: 10.1021/acsanm.9b00808.

[35] S. S. Jeong, A. Mittiga, E. Salza, A. Masci, and S. Passerini, ‘Electrodeposited ZnO/Cu2O heterojunction solar cells’, *Electrochimica Acta*, vol. 53, no. 5, pp. 2226–2231, 2008, doi: https://doi.org/10.1016/j.electacta.2007.09.030.

[36] Y. Ievskaya, R. L. Z. Hoye, A. Sadhanala, K. P. Musselman, and J. L. MacManus-Driscoll, ‘Fabrication of ZnO/Cu2O heterojunctions in atmospheric conditions: Improved interface quality and solar cell performance’, *Solar Energy Materials and Solar Cells*, vol. 135, pp. 43–48, Apr. 2015, doi: 10.1016/j.solmat.2014.09.018.

[37] A. Mysyrowicz, D. Hulin, and A. Antonetti, ‘Long Exciton Lifetime in Cu2O’, *Phys. Rev. Lett.*, vol. 43, no. 15, pp. 1123–1126, Oct. 1979, doi: 10.1103/PhysRevLett.43.1123.

[38] L. Shenje, S. Larson, Y. Zhao, and S. Ullrich, ‘Composition Effects on Ultrafast Optical Properties of CuxOy Thin Films: A Transient Absorption Study’, *J. Phys. Chem. C*, vol. 124, no. 45, pp. 24908–24918, Nov. 2020, doi: 10.1021/acs.jpcc.0c08716.

[39] H. Azimi *et al.*, ‘Effective Ligand Passivation of Cu2O Nanoparticles through Solid-State Treatment with Mercaptopropionic Acid’, *J. Am. Chem. Soc.*, vol. 136, no. 20, pp. 7233–7236, May 2014, doi: 10.1021/ja502221r.

[40] D. Abou-Ras, T. Kirchartz, and U. Rau, *Advanced Characterization Techniques for Thin Film Solar Cells*. Wiley, 2016. [Online]. Available: https://books.google.de/books?id=9J-tDAAAQBAJ

[41] J. Li, M. He, J. Yan, J. Liu, J. Zhang, and J. Ma, ‘Room Temperature Engineering Crystal Facet of Cu2O for Photocatalytic Degradation of Methyl Orange’, *Nanomaterials*, vol. 12, no. 10, 2022, doi: 10.3390/nano12101697.

[42] P. Wang *et al.*, ‘Temperature sensitive optical properties of exciton and room-temperature visible light emission from disordered Cu2O nanowires’, *RSC Adv.*, vol. 4, no. 71, pp. 37542–37546, 2014, doi: 10.1039/C4RA05595K.

[43] S. Parola *et al.*, ‘Study of Photoluminescence Decay by Time-correlated Single Photon Counting for the Determination of the Minority-carrier Lifetime in Silicon’, *Energy Procedia*, vol. 55, pp. 121–127, 2014, doi: https://doi.org/10.1016/j.egypro.2014.08.091.

CONCLUSION AND PERSPECTIVES

This work opens the door for a better understanding on the influence of preparation methods of Cu_2O on their absorber properties when grown via popular techniques of Pulsed Laser Deposition (PLD), Magnetron Sputtering and Thermal Oxidation. By optimising the PLD deposition temperature and oxygen partial pressure, we obtained pure Cu_2O phase at both high temperature (750 ℃) and low temperature (300 ℃) by varying the oxygen partial pressure. By following a detailed study on the PLD films, we have shown that the phase of the film, crystallinity, electrical and optical properties could be controlled by varying the deposition conditions and only in a narrow window of temperature and pressure good quality phase pure Cu_2O film could be obtained via PLD. We have shown the variation in the stoichiometry (oxygen to copper ratio) of the PLD films at different deposition conditions using a more reliable technique of Rutherford Back scattering Spectroscopy (RBS) which was not reported yet as most of the work in literature rely on more local techniques such as Raman spectroscopy for the phase determination. By comparing the quality of the films, their structural, electrical and optical properties, the best deposition condition for Cu_2O absorber using PLD was found to be 750 ℃ and 10^{-2} mbar oxygen partial pressure. This film was found to be better crystallized with lattice parameters close to pure Cu_2O, a direct bandgap of 2.05±0.05 eV from Tauc plot and a high absorption coefficient of ~10^6 cm^{-1} in the 400-600 nm range which makes it suitable for the application as an absorber. The optimized PLD film was p-type with a low resistivity of 40 Ω.cm, a high mobility of 30 cm^2/ (V. s) and bulk concentration of about 10^{15} cm^{-3}. Typically, low mobility of Cu_2O film is always a major concern for the implementation of the film in photoelectronic applications. Thus, achieving Cu_2O films with high mobility as reported in this work without compromising the carrier concentration is difficult.

Even though Na doped Cu_2O solar cell currently hold the highest reported efficiency for Cu_2O solar cell in the literature, the methods reported for Na doping of Cu_2O hardly allows for a control on the dopant amount. To the best of our knowledge this was the first time the electrical properties of Cu_2O films were studied by controlling the amount of Na inside Cu_2O lattice. Initial results on the impact of ion implantation of Na at various doses on the electrical properties of PLD Cu_2O were also discussed in this work. The carrier concentration was found to increase by a factor of 100 as Na substitutes Cu forming Na_2O thus increasing the copper

vacancies. Using a simulation software AFORS-HET, the influence of the increase in the carrier concentration of the Cu_2O absorber on the photovoltaic efficiency was also elucidated.

Despite sputtering deposition being a common growth technique for Cu_2O film, most of the studies are using DC Magnetron Sputtering. However, in this work we have optimized deposition conditions to obtain pure Cu_2O film using RF Magnetron Sputtering. The deposition temperature, sputtering gas flow rate, sputtering chamber pressure were varied to obtain good quality phase pure Cu_2O thin film at a lower temperature of 300 ℃. Compared to the PLD film at similar temperature, this film was found to have superior structural quality, flat morphology with uniform coverage, lower resistivity of 16 Ωcm and carrier concentration of about 10^{17} cm^{-3}. The mobility of this film was however lower at ~ 8 $cm^2/V.s$.

In order to compare the films deposited via PLD and magnetron sputtering, with thermally oxidised Cu_2O sheets, thermal oxidation conditions were also optimized. The oxidised sheets were etched in HNO_3 etchant at optimized etching conditions to remove any CuO on the surface. In the basic structural characterizations, the thermally oxidised sheets were found to have higher grain size even though there is higher stress.

Solar cells were prepared using Cu_2O from PLD, magnetron sputtering and thermal oxidation to compare their photovoltaic behaviour. The highest open-circuit voltage of 0.56 V was obtained for epitaxially grown PLD Cu_2O/Nb:STO heterojunction solar cell. However higher current of 1.9 mA/cm^2 was obtained for thermally oxidised Cu_2O solar cell (AZO/ZnO/Cu_2O/Au). The lower open-circuit voltage of thermally oxidised sheet was found to be due to difficulty in physically contacting the electrodes using probes during I-V measurements as the Surface photovoltage measurement of the junction of thermally oxidised Cu_2O/ZnO/AZO was found to be 500 mV. The sputtered Cu_2O based solar cell with architecture ITO/Cu_2O/AZO was also found to have comparable current of 1.76 mA/cm^2 but a lower open-circuit voltage of 0.26V.

The last part of this work focussed on the investigation of carrier dynamics in Cu_2O prepared via different techniques to better understand the influence of absorber preparation method on the obtained photovoltaic performance. A detailed comparison study of the Cu_2O films using advanced characterization techniques such as Transient absorption, time resolved photoluminescence, photothermal deflection spectroscopy, surface photovoltage spectroscopy were carried out which was not reported before and this will help to understand why high performing Cu_2O solar cells are not obtained when the preparation methods were varied.

Despite the good quality and electrical properties of the PLD film, The lower performance of PLD Cu_2O absorber was found to be due to lower exciton lifetime in the range of less than 1 ps from the Transient Absorption measurements whereas for the sputtered film, a photo-induced absorption (PIA) peak was visible even after 1μs. A long lifetime component at a higher energy state than the bandgap, possibly a trap, was observed in the long time TA measurements in the PLD Cu_2O which could be the factor affecting the exciton lifetime. This was not observed in the sputtered film. An exciton lifetime in the micrometer range is expected in a Cu_2O absorber without defects. Even though sub-band gap absorption due to defects were found in the absorbance spectra from PDS in both PLD and sputtered films, it was found to be more prominent in the sputtered Cu_2O film. Hence the sub-bandgap defects could be the factor affecting the exciton lifetime in sputtered film.

From PL decay kinetics analysis, it was also clear that the carrier lifetime is much lower for PLD film (315 ps). The oxidised sheet however was found to have a higher carrier lifetime of 4 ns. This better minority carrier lifetime in thermally oxidised sheets could be the key factor in obtaining high performance solar cells with thermally oxidised Cu_2O. From all the analysis done on the thermally oxidised Cu_2O, both basic and advanced it was clear that higher grain size, and better minority carrier lifetime are the key factors improving its efficiency as an absorber.

It is worth noting that there is potential for the sputtered Cu_2O film if the mobility of the film could be further improved as the carrier lifetime is comparable to the thermally oxidised sheet and since the deposition is carried out at a lower temperature, it is indeed a promising growth technique for Cu_2O absorber. Moreover, further optimization of the ion implantation doses on the sputtered Cu_2O film could eventually improve its properties and further studies in this direction is promising. Detailed studies on the PLD Cu_2O film using techniques such as Positron Annihilation Spectroscopy could help to understand more about the traps/defects which is reducing its exciton lifetime and will be useful to find a solution to overcome this limitation. We also believe there is further scope in the improvement of Cu_2O solar cell with sputtered film and thermally oxidised sheet by improving the heterojunction. Especially for the thermally oxidised sheet, since the surface is very reactive to oxidation, by reducing the etching time and top electrode deposition time to almost negligible can significantly improve the solar cell performance. Finding the right heterojunction with optimum barrier height is also a key factor to improve the photovoltaic properties. Thus, in spite of Cu_2O absorber being a long-researched

semiconductor, there is still a lot of room for improvement in both the material and heterojunction to obtain better performing solar cells.

APPENDIX

A.1 PHOTOVOLTAIC PRINCIPLE

The basic principle behind solar cells can be put in simple words as the conversion of sunlight into electricity using photoelectric effect. This concept was first introduced in the 1950s and since then there has been detail research to understand the mechanism to further improve the efficiency of the process and to utilize the full potential from the largest energy source available to mankind. The entire process can be divided into three steps, namely photoinduced charge generation, separation, and charge extraction. Upon illumination of a photoactive material electron-hole pairs (excitons) are generated which are then separated and extracted at two terminals leading to the generation of electric current. The entire process is fulfilled using different layers/stack of materials with desirable properties, such a device is called a photovoltaic cell or solar cell.

Semiconductor materials are the mostly used materials for photovoltaics. As atoms have discrete energy levels for electrons in the isolated state and in a solid when atoms are brought together in a crystalline lattice, due to the partial overlap of atomic wave functions of electrons, the allowed energy state of electrons split up leading to negligible difference in the discrete energy levels thus forming a continuum. This continuous density of states (DoS) is called a band. The energy of the bands determines its occupancy. The highest fully occupied band is called the valence band (VB) and the lowest unoccupied band is called conduction band (CB). The energy difference between these two bands is called the bandgap (E_g). The occupancy of the bands depends on temperature and the material. At ground state (zero Kelvin temperature), the conduction band will be empty, and the valence band will be fully occupied. Upon gaining a discrete amount of energy higher than the bandgap of the material, the electrons in the valence band will shift to the conduction band. The bandgap of semiconductors can further be tuned according to applications by adding impurities. In an intrinsic semiconductor (pure/ undoped) above zero Kelvin, electron-hole pairs are excited. When an electron is excited to the conduction band, the void created in the valence band is called a ``hole`` and can be considered as a positive charge particle. The distribution of electrons over the energy states is given by the Fermi distribution function (Figure A.1.1):

$$f(E) = \frac{1}{\exp\left[\frac{E-E_f}{k_B T}\right]+1} \quad \textbf{0.1}$$

where E is the energy of electron, T is the temperature and E_f is the Fermi energy. The Fermi level occupation probability is ½ and states above the energy is unoccupied and below are occupied at zero Kelvin. In an intrinsic semiconductor, the density of electrons and holes are equal, and the intrinsic density is given by:

$$n_i^2 = N_C N_V \exp\left(\frac{-E_G}{kT}\right) \quad \textbf{0.2}$$

The Fermi energy when $n_e = n_h$ is given by

$$E_F = \frac{1}{2}(E_V + E_c) + \frac{1}{2}kT \ln\frac{N_v}{N_c} \quad \textbf{0.3}$$

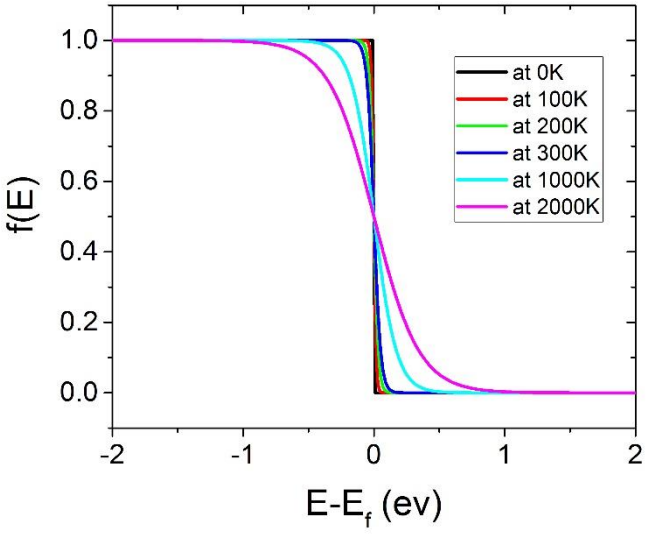

Figure A.1.1 Fermi distribution function at different temperatures**[195]**

Intentional doping of an intrinsic semiconductor with acceptor (donor) atoms, results in p(n) doping and n_h (n_e) increases and Fermi energy shifts close to valence (conduction) band. The number of "free carriers" increases with the intentional doping. The new Fermi energy level E_{FA} (E_{FD}) is given by the equations:

$$E_{FA} = E_V + kT \ln \frac{N_v}{n_h} \quad \textbf{0.4}$$

$$E_{FD} = E_c - kT \ln \frac{N_c}{n_e} \quad \textbf{0.5}$$

As depicted in Figure A.1.2, when a semiconductor is illuminated, it absorbs the photons, and if the absorbed photon energy, ħω is higher than the band gap energy of the semiconductor, it generates electron-hole pairs (excitons) which are bound together by coulombic forces. These excitons are unstable at room temperature (in inorganic solar cells) resulting in the shift of electron from valence band to the conduction band. By generating phonons, the excited electron relaxes to the lower edge of the conduction band, however further relaxation to the valence band is not probable as it involves higher energy. Thus, the hole and electron densities in the valence band and conduction band respectively increase upon illumination so that $n_h n_e > n_i^2$. The charge density is given by,

$$n_e n_h = n_i^2 \exp\left(\frac{E_{FC} - E_{FV}}{kT}\right)$$

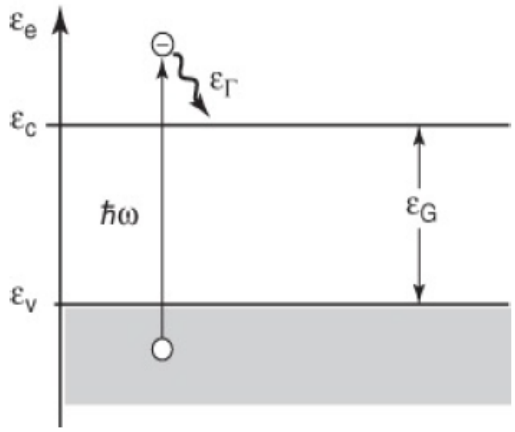

Figure A.1.2 Excitation of an electron from valence band to conduction band in a semiconductor upon illumination by absorbing a photon of energy ħω[2]

The separation of an exciton and their extraction is achieved in a solar cell with the help of a potential barrier. In most of the types of solar cells, the potential barrier is achieved with the help of a p-n junction. The junction is achieved with the help of two semiconductors. A solar cell with p-n junction from the same semiconductor material is a homojunction solar cell,

wherein if the p and n type material are of two different semiconductors it is called a heterojunction solar cell. A junction of metal and semiconductor is called a Schottky junction. An intrinsic semiconductor is charge neutral; however, they can be modified to n or p type with appropriate dopants. The most popular Si based solar cells are mostly homojunction with p-type and n-type doped Si contributing to the junction. When an n and p type semiconductor form a junction, the free electrons from the n- side and free holes from the p-side diffuses at the junction creating a space charge region (depletion region) with a built-in voltage. Due to the built-in voltage, there will be band bending at the junction and Fermi energy mismatch. The width of the space charge region can be modified by applying voltage (biasing) and by making it zero, the electric current flows. The energy band diagram of a typical n-p junction solar cell is shown in Figure A.1.3.

The very basic structure of a typical solar cell includes a window layer (n or p type), the light absorbing layer called absorber layer (i/n/p-type). On top, there will be electrodes (TCO) to collect the charges, which are also transparent to allow the sunlight to pass through and fall onto the absorber. At the bottom as well, there will be electrodes to collect the current. The different layers are fabricated onto a substrate. As the properties of each material influences the performance of the solar cell, in order to achieve a photovoltaic cell with high performance, it is important to carefully design the different layers. Another critical factor is the interfaces of different layers and hence it is important to consider the properties such as lattice constant, work function, electron affinity, thermal expansion coefficient. The important parameter for transparent conducting oxide (TCO) is good carrier concentration, mobility, and high transparency in the visible spectrum. A low resistance contact to the absorber is also crucial. Most of the n- type semiconductors have good conductivity, and a wider bandgap is preferred to allow maximum incident sunlight to pass through to the absorber. The window layer forms the junction with the absorber and should be thin for low series resistance and have high bandgap. For epitaxial deposition the lattice mismatch at the junction is also important. The back contact should have a work function matching the type of absorber as it makes an ohmic contact to the absorber. A high work function metal such as Au and Mo for hole collection and low work function metal such as Al, Ag for electron collection. The substrate should be mechanically stable, match the thermal expansion coefficients of deposited layers and moreover inert during device fabrication. Depending on the criteria different substrates such as flexible substrates (polymer film, stainless steel foils), metal, glass, transparent substrates (superstrate

device), conductive substrates.[8] There are different architectures, and possibility of additional further layers to improve the output efficiency of a solar cell.

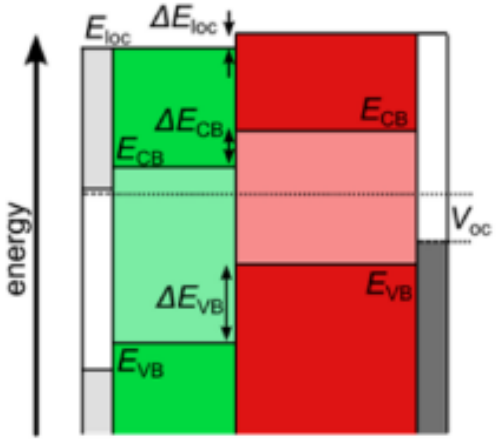

Figure A.1.3 Band diagram of a n-p junction solar cell[4]

As the top layer will be thinner, upon irradiation, the photons reach the junction easily and breaks the thermal equilibrium of the junction such that the minority carriers (electrons on the p- side and holes in the n-side) can cross the depletion region. Because of the junction barrier potential, the movement of the minority carriers in the opposite direction once they crossed the junction is not favourable because of the same barrier potential. Hence, the concentration of electrons and holes in the n and p side increases respectively thus resulting in a photovoltage and a small current flow when a load is connected across the junction. The total photocurrent generated have two components depending on where the charge carriers are generated upon photon absorption. If the charge carriers are in the p or n region, which further reaches the depletion region and then drifted across the junction to the region where they are majority carriers, they contribute to the diffusion current. If the charge carriers generated at the depletion region are separated by the electric field, they also contribute to the generated photocurrent. The total photocurrent is the sum of these two currents. The total current density upon illumination is only a portion of the photogenerated current (J_{ph}) after considering the reverse saturation current density (J_s) flowing through the diode. Hence the total current density J(V) under illumination is given by:

$$J(V) = J_s \left[\exp\left(\frac{e_0 V}{kT}\right) - 1\right] - J_{ph} \qquad \textbf{0.6}$$

In a solar cell, there will be additional ohmic losses and morphological defects further affecting the current density extracted. Hence if a solar cell is represented by an equivalent circuit (Figure A.1.4(a)), the losses can be modelled by taking also into consideration the losses from contact resistance of the wiring represented by a series resistance and a shunt or parallel resistance representing the morphological defects.

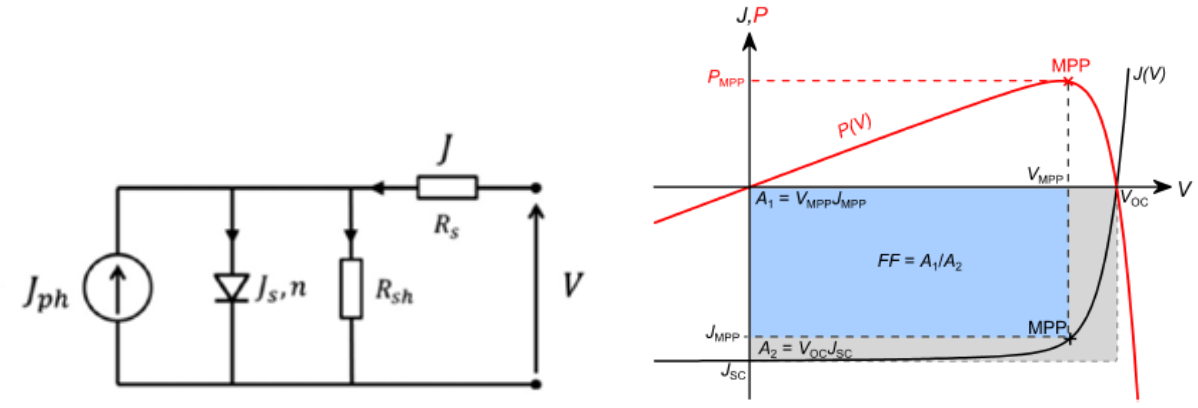

(a) (b)

Figure A.1.4 (a) Equivalent circuit model of a solar cell also considering the recombination and transport losses (b) J-V curve of an ideal solar cell[1]

The current density J and open circuit voltage V_{OC} of an ideal solar cell is then given by:

$$J = J_s \left[\exp\left(\frac{e_0 V - JR_s}{kT}\right) - 1\right] + \frac{V - JR_s}{R_{sh}} - J_{ph} \qquad \textbf{0.7}$$

$$e_0\, V_{oc} = E_g - k_B\, T \ln\left(\frac{N_C N_V}{n_e n_h}\right) \qquad \textbf{0.8}$$

The J-V curve of an ideal solar cell is represented as the black curve in Figure A.1.4(b). This is a basic characterization technique to measure the performance of a solar cell. From the curve, the voltage at zero current gives the open circuit voltage V_{OC} and the current density at zero voltage is the short-circuit current density, J_{SC}. The power output P is the product of the current density J and voltage V. The red curve in the Figure A.1.4(b) shows the power curve extracted from the current and voltage. The peak of the curve gives the maximum power that can be

extracted from the solar cell (Maximum Power Point) and the corresponding voltage at P_{MPP} is V_{MPP} and current is J_{MPP}. The measure of the quality of charge extraction from a solar cell is given by a parameter called fill factor (FF). It is the ratio of grey and blue rectangle in Figure A.1.4(b) and is given by the equation:

$$FF = \frac{J_{MPP}\, V_{MPP}}{J_{SC}\, V_{OC}} \qquad \textbf{0.9}$$

The power conversion efficiency of a solar cell which is the ratio of maximum power generated to the irradiated power, can be calculated from the above parameters, and is given by:

$$\eta = \frac{P_{MPP}}{P_{light}} = \frac{V_{OC} J_{SC} FF}{P_{light}} \qquad \textbf{0.10}$$

The solar radiation on different parts of Earth is different, hence a standard of AM called Air Mass is established to easily quantify the irradiation and to compare. An AM 1.5G spectrum with a power density of 1000 W/m^2 is used to calculate the PV performance as a standard. This value is considered as 1 sun.

The quality of energy conversion can also be quantified by another parameter called Quantum Efficiency (QE) which can be expressed either as External Quantum Efficiency (EQE) and Internal Quantum Efficiency (IQE). External Quantum Efficiency (EQE) is the ratio of the number of carriers collected to number of incident photons at a particular wavelength. Whereas Internal Quantum Efficiency (IQE) is the ratio of amount charge carriers collected to the number of photons absorbed by the absorber with wavelength.

A.2 PULSED LASER DEPOSITION (PLD)

Pulsed Laser Deposition is one of the commonly used thin film fabrication technique. It is a physical vapour deposition technique. Even though PLD was first reported in literature in the 1965 where it was used to grow semiconductor films and dielectric using a ruby laser[5]. A breakthrough happened in 1987 at Bell Communications Research when this deposition method was used for in situ growth of epitaxial high-temperature superconductor films[6]. Since that time PLD is popular technique for the deposition of several complex oxide films. Advancement in the PLD process have led to layer-by-layer growth of the film which can be monitored by Reflection high energy Electron Diffraction (RHEED)[7]. This allows for the better use of the technique for complex depositions tailored made for specific applications.

PLD is a simple technique conceptual and operational point of view as illustrated in the schematics in FigureA.2.1(a). A 20-30 ns wide high energy laser pulse (~ 1-10 J/cm^2) ablate the "target" thus rapidly removing material from it generating plasma plume (laser plume). A plasma plume is a transient and highly luminous collection of neutral or ionic atoms and molecules generated by vaporizing the surface material of the target. "Target" is a pellet made of the material whose thin film is to be deposited. It is attached on the target carousel and rotates throughout the deposition. The substrate onto which the film should be deposited is attached on a substrate holder which is also a heater and is placed opposite to the target. The heating element allows for the deposition of films at varied temperatures. The generated plasma plume expands while it travels away from the target towards the substrate and condenses onto the substrate forming a film. The typical velocity of the plasma plume is 106 cm^{-1}, however neutral atoms, electrons and ions travel at different velocities. Per pulse approximately 1 Å of film is deposited (for ~ 200 mJ/pulse) and laser pulse rate can be controlled from 1 to 100 Hz. The schematics shown here in Figure A.2.1(a) corresponds to the setup used in this work. However, it is possible to have several other arrangements such that the substrate can be positioned parallel to the plume propagation or in the same plane as the target.

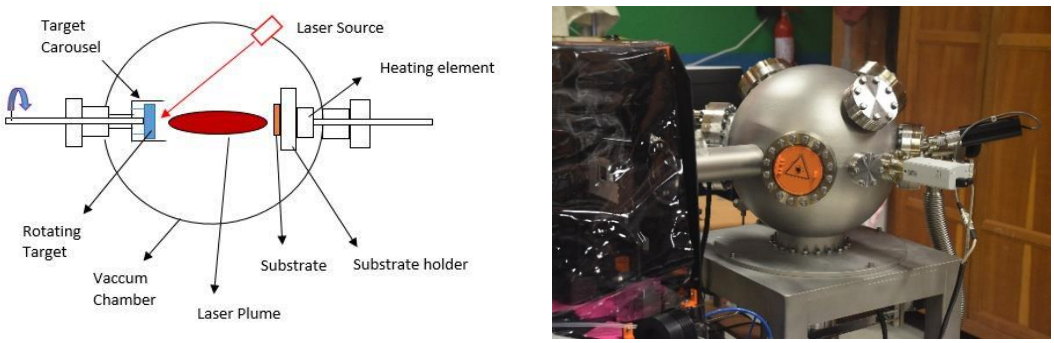

(a) (b)

Figure A.2.1 (a) Schematics of PLD setup (b) Photo of PLD system at ICube Laboratory

Laser ablation on the target can cause heating rates as high as 10^{11} K/s on the target surface and gas pressure of 10-500 atm[8]. The wavelength of the laser used determines the penetration depth on the target. To avoid subsurface boiling which will cause numerous large particulates on the film surface, it is preferrable to use a laser with smaller penetration depth so that the energy is absorbed on the surface of the target within a shallow layer. Practically possible lower wavelength limit for the laser is approximately 200 nm as there will be absorption of photons in the beam path by optical elements and oxygen molecules[7]. Lasers using KrF excimers (248 nm, 20-35 ns pulse duration) is the most used for PLD, while ArF (193 nm) and XeCl (308 nm) excimers are also used for film growth. Longer pulse durations (tens of nanoseconds) can lead to higher interaction between the incident beam and the plasma plume which can lead to increased heating. Additionally, the laser fluence must be higher than a threshold value to emit the species from the target surface which is typically in the range of 1-3 J/cm^2 for 25 ns pulse. The growth rates of PLD can be easily manipulated by adjusting the laser parameters.

One of the greatest advantages of PLD technique is the stoichiometric transfer of material from the target. However, that doesn't guarantee the growth of stoichiometric films as all the species in the plasma does not get deposited at the same rate as processes like re-sputtering (by high energy ions) or re-evaporation of volatile elements might occur. For the deposition of oxide films, the control of oxygen content is the most important factor and deposition at different background pressure highly influence the film stoichiometry. The nucleation and film growth in PLD is highly material dependent.

As there are no ion or evaporation sources involved in this technique, it is relatively simple to operate in high pressures using reactive gases like oxygen. The thickness of the deposited film

can be controlled using the laser fluence and deposition time, also, PLD have relatively high deposition rate. Even though the process of PLD involves an interplay of several factors determining the properties of the deposited film, it involves simple clean processing and laser is used as an external energy source. Additionally, since several targets can be attached to the target carousel, deposition of multilayer film is possible without taking the substrate from vacuum.

One of the main limitations of this deposition techniques is that since the plasma plume is highly forward directed, the composition of the deposited film is not controllable, and thickness of the film will not be uniform. In PLD, the area of deposition is small which limits the usage of this technique in large industrial processes which usually require large processing area. Even though the technique is simple, the mechanisms involved in the PLD is rather complex including the ablation, plasma generation, propagation of the plume and nucleation and growth of the film. Several factors influence the properties of the deposited thin film, laser fluence, background gas, target-substrate distance, temperature of deposition etc to name a few. Hence, a lot of optimizations is necessary for the deposition of new materials. The ablated material can contain large globules of molten materials (up to 10 μm diameter) which when deposited onto the substrate can increase the roughness of the film thus adversely affecting its applications.

A.3 MAGNETRON SPUTTERING

Magnetron sputtering is a vacuum-based physical technique just like PLD. It is a popular technique for the deposition of oxide thin films. The main advantage of the sputtering technique is that even at low temperature high deposition rate can be achieved in this technique. Moreover, accurate control of the stoichiometry of the deposited thin film is possible. Similar to other thin film deposition techniques, the property of the thin film depends on the oxygen partial pressure, gas flow rate, temperature of the substrate and chamber pressure.

In a "normal" sputtering process, a target is bombarded with high energy ions which emit molecules from the target. These molecules with high kinetic energy travel to the substrate to form a film.

In magnetron sputtering technique, the ionization of the atoms hitting the target is increased with the help of magnetic fields. This in turn increases the sputtered atoms. Figure A.3.1(a) shows the principle of magnetron sputtering. With the help of horseshoe magnet, magnetic field is created close to the target surface (parallel to target surface $\mathbf{B_p}$). In addition to the magnetic field, by applying a negative potential at the target, an electric field **E** perpendicular to the target surface is also created. A DC (direct-current) high voltage or RF (radio-frequency) or HF (high-frequency) supply can be applied to the target to ignite the magnetron discharge. Based on this there are two types of sputtering, DC Magnetron Sputtering and RF Magnetron Sputtering. A sputtering gas most probably Argon is introduced into the sputtering chamber with the help of a gas regulating system. The high voltage inside the vacuum chamber argon gas gets ionized creating a magnetron plasma in which the ions and electrons are separated. The free electrons experience a force **F** given by

$$\mathbf{F} = -q * (\boldsymbol{E} + \boldsymbol{v} * \boldsymbol{B_p}) \qquad \textbf{0.11}$$

where q is the elementary charge and $\boldsymbol{v}$ is the velocity of electron.

The secondary electrons emitted perpendicular to the target are only influenced by the electric field and hence moves away from the target surface and exhibits helical motion (depicted by green circle in Figure A.3.1(a)) and are trapped above target surface. Each of these electrons improves the ionization of the Argon gas. After ionization of the Argon gas, the positively charges ions accelerate towards the negatively charged target sputtering the target material. The sputtered material then travels to the substrate and deposit. The formation of trapped electrons

in magnetron sputtering enhances the efficiency of sputtering by increasing the sputtering rate up to 1 μm/min.

Using magnetron sputtering, by combining a reactive gas such as oxygen, nitrogen or any carbon-containing gas, the concept of "reactive sputtering" can be achieved. Under the right conditions of deposition parameters such as substrate temperature, sputtering gas pressure, rate, energy of the ions hitting the substrate etc a compound material can be formed with the help of condensation and chemical reactions on the substrate surface in reactive sputtering. By introducing oxygen gas as the reactive gas, thin oxide films can be formed on the substrate. Figure A.3.1(b) shows the schematics of the setup. In this thesis, Cu_2O films were deposited using Argon as the sputtering gas and oxygen as the reactive gas and a Cu target.

The key factors to consider for getting good quality film with rather homogenous coverage are suitable ion energies/intensity, right substrate temperature and optimum base pressure of the sputtering chamber. Much higher ion energies are not favorable as higher energy ions might get implanted at a depth in the bulk material which is a radiation damage. Relatively low ion energies (30-90 eV corresponding to bias voltage of -30 to -90 V) a rather homogenous film will be formed on the substrate surface due to close packing procedure of the sputtered particles reaching the substrate. The influence of substrate temperature is also critical as too low temperatures leads to island formation. The deposited atoms will be less bonded to the substrate as they are more strongly bonded together which leads to voids in the deposited film. Higher substrate temperature enhances the lateral movement sputter atoms due to increase in the vibrational energies. Additionally, the base pressure of the vacuum chamber should not exceed 10^{-6} mbar as at too high pressures, impurities such as oxygen and other gases influence the film.

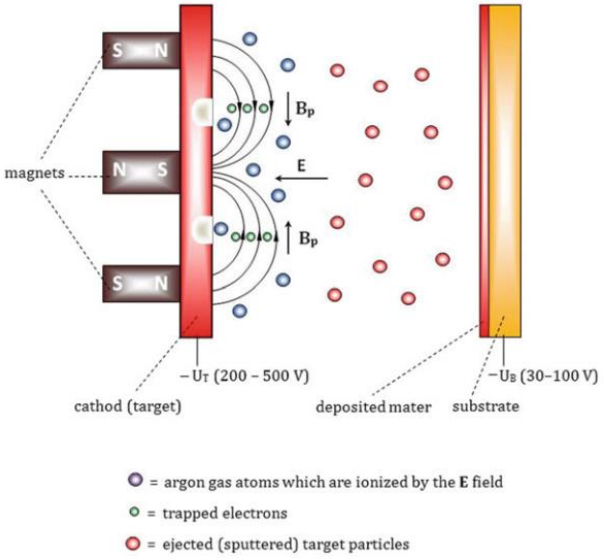

(a)

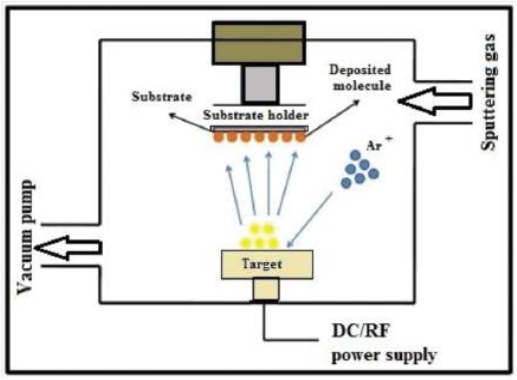

(b)

(c)

Figure A.3.1 Principle of magnetron sputtering with the arrangement of magnets behind the target which is at negative potential (copied from **[9]**) (b) Schematics of Magnetron sputtering technique (copied from [10]) (c) Photograph of the sputtering setup at ICube Laboratory

One disadvantage of reactive sputtering is the different stresses that could be developed on the deposited film which could be thermal stress (due to difference in the thermal expansion coefficient of the two materials) or internal stress (due to impurities in the film, microscopic lattice defects, lattice mismatch of film and substrate). Excessive build up of stress leads to poor adhesion to the substrate and result in peel off.

It is also worth noting that the sputtering rate will be reduced for reactive sputtering due to the formation of compounds also on the target surface which eventually reduces the sputtering yield. More than 50 % decrease can be expected as the target may become less conducting and the deposition conditions completely changes. This can be avoided by keeping the reactive gas flow rate below the threshold or by pulsing the magnetron bias supply.

Some of the main advantages of magnetron sputtering are the films will have lower surface roughness, moderate deposition rate, possibility of columnar growth, good quality and high film density.[9]

REFERENCES OF APPENDIX

[1] C. Venugopalan Kartha, 'Investigation of Degradation Phenomena in Organic Solar Cells upon Air Exposure', Faculty of Engineering,University of Freiburg, Freiburg, 2019.

[2] P. Würfel and U. Würfel, *Physics of Solar Cells: From Basic Principles to Advanced Concepts*. John Wiley & Sons, 2009.

[3] K. L. Chopra, P. D. Paulson, and V. Dutta, 'Thin-film solar cells: an overview', *Progress in Photovoltaics: Research and Applications*, vol. 12, no. 2–3, pp. 69–92, 2004, doi: https://doi.org/10.1002/pip.541.

[4] S. Rühle *et al.*, 'All-Oxide Photovoltaics', *J. Phys. Chem. Lett.*, vol. 3, no. 24, pp. 3755–3764, Dec. 2012, doi: 10.1021/jz3017039.

[5] H. M. Smith and A. F. Turner, 'Vacuum Deposited Thin Films Using a Ruby Laser', *Appl. Opt.*, vol. 4, no. 1, pp. 147–148, Jan. 1965, doi: 10.1364/AO.4.000147.

[6] D. Dijkkamp *et al.*, 'Preparation of Y-Ba-Cu oxide superconductor thin films using pulsed laser evaporation from high Tc bulk material', *Applied Physics Letters*, vol. 51, no. 8, pp. 619–621, 1987, doi: 10.1063/1.98366.

[7] H. M. Christen and G. Eres, 'Recent advances in pulsed-laser deposition of complex oxides', *Journal of Physics: Condensed Matter*, vol. 20, no. 26, p. 264005, Jun. 2008, doi: 10.1088/0953-8984/20/26/264005.

[8] D. Geohegan, D. Chrisey, and G. Hubler, 'Pulsed laser deposition of thin films', *Chrisey and GK Hubler (eds), Wiely, New York*, pp. 59–69, 1994.

[9] M. Braun, 'Magnetron Sputtering Technique', in *Handbook of Manufacturing Engineering and Technology*, A. Y. C. Nee, Ed. London: Springer London, 2015, pp. 2929–2957. doi: 10.1007/978-1-4471-4670-4_28.

[10] A. Jilani, M. S. Abdel-wahab, and A. H. Hammad, 'Advance Deposition Techniques for Thin Film and Coating', in *Modern Technologies for Creating the Thin-film Systems and Coatings*, N. N. Nikitenkov, Ed. InTech, 2017. doi: 10.5772/65702.

Résumé en français

La plupart des cellules solaires disponibles commercialement sont basées sur le silicium (Si). Cependant, comme leurs étapes de fabrication sont coûteuses, avec une durée d'amortissement énergétique longue, les matériaux pour cellules solaires alternatifs et à bas coût sont importants et sont fortement étudiés depuis quelques dizaines d'années. Dans une cellule solaire, les oxydes sont largement utilisés pour le transport électronique, les électrodes transparentes, et les couches intermédiaires dans les cellules tandem. De plus, les oxydes sont aussi pertinents comme couche photoactive en tant qu'absorbeur de photons, du fait de leur abondance, faible toxicité, et stabilité sous condition atmosphérique. Ainsi, une des technologies les plus investiguées et en pleine croissance est les cellules solaires tout oxyde. Parmi les oxydes absorbeurs, Cu_2O est l'un des matériaux les plus prometteur et abondant. Il est un absorbeur prometteur du fait de nombreux facteurs comme un coefficient d'absorption élevé, une bande interdite directe favorable, un élément de base le cuivre abondant, et la non-toxicité. C'est un semiconducteur de type p avec une bande interdite d'environ 2,0-2,2 eV. Cependant, le rendement de conversion des cellules solaires à base de Cu_2O à ce jour est en-dessous des 10% ce qui est bien en-dessous de la limite de Schockley-Queisser (~ 23 %). Beaucoup d'efforts ont été entrepris pour augmenter le rendement de conversion de cellules à base de Cu_2O depuis que l'effet photoélectrique a été découvert dans les années 1930 dans cet oxyde. L'une des difficultés majeures est la faible stabilité de Cu_2O à température ambiante et ainsi l'obtention de la phase de Cu_2O sans la phase parasite CuO est très difficile. De plus, pour les cellules solaires à hétérojonction, des facteurs clé pour améliorer le rendement sont l'alignement des niveaux d'énergie, la réduction des offsets d´alignement des bandes des différents matériaux et la réduction des défauts d'interface.

La nature de la technique de croissance pour obtenir l'absorbeur Cu_2O joue énormément sur le rendement de conversion. Les films de Cu_2O peuvent être élaborés par différentes techniques par voie physique ou chimique. La conductivité du Cu_2O provient principalement des vacances de Cu qui dépendent des conditions de température et de pression durant la synthèse. Ainsi, il est important de bien maîtriser la croissance d'absorbeurs de Cu_2O via ces différentes techniques pour améliorer ses performances photovoltaïques. Les cellules solaires Cu_2O préparées par oxydation thermique de feuilles de cuivre fournissent les meilleurs rendements de conversion à ce jour (Figure 1). Cependant, comme cette oxydation requiert une température

supérieure à 1000°C, des voies alternatives de croissance de Cu_2O sont nécessaires pour des applications performantes à grande échelle et en particulier permettant l'utilisation de substrats flexibles. Mais pour atteindre cela, il est important de comprendre les différences entre les propriétés des absorbeurs de Cu_2O obtenus par différentes techniques, afin que cet absorbeur puisse être façonné pour obtenir les propriétés désirées, pour obtenir un meilleur rendement de conversion.

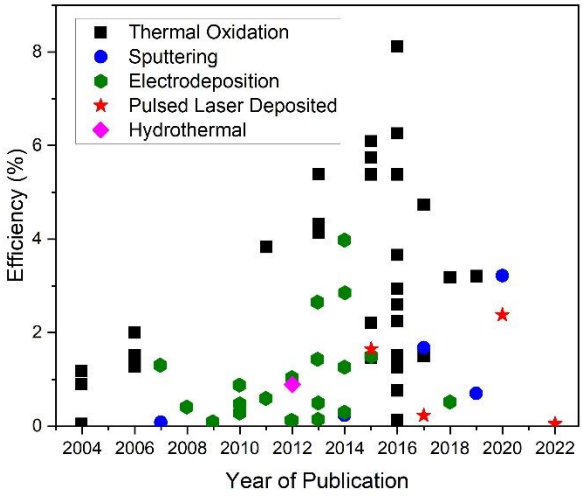

Figure 1 Rendements de conversion de cellules solaires à base de Cu_2O fabriqué par différentes techniques

Dans ce travail, des absorbeurs de type p de Cu_2O sont préparés en utilisant trois techniques différentes, l'ablation laser pulsé (PLD), la pulvérisation cathodique, et l'oxydation thermique. Bien que la PLD et la pulvérisation cathodique soient deux techniques connues pour fournir des films de haute qualité, les absorbeurs de Cu_2O par ces voies ne fournissent pas de cellules solaires à rendement de conversion élevé. Une étude détaillée des films de Cu_2O préparés par ces différentes techniques, au niveau des propriétés structurales, optiques, électriques, permettra de mieux comprendre les facteurs limitants visant à améliorer encore les propriétés de cet absorbeur. L'exploration d'hétérojonctions pour obtenir des cellules solaires à base de Cu_2O avec différents oxydes transparents conducteurs (TCOs) est également proposée dans ce travail.

Dans le **chapitre 1** nous introduisons les propriétés de base d'un absorbeur photovoltaïque et en détaillant les différents types d'absorbeurs à base d'oxyde. Nous proposons un état de l'art

sur les cellules solaires tout oxyde avec différents absorbeurs. Les propriétés de base du Cu_2O sont également décrites, incluant la structure cristallographique, les propriétés optiques et électriques et les différentes méthodes de fabrication.

Le **chapitre 2** est dédié à la fabrication de Cu_2O par PLD. Les couches minces de Cu_2O obtenues par PLD ont été déposées à différents températures et pressions en utilisant une cible de CuO préparée à partir de poudre de CuO. Des couches minces de Cu_2O ont été obtenues à des températures de dépôt élevées de 750 °C (marqué A dans la Figure 2) et à 300 °C les couches sont du Cu_xO (marqué B dans la Figure 2) en variant la pression partielle d'oxygène. Le ratio cuivre vs. oxygène dans les films a été étudié par spectroscopie de rétrodiffusion de Rutherford (RBS). La Figure 2 montre clairement la variation de la stœchiométrie dans les films de Cu_xO avec la température de dépôt et la pression partielle d'oxygène. La RBS est une technique à plus grande zone d'analyse que les caractérisations locales comme la spectroscopie Raman, et de fait fournit des résultats plus fiables. Les propriétés des différents films obtenus par PLD sont décrites dans ce chapitre et l'évolution de la qualité de la surface, des propriétés optiques et électriques sont aussi décrites en mettant en évidence quatre films caractéristiques (A, B, C, D dans la Figure 2).

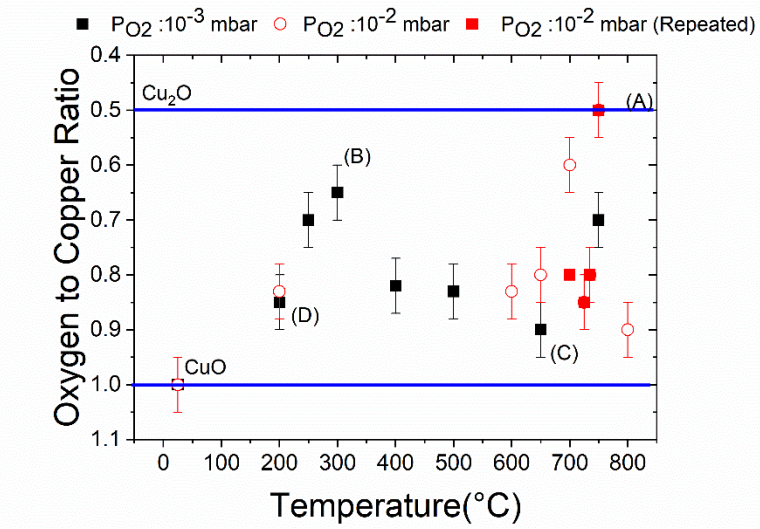

Figure 2 Ratio cuivre vs. oxygène déterminé par RBS de films PLD de Cu_xO

Le **chapitre 3** porte sur les films de Cu_2O obtenus par pulvérisation cathodique. Ils ont été déposés grâce à une cible de Cu commerciale et les paramètres de dépôt tels que la température et les pressions et flux de gaz ont été optimisés. L'obtention d'une stœchiométrie de type Cu_2O

a été confirmée par RBS, diffraction de rayons X et spectroscopie Raman. L'influence du débit d'oxygène sur la stœchiométrie des films déterminée par RBS est montrée dans la Figure 3. Les paramètres de dépôt pour obtenir des films de Cu_2O purs sont P : 53W, Ar/O_2 : 16 / 1.8 sccm, T : 300°C. La qualité de ces films et leurs propriétés optiques et électriques ont été ensuite analysées par différentes techniques pour évaluer leur potentiel comme absorbeur photovoltaïque.

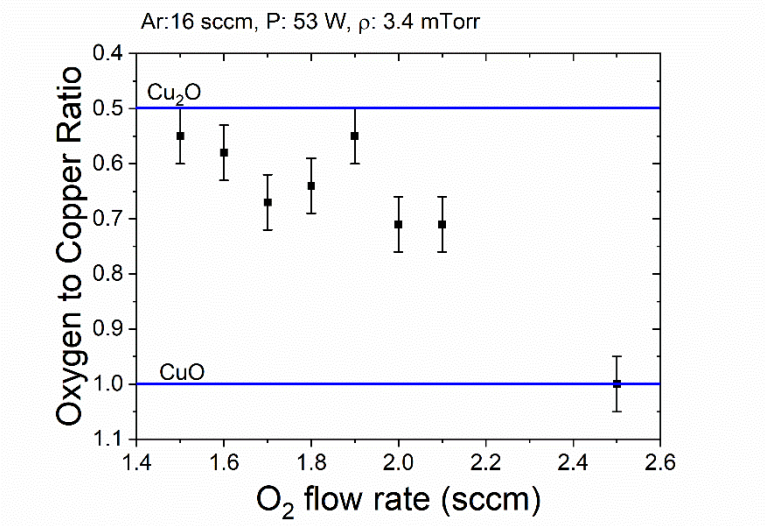

Figure 3 Ratio cuivre vs. oxygène de films Cu_xO par pulvérisation cathodique avec différents débits d'oxygène

L'oxydation thermique de feuilles de Cu à température élevée est la troisième technique d'élaboration de Cu_2O étudiée, présentée dans le **chapitre 4**. Les cellules solaires à base de Cu_2O les plus performantes dans la littérature sont obtenues par cette méthode. Afin de comprendre pourquoi, les conditions de fabrication ont été optimisées pour obtenir des feuilles de Cu_2O bonne qualité. Après oxydation les feuilles sont attaquées avec de l'acide nitrique pour enlever le CuO résiduel en surface.

Les caractérisations structurales du Cu_2O, préparé par les trois différentes techniques, par diffraction de rayons X et spectroscopie Raman, révèlent que la qualité des films déposés par PLD à haute température est meilleure qu'à basse température. Tandis que les films par pulvérisation cathodique à cette même basse température sont de bonne qualité avec un signal T_{1u} meilleur que le film de PLD (Figure 4). Le film PLD déposé à 300°C montre la moins bonne qualité de surface (ratio T_{1u} sur $2E_u$ de 0.80). Le plus faible ratio est pour le film PLD à 750°C (ratio 0.43) puis le film de pulvérisation cathodique à 300°C (ratio 0.66).

La feuille oxydée thermiquement a des pics Raman caractéristiques avec un signal T_{1u} très élevé, ce qui correspond à des photons activés par des défauts tels que les vacances de cuivre et les défauts interstitiels, qui contribuent à la conductivité du film. Le ratio d'intensité des pics Raman (0.36) révèle également que ces feuilles sont de meilleure qualité que les films obtenus par les deux autres techniques. Ce résultat est une indication que l'oxydation thermique produit du Cu_2O de bonne qualité avec moins de dommages de surface ce qui peut conduire à de meilleures performance photovoltaïques.

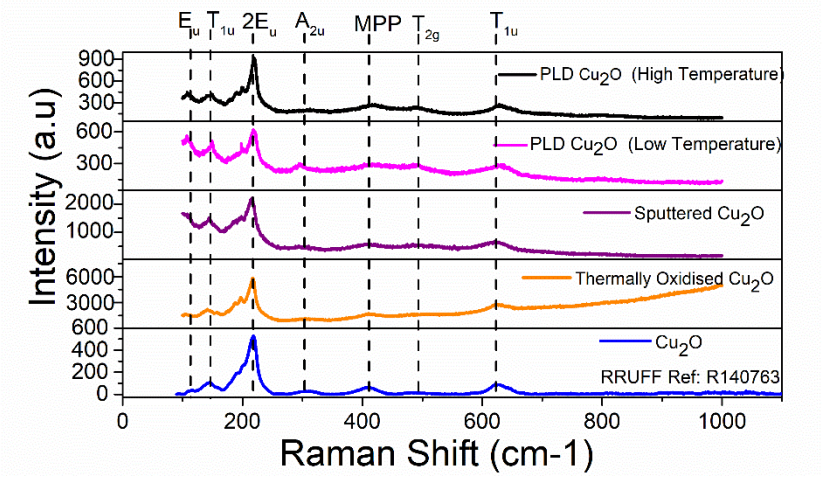

Figure 4 Spectres Raman de Cu_2O obtenus par les trois différentes techniques (longueur d'onde d'excitation de 532 nm)

L'analyse par diffraction de rayons X montre que les films par PLD à haute température ont des paramètres (0.427 nm) plus proche de la valeur idéale et moins de contraintes ce qui indique une meilleure qualité de film. Le film par pulvérisation cathodique a un paramètre de 0.428 nm et le film par oxydation 0.426 nm ce qui est aussi proche du Cu_2O pur. Les feuilles oxydées ont une taille de grain plus importante de ~110 nm ce qui est sept fois plus élevé que la taille de grain moyenne du film PLD. L'augmentation de la taille des grains permet de réduire les recombinaisons et la diffusion au joints de grain, ce qui améliore les propriétés électriques de films.

L'analyse de la morphologie par microscope électronique à balayage (MEB) montre des grains de forme rectangulaire de couverture uniforme pour le film PLD à 750 °C tandis que le film à 300°C est plus plat mais avec la présence de trous (Figure 5 a et b). Les films par pulvérisation cathodique déposés à 300°C sont encore plus plats, avec une bonne couverture et sans trous (Figure 5c). La rugosité RMS obtenue par AFM est de 2.7 nm seulement ce qui est bien plus

faible que par la PLD (47 nm à haute température et 7 nm à basse température) et la feuille oxydée (24 nm). Les larges grains de la feuille sont également visibles en MEB.

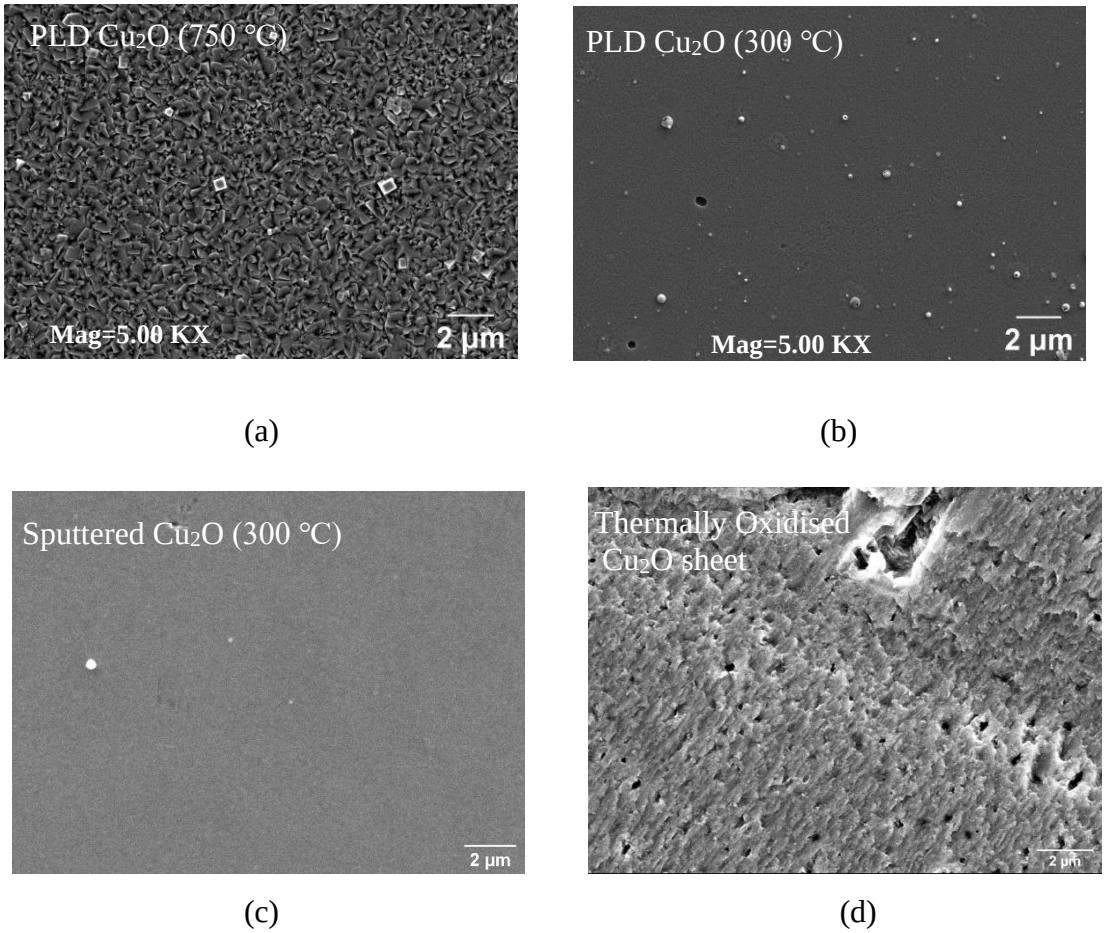

Figure 5 Images électrons secondaires de l'absorbeur Cu_2O préparé à (a) 750 °C, 10^{-2} mbar par PLD (b) 300 °C, 10^{-3} mbar par PLD (c) P: 53 W, Ar/O_2 : 16 /1.8 sccm, T:300 °C par pulvérisation cathodique (d) à 1050 °C par oxydation thermique

Les propriétés électriques des absorbeurs sont listées dans le Tableau 1. Le film PLD à haute température a la plus forte mobilité sans compromettre la densité de porteur, ce qui est généralement difficile pour Cu_2O. Les propriétés électriques du film PLD à basse température sont mauvaises du fait de la faible qualité de la surface. Le film par pulvérisation cathodique a une faible résistivité et une forte densité de porteurs mais également une mobilité faible. Pour les films déposés à faible température, la mobilité est limitée du fait de la diffusion par les centres ionisés. Une faible mobilité est également observée pour les films PLD à basse température. De plus, comme les films par pulvérisation cathodique ont une forte densité de

porteurs, la diffusion par les centres ionisés est élevée et ce sont probablement des défauts natifs. Tous les films montrent une conduction de type p. D'après l'analyse par effet Hall, le film PLD à haute température a de meilleures propriétés électriques que par pulvérisation cathodique.

Tableau 1 Propriétés électriques des films par mesure d'effet Hall

Echantillon	**Température (°C)**	**Epaisseur approx.**	**Résistivité (Ω.cm)**	**Mobilité Hall ($cm^2/V.s$)**	**Densité de porteurs (cm^{-3})**
PLD Cu_2O	750	100 nm	40±24	22.5±8.5	$+5x10^{15}±4x10^{15}$
PLD Cu_2O	300	100 nm	329.0±0.8	9.0±0.2	$+2.4x10^{15}±1.0x10^{15}$
Pulv. Cath. Cu_2O	300	100 nm	16.2±0.01	4.7±4.1	$+3.1x10^{17}$ $±2.6x10^{17}$

Les trois types d'absorbeurs ont un fort coefficient d'absorption, supérieur à 10^5 cm^{-1} ce qui est typique du Cu_2O, et une largeur de bande interdite entre 2 et 2.3 eV. La comparaison de la photoluminescence (PL), montrée dans la Figure 6, montre que le pic d'émission correspondant à l'émission en bord de bande est à la même longueur d'onde pour les trois techniques bien que la longueur d'excitation soit différente pour les films par pulvérisation cathodique. La forme du pic de PL est identique pour la PLD et l'oxydation thermique et ce dernier montre une forte intensité ce qui indique de plus faibles recombinaisons non radiatives, et donc moins de défauts. Dans les films par pulvérisation cathodique, des pics PL à plus haute longueur d'onde sont visibles. Leur origine n'est pas encore claire, mais pourrait être des vacances de Cu et des défauts interstitiels qui n'étaient pas visibles avec les autres longueurs d'onde d'excitation. Comme le pic est plus large dans la région proche infrarouge, il pourrait être dû à de l'émission de défauts multiples se recouvrant, liés à des centres de recombinaison n'étant pas observé pour la PLD et l'oxydation thermique.

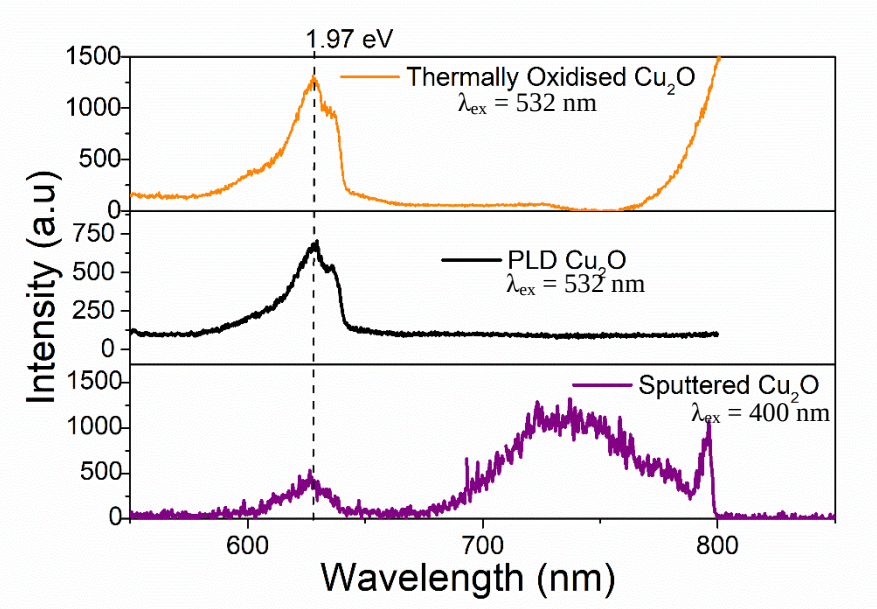

Figure 6 Spectres PL de Cu_2O obtenu par les différents techniques

Le **chapitre 5** et dernier chapitre de cette thèse concerne les comparaisons des propriétés photovoltaïques des différents absorbeurs Cu_2O formant des hétérojonctions avec différents TCOs et les caractérisations avancées pour mieux comprendre l'influence de la méthode de préparation sur les performances et la dynamique des porteurs.

La meilleure cellule solaire avec une couche de Cu_2O épitaxiée par PLD d'environ 100 nm d'épaisseur est obtenue sur Nb:STO avec une électrode supérieure semi-transparente d'or. La tension de circuit ouvert est de 0.56 V sous illumination AM 1.5G. La cellule montre une faible densité de courant de court-circuit de 0.21 mA/cm^2 qui peut être dû à la faible épaisseur de l'absorbeur et l'absorption de la couche supérieure d'or. Les cellules solaires par pulvérisation cathodique avec ITO en contact arrière et de l'AZO par PLD en contact avant donnent une densité de courant de court-circuit de 1.76 mA/cm^2 et une tension de circuit ouvert de 0.26 V. Les cellules solaires des feuilles de Cu_2O oxydé ont un contact arrière en or et un contact avant de ZnO/AZO. Elles fournissent une densité de courant de court-circuit de 1.9 mA/cm^2 et une tension de circuit ouvert de 0.19 V. En comparant les différents résultats dans la Figure 7 et le Tableau 2, le facteur de forme est une source majeure de perte de rendement de conversion. Mis à part les effets de l'hétérojonction, nous observons l'influence de l'absorbeur de Cu_2O sur les performances photovoltaïques et les caractéristiques I-V sont meilleures pour l'épitaxie par PLD.

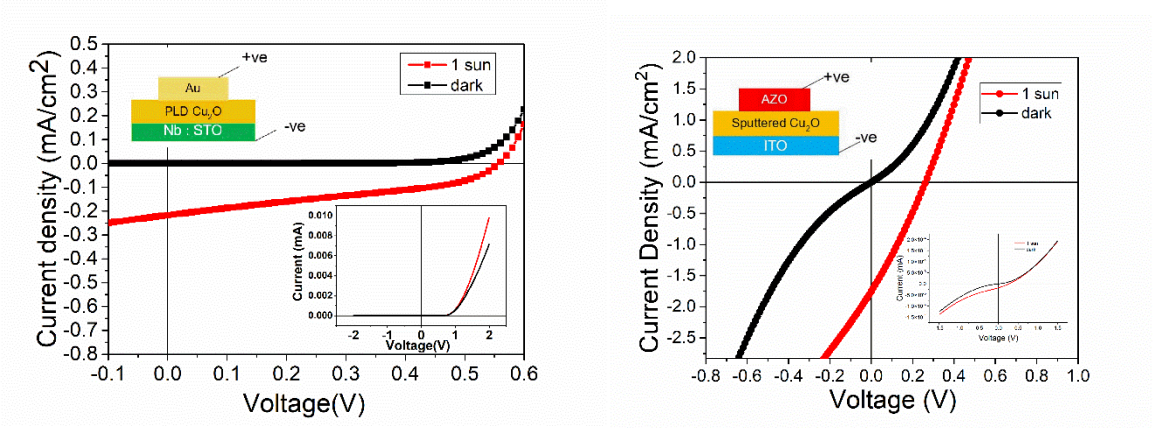

(a) (b)

(c)

Figure 7 Caractéristiques I-V de cellules solaires avec Cu_2O préparé par (a) PLD (b) pulvérisation cathodique (c) oxydation thermique. Les schémas des architectures sont indiqués dans les encarts.

Tableau 2 Paramètres des cellules solaires de Cu_2O préparé avec les différentes techniques

Architecture	Méthode de préparation de Cu_2O	Densité de courant de court-circuit	Tension de circuit ouvert	Rendement de conversion	Facteur de forme
Au/Cu_2O/Nb:STO	PLD	0.21 mA/cm^2	0.56 V	0.053 %	45.0 %
AZO/ Cu_2O/ITO	Pulv. Cath.	1.76 mA/cm^2	0.26 V	0.127 %	27.8 %
AZO/ZnO/ Cu_2O/Au	Oxydation thermique	1.90 mA/cm^2	0.19 V	0.09 %	25 %

Les résultats montrés dans le Tableau 2 correspondent aux meilleures cellules solaires obtenues. Nous pensons que l'écart par rapport aux valeurs de la littérature pour les feuilles de Cu_2O provient des défauts de l'hétérojonction et de la qualité de la surface car l'oxydation de la surface après la gravure chimique n'est pas contrôlée et la formation de CuO au niveau de l'hétérojonction est pratiquement inévitable. Même si les performances sont bien inférieures à d'autres types de cellules comme celles basées sur le silicium, les valeurs montrées ici sont comparables à celles obtenues dans la littérature par d'autres techniques telles que l'ALD et l'électrodépôt.

Dans le chapitre 5, nous utilisons également des techniques avancées de caractérisation pour mieux comprendre les différentes propriétés et la qualité des absorbeurs obtenus par les différentes techniques, en particulier la dynamique des porteurs dans Cu_2O. Nous utilisons différentes méthodes comme l'absorption transitoire (TA), la photoluminescence résolue en temps, la technique TCSPC (Time Correlated Single Photon Counting), PDS (Photothermal Deflection Spectroscopy), et Surface Photovoltage Spectroscopy (SPS).

Malgré la bonne qualité des films PLD, le faible rendement de conversion avec cet absorbeur est dû à un temps de vie de l'exciton de moins de 1 ps mesuré par absorption transitoire tandis que des pics d'absorption photo-induite (PIA) sont visibles même après 1 µs. Les pics GSB et TIA pour la PLD ont un déclin rapide de type mono-exponentiel. Les pics GSB des films par pulvérisation cathodique ont un déclin bi-exponentiel avec des constantes de ~1 ps et ~138 ps plus élevées que par PLD. Une composante à temps de vie long à une énergie supérieure au

bandgap est observée dans la mesure TA longue des films PLD, ce qui pourrait affecter le temps de vie de l'exciton et n'est pas visible dans les films par pulvérisation cathodique. Un temps de vie de l'exciton de plusieurs microsecondes est attendu dans le Cu_2O sans défauts, ce qui n'est pas observé dans les films. Ainsi la meilleure performance PV des films par pulvérisation cathodique par rapport aux films par PLD pourrait être due au plus grand temps de vie de l'exciton malgré des propriétés électriques et de surface inférieures.

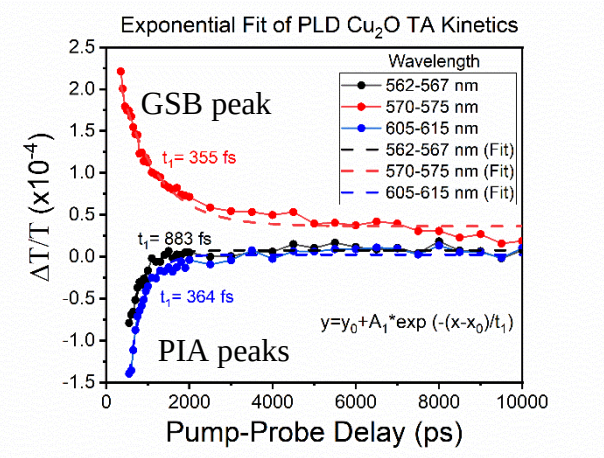

(a)

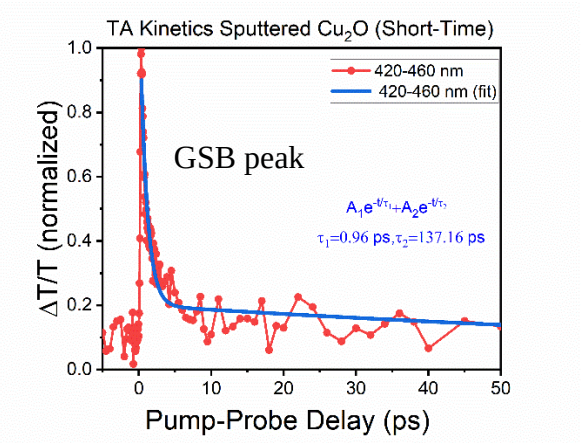

(b)

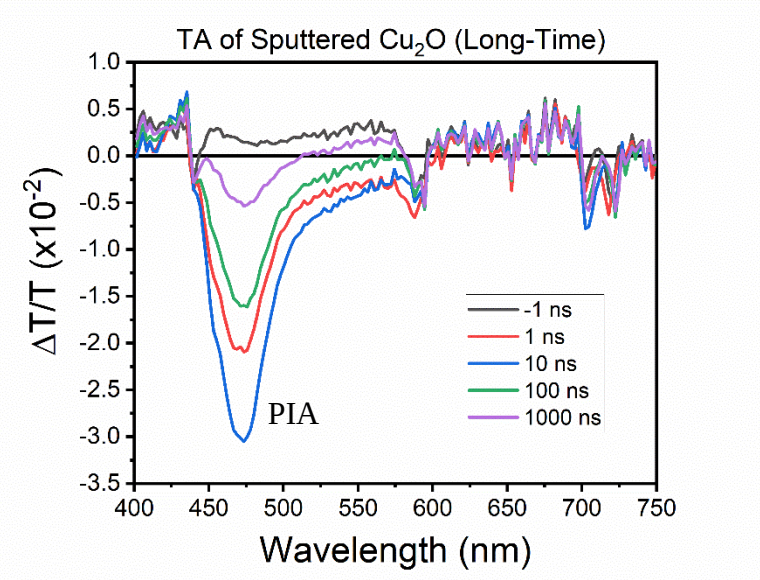

(c)

Figure 8 Cinétique de la mesure TA de (a) pics GSB et PIA de Cu_2O par PLD (temps courts) (b) pics GSB de Cu_2O par pulvérisation cathodique (temps courts) (c) spectres TA longs avec fort signal PIA

Bien que de l'absorption en-dessous du bandgap due à des défauts ait été observée dans les spectre d'absorbance par PDS à la fois dans les films PLD et pulvérisation cathodique, celle-ci est plus élevée dans les films par pulvérisation cathodique. Ainsi, ces défauts sous-bandgap pourraient être le facteur influençant le temps de vie de l'exciton dans les films par pulvérisation cathodique.

Le temps de vie dans Cu_2O a été analysé par ajustement des spectres de dynamique de PL par TCSPC (Figure 9). D'après cette analyse, il est clair que le temps de vie des porteurs est bien plus faible pour les films PLD avec un temps de déclin moyen de ~315 ps. Les feuilles oxydées ont un temps de vie des porteurs plus élevé, de 4 ns. Ce temps de vie des porteurs minoritaires plus élevé dans les feuilles pourrait être la clé pour l'obtention de cellules solaires performantes par oxydation du cuivre. Un temps de déclin rapide n'est pas souhaitable car les photoporteurs sont perdus plus rapidement par recombinaison radiative. Le déclin de PL aux deux longueurs d'ondes dans les feuilles oxydées est à peu près identique mais tri-exponentiel, avec un temps de déclin de 3.83 ns (pour le pic à 585 nm) et 4.14 ns (pour le pic à 476 nm). Le défaut pourrait avoir un temps de vie de fluorescence plus long que les recombinaisons de bord de bande. Le pic à 476 nm pourrait être dû à des défauts. Pour le film par pulvérisation cathodique aucun pic de PL n'était visible dans la mesure TCSPC. Mais le temps de vie de PL obtenu par TRPL pour le film par pulvérisation cathodique est le meilleur et d'environ 0.1 ns.

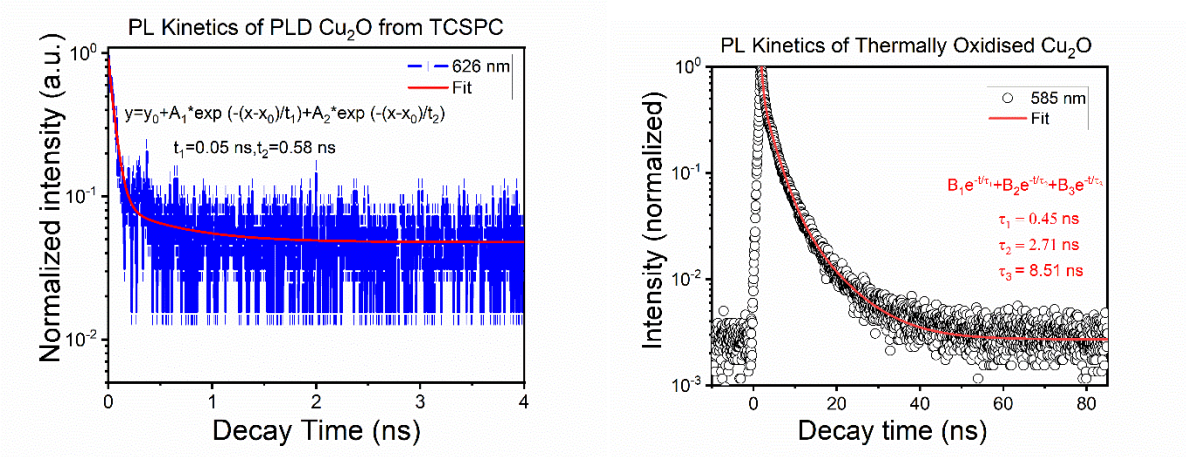

(a) (b)

Figure 9 Déclin de PL du pic d'émission en bord de bande de (a) film PLD de Cu_2O (b) feuille de Cu_2O oxydée thermiquement, par mesure TCSPC

D’après les analyses basiques et avancées sur les feuilles oxydées de Cu_2O, il est clair qu’une plus grande taille de grain et un meilleur temps de vie des porteurs minoritaires sont des facteurs clé pour améliorer les performances de l’absorbeur. Le tableau 3 résume les performances de cet absorbeur préparé soit par PLD, pulvérisation cathodique ou oxydation thermique. Ce travail ouvre la voie vers une meilleure compréhension des méthodes de croissance pour obtenir une phase pure de Cu_2O par PLD, pulvérisation cathodique et oxydation thermique et une comparaison des différents films est proposée. En implémentant ces films dans des cellules solaires tout oxyde nous illustrons les applications possibles. Ceci est un point de départ pour l’optimisation des absorbeurs de Cu_2O via les techniques répandues de la PLD et la pulvérisation cathodique, en identifiant les facteurs limitant leur performance par rapport aux feuilles oxydées de Cu_2O.

Tableau 3 Résumé des performances de l’absorbeurCu_2O fabriqué par différentes techniques dans le cadre de ce travail

Properties	**Parameters**	**Cu_2O Absorber**		
		PLD	Magnetron Sputtering	Thermal Oxidation
Surface Quality	Average Grain size	15 nm	10 nm	109 nm
Absorption	Bandgap	2.05±0.05 eV	2.24±0.02 eV	1.97 eV (PL)
Defects	Sub-Bandgap states	Low	High	
Minority Carriers	Carrier lifetime	< 1ps	~ 69 ps	~ 1000 ps
J-V Performance	V_{OC}	560 mV (epitaxial Cu_2O)	260 mV	190 mV
	J_{SC}	0.21 mA/cm^2 (epitaxial Cu_2O)	1.76 mA/cm^2	1.9 mA/cm^2

Publication

C. V. Kartha, J.-L. Rehspringer, D. Muller, S. Roques, J. Bartringer, G. Ferblantier, A. Slaoui, and T. Fix: Insights into Cu_2O thin film absorber via pulsed laser deposition. *Ceramics International* **48**(11), 15274 (2022).

Communications

1. Poster : C. V. Kartha, G. Schmerber, J.-L. Rehspringer, D. Muller, S. Roques, G. Ferblantier, A. Slaoui, T. Fix "Synthesis and Characterization of Cuprous Oxide Thin Films" at KSOP-QMat Summer School 2020, Karlsruhe,Germany
2. Présentation orale : C. V. Kartha, G. Schmerber, J.-L. Rehspringer, D. Muller, S. Roques, A. Slaoui, and T. Fix "Pulsed Laser Deposition of Cu_2O Thin Film for Photovoltaics", at E-MRS Spring Meeting 2021
3. Présentation orale : C. V. Kartha, D. Muller, S. Roques, G. Ferblantier, A. Slaoui, T. Fix, "An Experimental Comparison Study on the Cu_2O Thin Films via Different Preparation Techniques", at E-MRS Spring Meeting 2022

Chithira VENUGOPALAN KARTHA

Croissance et caractérisation d'absorbeurs à base d'oxyde cuivreux pour le photovoltaïque

Résumé

L'oxyde cuivreux (Cu_2O) est un candidat prometteur comme absorbeur photovoltaïque. Dans ce travail, nous avons tout d'abord optimisé les conditions de dépôt de films de Cu_2O purs sans phase parasite de CuO par ablation laser pulsé (PLD) et pulvérisation cathodique RF. Nous avons également optimisé l'oxydation thermique de feuilles de cuivre pour obtenir Cu_2O. Nous avons montré que la stœchiométrie des films peut être contrôlée en variant les conditions de dépôt. Les propriétés des films en tant qu'absorbeur ont été investiguées en détail avec différentes techniques structurales, optiques et électriques. Pour étudier l'influence de la technique de croissance de Cu_2O sur les propriétés en tant qu'absorbeur, les films de Cu_2O optimisés par PLD et pulvérisation cathodique ont été comparés aux feuilles de Cu_2O oxydées thermiquement. La réponse photovoltaïque de ces absorbeurs préparés via les différentes techniques a été mesurée en élaborant des cellules solaires à base d'hétérojonctions adaptées. Une tension de circuit ouvert de 0.56 V a été mesurée à partir de films épitaxiés par PLD avec une hétérojonction à base de $Nb:SrTiO_3$. Le meilleur courant a été obtenu avec des cellules solaires de feuilles de Cu_2O oxydé thermiquement, fournissant une densité de courant de 1.90 mA/cm^2. Les cellules solaires à base de Cu_2O obtenu par pulvérisation cathodique offrent également une réponse photovoltaïque intéressante. Pour finir, la variation des performances des différents absorbeurs de Cu_2O a été analysée en utilisant des techniques de caractérisation avancées comme l'absorption transitoire et la technique de TCSPC (Time-Correlated Single Photon Counting). Nous montrons que la présence de défauts ou pièges influence le temps de vie des porteurs dans les films obtenus par PLD et pulvérisation cathodique, ce qui affecte l'efficacité de la séparation des porteurs de charge dans les cellules solaires

Mots clés : oxydes, PLD, pulvérisation cathodique, oxydation thermique, cellule solaire, Cu_2O

Résumé en anglais

Cuprous Oxide (Cu_2O) is a promising candidate as an absorber in photovoltaics. In this work, initially we have optimized the deposition conditions for pure Cu_2O film without any parasitic CuO phase via Pulsed Laser Deposition (PLD) and RF Magnetron Sputtering. Optimization of the thermal oxidation of copper sheets to obtain Cu_2O was also carried out. We have shown that the stoichiometry of the film can be controlled by varying the deposition conditions. The absorber properties of the films were investigated in detail with several structural, optical, and electrical characterization techniques. To study the influence of the Cu_2O growth technique on the absorber properties, optimised PLD and sputtered Cu_2O films were compared to thermally oxidised Cu_2O sheets. The photovoltaic response of the same absorber prepared via different techniques was also investigated by constructing solar cells with suitable heterojunctions. An open-circuit voltage of 0.56 V was measured from epitaxially grown PLD Cu_2O with $Nb:SrTiO_3$ heterojunction. The highest current was obtained for solar cell with thermally oxidised sheet with a short-circuit current density of 1.90 mA/cm^2. The sputtered Cu_2O solar cell also showed promising photovoltaic response. Finally, the variation in the absorber efficiency of Cu_2O was analysed using advanced characterization techniques such as Transient Absorption and Time-Correlated Single Photon Counting. The presence of defects or traps were found to influence the carrier lifetime in the PLD and sputtered Cu_2O films, highly affecting the charge carrier separation efficiency when employed in a photovoltaic cell.

Keywords: Oxides, PLD, Magnetron Sputtering, Thermal Oxidation, Solar Cell, Cu_2O